TIMING AND ORIGIN OF INTERMEDIATE SULFIDATION EPITHERMAL VEINS AND GEOCHEMICAL ZONING IN THE FRESNILLO DISTRICT, MEXICO: CONSTRAINED BY ^{40}Ar/^{39}Ar GEOCHRONOLOGY, FLUID INCLUSIONS, GAS ANALYSIS, STABLE ISOTOPES, AND METAL RATIOS

By

Jesus M. Velador

Submitted to the Faculty in Partial Fulfillment of

the Requirements for the

Doctorate of Philosophy in Geology

New Mexico Institute of Mining and Technology

Department of Earth and Environmental Sciences

Socorro, New Mexico

May, 2010

To the memory of my mother who passed away in 2002, to my father who has dedicated over 35 years of his life to the arduous work of metals exploration in Mexico, and finally to my wife Magdalena, my children Elizabeth and Jesus, Jr. for all their support and understanding.

ABSTRACT

Fresnillo is a world class district that has produced silver almost continuously since the 1550's. Currently the district produces ore from several intermediate sulfidation epithermal veins with average grades between 300 and 700 grams per tonne of silver and contains approximate resources of 1BOz of silver. Two areas with epithermal mineralization are considered in this study: Fresnillo southeast, which contains the mine and the producing veins; and Fresnillo southwest, which contains veins discovered within the last six years, such as Jarillas and Valdecañas.

In this study of Fresnillo questions relevant to the understanding of epithermal deposits in general are addressed like: is it one large district formed by an extensive mineralizing event, or is it the result of several overlapping mineralizing events? What was the source of the mineralizing fluids and where was this source located? The answers to the previous questions are relevant for the understanding of intermediate sulfidation epithermal deposits in Mexico and have important implications for exploration in the district.

The intermediate sulfidation epithermal veins of Fresnillo are hosted by the Middle Jurassic to Lower Cretaceous volcanosedimentary sequence (Guerrero Terrane), which is locally covered by Paleocene to Eocene conglomerate, and Eocene to Oligocene volcanic rocks that locally bear acid sulfate alteration with alunite veins. An Oligocene quartz-monzonite intrusion also occurs in Fresnillo and is spatially

associated with manto, chimney and vein deposits in the historic part of the district. The reserves of the historic part of the district, Fortuna-Proaño area, have been exhausted.

Spatial association of Tertiary volcanics, intrusions, acid sulfate alteration and epithermal veins, makes the district ideal for evaluating the temporal relations between magmatism and hydrothermal activity using precise $^{40}Ar/^{39}Ar$ geochronology. Sanidine single crystal laser fusion analyses reveal discrete volcanic eruptions at 44.73 ± 0.04, 40.92 ± 0.04, 40.83 ± 0.04, 31.55 ± 0.03 and 31.04 ± 0.05 Ma. Dating of orthoclase from the Fortuna quartz-monzonite was problematic due to excess argon contamination, but a preferred age of 32.65 ± 0.05 Ma is suggested. Two adularia samples from the Jarillas vein give statistically identical ages of 29.75 ± 0.12 and 29.68 ± 0.10 Ma. Adularia from Valdecañas vein shows a climbing age spectrum related to hydrothermal alteration; however a terminal step with age of 29.74 ± 0.07 Ma suggests that the two veins may be coeval. Alunite recorded two distinct ages at 30.56 ± 0.04 and 31.03 ± 0.05 Ma. Alunite and adularia ages suggest that acid sulfate alteration and mineralization occurred separately well after emplacement of the dated phase of the Fortuna stock and consequently it can not be the source of heat for the hydrothermal system that formed those. Finally, the ~3 Ma difference in age between epithermal mineralization and the Fortuna stock are indicative of a long lived but episodic hydrothermal system which could have been driven by multiple pulses of small and shallow intrusions.

Core logging and petrography of Jarillas and Valdecañas reveals very similar mineralogy and paragenesis for both veins. The main ore minerals occurring in these veins are sphalerite, galena, pyrargyrite, polybasite and acanthite; the main gangue sulfide and non-sulfide minerals are pyrite, arsenopyrite, and quartz and calcite. Mineral

deposition occurred in five stages: 1) deposition of mostly base metal sulfides; 2) quartz and calcite with fewer sulfides; 3) alternating bands of chalcedonic quartz, calcite, adularia, epidote, base metals and silver minerals; 4) quartz, calcite and dolomite-ankerite with coarse grained pyrargyrite; and 5) barren quartz, calcite and fluorite.

Fluid inclusion microthermometry was performed in over 900 fluid inclusions hosted mainly by quartz and calcite in both veins. The fluid inclusion study resolved homogenization temperature and salinity ranges typical of intermediate sulfidation epithermal deposits; 160°C to 320°C and 0 to 11 wt% NaCl eq. respectively. Fluid inclusion gas analysis was also done in some samples and indicates that H_2O accounts for 99.17 to 99.86 % of the volatiles extracted, whereas the second and third most abundant volatiles are CO_2 (<0.5 mol %) and N_2 (<0.4 mol %). Calculated $\log fO_2$ (-42.5 to -34.2) and $\log fS_2$ (-11.9 to -3.6) ranges indicate that the hydrothermal fluids were reducing which is typical of low to intermediate sulfidation systems. $\delta^{18}O$ mineral values determined in quartz (n=44) and calcite (n=25) associated with ore stages range from 12.4 to 18.6 per mil and 7.4 to 15.3 per mil, respectively. The oxygen fluid values calculated for the homogenization temperatures determined by fluid inclusions range from 3.9 to 9.6 per mil (quartz) and 5.9 to 10.9 per mil (calcite). δD values (n=14) measured from fluid inclusions in quartz associated with ore in the two veins range from -79.3 to – 50.5 per mil. $\delta^{13}C$ values determined for calcite associated with ore in Jarillas range from -8.2 to -6.1 per mil, and for Valdecañas from -9.1 to -4.0 per mil.

Textures, mineralogy, and stable isotope data indicate that the intermediate sulfidation veins in Fresnillo are co-genetic. The maximum salinities up to 11 wt % NaCl, heavy oxygen and hydrogen isotope compositions of the fluids, and gas analysis in

conjunction suggest that the veins were formed by mixing of magmatic and deeply circulated meteoric water. The consistently light sulfur and carbon values of the veins throughout the district suggest that sulfur and carbon were partially derived from the Guerrero Terrane either by leaching of those elements at the time of hydrothermal fluid circulation or due to assimilation and melting of Guerrero Terrane xenoliths in a deep-seated magma chamber.

Variations in average homogenization temperatures and salinities, and sulfur and oxygen fugacity ranges across the district indicate a zonation pattern from southeast to northwest. These results also show that the gold and base metal concentrations of the veins in the west are consistently higher with respect to those of the veins in the east. Additionally, high Au/Ag ratios and low base metal contents in the Saucito, San Antonio and San Mateo veins suggests that these veins are distal with respect to the possible center of the district and therefore, the thermal center of the district could be to the northwest. Finally if the thermal center is an intrusion, then there is exploration potential to the northwest for more epithermal mineralization proximal to the intrusion or even for porphyry type mineralization at depth.

ACKNOWLEDGEMENTS

TABLE OF CONTENTS

LIST OF FIGURES

viii

LIST OF TABLES

INTRODUCTION

Purpose

Epithermal deposits form at shallow depths in volcanic-hydrothermal and geothermal environments. They define a spectrum with two end members; low and high sulfidation (Hedenquist et al., 1998). In addition it is recognized that epithermal deposits can form a continuum with porphyry deposits at depth, and that high sulfidation deposits are generally proximal with respect to the intrusion whereas low sulfidation deposits occur generally distal (Hedenquist et al., 1998). Intermediate sulfidation deposits form part of the spectrum and their genesis is complex due to the involvement of fluids with meteoric or magmatic origin during their formation and due to fluid evolution. According to several authors, the fluids that formed the Mexican epithermal deposits represent a mixture of fluids with diverse origin varying from meteoric to magmatic (Camprubí and Albinson, 2007; Simmons et al., 1988; Benton, 1991; Norman et al., 1997; Simmons, 1991; Albinson et al., 2001; Camprubí et al., 2001; Camprubí and Albinson, 2007).

Globally, epithermal deposits produce about 30% of the gold and silver, and they are economically the most important precious metal producers in Mexico. Important intermediate sulfidation epithermal deposits occur in the Great Basin of the United States, Peru and the Mesa Central of Mexico. Mexico is ranked as the second silver producer in the world with 104.2 BOz produced in 2008, most of which comes from epithermal deposits and approximately 30% comes from Fresnillo (The Silver Institute;

1

Fresnillo Plc). Several silver-rich low and intermediate sulfidation epithermal deposits have given the status of top silver producing country to Mexico; e.g. Pachuca-Real del Monte, Taxco, Guanajuato, Zacatecas and Fresnillo (Camprubí and Albinson, 2007). Study of the epithermal deposits of Fresnillo provides an opportunity to investigate the temporal and chemical evolution of this world class district. This thesis will address major questions in epithermal ore deposits that are generally applicable to the other IS deposits in Mexico and around the world such as: age of mineralization, duration of hydrothermal activity and sources of fluids and metals.

Statement of the problem

Despite the fact that the Fresnillo mine has produced silver almost continuously for over 450 years, at present it still contains total resources approximately of 1 BOz. In the mid 1970's intermediate sulfidation mineralization was discovered in Fresnillo (Santo Niño vein), which raised some questions about its genesis. Between the 1980's and 1990's more veins were discovered (San Carlos and many others) and several studies were performed on different veins to understand the characteristics of the mineralizing fluids and the genesis of the veins (Chico, 1986; Gemmell, 1986; Simmons, 1988; Benton, 1991, Dilley, 1993; Eckberg, 1999). In 2003, intermediate sulfidation mineralization was also discovered about 8 km to the southwest of the mine (Saucito vein). Discovery of Valdecañas and Jarillas followed the discovery of Saucito vein. The new discoveries in what is now referred to as the Fresnillo-SW area raised questions not only about the genesis of those veins in themselves, but also questions involving the genesis of the district as a whole: is it one large and rich district? Or, is big because it is the result of several overlapping mineralizing events over time? If it is one large district,

what was the source of the mineralizing fluids and where was it located? To which side of the district is there potential for more mineralization?

In order to provide answers to the broad questions mentioned above, we have designed our study to answer more specific questions (relevant to the understanding of epithermal deposits):

1) What is the age of mineralization, its temporal relation with volcanism and intrusion, and how long the hydrothermal system remained active?

2) What are the physiochemical characteristics and the source of the hydrothermal fluids, and what is the genetic relation between the veins across the district?

3) Is there a physiochemical zonation across the district that can help us infer the possible location of the thermal center of the district?

4) What exploration recommendations can be made for the Fresnillo district as a result of this study?

Approach

The approach selected in this research project is to perform $^{40}Ar/^{39}Ar$ geochronology, ore petrography, fluid inclusion, gas analysis, and stable isotope studies and to interpret an extensive data base of metal assays. The results of the investigations allow interpretations about the timing of mineral deposition, temporal relations between magmatism, mineralization and hydrothermal activity, and the duration of hydrothermal activity in the district, as well as about the physiochemical characteristics of the hydrothermal fluids, its source (s) and its evolution. In conjunction our results allow us to provide a genetic model of the district that has important implications for future exploration in the district.

3

Organization

This thesis is organized into four parts, the first part is an introduction and the following three parts are papers that are intended to be published in scientific journals. The first paper (Chapter I) is about the $^{40}Ar/^{39}Ar$ geochronology and it has been submitted to ECONOMIC GEOLOGY. The second paper (Chapter II) is about the genesis and it is also going to be submitted to a journal for publication. The third and last paper (Chapter III) is about the physiochemical zoning across the district and is also going to be submitted to a journal. Following chapter III there is a section with general conclusions based on the three papers. Finally at the end there are appendices with the analytical data tables for argon geochronology, sample locations, petrographic descriptions, microthermometry data and gas chemistry data.

CHAPTER I

TIMING OF MAGMATIC ACTIVITY AND MINERALIZATION AND EVIDENCES OF A LONG-LIVED HYDROTHERMAL SYSTEM IN THE FRESNILLO SILVER DISTRICT, MEXICO: CONSTRAINED BY ^{40}Ar/^{39}Ar GEOCHRONOLOGY

Abstract

The ore deposits of Fresnillo have produced silver for over 450 years and contain resources of approximately 1 BOz. Mineralization in Fresnillo occurs in epithermal veins hosted by a Middle Jurassic to Lower Cretaceous volcanosedimentary sequence (Guerrero Terrane). Late Paleocene conglomerates and Eocene to Oligocene tuffs and flows of trachyte, rhyolite and rhyodacite lay unconformably on top of the Guerrero Terrane. Acid-sulfate alteration with alunite veins, of steam-heated origin, occurs in Eocene tuffs above some of the mineralized veins. Oligocene rhyolitic domes and a quartz-monzonite stock also occur in the area, whereas sparse Miocene basaltic-flows and dikes are the youngest igneous rocks in the district.

Spatial association of Tertiary volcanics, intrusions, acid sulfate alteration and epithermal veins, makes the district ideal for evaluating the temporal relations between magmatism and hydrothermal activity using precise ^{40}Ar/^{39}Ar geochronology. Sanidine single crystal laser fusion analyses reveal discrete volcanic eruptions at 44.73 ± 0.04,

40.92 ± 0.04, 40.83 ± 0.04, 31.55 ± 0.03 and 31.04 ± 0.05 Ma. Dating of orthoclase from the Fortuna quartz-monzonite was problematic due to excess argon contamination, but a preferred age of 32.65 ± 0.05 Ma is suggested. Two adularia samples from the Jarillas vein give statistically identical ages of 29.75 ± 0.12 and 29.68 ± 0.10 Ma. Adularia from Valdecañas vein shows a climbing age spectrum related to hydrothermal alteration; however a terminal step with age of 29.74 ± 0.07 Ma suggests that the two veins may be coeval. Alunite recorded two distinct ages at 30.56 ± 0.04 and 31.03 ± 0.05 Ma. Alunite and adularia ages suggest that acid sulfate alteration and mineralization occurred separately well after emplacement of the dated phase of the Fortuna stock and consequently it can not be the source of heat for the hydrothermal system that formed those. Finally, the ~3 Ma difference in age between epithermal mineralization and the Fortuna stock are indicative of a long lived but episodic hydrothermal system which could have been driven by multiple pulses of small and shallow intrusions.

Introduction

A genetic connection between spatially associated porphyry and epithermal ore deposits has been suggested or demonstrated in many districts around the world (Sillitoe, 1989; Vila and Sillitoe, 1991; and Hedenquist et al., 1997; Muntean and Einaudi, 2001; Valencia et al., 2008; and Pudack et al., 2009). Geochemical studies have also revealed the participation of magmatic fluids in the generation of high sulfidation and some intermediate sulfidation epithermal deposits, including the Santo Niño vein in Fresnillo (Simmons, 1986; Heald et al., 1987; Hedenquist et al., 1998; Sillitoe, 2008). In contrast with high sulfidation deposits, low and intermediate sulfidation equivalents occur generally distal with respect to any intrusive rock (Hedenquist, 1987), but in many cases,

K/Ar and ^{40}Ar/^{39}Ar studies have demonstrated a temporal link between mineralization and the spatially associated igneous rocks (Marsh et al., 1997; Camprubí et al., 2003; Rice et al., 2005; Warren et al. 2008).

The spatial association of igneous rocks, steam-heated alteration and epithermal veins, makes the Fresnillo district ideal for evaluating the temporal relations between magmatism and hydrothermal activity using precise ^{40}Ar/^{39}Ar geochronology. Precise and accurate determinations of the age relations between igneous activity, acid sulfate alteration and epithermal mineralization help determine not only whether a temporal link exists between magmatism and mineralization but also the duration of hydrothermal activity. These data can be used as a basis for further geochemical studies aimed to evaluate the genetic evolution of the Fresnillo District. In this study we have conducted single crystal laser fusion analysis on sanidines from Tertiary volcanic rocks and step heating age spectrum experiments on orthoclase from the Fortuna quartz-monzonite (Fortuna stock) associated with skarn and manto mineralization, adularias from two intermediate sulfidation epithermal veins and alunites from acid sulfate alteration occurring in Eocene volcanics.

Geology

Fresnillo is located within the Mesa Central physiographic province (MC) which is an elevated plateau comprised of marine sedimentary rocks of the Sierra Madre Oriental (SMOr) terrane to the east and northeast and a sequence of volcanosedimentary rocks of the Guerrero Terrane (GT) to the southwest. These terranes are partially and unconformably overlain by volcanic rocks of the Sierra Madre Occidental (SMOc) in the

western portions of the MC (Fig. 1). The GT forms part of a collage of suspect terranes

that were accreted to the west margin of Mexico by the Upper Jurassic to Early Tertiary
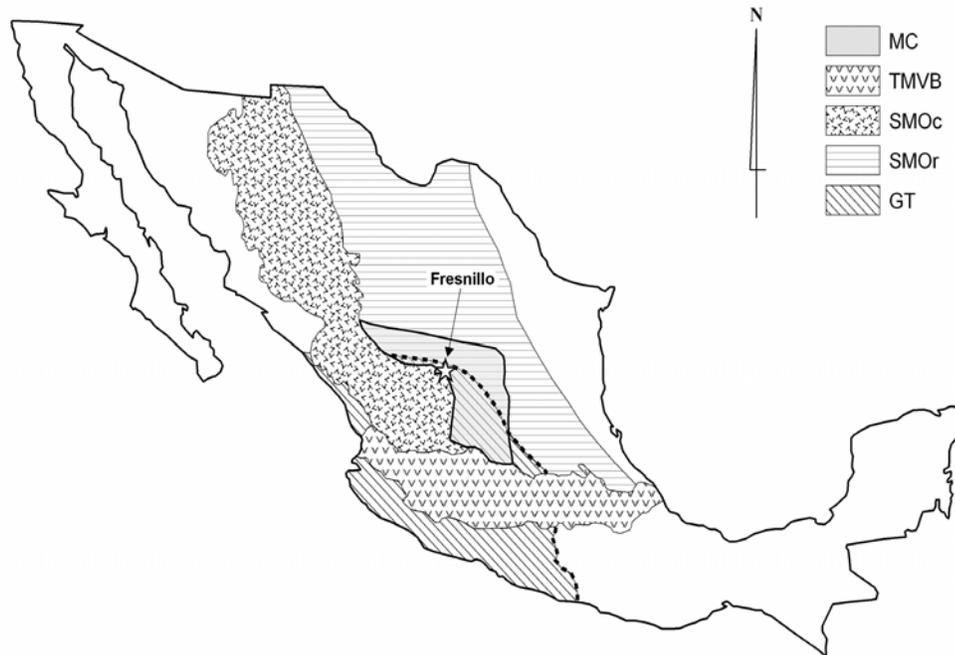
Fig. 1. Map of Mexico showing the location of the Mesa Central and Fresnillo. Adapted from Campa and Coney (1982) and Nieto-Samaniego et al. (2007). Abbreviations are as follow: MC (Mesa Central), TMVB (Trans Mexican Volcanic Belt), SMOc (Sierra Madre Occidental), SMOr (Sierra Madre Oriental), GT (Guerrero Terrane).

(Campa and Coney, 1982) and its age has been bracketed by U-Pb zircon geochronology

between 157.4 +/-4.1 Ma to 139.7 +/- 2.5 Ma from samples of felsic volcanics spatially

associated with Volcanogenic Massive Sulfide (VMS) deposits in Zacatecas, Guanajuato

and Guerrero states (Mortensen et al., 2008) and between ~160 Ma to ~132 Ma from

samples of metamorphosed volcanosedimentary rocks near Zacatecas City (Escalona-

Alcázar et al., 2009). In Fresnillo the GT is separated into two domains, one consisting

primarily of graywackes and black shales at the base, and the other consisting primarily

of andesitic lava flows on top (Chilitos formation) (Fig. 2). A detailed description of the

stratigraphy of the GT in Fresnillo can be found in De Cserna (1976), and Ruvalcaba-

Ruiz and Thompson (1988). Outcrops of the GT in Fresnillo are sporadic and relatively small.

The Tertiary section contains the Late Paleocene to Early Eocene Fresnillo conglomerate at the base (De Cserna, 1976; Ruvalcaba-Ruiz and Thompson, 1988), with overlying Eocene trachytic to dacitic tuffs, and Oligocene rhyolite to rhyodacite tuffs, flows and domes on top (J. M. Velador, unpublished data, 2005). Informal names of Valdecañas and Cierpe (Eocene units), and Piedras and Altamira (Oligocene units) have been assigned here to the Tertiary volcanics (Fig. 2). Changes in geochemical composition between the Eocene and Oligocene volcanics have been attributed to the onset of crustal extension of the MC (Orozco-Esquivel et al., 2002). Finally, common but sparse Miocene basalt flows represent the latest volcanism in the area (Nieto-Samaniego et al., 2007).

There are three types of intrusive rocks identified in Fresnillo; Middle Jurassic to Early Cretaceous mafic sills and dikes that form part of the GT; Oligocene quartz-monzonite and granodiorite in Fresnillo and Plateros, respectively; and Miocene basalt dikes. The Oligocene Fortuna stock is spatially associated with mineralization in the Fortuna and Proaño areas (De Cserna et al., 1977; Ruvalcaba-Ruiz, 1980; Chico, 1986). This intrusion has been proposed as the ore generating stock for skarn, chimney (De Cserna, 1977) and vein mineralization (Eckberg, 1999). Based on cross cutting relations between the stock, manto and vein deposits, De Cserna (1977), proposed a Late Eocene age for this intrusion, and suggested that it was older than the veins.
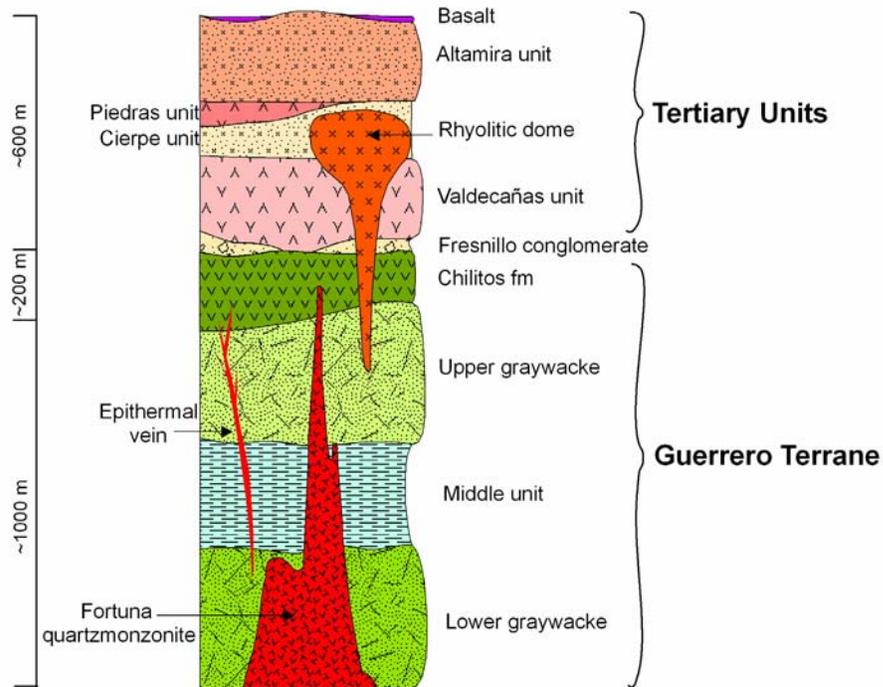
Fig. 2. Stratigraphic column of the Fresnillo district showing approximate thickness of the main units.

Ore Deposits

Mineralization in Fresnillo occurs in four areas: the Proaño area, the site for ore discovery in 1554, which contained silver mineralization in an oxidized stockwork; the Fortuna area, which contained silver, lead and zinc mineralization occurring in manto, chimney, skarn and vein deposits, spatially related to the Fortuna stock (De Cserna et al., 1977; Ruvalcaba-Ruiz, 1980; Chico, 1986); the Fresnillo-SE area (Trejo, 2001), which consists of high grade silver, lead and zinc, intermediate sulfidation epithermal veins such as Santo Niño and San Carlos; and finally the recently discovered Fresnillo-SW area comprising the high-grade silver, gold, lead and zinc, intermediate sulfidation Saucito, Jarillas and Valdecañas veins.

Mineralization in Fresnillo-SE and Fresnillo-SW is blind to surface and for the most part hosted by the sedimentary units of the GT. The veins trend E-W to NW-SE, dip

steeply north or south, and have lengths varying between 1.3 to ~8 km and widths of 10's

cm to 10's m. Textural and mineralogic similarities between the veins of the two areas

suggest a genetic connection. Additionally, fluid inclusion data (Velador et al., 2009),

and preliminary stable isotope and fluid inclusion gas analysis results suggest that the

Santo Niño, Jarillas and Valdecañas veins are genetically related. The veins are

characterized by occurrence of: argillic alteration, silicification and early brecciation of

wall rock; deposition of massive sphalerite and galena at depth; deposition of alternating

bands of sulfides (galena, sphalerite, pyrite, arsenopyrite, chalcopyrite and pyrrhotite),

quartz, chalcedony, calcite, epidote and minor adularia, with complex paragenetic

relations; and deposition of late stage veins of barren quartz, calcite and locally fluorite.

The silver sulfosalts (pyrargyrite, polybasite, stephanite and miargyrite), sulfides

(acanthite, aguilarite) and electrum are the most important Ag-bearing minerals, and

occur generally associated with galena and sphalerite or disseminated in quartz and

calcite bands. In Santo Niño (Rubalcaba-Ruiz and Thompson, 1988), and in Jarillas and

Valdecañas, adularia forms thin bands and more commonly occurs as large (up to 5 mm),

weakly to moderately sericitized sub-rhombic crystals, embedded in bands of quartz and

calcite.

Hydrothermal Alteration

Clay mineral characterization of core samples from the Saucito vein in Fresnillo-

SW revealed that at ore-shoot elevations, illite and interlayered illite-smectite sometimes

associated with calcite, are the main clays filling fractures, whereas at higher elevations

(i.e, close to surface) the alteration envelope broadens and the assemblage changes to

advanced argillic bearing kaolinite and interlayered illite-smectite in a denser network of

11

fractures (J. M. Velador, unpublished data, 2005). A similar mineral assemblage and zoning is observed in the Santo Niño, San Carlos, Jarillas and Valdecañas veins with core logging. The only surface expressions of the blind epithermal veins at depth are calcite, barite and quartz veinlets, which occur in some of the scant outcrops of the GT in Fresnillo-SE. Outside the influence of the argillic and advanced argillic alteration envelopes the rocks of the GT are chloritized, but because of its regional character, it is possible that this alteration is related to greenschist facies metamorphism produced during accretion.

In contrast to Saucito and the other veins in the valley, intense zones of silicification, quartz-alunite-kaolinite alteration, alunite stockworks and less abundant quartz veinlets occur above the Valdecañas vein in the Eocene volcanic units forming an acid sulfate alteration blanket of steam-heated origin. Similar, but less intense alteration occurs in other areas with more restricted aerial extension in Cerro del Cristo and Cerro Proaño, in Fresnillo-SE (Ruvalcaba-Ruiz, 1980; Simmons, 1991). In the Piedras area, south of Saucito vein, the volcanic units have mercury anomalies, lenticular-hydrothermal explosion breccias and strong to pervasive silicified zones, which have been interpreted to be proximal to the paleosurface (Simmons, 1986; Albinson, 1988; Simmons et al., 1988).

Previous Geochronology

The first attempt in the district to define the temporal relationships between volcanism, magmatism and hydrothermal activity was done by Lang et al. (1988), using K/Ar dating on whole rock samples of altered and unaltered volcanic and intrusive rocks (Table 1). They suggested that the timing of volcanic activity was between 38.3 ± 0.8 and

27.4 ± 1.5 Ma and intrusive activity was between 33.5 ± 0.8 and 32.1 ± 1.3 Ma. Additionally, they dated feldspar-rich fractions separated from the Fortuna stock and Plateros granodiorite (~7.5 km north of Fresnillo) and reported distinct ages of crystallization: the Fortuna stock crystallizing at 31.6 ± 0.7 Ma and the Plateros stock at 33.0 ± 0.7 Ma. Dating of hydrothermal K-feldspar occurring in the altered Valdecañas unit provided an age of 29.1 ± 0.8 Ma, and was interpreted as the age of hydrothermal activity related to mineralization in Fresnillo (Lang et al., 1988).

In 2003, discovery of the Saucito vein in Fresnillo-SW, and proximal to the altered volcanics, created the necessity for a better understanding of the temporal relations between volcanism, mineralization and acid-sulfate alteration. Thus, a second K/Ar study was undertaken, and samples were collected from fresh and altered volcanics in the Valdecañas range and three samples were collected from drill core of the Saucito vein (Table 1). The whole rock samples were analyzed at the Geochronology and Isotopic Geochemistry laboratory of Actlabs in Canada (Kapusta, 2005). The dates of Kapusta (2005), did not agree with all of the results of Lang et al. (1988), but his work on the quartz-alunite altered tuff, in approximately the same location of Lang's SS-179 sample, produced an analytically identical age of 29.9 ± 0.9 Ma. Combined, these efforts indicate that acid-sulfate alteration occurred between ~29 and ~30 Ma. The older limit for volcanic activity was determined to be 42.2 ± 1.1 Ma. Finally, the three samples from Saucito vein reported two anomalously old ages of 42.4 ± 2.2 and 54.6 ± 2.4 Ma and one age of 27.4 ± 1.2 Ma which overlaps within reported error with the 29.1 ± 0.8 date determined for hydrothermal K- feldspar by Lang et al. (1988), (Table 1).

Table 1. K/Ar ages (Ma) with errors at 1σ by Lang et al. (1988) and Kapusta (2005).

Lithologic unit	Description	Lang et al. (1988)	Kapusta (2005)
Saucito vein	Banded vein with clays		27.4+/-1.2
	Banded vein with clays		42.4+/-2.2
	Banded vein with clays		54.6+/-2.4
Acid sulphate alt.	K-feldspar veinlets / qtz alunite aleteration	29.1+/-0.8	29.9 +/- 0.9
	Duplicate	29.1+/-0.6	
Altaminara unit	Rhyodacite	27.4+/-1.5	28.7 +/- 1.1
	Rhyodacite		30.5 +/- 1.0
	Rhyodacite		31.5 +/- 1.1
Rhyodacite	Silicified rhyodacite, 6.5 km SW of Altamira		48.7+/- 6.5
Piedras unit	Rhyolitic tuff	27.7+/-0.6	30.1 +/- 0.8
	Rhyolitic tuff		31.2 +/- 0.8
	Rhyolitic tuff		32.7 +/- 1.3
Cierpe unit	Rhyolitic - trachytic tuff	38.3+/-0.8	40.1 +/-1.1
	Rhyolitic - trachytic tuff		42.2 +/- 1.1
Valdecañas unit	Silicified rhyolitic - trachytic tuff		32.2 +/- 1.0
	Silicified rhyolitic - trachytic tuff		49.0 +/- 1.5
Fortuna stock	Quartz-monzonite	32.1+/-1.3	
	Quartz-monzonite, feldspar-rich fraction	31.6+/-0.7	
	Quartz-monzonite, feldspar-rich fraction	32.3+/-0.7	
Plateros granodiorite	Granodiorite	32.7+/-1.2	
	Duplicate	32.2+/-0.7	
	Granodiorite, feldspar-rich fraction	33.0+/-0.7	
	Sericitized granodiorite	31.0+/-0.6	
Plateros dike	quartz trachyte	33.5+/-0.8	
Chilitos fm	Altered basalt	36.3+/-0.7	

^{40}Ar/^{39}Ar Methods

Hand samples were collected from rhyolitic tuffs and flows at different
stratigraphic levels of the Tertiary section and one sample of the Fortuna stock was
collected from drill core of the Fortuna area. Petrographic studies revealed that the
sanidines are unaltered and that the Fortuna orthoclase is weakly to moderately
sericitized. The rock samples were crushed, grounded and subsequently sieved to obtain
phenocryst-rich fractions. Separation of potassium feldspars was done primarily by hand
picking under a binocular microscope. The separated crystals were cleaned ultrasonically
with 25 percent HF and repeatedly rinsed with distilled water to remove glass, matrix

and/or sericite. The mineral separate purity was assessed by examination in immersion oil under a polarizing microscope.

Calcite and quartz bands bearing sub-rhombic adularia grains up to 5 mm were obtained from core samples of the Jarillas and Valdecañas veins. Identification of adularia was done on hand sample using the binocular microscope, thin section and in some cases by staining with sodium cobaltinitrite following the methodology of Bailey and Stevens (1960). Petrographic studies of these samples revealed moderate to weak sericitization of the adularia grains. The bands containing adularia were crushed using a mortar and pestle and the adularia was concentrated by hand picking. The separated grains were ultrasonically cleaned with concentrated HCl for a few minutes to remove calcite and sericite, and then repeatedly rinsed with distilled water.

Alunite samples were obtained from veinlets hosted by the steam-heated acid sulfate alteration zone in the Eocene volcanics. Petrographic examination of one sample revealed randomly oriented, 10 to 20-µm long crystals of alunite associated with clay minerals, mostly kaolinite. The alunite veins were crushed with a mortar and pestle and then cleaned ultrasonically with 10 percent HCl and rinsed with distilled water to remove clays. Purity greater than 98 percent was assessed by binocular microscope investigation.

After separation, samples and inter-laboratory standard, Fish Canyon-tuff sanidine (age 28.02 Ma), were loaded in aluminium disks and irradiated in two batches (NM-213 and NM-220) at the Nuclear Science Center Reactor at Texas A&M University for 7.22 hours and at the Triga Reactor at Denver for 10 hours, respectively. Argon extraction for sanidine was conducted by single-crystal laser fusion (SCLF) using a CO_2 laser, by incremental step heating with a defocused CO_2 laser beam for alunite, and by resistance

15

furnace step heating for adularia and orthoclase at the New Mexico Geochronology

Research Laboratory (NMGRL) at New Mexico Tech. Argon isotope intensities were

measured using a MAP 215-50 mass spectrometer operated at a resolution of 450 at mass

40 that is equipped with a Pfeiffer SEM 217 electron multiplier at New Mexico Tech.

Blanks were run routinely to correct for isotope contribution from the extraction system

and interfering reaction correction factors were determined by analysis of CaF_2 and K-

glass. Data reduction and age calculation was done using the program Mass Spec v. 7.687

written by A. Deino at the Berkley Geochronology Center. The sanidine dates are plotted

on ideograms and the eruption ages are calculated using the inverse variance weighted

mean method of Taylor (1982). Adularia, alunite and orthoclase data were plotted on age

spectrum and inverse isochron diagrams and plateau ages were calculated using the

inverse variance weighted mean of the selected steps.

$^{40}Ar/^{39}Ar$ Results

A total of 11 samples of sanidine, orthoclase, adularia and alunite were dated;

tables A1 and A2 in the appendix show the analytical data. Figure 3 summarizes the

$^{40}Ar/^{39}Ar$ results.

Sanidine: Ideograms for sanidines of the Valdecañas unit (VR-07-12), Cierpe unit (VR-

07-17 and LL-07-01), the rhyolitic dome (VR-07-38) and the Altamira unit (VR-08-02)

reveal mostly normally distributed populations with the exception of a few outliers (Fig.

4). Except for sample VR-08-02, all the sanidines for each sample were used to

determine eruption ages despite the fact that MSWD values (2.3 to 2.6) are slightly

elevated. For VR-08-02, two crystals are omitted from age calculation. Weighted mean

16

ages of 44.73 ± 0.04, 40.92 ± 0.04, 40.83 ± 0.04, 31.55 ± 0.03 and 31.04 ± 0.05 Ma were

determined for these units and fall correctly in stratigraphic sequence.
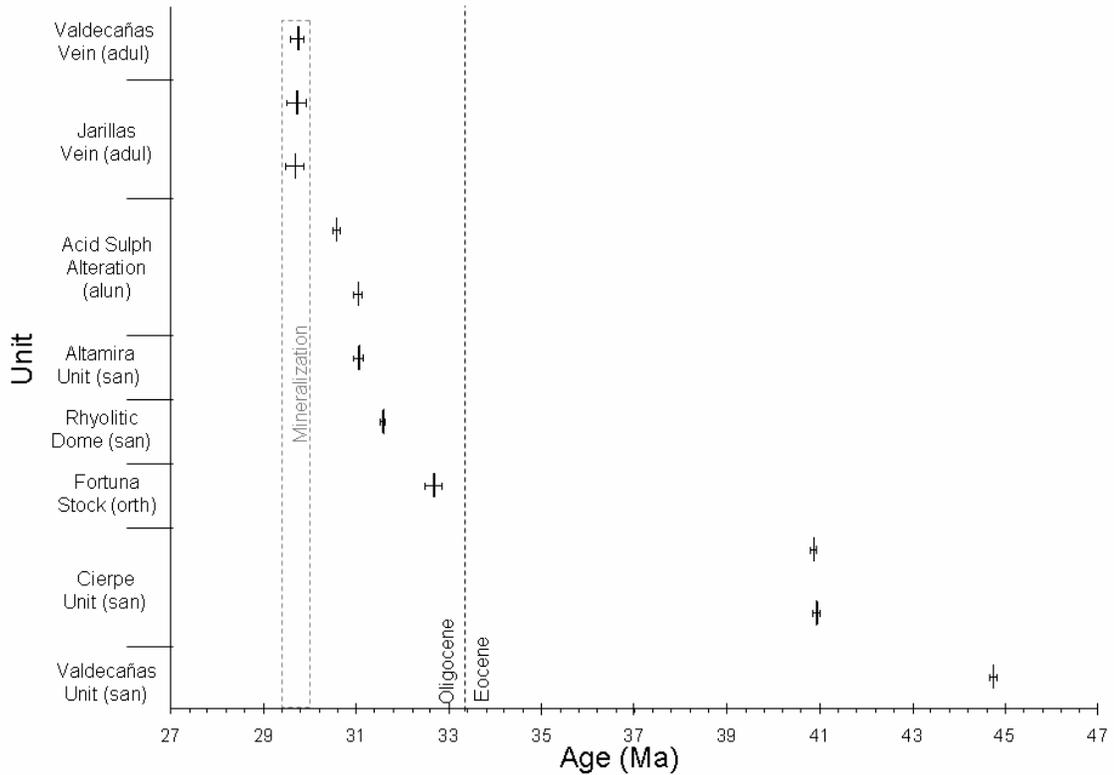
Fig. 3. Summary plot of ^{40}Ar/^{39}Ar ages; 2σ error bars are used in this figure instead of 1σ for a better visualization of the error bars. Abbreviations: sanidine (san), adularia (adul), orthoclase (orth), alunite (alun).

Orthoclase: The orthoclase age spectrum derived of the Fortuna stock (MP-08-01) has an

overall climbing pattern of ages between about 30.2 and 36.0 Ma. The spectrum shows

alternating old and young ages for isothermal duplicate steps at the beginning, followed

by an undulatory plateau segment and then by anomalously old steps for the rest of the

extraction (Fig. 5). The shape of this spectrum could be indicative of argon loss

associated with slow cooling or episodic heating. Alternatively, the complex spectra

17

could indicate excess [40]Ar contamination. Foster et al. (1990) described similar spectra as that revealed by MP-08-01 and interpreted the initial ages as reliable and the older ages as excess argon contamination. We tentatively adopt this interpretation for the Fortuna stock and suggest a preferred age of 32.65 ± 0.05 Ma that is described from the initially flat age spectrum segment.
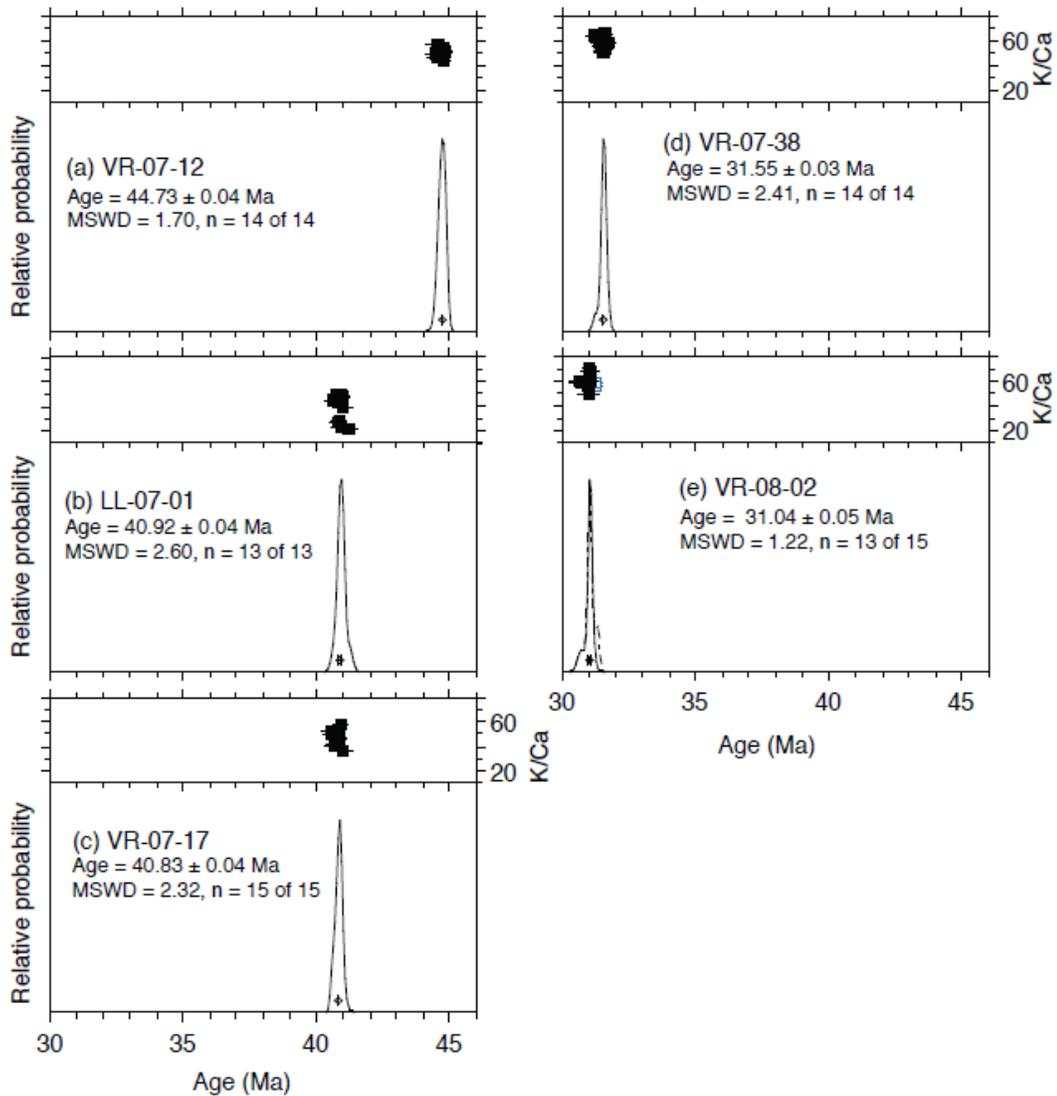
Fig. 4. [40]Ar/[39]Ar age probability and K/Ca diagrams for sanidine single crystal data. Eruption ages range from 44.73 to 31.04 Ma and indicate at least 4 analytically distinct eruptions. Open symbols for VR-08-02 are data omitted from mean age calculations.
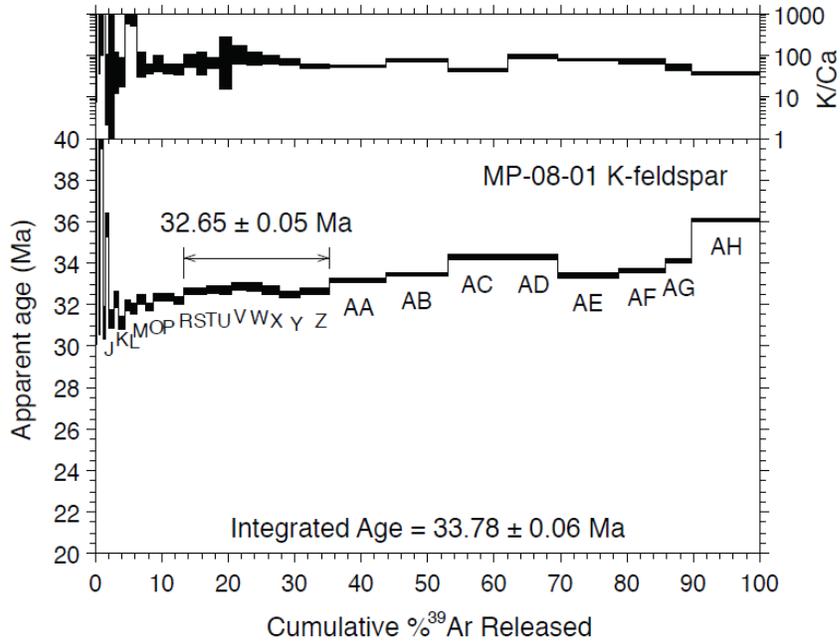
Fig. 5. Age and K/Ca spectra for K-feldspar from the Fortuna stock. Rising ages from steps AA-AH are tentatively interpreted to be caused by excess ^{40}Ar with the flat segment at 32.65 Ma representing the possible intrusion age. Increasing ages over the initial ~10% ^{39}Ar released could record argon loss associated with younger hydrothermal activity.

Adularia: Step heating experiments were conducted on two adularia samples (JV-G5-9 and JV-K9-17) from the Jarillas vein and one adularia (VV-GD-13) from the Valdecañas vein (Figs. 6, 7). Age spectra of the Jarillas adularias reveal initial old steps followed by apparent ages between about 29 to 31 Ma (Figs. 6A, 6B). Inverse isochron plots for these samples produce two statistically identical ages of 29.75 ± 0.12 and 29.68 ± 0.10 Ma, with ^{40}Ar/^{36}Ar initial components greater than atmospheric (Figs. 6C, 6D). These isochron ages are the preferred ages of the samples, and the excess argon component explains the minor age spectrum complexity. The age spectrum of the Valdecañas adularia (VV-GD-13) is disturbed, and starts with an anomalously old step that is followed by an age gradient between 24.08 and 29.74 Ma (Fig. 7). This sample is somewhat sericitized and the complexity likely stems from this alteration. We do not

19

think that the 29.74 ± 0.07 Ma age of step "N" is in coincidental agreement with the

Jarillas vein adularias, but rather suggests a common age for the veins.

Alunite: Two alunites sampled from drill-core VV-IC-01 and outcrop VR-07-05 of the

acid sulfate alteration zone affecting the volcanics above Valdecañas vein were step

heated with a defocused CO_2 laser. The age spectrum for sample VV-IC-01 shows

initially old apparent ages for steps A-D followed by a well defined plateau for steps E-

G, whereas VR-07-05 shows a well defined plateau for almost 100 percent of the total

[39]Ar released (Figs. 8A, 8B; appendix). Plateau ages of 30.56 ± 0.04 and 31.03 ± 0.05 Ma

are given by these alunites and they are analytically distinct. Isochron ages are

statistically identical to the plateau ages (Figs. 8C, 8D; appendix). Tables 2A and 2B

summarize the [40]Ar/[39]Ar results and figure 9 is a regional geologic map of Fresnillo

showing the location of the dated samples.

Table 2a. [40]Ar/[39]Ar ages of sanidines from volcanic units.

Sample ID	Mineral	Description	Irradiation batch	No. of steps	%[39]Ar	Plateau age (Ma)	1σ	Inverse isochron age (Ma)	1σ	[40]Ar/[36]Ar
MP-08-01	Orthoclase	Fortuna quartz-monzonite	NM-220B	9	21.9	32.65	0.05	no isochron age		
JV-G5-9	Adularia	Hole G5 Jarillas vein	NM-213H	10	86.7	29.89	0.13	29.75	0.12	304
JV-K9-17	Adularia	Hole K9 Jarillas vein	NM-213H	3	44.7	30.71	0.07	29.68	0.10	322
VV-GD-13	Adularia	Hole GD Valdecañas vein	NM-220B	1	36.8	29.74	0.07	no isochron age		
VV-IC-01	Alunite	Hole IC, altered Valdecañas unit	NM-213H	3	82.5	30.56	0.04	30.73	0.11	240
VR-07-05	Alunite	vein in altered Valdecañas unit	NM-213H	7	98.6	31.03	0.05	31.05	0.07	294

Table 2b. [40]Ar/[39]Ar ages of adularias, alunites and orthoclase.

Sample ID	Mineral	Description	Irradiation batch	No. of analyses	Age (Ma)	1σ
VR-07-12	Sanidine	Valdecañas unit	NM-213G	14	44.73	0.04
LL-07-01	Sanidine	Cierpe unit (Lomas largas)	NM-213G	13	40.92	0.04
VR-07-17	Sanidine	Cierpe unit (Valdecañas range)	NM-213G	15	40.83	0.04
VR-07-38	Sanidine	Rhyolitic dome	NM-213G	14	31.55	0.03
VR-08-02	Sanidine	Altamira unit	NM-220B	13	31.04	0.05
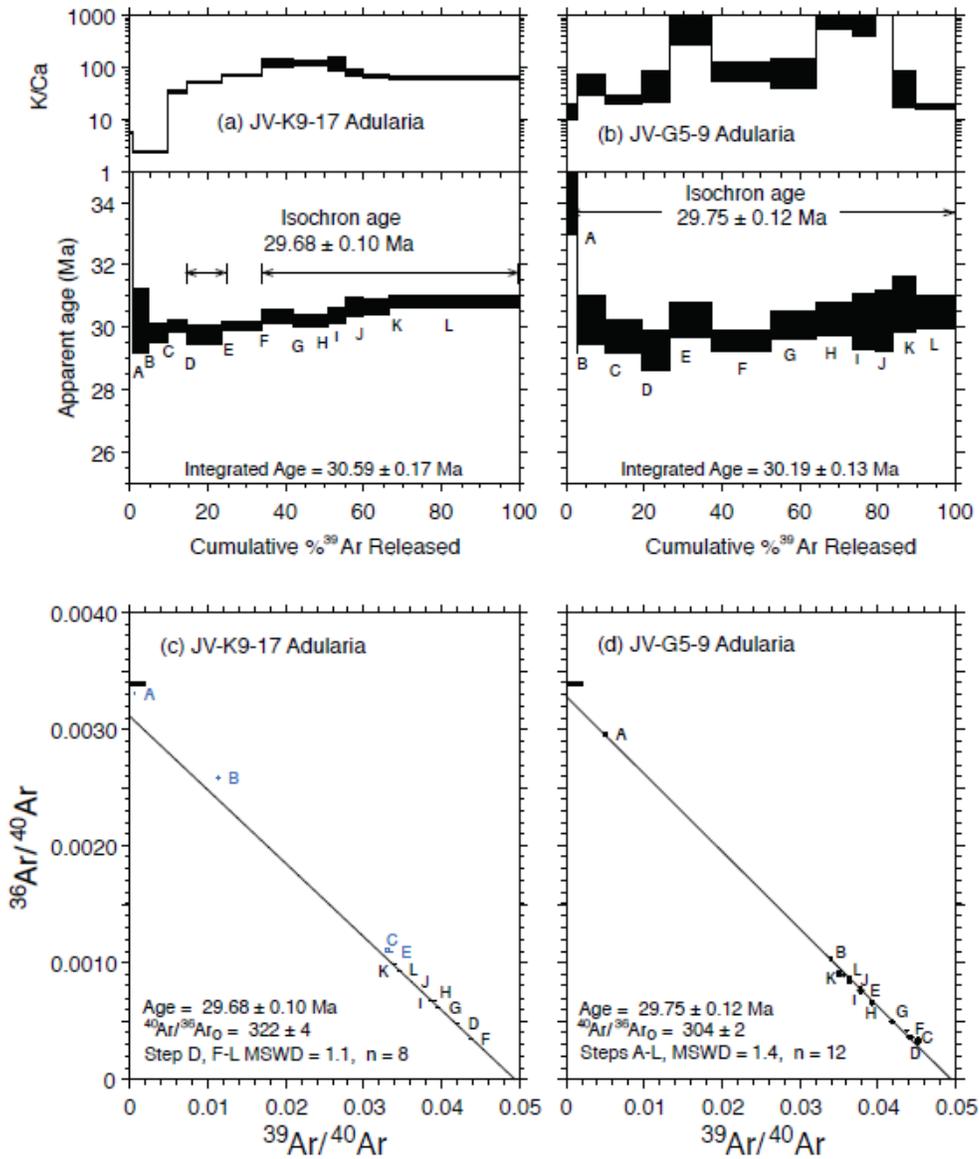
Fig. 6. Jarillas vein adularia age spectra and isochron diagrams. Both samples yield somewhat disturbed age spectra that are apparently explained by minor excess ^{40}Ar contamination revealed by isochron analysis. Isochron ages are concordant at ~29.7 Ma and yield the preferred age of the Jarillas vein.
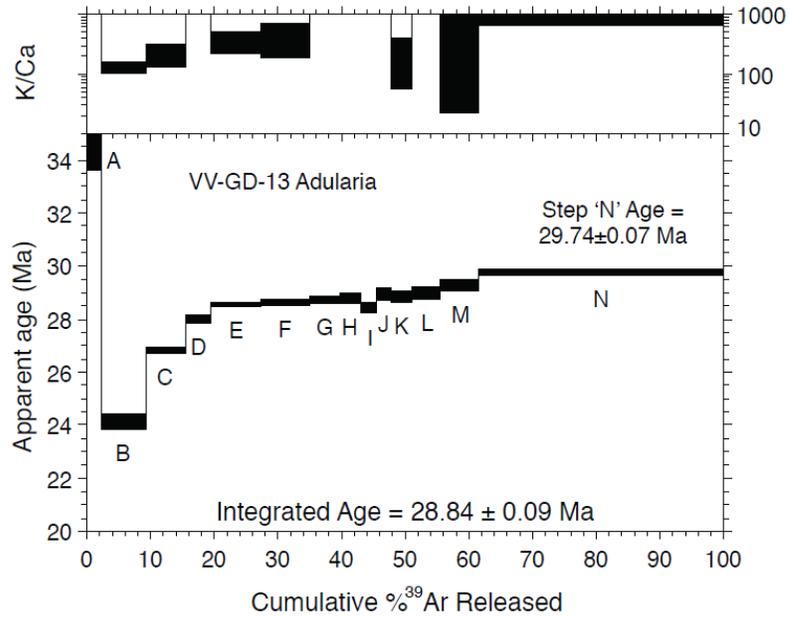
Fig. 7. Valdecanas vein adularia age spectrum. Climbing ages likely reflect alteration of the sample that is documented by petrography showing sericitization. The 29.74 Ma date recorded by step 'N' is suggested as an accurate date for the Valdecanas vein due in part to its (none coincidental?) agreement with the Jarillas vein adularia ages.
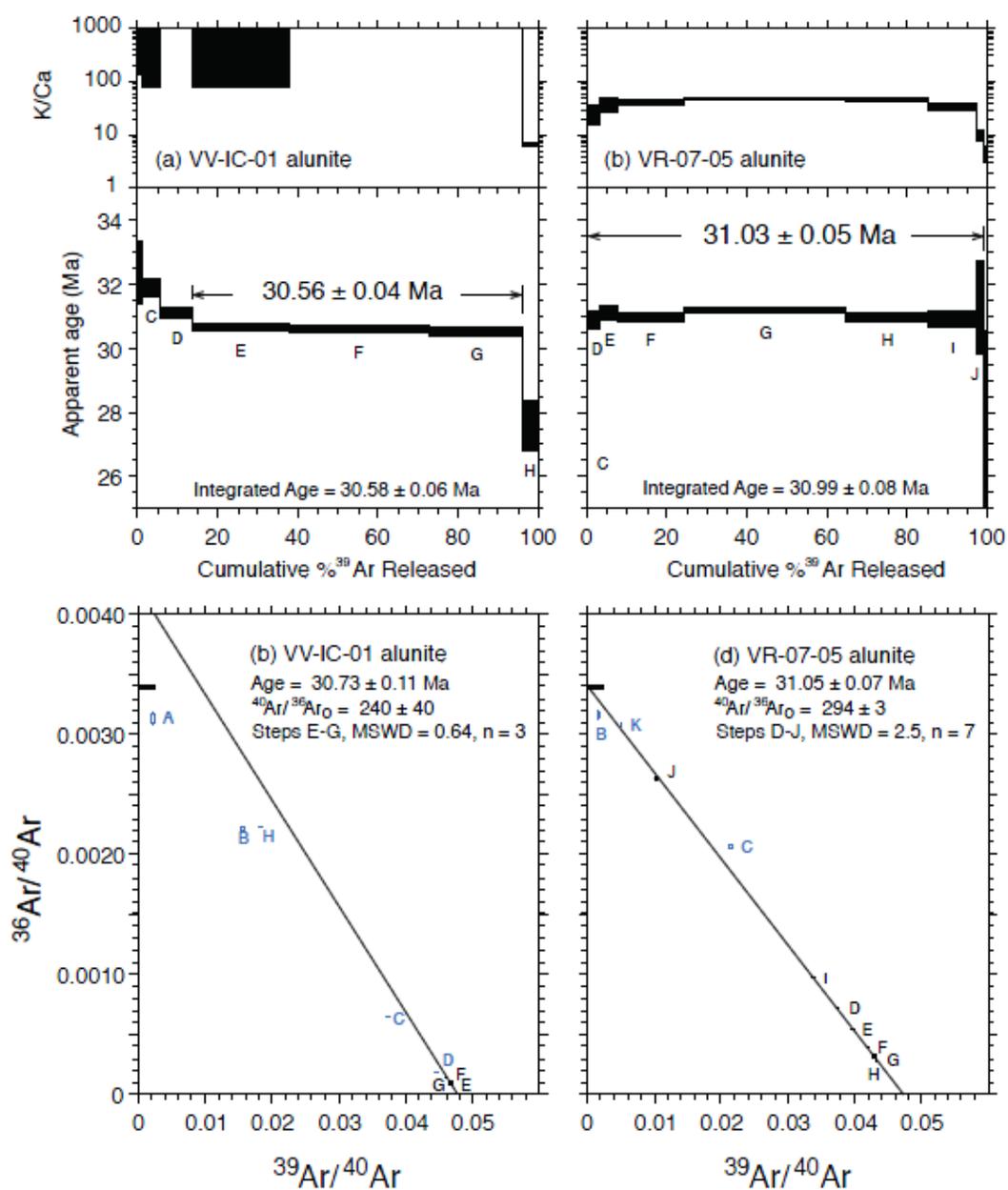
Fig. 8. Alunite age and K/Ca spectra and isochron diagrams. Flat segments of the age spectra with preferred dates of 30.56 and 31.03 Ma indicate two distinct acid sulfate alteration events.
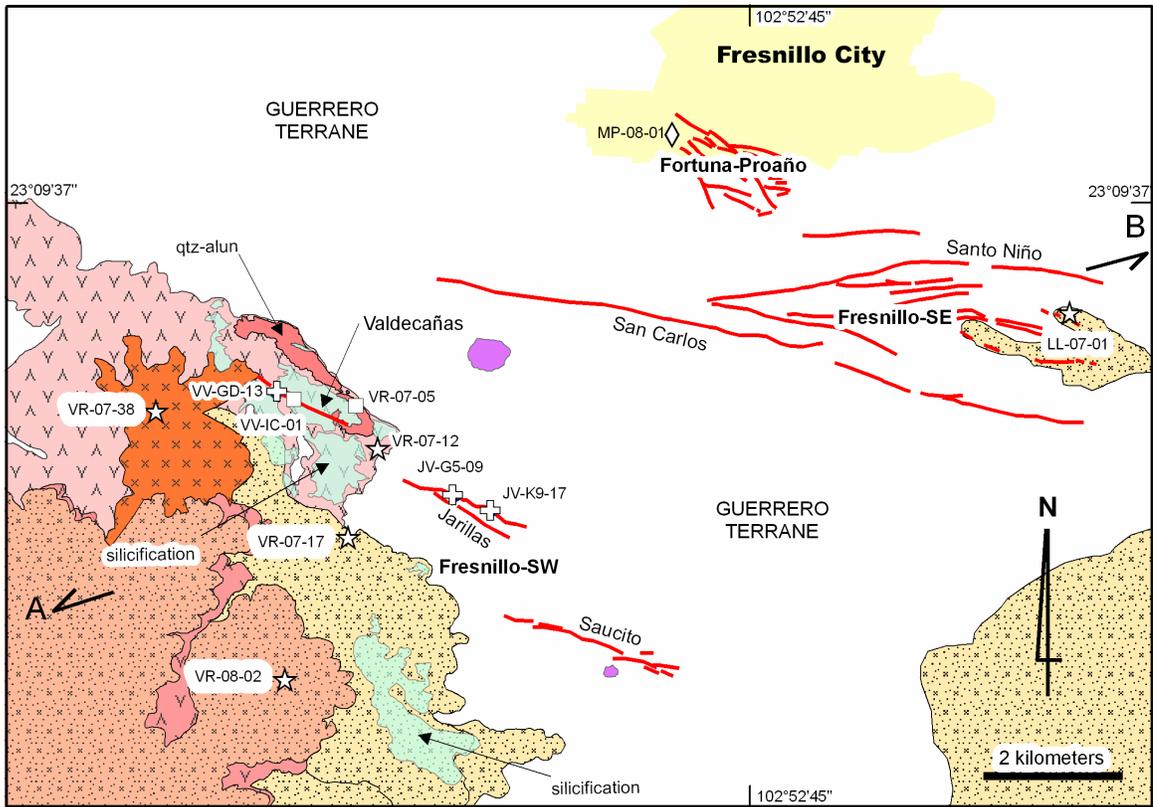
Fig. 9. Geologic map of Fresnillo showing sample locations and approximate location of the schematic section (A-B) in figure 10, see figure 1 for explanation of lithologic units. Crosses represent adularia samples, squares alunite, diamond orthoclase and stars sanidine. Surface elevation varies from 2000 to 2850 meters above sea level (m.a.s.l) and the veins are projected from approximately 1800 m.a.s.l.

Discussion and Conclusions

Compared to existing K/Ar geochronology, the new ^{40}Ar/^{39}Ar geochronology provides a much more precise and accurate definition of timing of volcanism and hydrothermal activity. The volcanic record is constrained by sanidine dating and reveals distinct volcanic eruptions between 44.73 ± 0.04 and 31.04 ± 0.05 Ma with a hiatus that is coincident with the unconformity of the Upper Eocene described by Albinson (1988), and with a change in chemical composition of the magmatism in response to uplift and crustal thinning in the MC (Nieto-Samaniego et. al., 2007).

The geochronology of the Fortuna quartz-monzonite is somewhat ambiguous; however we tentatively suggest an intrusion age of 32.65 ± 0.05 Ma (Fig. 5). We propose that this age provides a maximum age of the Fortuna stock and that the initial steps of the spectrum at ~30 Ma could record argon loss related to the hydrothermal event responsible for the adularia formation.

For the Jarillas vein adularias, two statistically identical inverse-isochron ages of 29.75 ± 0.12 and 29.68 ± 0.10 Ma provide the timing of epithermal mineralization at Fresnillo. Complications in the Valdecañas age spectrum are probably due to sericitization of the adularia and do not allow unambiguous age calculation, however adularias from both veins are apparently coeval at ~29.7 Ma. Preliminary fluid inclusion data (Velador et al., 2009) suggests that the Jarillas and Valdecañas veins in Fresnillo-SW and other veins in Fresnillo-SE could be cogenetic which will be evaluated further in more detail with stable isotope and gas analysis studies.

Dating of two alunites from the hydrothermally altered Valdecañas unit resolved two pulses of acid sulfate alteration at 30.56 ± 0.04 and 31.03 ± 0.05 Ma. These ages

suggest that acid sulfate alteration occurred before mineralization, and define a

hydrothermal activity duration related to alunite deposition of at least 0.47 Ma. A

difference in age of ~1 Ma between the adularias and the alunites could indicate that they

are not related to the same hydrothermal pulse and/or that a long-lived but episodic,

hydrothermal system prevailed.

Duration of Hydrothermal Activity

Long-lived hydrothermal systems of ~0.8 Ma have been modelled by Cathless et

al. (1997), for a single episode of intrusion of mafic composition (high temperature)

undergoing conductive (i.e., slow) cooling. They also suggest that near-surface

hydrothermal systems lasting ~1 Ma can result from multiple pulses of intrusion with

associated hydrothermal circulation. Marsh et al. (1997) modelled a shallowly emplaced

500 m wide porphyry undergoing conductive cooling and showed that it would cool

below the closure temperature of minerals dated by $^{40}Ar/^{39}Ar$ methods in less than 40,000

years. Therefore they proposed that the duration of many ore forming, porphyry-related

hydrothermal systems with resolvable ages form by prolonged, multiple and spatially

coincident intrusive events.

$^{40}Ar/^{39}Ar$ dating at Cerro de Pasco, Peru (Baumgartner et al., 2009) and El Peñon,

Northern Chile (Warren et al., 2008) define long-lived (~1 Ma) hydrothermal activity. At

the Sleeper deposit in Nevada, an age difference of ~2 Ma, determined with $^{40}Ar/^{39}Ar$

geochronology, between alteration and mineralization has been interpreted to reflect

multiple pulses of alteration and mineralization (Conrad et al., 1993). Differences of up

to 2 Ma between mineralization and the youngest volcanic event have been observed in

Mexican epithermal deposits of the MC and it has been hypothesized that mineralization

there occurred during the late stages of crystallization of the intrusive rocks (Camprubí et al., 2003). Based mostly on K/Ar data from various volcanic-hosted epithermal deposits in the Great Basin, Silberman (1985), proposed that hydrothermal activity typically persists for 0.5 to 1.5 Ma and that it comprises multiple pulses of alteration and mineralization with lifetimes of 0.1 to 0.2 Ma. In Fresnillo, mineralization occurred ~1.3 Ma after the youngest dated volcanic event and thus it appears that mineralization is not temporally associated with local volcanism. On the other hand, alunite VR-07-05 (31.03 ± 0.05 Ma) coincides within the age of the Altamira rhyodacite (VR-08-02; 31.04 ± 0.05) and thus they could be genetically related.

Short-lived hydrothermal systems have been interpreted based on high resolution $^{40}Ar/^{39}Ar$ studies for the epithermal Au-veins in Borovitsa Caldera, Southern Bulgaria (~100 to ~500 ka; Singer and Marchev, 2000), Round Mountain Nevada (<50 ka; Henry et al., 1997), Cerro Rico de Potosi in Bolivia (~200 ka Rice et al., 2005) and Midas in Northern Nevada (<600 ka; Leavitt et al., 2004). Duration of mineralization processes have been determined in the Hosen-1 vein, Hishikari in Japan (~260 ka; Sanematsu et al., 2006) and the La Guitarra vein, Temascaltepec in Mexico (~400 ka; Camprubí et al., 2003).

We believe that the significant difference in age between mineralization and the Fortuna stock (~3 Ma) reflects undiscovered multiple pulses of intrusions with associated hydrothermal activity, which is supported by the occurrence of the Plateros intrusion north of Fresnillo, rather than mineralization occurring during the very late stages of crystallization of the intrusion. The dated phase of the Fortuna stock appears to be too old to be genetically related to the dated epithermal mineralization. However, because of its

close spatial association with the mineral deposits of the Fortuna and Cerro Proaño areas, we agree with De Cserna (1977), that the Fortuna stock may be genetically related to at least some of the mineralization in those areas. Figure 10 is a SW - NE schematic representation of the Fresnillo district showing two pulses of intrusions; the Fortuna stock and an unidentified later intrusion responsible for mineralization at Fresnillo-SE and Fresnillo-SW. It is likely that multiple pulses of small, shallow intrusions drove hydrothermal systems at Fresnillo and were responsible for Fresnillo's large size and richness.
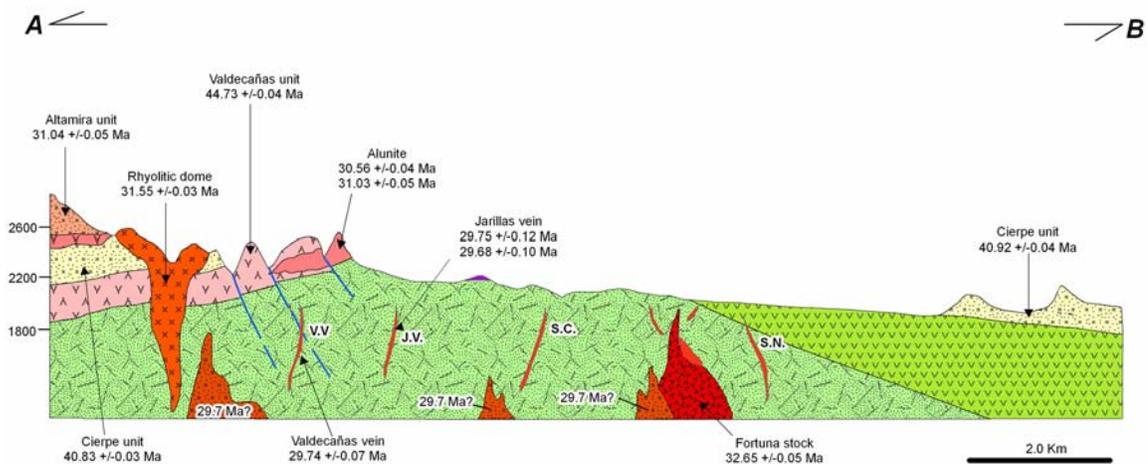
Fig. 10. Schematic cross section (A – B) looking north showing the approximate positions of epithermal veins and two pulses of intrusions. Notice that the Fortuna stock and the mineral deposits associated with it are projected from approximately 2.5 km north from the location of the cross section. The intrusions with ages with question mark (~29.70 Ma?) represent the hypothesized intrusions that could be genetically related to epithermal mineralization. Elevations in the vertical scale are approximate and in meters above sea level.

CHAPTER II

PHYSIO-CHEMICAL CHARACTERISTICS AND EVOLUTION OF THE HYDROTHERMAL FLUIDS THAT FORMED INTERMEDIATE SULFIDATION VEINS IN FRESNILLO

Abstract

Fresnillo is a world class silver district with intermediate sulfidation epithermal veins that has produced silver almost continuously since the 1550's. Annual silver production in the last five years has increased progressively from 33 to over 35 Moz and the total resources of the district approximate 1BOz. Epithermal mineralization is hosted by the Middle Jurassic to Lower Cretaceous Guerrero Terrane, which is locally covered by Paleocene-Eocene conglomerate, Eocene and Oligocene volcanic rocks, and Quaternary alluvium.

Core logging and petrography reveals that the mineralogy and paragenesis of the Jarillas and Valdecañas veins in Fresnillo-SW is very similar to that of the Santo Niño vein in Fresnillo-SE. The main ore minerals occurring in these veins are sphalerite, galena, pyrargyrite, polybasite and acanthite; the main gangue sulfide and non-sulfide minerals are pyrite, arsenopyrite, and quartz and calcite. In Jarillas and Valdecañas mineral deposition occurred in five stages: 1) deposition of mostly base metal sulfides; 2) quartz and calcite with fewer sulfides; 3) alternating bands of chalcedonic quartz, calcite,

adularia, epidote, base metals and silver minerals; 4) quartz, calcite and dolomite-ankerite with coarse grained pyrargyrite; and 5) barren quartz, calcite and fluorite.

Determination of homogenization and ice-melting temperatures in over 900 fluid inclusions hosted by quartz and calcite in Jarillas and Valdecañas resolved homogenization temperature and salinity ranges typical of intermediate sulfidation epithermal deposits; 160°C to 320°C and 0 to 11 wt% NaCl eq. respectively. Fluid inclusion gas analysis indicates that H_2O accounts for 99.17 to 99.86 % of the volatiles extracted, whereas the second and third most abundant volatiles are CO_2 (<0.5 mol %) and N_2 (<0.4 mol %). Calculated log$f$O$_2$ (-42.5 to -34.2) and log$f$S$_2$ (-11.9 to -3.6) indicate that the hydrothermal fluids were reducing which is typical of low to intermediate sulfidation systems. $\delta^{18}O$ mineral values determined in quartz (n=44) and calcite (n=25) associated with ore stages range from 12.4 to 18.6 per mil and 7.4 to 15.3 per mil, respectively. The oxygen fluid values calculated for the homogenization temperatures determined by fluid inclusions range from 3.9 to 9.6 per mil (quartz) and 5.9 to 10.9 per mil (calcite). δD values (n=14) measured from fluid inclusions in quartz associated with ore in the two veins range from -79.3 to – 50.5 per mil. $\delta^{13}C$ values determined for calcite associated with ore in Jarillas range from -8.2 to -6.1 per mil, and for Valdecañas from -9.1 to -4.0 per mil.

Salinities up to 11 wt % NaCl, heavy oxygen and hydrogen isotope compositions of the fluids, and gas analysis indicate that the veins were formed by magmatic water mixing with deeply circulated meteoric water. The consistently light sulfur and carbon values of the veins throughout the district indicate that sulfur and carbon were partially derived from the Guerrero Terrane either by leaching of those elements at the time of

hydrothermal fluid circulation or due to assimilation and melting of Guerrero Terrane xenoliths in a deep-seated magma chamber.

Textures, mineralogy, and stable isotope data suggests that the veins from Fresnillo-SE and Fresnillo-SW are cogenetic. Conversely, variations in average homogenization temperatures and salinities, sulfur fugacities, and Au/Ag ratios between the veins indicate a district-wide zoning pattern from east to west. It is determined that temperature, salinity, sulfur fugacity and Au/Ag ratios increase from east to west, which could indicate that the source of heat and fluids lies to the west. At the vein scale, it is noted in Jarillas and Valdecañas that the concentration of base metals increases at depth and that the fluids evolved from reduced low sulfidation to more oxidized and intermediate sulfidation through paragenesis. We propose that the veins in both areas are genetically related and that the geochemical variations observed could have been the result of complex fluid evolution.

Introduction

Fresnillo is a district with silver resources of approximately 1 BOz hosted in intermediate sulfidation (IS) epithermal veins. Camprubí and Albinson (2007), proposed an empirical classification for the IS and low sulfidation (LS) deposits in Mexico. In that classification, they include Fresnillo, based on data from Santo Niño vein, in a type exhibiting dominantly LS characteristics with polymetallic IS roots. For ease of description in this paper, we separate the Fresnillo district into three areas: 1) the Fortuna-Proaño area, which hosted mostly northwest trending veins with abundant base metals, spatially associated with the Fortuna stock and manto, chimney and stockwork mineralization; 2) the Fresnillo-SE area (site of the currently producing veins; Santo Niño

31

and San Carlos), which hosts northwest to east-west trending banded IS epithermal veins rich in silver with lengths of 1.3 km or more; and 3) the Fresnillo-SW area with northwest trending IS veins very similar to those of Fresnillo-SE, that were discovered in the last 7 years (Saucito, Jarillas, and Valdecañas).

In 2003, drilling led to the discovery of the Saucito vein in Fresnillo-SW (Fig. 11); this discovery motivated extensive exploration in the area that later resulted in the discovery of Valdecañas and Jarillas. Those discoveries extended the boundaries of the known mineralization in the district to the southwest, and raised questions about the actual size of the district and the genetic relation between the veins. In this study, we focus on determining the source or sources of the hydrothermal fluids that formed the Jarillas and Valdecañas veins, as well as on the potential for a genetic link between the veins in Fresnillo-SE and Fresnillo-SW. We evaluate the possible sources of the hydrothermal fluids by analyzing fluid inclusions, fluid inclusion gases and stable isotopes from Jarillas and Valdecañas; we also analyze the possible genetic relations between the veins by comparing the mineralogy and geochemical characteristics of the Jarillas and Valdecañas veins in Fresnillo-SW with those of the well studied Santo Niño vein in Fresnillo-SE. This study provides new geochemical data that is very important to the understanding of the famous and complex Mexican intermediate sulfidation deposits.

Large and rich, low and intermediate sulfidation epithermal deposits like Fresnillo can result from multiple small short-lived hydrothermal systems or from one big long-lived hydrothermal system. New $^{40}Ar/^{39}Ar$ results (Velador et al., 2010a; submitted) indicate that hydrothermal activity in Fresnillo was episodic and could have lasted for ~3 Ma. This study will also help us determine whether deposition of IS veins in

32

Fresnillo-SE and Fresnillo-SW occurred in response to one large hydrothermal system, or

from separate and distinct hydrothermal systems.
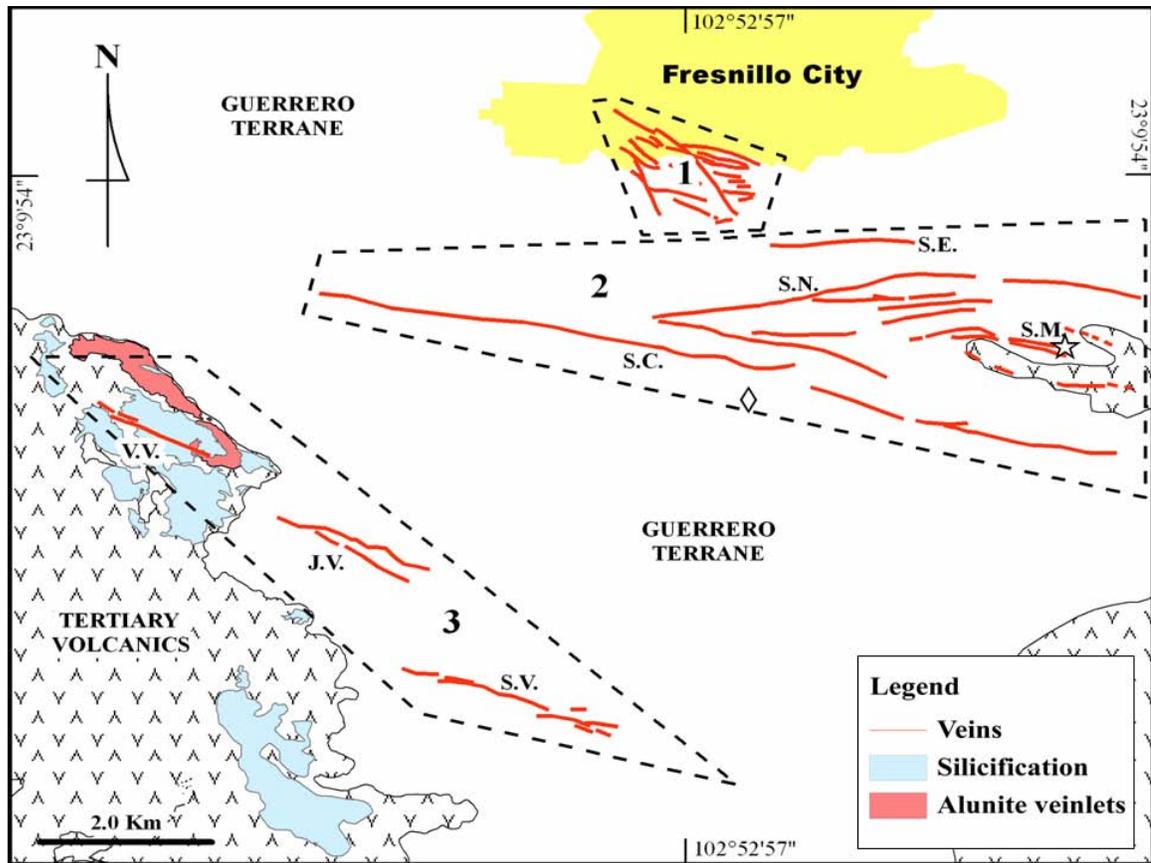
Fig. 11. Map of the Fresnillo district showing Fortuna-Proaño (1), Fresnillo-SE (2) and
Fresnillo-SW (3) areas and veins projected from approximately 200 meters below
surface. Abbreviations: S.E. (Santa Elena), S.M. (San Mateo), S.N.V. (Santo Niño Vein),
S.C.V. (San Carlos Vein), S.V. (Saucito Vein), J.V. (Jarillas Vein), V.V.
(ValdecañasVein). Surface elevation varies from 2100 to 2850 meters above sea level
(m.a.s.l) and the veins are projected from approximately 1800 m.a.s.l. Sample locations:
star (CC-07-01); rhomb (CH-09-01).

Geology

The IS epithermal veins of Fresnillo are hosted by the volcanosedimentary

sequence of the Guerrero Terrane (GT). The GT is subdivided in a lower sedimentary

domain consisting mainly of graywackes and black shales and an upper volcanic domain

on top consisting mainly of submarine andesitic to basaltic lavas. The age of the GT has

33

been constrained in different locations in Zacatecas between ~132 Ma and ~160 Ma (Mortensen et al., 2008; Escalona-Alcázar et al., 2009). The local geology and stratigraphy of Fresnillo have been described in detail by De Cserna, (1976) and summarized by Ruvalcaba-Ruíz and Thompson, (1988), and Gemmell et al., (1988). In Fresnillo, the GT is covered unconformably by a Late Paleocene to Early Eocene conglomerate (De Cserna, 1976; Ruvalcaba-Ruíz and Thompson, 1988) and by Eocene to Early Oligocene (44.73 +/- 0.06 Ma to 31.07 +/- 0.04 Ma) trachytic to dacitic tuffs and rhyolitic to rhyodacitic flows and domes (Velador et al., 2010a; submitted). Basalts of possible Miocene age form small and disperse outcrops around the area. There are three types of intrusive rocks identified in Fresnillo; Middle Jurassic to Early Cretaceous mafic sills and dikes that form part of the GT; Oligocene quartz-monzonite and granodiorites in Fresnillo and Plateros, respectively; and Miocene basalt dikes.

Ore deposits

Mineralization in the Fortuna-Proaño area in the north part of the district contained silver mineralization in an oxidized stockwork and silver, lead-zinc mineralization in vein, manto, chimney, and skarn deposits. Those deposits are spatially associated with the 32.65 +/- 0.05 Ma (Velador et al., 2010a; submitted) Fortuna quartz-monzonite. The Fresnillo-SE area consists of a system of high grade silver, lead and zinc with minor gold, epithermal veins e.g. Santo Niño, San Carlos, San Mateo, Santa Cruz and Santa Elena. The Fresnillo-SW is a recently discovered area with high-grade silver-gold, lead and zinc veins with mineralogic and textural characteristics that suggest a genetic relation with the veins in Fresnillo-SE. The most important veins in Fresnillo-SW are: Saucito, Jarillas and Valdecañas; however other prospects are being explored in the

area. Based on their physical characteristics, e.g. high Ag/Au ratio and high base metal contents, the veins in both areas fit with the IS type proposed by Hedenquist et al., (2000) and Sillitoe and Hedenquist, (2003).

Mineralization in the Fresnillo-SE and Fresnillo-SW areas occurs in blind to surface, northwest-southeast to west-east trending IS veins. The veins dip steeply north or south and range in length from ~1.3 to ~8 km and in thickness from a few 10's of centimetres to 10's of meters. Vein width typically pinches and swells along strike and cymoid-loop structures are also common. In some portions they show banding, indicative of deposition in open spaces, whereas in other areas they show brecciation or narrow veins in stock-work fashion that indicate that the structure was closed or partially closed to fluid passage. Typically the ore zones of the veins form undulatory bands with vertical extents of ~200 to 450 meters (Fig. 12). These ore bands are analogous to the "ribbons" described in the Topia veins in Durango, Mexico by Loucks and Petersen (1988). At depth the veins commonly contain coarse massive veins of sulfides, sphalerite and galena, whereas the upper portions generally show barren or low grade coarsely banded veins of quartz and calcite.

Hydrothermal alteration

At ore-shoot elevations, illite and interlayered illite-smectite (sometimes associated with calcite), are the main clays filling fractures in the host rock. At higher elevations the alteration envelope broadens and the assemblage changes to advanced argillic bearing kaolinite and interlayered illite-smectite in a denser network of fractures (J. M. Velador, unpublished data, 2005) (Fig. 13). A similar mineral assemblage and zoning is observed in the Santo Niño, San Carlos, Jarillas and Valdecañas veins. The only

35
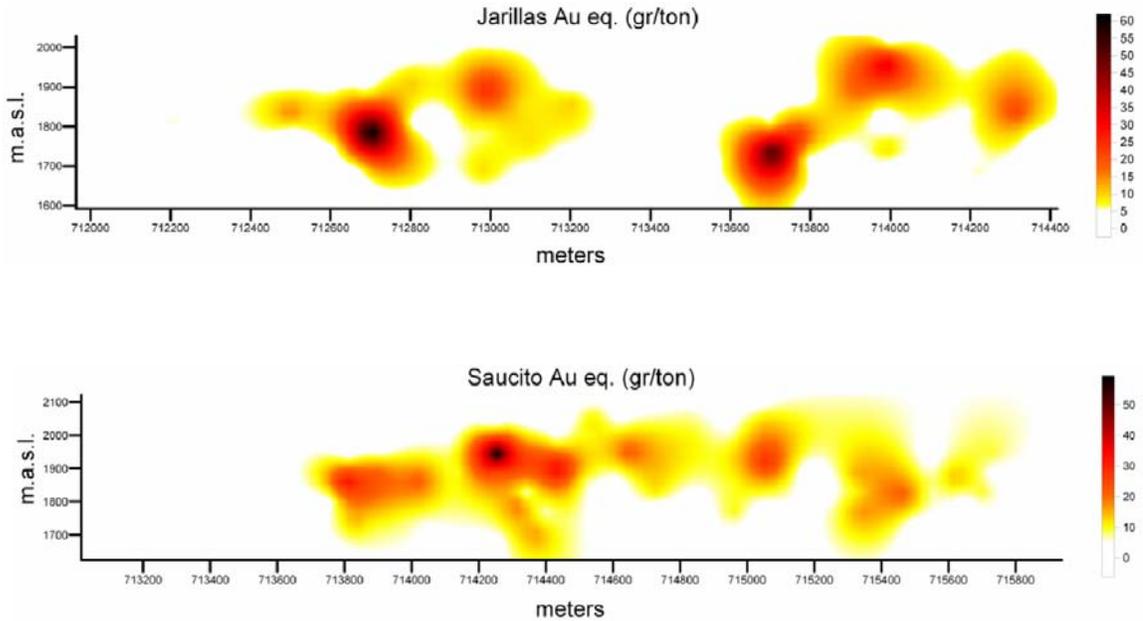
Fig. 12. Undulatory ore bands for the Jarillas and Saucito veins defined by Au equivalent >5 gr/ton. Abbreviations; m.a.s.l. (meters above sea level), horizontal axis shows the UTM easting coordinate in meters.

surface expressions of the epithermal veins at depth are calcite, barite and quartz veinlets, which occur in some of the scant outcrops of the GT in Fresnillo-SE. Outside the influence of the argillic and advanced argillic alteration envelopes the rocks of the GT are chloritized, but because of the regional character of this alteration, it is possible that it is related to green-schist facies metamorphism produced during accretion. To the west, above the Valdecañas vein, the Eocene tuffs are strongly silicified and contain zones with abundant alunite veinlets or stockworks (Fig. 14). Sporadically, at elevations varying around 2450 meters above sea level (m.a.s.l.), there are zones within the tuffs replaced by crystobalite and containing opaline-chalcedony that could have been formed near the paleosurface. South of Saucito vein, in the Piedras area, the alunite veins contain cinnabar.

36
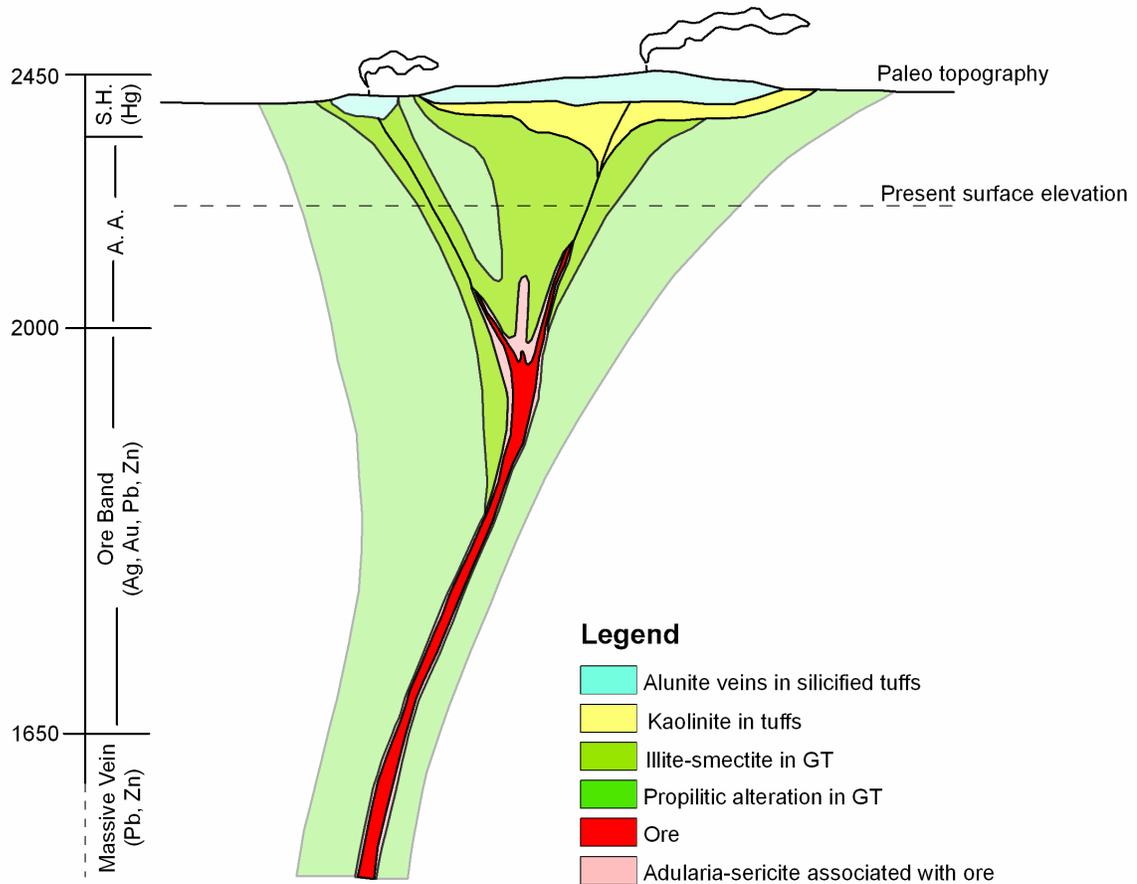
Fig. 13. Epithermal model for Valdecañas vein showing alteration envelopes and ore zone: adapted from Buchanan (1981). The elevations are approximate, in meters above sea level, and the horizontal scale is exaggerated to represent the vein. Abbreviations; A. A. (argillic alteration), S. H. (steam heated blanket).

Fig. 14. Alunite veinlets of the acid sulfate alteration blanket in Fresnillo-SW above Valdecañas vein.

Mineralogy

The mineralogy and paragenesis of the Fortuna and Proaño areas has been described previously by several authors (Stone and McArthy 1942; De Cserna et al., 1977; Kreczmer 1977; Ruvalcaba-Ruíz 1980; Chico 1986; and Ruvalcaba-Ruíz and Thompson 1988). Ruvalcaba-Ruíz and Thompson (1988) provide a detailed summary of the mineralogy of those areas. The mineralogy and paragenesis of the Santo Niño, San Mateo and San Carlos epithermal veins in the Fresnillo-SE area are described in Gemmell et al., (1988), Dilley, (1993) and Eckberg, (1999) respectively. Gemmell et al., (1988) provides a thorough description of the vein stratigraphy, paragenesis, mineralogy and mineral chemistry of Santo Niño vein.

Previous knowledge of the mineralogy of the Fresnillo-SW veins is restricted to a study of a few samples from the Saucito vein (Enriquez 2004; internal report) and to some XRD and XRF analyses, carried out at the "Centro de Investigación y Desarrollo Tecnológico" of Peñoles (CIDT), complementing metallurgical testing of the Saucito, Jarillas and Valdecañas veins. The minerals identified with these studies are: quartz, calcite, pyrite, sphalerite, galena, pyrargyrite, acanthite, polybasite, arsenopyrite, chalcopyrite, freibergite, aguilarite and electrum in order of abundance. Silver species occurring in minor concentrations in Jarillas and Valdecañas are argentotennantite, naumanite, proustite and native silver. Other minerals detected in either minor or trace amounts are adularia, chlorite, hematite, siderite, fluorite, ankerite, goethite and pyrrhotite.

Detailed core logging of vein intercepts from Jarillas and Valdecañas veins was carried out in order to define the mineralogy and paragenesis and to select the most

38

representative samples for mineralogy, petrography, fluid inclusion analysis and stable isotope geochemistry. Petrographic studies were carried out on 83 polished thin sections of the Jarillas vein and 20 polished thin sections of the Valdecañas vein.

Three different types of breccia are identified in the Jarillas and Valdecañas veins based on clast and cement composition: 1) breccia consisting of clasts of country rock (mainly greywacke and black shale) cemented by quartz and calcite; 2) breccia of clasts of country rock cemented by sulfides (predominantly sphalerite, galena and pyrite), chlorite, calcite and quartz; and 3) breccia consisting of coarse sulfide fragments (sphalerite and galena) cemented by calcite and microcrystalline quartz (Fig. 15). Occasionally the sulfides, chlorite, quartz and calcite form cockade bands surrounding sub-angular rock fragments. Multiple brecciation events in epithermal veins can be evidence of episodic self-sealing-rupture events (Sillitoe, 1985).

The two most abundant non-sulfide gangue minerals in the two veins are quartz and calcite. Quartz forms bands, cements breccias, and/or fills or grows in vugs. Description of quartz textures under the microscope was based on the terminology proposed by Dowling and Morrison (1989). Quartz grains in bands are euhedral to anhedral, vary in size from microcrystalline to coarse grained (<50-μ to >1000-μ) and are interlocked or form mosaic-like textures. Colloform and chalcedonic bands of quartz show interlocked grains of irregular shape or spherulites with radial extinction or the typical feathery textures of chalcedony. Calcite, as well as quartz, forms bands, fills interstices between coarse-grained quartz crystals and/or fills vugs. Calcite crystals vary in grain-size from fine to coarse and the bands commonly contain microcrystalline quartz in the interstices. Calcite commonly has a dirty appearance and has pits left behind by

destruction of large fluid inclusions at the time of polishing, sometimes shows good

cleavage, and less frequently is clean (transparent) with well defined polysynthetic

twinning under polarized light. The calcite bands are generally <2 cm thick and alternate

with bands of quartz and sulfides. Other common gangue minerals associated with quartz

and calcite that may form bands are chlorite, dolomite – ankerite, adularia, hematite and

undifferentiated phylosilicates (illite and/or interlayered illite/smectite). Bands of quartz-

hematite and epidote have been observed alternating with bands of black and white

chalcedony in Jarillas and Valdecañas (Fig. 16). According to Henley et al., (1986),

epidote deposits due to vigorous boiling at temperatures between 250°C to 300°C and

indicates mCO_2 ~0.01 or less, i.e. CO_2 is too low for calcite to be stabilized. Adularia is

also present as coarse euhedral grains embedded in quartz and calcite (Fig. 17)

The sulfides in these veins can be coarse-grained and massive (massive veins of

sulfides), can form bands alternating with quartz, chalcedony and calcite, or can occur as

fine disseminations in quartz and calcite. Sulfides are generally fine to medium grained

when they form bands. The sulfide minerals present in these veins include pyrite,

sphalerite, galena, arsenian-pyrite – arsenopyrite, marcasite chalcopyrite and pyrrhotite.
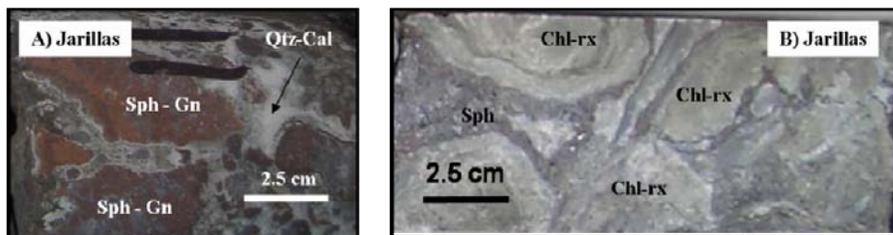
Fig. 15. Breccias. A) Sphalerite and galena fragments cemented by quartz and calcite. B) Chloritized rock fragments cemented by sphalerite and galena. Abbreviations: Qtz (quartz), Cal (calcite), Sph (sphalerite), Gn (galena), Chl-rx (chloritized rock).
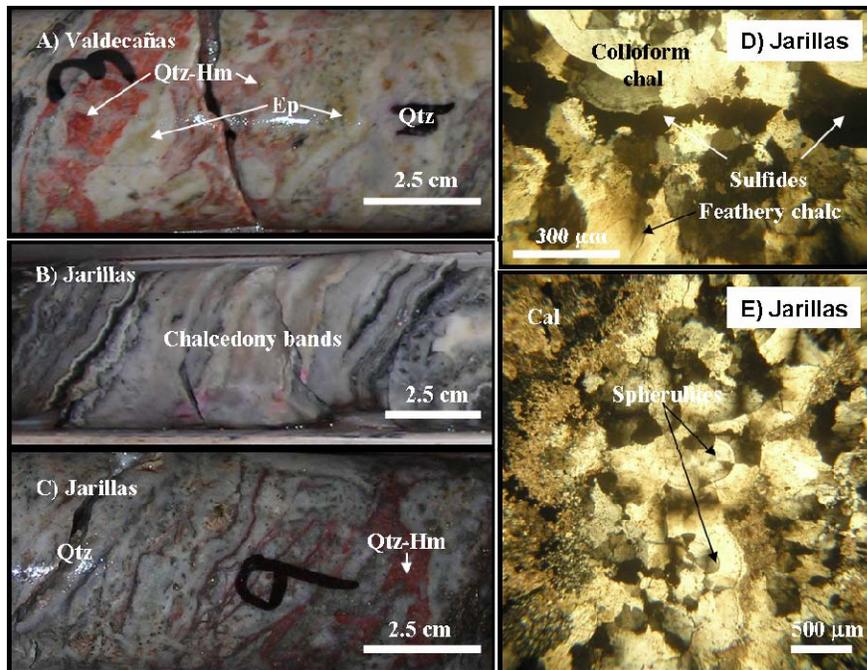
Fig. 16. Banded textures in Valdecañas and Jarillas veins. A) Valdecañas vein showing quartz-hematite and epidote associated with quartz and calcite. B) Jarillas vein showing black and white chalcedonic quartz. C) Jarillas vein showing quartz and chalcedonic-quartz bands associated with quartz-hematite bands. D) and E) photomicrographs of Jarillas showing colloform textures. Abbreviations: Qtz (quartz), Hm (hematite), Ep (epidote), Cal (calcite) Chal (chalcedony).
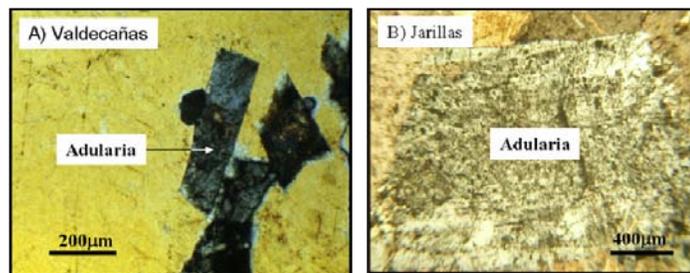
Fig. 17. Adularia crystals. A) embedded in quartz from Valdecañas vein and B) in calcite from Jarillas vein.

Chalcopyrite and pyrrhotite are generally fine-grained and occur more commonly as <10 μm inclusions in iron-rich cores of zoned sphalerite; other minerals observed as inclusions (<10 μm) in sphalerite are silver sulfosalts (pyrargyrite, tennantite-tetrahedrite) and acanthite (Fig. 18). Silver sulfosalts have also been observed included in galena. The most abundant silver sulfosalt is pyrargyrite, sometimes forming euhedral grains with

diameters of up to 1 cm when they occur in vugs. Euhedral grains of pyrargyrite that have

grown in cavities are associated with calcite, dolomite – ankerite and quartz (Fig. 19).
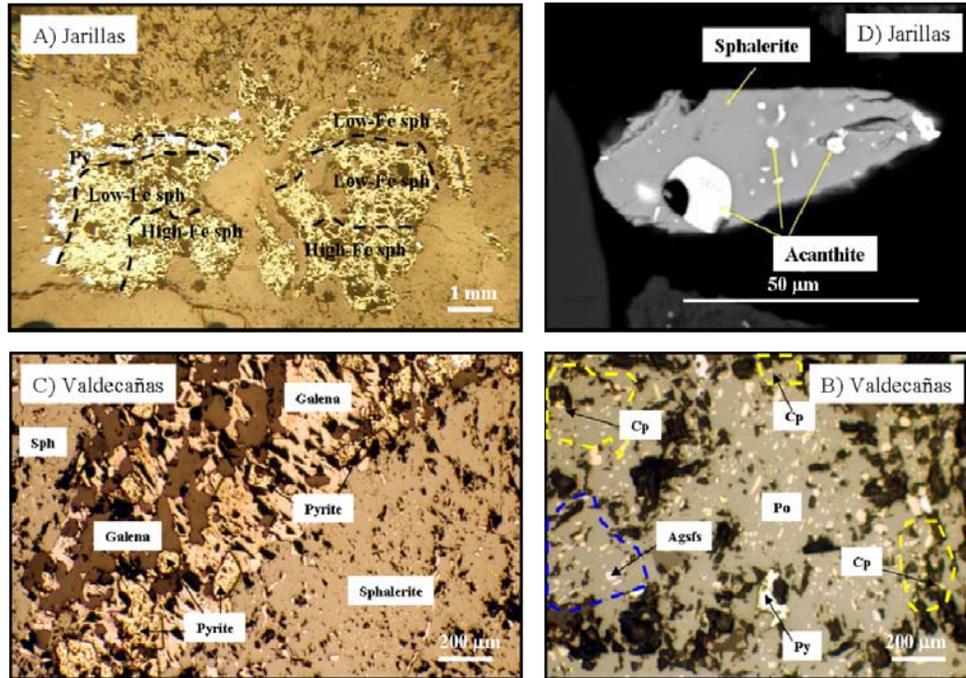
Fig. 18. Zoned sphalerites (Sph) with inclusions of pyrite (Py) and exsolution of chalcopyrite (Cp), silver sulfosalts (Agsfs), and pyrrhotite (Po). A) photomicrograph of zoned sphalerite with cores rich in iron (High-Fe) and rims poor iron (Low-Fe), notice that a band of pyrite was deposited between the two bands of low iron sphalerite. B) SEM image showing sphalerite with inclusions of acanthite. C) Microphotograph of sphalerite with chalcopyrite disease. D) Microphotograph of sphalerite rich in iron showing also pyrrhotite, chalcopyrite (within yellow polygons) and silver sulfosalts (within blue polygon) and inclusions of pyrite.

Other common silver species are acanthite and aguilarite which are generally fine

grained. Silver sulfosalts occurring in minor or trace amounts include polybasite,

stephanite and probably miargyrite. Sphalerite and galena occur in grain sizes up to a

couple of centimetres in massive veins or as small as 10 µm when they occur

disseminated in quartz and calcite or included in pyrite.

One conspicuous feature of these veins is the presence of coarsely banded or massive veins of coarse-grained sphalerite and galena at deeper levels. The sulfides deposited in this event occasionally cement breccias in the host rock. Commonly, the massive veins are cross-cut by the banded veins that extend to higher elevations, which suggest the multiple events of opening and mineralization occurred during vein formation. Banding in the banded veins can be either thinly-laminated, which is commonly associated with ore, or it can be coarse (thicker bands) which is generally low grade or barren (Fig. 20). Another important textural feature observed in 3 drill-hole intercepts in Jarillas, is the occurrence of bladed quartz after calcite. Etoh et al., (2002) proposed that bladed calcite in Hishikari formed due to a sudden loss of CO_2 caused by boiling. In Hishikari, the bladed calcite was coated by adularia and then dissolved, which created cavities that were subsequently filled by quartz (Etoh et al., 2002).

The bladed calcite in Jarillas is of the lattice type, according to the criteria proposed by Dong et al., (1995). It is possible that bladed calcite in Jarillas was deposited also due to boiling and concomitant loss of CO_2, then coated by quartz (instead of adularia), dissolved probably due to the passage of latter acidic fluids or decrease in temperature upon boiling (Corbett and Leach, 1988), which created cavities that were subsequently filled by quartz.
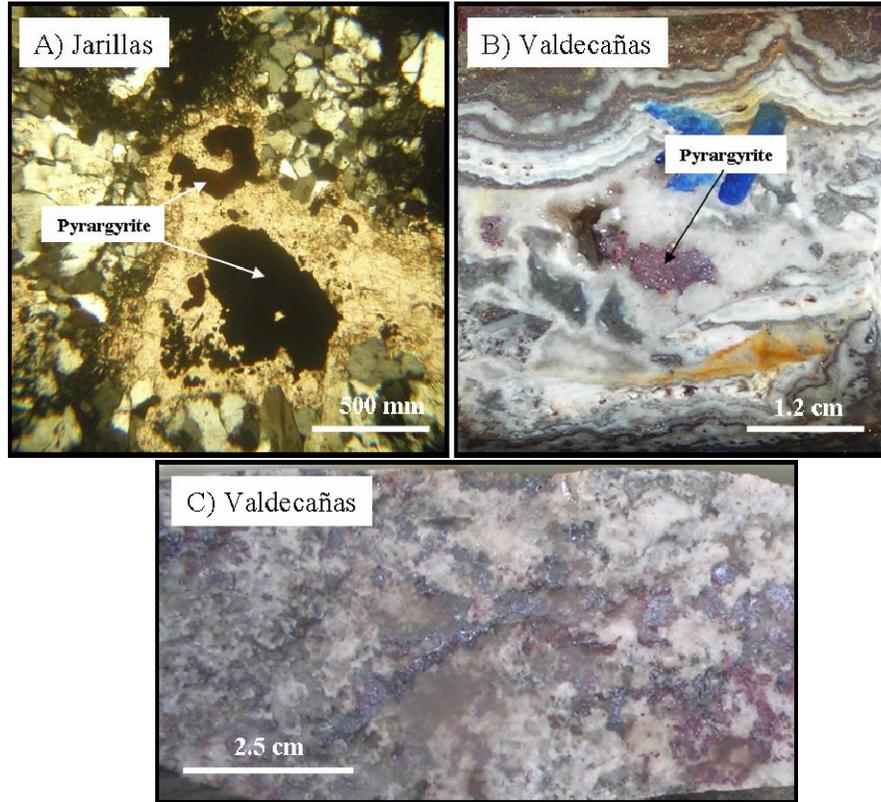
Fig. 19. Stage 4 mineralizing event showing coarse grained pyrargyrite associated with calcite and dolomite-ankerite. A) Pyrargyrite associated with calcite filling a cavity in quartz band; B) Pyrargyrite filling vug in a banded vein; C) Pyrargyrite associated with dolomite-ankerite.
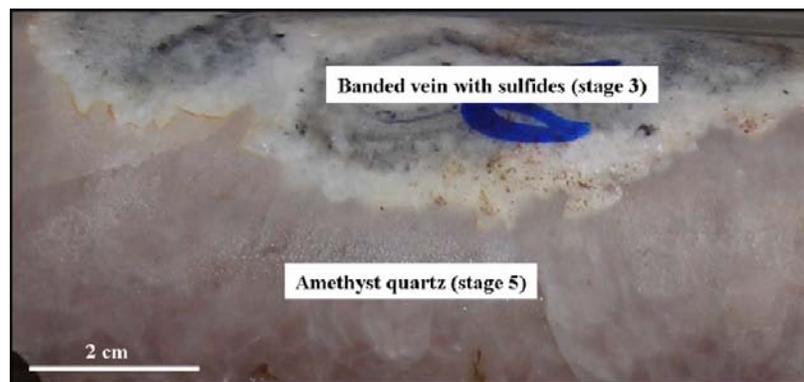
Fig. 20. Late amethyst quartz cross cutting mineralized banded vein in Jarillas.

Vein stratigraphy and paragenesis

Description and interpretation of cross-cutting relations between breccias, massive veins, banded veins and late-barren veins were used to describe the vein stratigraphy. This approach was used in the Santo Niño vein by Gemmell (1986) and in San Mateo vein by Dilley (1993). Mineral deposition is observed to occur in five stages in Jarillas and Valdecañas (Fig. 21).

Stage 1: This stage is characterized by deposition of coarse-grained galena and sphalerite with fine grained silver sulfosalts and minor chalcopyrite and pyrrhotite. Sphalerite in this stage is commonly zoned showing iron-rich cores, as indicated by the dark brown to black color, with yellow-orange rims low in iron. Inclusions of chalcopyrite and pyrrhotite are common in the high-Fe cores of sphalerite. Chlorite also occurs associated with this massive vein but it seems to be late with respect to sulfides. Stage 1 cements brecciated sedimentary rocks of the Guerrero Terrane and forms cockade bands of galena, sphalerite and chlorite around the rock fragments.

Stage 2: This stage is characterized by deposition of medium- to fine-grained quartz and calcite cross cutting the coarse-grained sulfides in Stage 1 and the host rock. This quartz and calcite typically show abundant disseminated sulfides and it is possible that at least some of them are reworked grains formed during Stage 1.
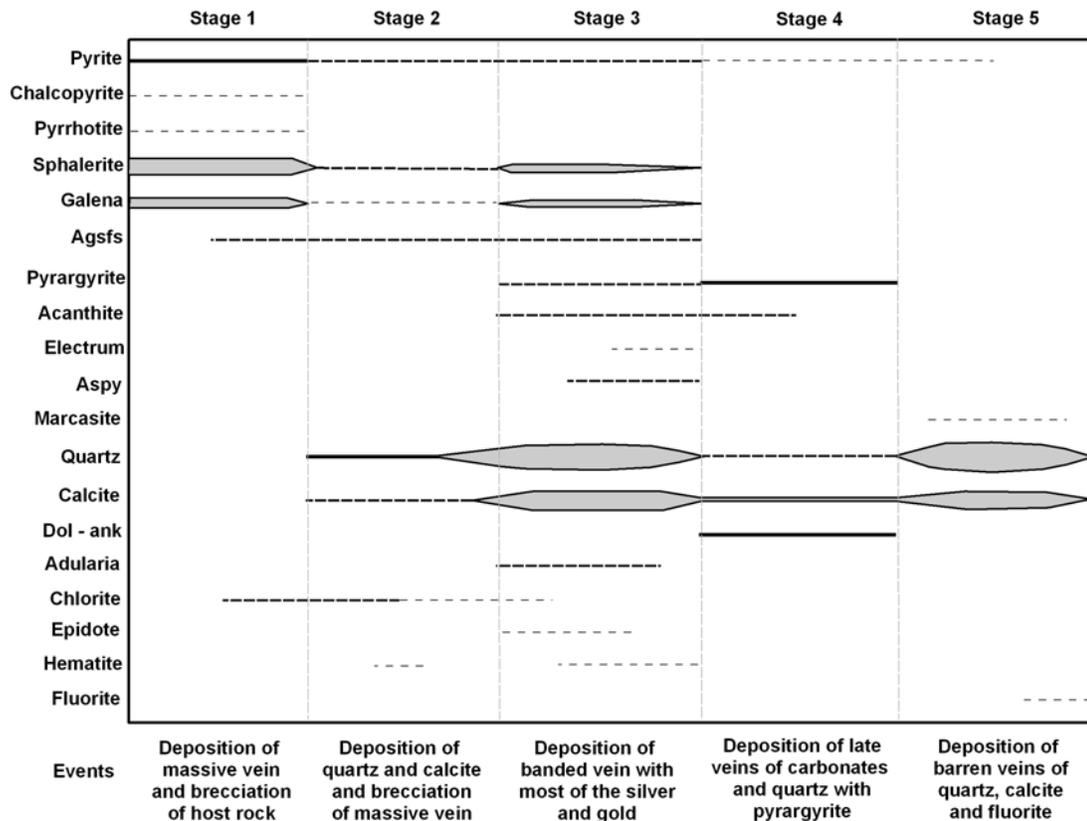
Fig. 21. Paragenesis of Jarillas vein and mineralizing events. Abbreviations: Agsfs (aguilarite, polybasite, stephanite and miargyrite), Gold (electrum), Aspy (arsenian-pyrite and arsenopyrite) and Dol – ank (dolomite – ankerite).

Stage 3: This stage is characterized by deposition of alternating bands, rarely symmetrical crustiform-banding, of quartz, calcite and sulfides (sphalerite, galena, pyrite, arsenian-pyrite, and arsenopyrite). Sphalerite in this stage is commonly low-Fe and does not show zoning. Minor constituents forming thin bands or included in quartz and calcite bands are adularia, epidote, hematite and clay minerals. Pyrargyrite and the other silver sulfosalts occur disseminated in quartz and calcite or associated with sphalerite and galena in the bands of sulfides.

Stage 4: This stage consists of calcite, dolomite – ankerite and quartz veins or stringers with pyrargyrite and less acanthite that cross cut stages 1, 2 and 3.

Stage 5: This stage is barren and consists of milky and amethyst quartz and calcite with minor disseminated pyrite and marcasite and sometimes fluorite. Fluorite appears to be the last mineral to have been deposited.

Mineral Zoning

Mineral zoning of the Santo Niño vein has been described in detailed by Gemmell et al. (1988). In general Santo Niño shows that sphalerite and galena are more abundant in the deeper levels of the vein where they occur associated with tetrahedrite and polybasite. Also at deeper levels, sphalerite shows inclusions of chalcopyrite, pyrargyrite, tetrahedrite, acanthite and pyrrhotite. At the upper levels pyrargyrite associated with pyrite is more common and the amount of sphalerite and galena decrease. A similar zoning pattern has been determined for Saucito (J. M. Velador, unpublished data, 2005). In Saucito sphalerite and galena are more abundant at depth, and are associated with black silver sulfosalts (tetrahedrite and polybasite), whereas at shallow depth, pyrargyrite is more abundant and the amount of sphalerite and galena decrease.

The same pattern is observed in Jarillas and Valdecañas. There is a deeper zone with abundant coarse grained sphalerite associated predominantly with tetrahedrite-tenantite and polybasite. Deep sphalerite has Fe-rich cores and Fe-poor rims, and the Fe-rich cores show abundant inclusions of chalcopyrite, silver sulfosalts (tetrahedrite-tenantite, polybasite), acanthite and pyrrhotite. At shallow elevations sphalerite and galena are less abundant and fine grained, and sphalerite is Fe-poor. Also at shallow levels the amount of quartz and calcite increases and pyrargyrite is the predominant silver sulfosalts.

Fluid Inclusions

Previous work

Previous fluid inclusion studies in the manto and vein deposits of the Fortuna-Proaño area include those by Kreczmer (1977), Macdonald (1978), Gonzalez (1984) and Chico (1986). Ruvalcaba-Ruíz and Thompson (1988) provide a detailed summary of the fluid inclusion studies in that area. Those studies have estimated that the temperatures of homogenization (Th) for the chimney and manto deposits range from 200°C to 400°C; whereas the Th of the 2137 and 2270 veins, in the same area, range from 175°C to 419°C. Salinity data ranges from 4 to 7.5 wt% NaCl eq. in the chimney deposits and from 0.2 to 15.1 wt% NaCl eq. in the 2137 and 2270 veins. No evidence for boiling is reported by any of these studies.

Fluid inclusion studies in the SE-Fresnillo area include those by Ruvalcaba-Ruíz (1980), Simmons (1986), Dilley (1993) and Eckberg (1999). A reconnaissance fluid inclusion study of the Saucito vein in the Fresnillo-SW was done by Enriquez (2004) on 14 samples of quartz, calcite, and fluorite. Evidence for fluid boiling is reported for Santa Elena, Santo Niño, San Mateo (Ruvalcaba-Ruíz, 1980; Simmons, 1986; Dilley, 1993 and Eckberg, 1999), and Saucito veins (Enriquez, 2004). Homogenization temperatures and salinities of these veins range between 168 to 298°C and 0.0 to 16.6 wt % NaCl eq. Table 3 is a summary the previous fluid inclusion studies done in Fresnillo-SE and the Saucito vein of Fresnillo-SW.

Methods

Samples for fluid inclusion analysis were collected from drill-core representing the horizontal and vertical extent of the Jarillas and Valdecañas veins. Over 580 fluid

48

inclusions from multiple bands or mineral-grains of quartz, calcite and epidote from

mineralizing stages 2, 3, 4 and 5 were studied in Jarillas and over 340 fluid inclusions

from multiple bands or mineral-grains of quartz and calcite from stages 3 and 5 were

studied in Valdecañas. Fluid inclusions in both veins are of three types: monophase

(liquid), monophase (vapor), and two phase (liquid + vapor), and they vary in size from 2

to 50-μm (Fig. 22); no daughter minerals were observed.

Table 3. Summary of fluid inclusion data from previous studies. Numbers in parenthesis
in the Th°C and Salinity columns represent the average value and the number of analyses,
respectively.

Reference	Vein	Minerals	Th°C range	Salinity range in wt% NaCl eq.
Ruvalcaba-Ruiz (1980)	Santo Niño/Santa Elena	qtz and cal	184 - 298 (234; 174)	0.0 - 1.1 (0.4;174)
Simmons (1986)	Santo Niño	qtz, cal and sl	180 - 260 (217; ~1000)	0.0 - 12.0 (2.5; ~1000)
Dilley (1983)	San Mateo	qtz, cal and sl	168 - 278 (219; 252)	0.0 - 16.6 (4.0; 65)
Eckberg (1999)	Santo Niño	qtz and cal	169 - 272 (220; 61)	0.3 - 6.8 (2.3; 61)
Eckberg (1999)	San Carlos	qtz and cal	168 - 280 (222; 70)	0.3 - 14.3 (2.4; 70)
Enriquez (2004)	Saucito	qtz, cal and flu	185 - 267 (222; 100)	0.5 - 3.4 (2.3; 100)

quartz (qtz), calcite (cal), sphalerite (sl) and fluorite (flu)

Homogenization and ice melting temperatures were determined using a Linkam TH600

heating and freezing stage with accuracy of +/- 2°C. Temperatures of homogenization

above 200°C were measured with precision of +/- 1°C and temperatures below 200°C

(homogenization and melting) with precision of +/- 0.1°C. Melting temperatures of solid

potassium dichromate, CO_2 and H_2O fluid inclusion standards were measured

periodically for calculation of calibration curves and data correction. Salinities in wt%

NaCl eq. and pressures in bars where calculated using FLINCOR ver. 1.4 (Brown, 1992).

Classification of inclusions into primary, pseudo-secondary and secondary was done

based on the criteria established by Roedder (1984).

Results

Homogenization temperatures measured in primary fluid inclusions hosted by quartz, calcite and epidote of ore and barren stages, range from 160 to 320°C in Jarillas (Fig. 23). The salinity range determined for primary inclusions is 0.2 to 11.0 NaCl wt% eq. (Fig. 24). Coexisting liquid-rich and vapor-rich inclusions were observed in many of the studied samples which could indicate boiling conditions at the time of trapping; however, only a couple of vapor-rich inclusions were homogenized into vapor phase and they gave temperatures consistent with the adjacent liquid dominated inclusions. Homogenization temperatures and salinities determined from primary inclusions in Valdecañas vein range from 160 to 320°C and 0 to 11.0 wt% NaCl eq. respectively (Figs. 25, 26). Coexisting liquid and vapor-rich inclusions occur in Valdecañas, although they are less common than in Jarillas. This evidence was observed mainly in stages 3 and 5 in both veins and may indicate that boiling occurred more than once during vein formation.
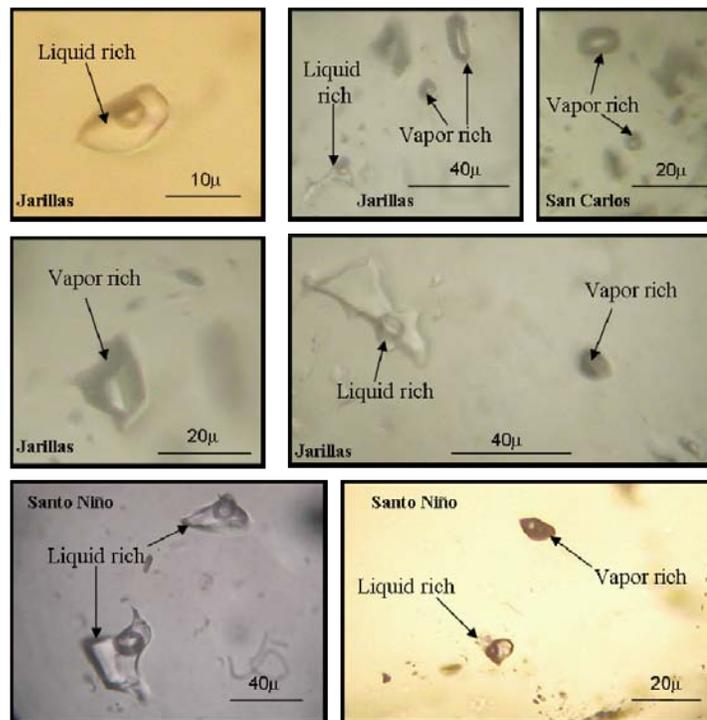
Fig. 22. Two phase fluid inclusions, liquid-rich and vapor-rich, in Jarillas, Santo Niño and San Carlos veins.

Adularia, epidote and bladed quartz after calcite were observed in some samples, and add

supporting evidence for boiling (Fournier, 1985; Drummond and Ohmoto, 1985; Henley

et al., 1986; White and Hedenquist, 1990). Additionally, the presence of chalcedony or

colloform quartz may indicate boiling and rapid cooling (White and Hedenquist, 1990,

Hedenquist et al., 2000). Evidence of boiling conditions allow us to assume that most of

our measured Th's represent actual trapping temperatures (Tt) and therefore they do not

need pressure correction (Roedder and Bodnar, 1980). The calculated pressures and the

modal temperatures of Jarillas and Valdecañas are 25 and 45 bars respectively. Assuming

hydrostatic conditions of pressure we estimate that the paleowater table was at an

elevation of ~2200 to ~2400 m.a.s.l. (meters above sea level). Geologic mapping

suggests that the paleosurface was at an elevation between 2350 and 2550 m.a.s.l.; based

on the occurrence of crystobalite, chalcedony blankets and alunite veins with cinnabar.

 Despite the fact that the fluid inclusions in Jarillas and Valdecañas show the same

range in Th, it is clear from figures 25 and 26 that Jarillas has a lower Th mode than

Valdecañas. Similarly the two veins show almost the same salinity range and even almost

the same mode at ~2.5 wt% NaCl eq., however it is evident from figures 23 and 25 that

more inclusions with salinity greater than 5 wt% NaCl eq. occur in Valdecañas.
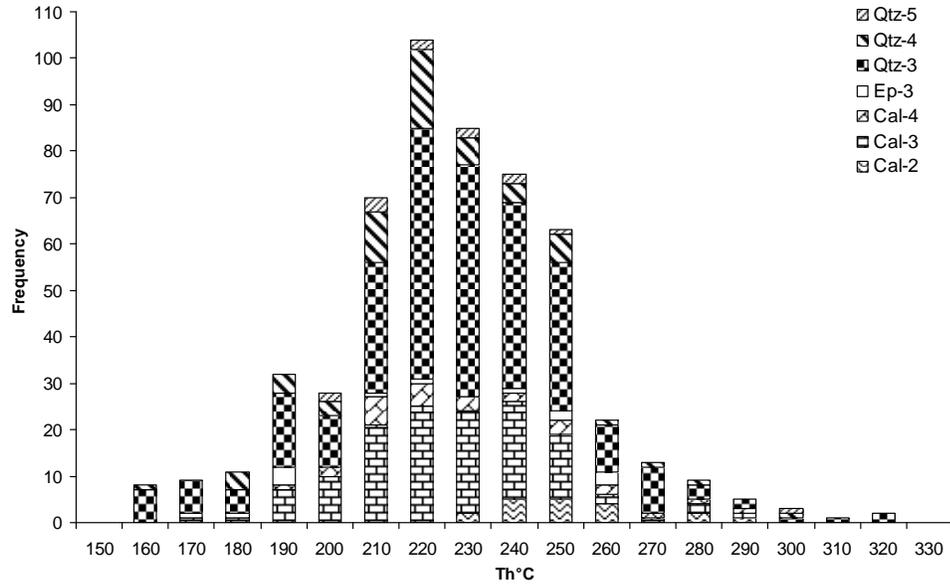
Fig. 23. Histogram of homogenization temperatures for primary inclusions in Jarillas vein. Mineral abbreviations are as follows: calcite (cal), quartz (qtz), epidote (ep). The numbers indicate the paragenetic stage.
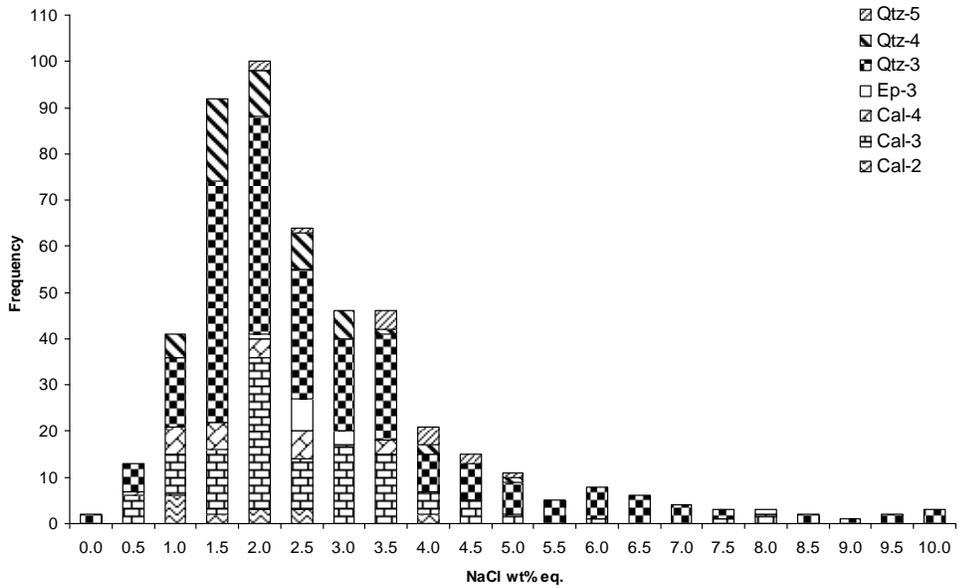
Fig. 24. Histogram of salinity for primary inclusions in Jarillas vein. Abbreviations as in figure 3.
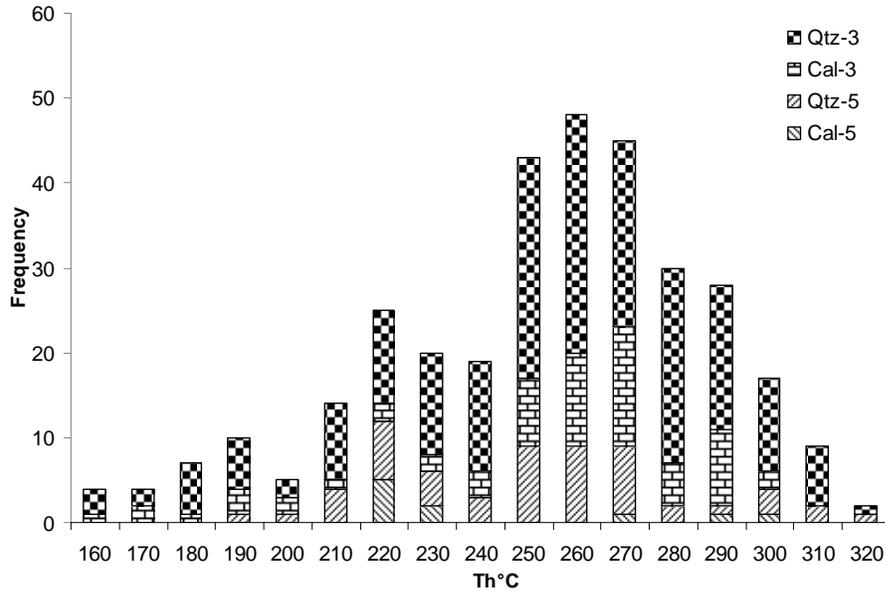
Fig. 25. Histogram of homogenization temperatures for primary inclusions in Valdecañas vein. Abbreviations as in figure 3.
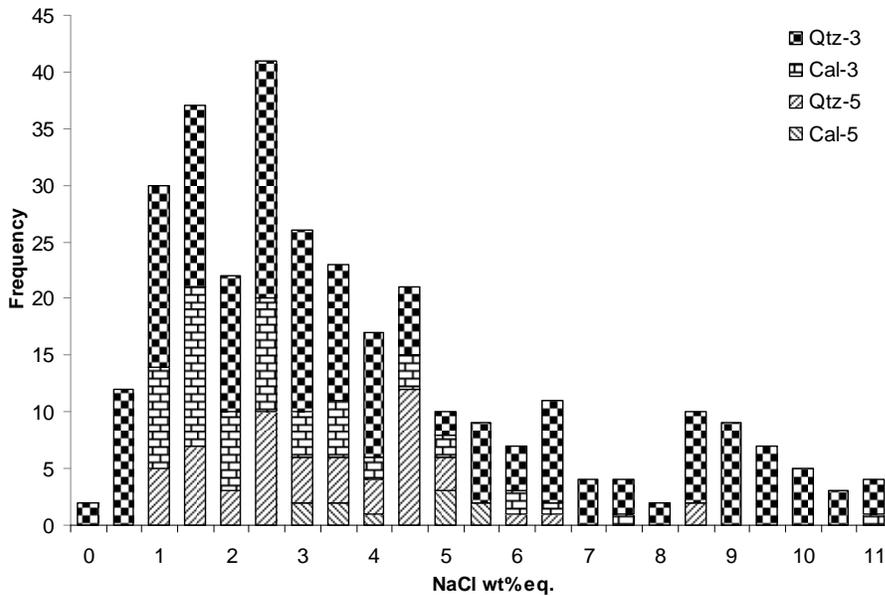
Fig. 26. Histogram of salinity for primary inclusions in Valdecañas vein. Abbreviations as in figure 3.

Fluid inclusion gas analysis

Previous work

In addition to the various microthermometry studies done in Fresnillo, one fluid

inclusion study focused on the fluid gas composition of the Santo Niño vein. Benton

(1991) analyzed gases from quartz-hosted fluid inclusions in 16 samples by thermal

decrepitation. The predominant gases identified in that study were H_2, CO_2, CH_4, N_2,

H_2S, SO_2, NO, CO and C_xH_n (combined organics) and lesser amounts of He, Ne, Ar, O_2

and NH_3. Total gas content varied between 0.1 and 3.3 mol percent, however CO_2 was

found only in concentrations of <1.57 mole percent, which is low for inclusions to

present clathrate formation behavior and to depress the melting point of ice significantly.

Benton (1991), calculated a small range in oxygen fugacity (log fO_2= -39.8 to -42.5) and

a wide range in sulfur fugacity (log fS_2= -10.5 to -17.9) and interpreted that those

represent a combination of boiling and mixing processes.

Methods

A total of 23 samples were separated from banded vein in two drill-hole intercepts

in Jarillas and two more in Valdecañas veins; quartz (n=14) and calcite (n=4) samples

weighting approximately 20 mg were separated from individual mineral bands in Jarillas

and quartz (n=5) samples with the same weight were separated from Valdecañas. The

samples were collected from different bands throughout the width of the veins in order to

detect gas chemistry variations through paragenesis and between the veins. The mineral

separates were cleaned with NaOH and deionized water before crushing in vacuo by the

crush-fast-scan (CFS) method described by Norman et al. (1997). Analysis of inclusions

by CFS method opens one or several inclusions at a time, however the spatial and time

relationship among the inclusions is not known (Norman et al., 1997). Incremental crushing also allows multiple gas analyses per sample; in this study 7 to 17 analyses per sample were obtained. The gases were analyzed using a quadrupole mass spectrometer which determines quantitative amounts of volatiles in fluid inclusions. The species detected were: H_2, He, CH_4, H_2O, N_2, H_2S, Ar, CO_2, SO_2, C_2H_4, C_2H_6, C_3H_6, C_3H_8, C_4H_8, C_4H_{10} and benzene.

Results

The weighted mean values for the gas species H_2, He, CH_4, H_2O, N_2, H_2S, Ar, CO_2 and hydrocarbons in mol percent, for the Jarillas and Valdecañas veins are reported in table 4. In this study, H_2O accounted for 99.17 to 99.86 mol % of the volatiles extracted; the most abundant gases were CO_2 (<0.5 mol %) and N_2 (<0.4 mol %). Oxygen and sulfur fugacities were calculated using the H_2, CH_4, CO_2 and H_2S values, homogenization temperatures measured in fluid inclusions and the equilibrium equations provided by Henley, (1984). Log fO_2 and log fS_2 for Jarillas range from -34.22 to -42.49 and -3.63 to -11.90 respectively; whereas log fO_2 and log fS_2 for Valdecañas range from -35.03 to -41.52 and -5.24 to -11.74 respectively.

Table 4. Weighted mean values of gas species determined for Jarillas and Valdecañas.

Sample	Mineral	H$_2$	He	CH$_4$	H$_2$O	N$_2$	H$_2$S	Ar	CO$_2$
K9-13-GAQ	quartz	0.000E+00	5.533E-05	2.824E-02	9.951E+01	2.021E-01	9.357E-04	3.742E-03	2.442E-01
K9-20-GAQ	quartz	0.000E+00	4.081E-05	1.660E-02	9.917E+01	3.608E-01	2.878E-03	6.207E-03	4.057E-01
K9-8-GAQ	quartz	0.000E+00	3.987E-05	6.135E-03	9.977E+01	7.772E-02	2.073E-03	1.518E-03	1.351E-01
K9-19-GAQ3	quartz	1.224E-05	5.902E-05	7.719E-03	9.978E+01	7.830E-02	2.577E-03	2.487E-03	1.067E-01
K9-5-GAQ	quartz	0.000E+00	5.381E-05	5.789E-02	9.962E+01	1.162E-01	9.373E-04	1.629E-03	1.832E-01
K9-19-GAQ1	quartz	4.739E-04	6.118E-05	1.358E-02	9.956E+01	4.631E-02	2.937E-03	1.359E-03	3.702E-01
K9-20-GAQ2	quartz	0.000E+00	3.039E-05	1.683E-02	9.971E+01	5.783E-02	1.178E-03	1.160E-03	2.062E-01
K9-1-GAQ	quartz	0.000E+00	3.520E-05	8.831E-03	9.986E+01	5.558E-02	2.412E-03	1.229E-03	6.862E-02
K9-14-GAQ	quartz	0.000E+00	2.982E-05	1.935E-02	9.961E+01	1.977E-01	2.767E-04	2.563E-03	1.609E-01
K9-3-GAC	calcite	0.000E+00	5.872E-05	1.460E-02	9.970E+01	1.086E-01	2.897E-03	1.937E-03	1.643E-01
K9-8-GAC	calcite	1.490E-04	6.945E-05	7.324E-03	9.969E+01	4.963E-02	7.108E-03	1.685E-03	2.315E-01
K9-22-GAQ	quartz	1.933E-06	5.737E-05	8.441E-03	9.974E+01	1.319E-01	2.262E-03	2.440E-03	1.105E-01
K9-21-GAC	calcite	0.000E+00	2.097E-04	4.544E-03	9.965E+01	5.701E-02	3.728E-03	1.773E-03	2.742E-01
K9-19-GAC	calcite	3.543E-04	4.442E-05	5.032E-03	9.954E+01	2.705E-01	2.380E-03	4.352E-03	1.713E-01
G5-1-GAQ1	quartz	0.000E+00	4.771E-05	1.976E-02	9.956E+01	3.355E-02	8.799E-04	5.609E-04	3.786E-01
G5-3-GAQ	quartz	0.000E+00	5.804E-05	2.532E-02	9.925E+01	3.513E-01	5.573E-03	7.390E-03	2.757E-01
G5-5-GAQ	quartz	0.000E+00	5.347E-05	6.464E-03	9.933E+01	3.695E-01	2.403E-03	6.132E-03	2.767E-01
G5-10-GAQ1	quartz	0.000E+00	1.242E-04	1.171E-02	9.981E+01	3.369E-02	3.336E-03	1.971E-03	1.113E-01
GD-4-GAQ1	quartz	2.053E-04	6.476E-05	1.495E-02	9.954E+01	2.943E-02	3.026E-03	1.265E-03	4.016E-01
GD-4-GAQ2	quartz	4.505E-04	5.362E-05	1.342E-02	9.949E+01	2.608E-02	2.962E-03	1.269E-03	4.576E-01
GD-8-GAQ	quartz	7.777E-05	4.472E-05	6.511E-03	9.962E+01	2.152E-01	2.640E-03	3.661E-03	1.468E-01
GD-10-GAQ	quartz	0.000E+00	2.120E-04	7.515E-03	9.967E+01	1.792E-01	2.958E-03	3.384E-03	1.317E-01
OF-09-GAQ	quartz	0.000E+00	7.412E-05	9.868E-03	9.961E+01	1.181E-03	2.960E-03	4.013E-04	3.680E-01

Gas species are reported in mol%

Table 4. Continued.

Sample	Mineral	SO$_2$	C$_2$H$_4$	C$_2$H$_6$	C$_3$H$_6$	C$_3$H$_8$	C$_4$H$_8$	C$_4$H$_{10}$	Benzene
Jarillas vein									
K9-13-GAQ	quartz	4.071E-04	1.077E-03	3.545E-03	2.144E-04	2.434E-03	2.650E-04	4.141E-04	1.645E-04
K9-20-GAQ	quartz	1.500E-02	1.188E-03	2.919E-03	8.907E-03	2.049E-03	1.466E-04	5.703E-04	6.250E-03
K9-8-GAQ	quartz	1.390E-04	6.609E-04	2.263E-03	6.688E-05	1.170E-03	9.567E-05	1.874E-04	1.049E-04
K9-19-GAQ3	quartz	3.210E-04	3.137E-03	1.739E-03	3.538E-06	1.278E-02	2.018E-04	1.841E-03	1.047E-04
K9-5-GAQ	quartz	4.389E-04	1.816E-03	5.585E-03	2.152E-04	6.083E-03	4.596E-04	5.919E-04	2.538E-04
K9-19-GAQ1	quartz	3.411E-04	1.323E-03	2.382E-03	2.012E-05	2.464E-03	1.837E-04	4.069E-04	1.198E-04
K9-20-GAQ2	quartz	2.713E-04	7.592E-04	1.876E-03	8.803E-05	1.844E-03	1.475E-04	4.800E-04	1.461E-04
K9-1-GAQ	quartz	2.845E-04	9.507E-04	2.538E-03	0.000E+00	2.240E-03	1.866E-04	4.506E-04	1.139E-04
K9-14-GAQ	quartz	2.147E-04	4.694E-04	2.798E-03	2.191E-05	2.818E-03	2.128E-04	1.155E-03	2.546E-04
K9-3-GAC	calcite	2.437E-04	9.095E-04	2.094E-03	8.223E-06	1.588E-03	1.409E-04	2.827E-04	8.452E-05
K9-8-GAC	calcite	3.965E-04	1.306E-03	2.686E-03	0.000E+00	2.861E-03	2.017E-04	5.155E-04	1.111E-04
K9-22-GAQ	quartz	2.029E-04	9.105E-04	1.579E-03	5.166E-06	1.418E-03	1.540E-04	2.328E-04	6.709E-05
K9-21-GAC	calcite	2.790E-04	9.677E-04	2.510E-03	1.901E-05	3.270E-03	1.532E-04	3.021E-04	9.157E-05
K9-19-GAC	calcite	1.368E-04	6.400E-04	2.105E-03	9.432E-05	1.343E-03	9.890E-05	1.749E-04	5.017E-05
G5-1-GAQ1	quartz	2.535E-04	2.378E-04	1.852E-03	6.124E-05	1.482E-03	1.559E-04	2.331E-04	1.305E-04
G5-3-GAQ	quartz	7.899E-04	0.000E+00	8.121E-02	4.299E-04	2.647E-03	3.847E-04	4.877E-04	2.024E-04
G5-5-GAQ	quartz	2.299E-04	6.214E-04	2.584E-03	1.816E-05	1.673E-03	1.009E-04	2.093E-04	6.013E-05
G5-10-GAQ1	quartz	3.664E-04	3.492E-03	1.493E-03	0.000E+00	1.537E-02	2.141E-04	2.166E-03	1.327E-04
Valdecañas vein									
GD-4-GAQ1	quartz	3.437E-04	1.502E-03	3.146E-03	1.407E-05	2.913E-03	2.157E-04	4.319E-04	1.093E-04
GD-4-GAQ2	quartz	2.568E-04	9.578E-04	2.300E-03	0.000E+00	2.102E-03	1.593E-04	4.095E-04	9.273E-05
GD-8-GAQ	quartz	2.375E-04	9.420E-04	2.208E-03	6.035E-08	1.844E-03	1.349E-04	2.588E-04	6.727E-05
GD-10-GAQ	quartz	2.800E-04	8.432E-04	1.953E-03	4.317E-06	1.996E-03	1.849E-04	3.699E-04	1.060E-04
OF-09-GAQ	quartz	2.370E-04	7.845E-04	2.245E-03	1.898E-05	1.786E-03	1.583E-04	2.352E-04	8.714E-05

Stable Isotopes

Previous work

Oxygen and hydrogen stable isotopes were analyzed from quartz, calcite and fluid

inclusions of the Santo Niño vein by Simmons (1986) and Benton (1991). The $\delta^{18}O$ and

δD fluid values reported in those studies range between 0.6 to 17.0 ‰ and -82 to -30 ‰

respectively (Simmons, 1986; Benton, 1991). Carbon isotopes were also analyzed from

calcites by Simmons (1986), and Benton (1991). The $\delta^{13}C$ values determined in those

studies for ore related and late stage calcite range between -9.8 and -3.9 ‰. Gonzalez et

al. (1984), analyzed sulfur isotopes from 50 samples of sphalerite and galena of the

manto and vein deposits in the Fortuna–Proaño area. The values reported in that study for

sphalerite and galena are $\delta^{34}S_{sl}$= -2 to -6 ‰ and $\delta^{34}S_{gn}$= -5 to -8 ‰, and the average

calculated fluid value was $\delta^{34}S_{H_2S}$= -2.6 ‰. Earthman et al. (2010; in preparation),

analyzed sulfur isotopes in 121 samples of sphalerite, galena and pyrite from veins in

Fresnillo-SW. The mineral $\delta^{34}S$ values for pyrite range from -1.5 to -4.6 ‰ and for

sphalerite and galena from -4.0 to -6.8 and from -5.7 to -9.2 ‰ respectively. The

calculated $\delta^{34}S_{H_2S}$ (fluid) values for sphalerite and galena are remarkably consistent

between -4.0 and -6.0 ‰, whereas the $\delta^{34}S_{H_2S}$ values calculated for pyrite are more

spread, between -2.0 and -7.0 ‰ (Earthman et al., 2010; in preparation).

Methods

Core samples were collected from 33 drill-holes with spatial distribution

representative of the known length and height of Jarillas and Valdecañas veins. Quartz

and calcite minerals from all mineral stages were separated and cleaned for oxygen,

hydrogen and carbon isotope analyses. In many cases multiple bands of quartz and calcite

within a particular sample were separated for analysis of oxygen and carbon isotopes to determine variations between adjacent bands or be able to calculate temperatures using fractionation equations. Additionally, late stage calcite veins were sampled from two drill-holes that intercepted Jarillas vein and were analyzed for oxygen and carbon isotopes. The late stage calcite samples were obtained typically at 100 m intervals from approximately the beginning of the holes (100 m depth) to the end (800 meters). Alunite veins were sampled from the steam-heated acid sulfate alteration blanket in the Eocene tuffs above Valdecañas vein in Fresnillo-SW; three samples were collected at surface (VR-07-01, VR-07-05 and VR-07-07) and one sample was collected from core at an approximate depth of 50 m (VV-IC-01). Sulfur, oxygen and hydrogen isotopes were analyzed from the SO_4 and OH sites of the alunites. Quartz (CH-09-01) and barite (CC-07-01) veins were also sampled on outcrops of the GT in Fresnillo-SE. The details on separation and cleaning procedures are described individually for each mineral below. Quartz: Quartz samples from Jarillas (n=35), Valdecañas (n=9) and veinlets outcropping in Fresnillo-SE (sample CH-09-01) were cleaned ultrasonically with diluted HCl to remove calcite and clays, rinsed with distilled water and dried. The cleaned samples (20 mg), duplicates and standard (NBS 28) were grinded and placed in nickel vessels for oxygen extraction by the fluorination method with ClF_3 (Clayton and Mayeda, 1963). The evolved O_2 was reduced and converted to CO_2 gas with a graphite rod heated under vacuum with a platinum catalyst. The CO_2 gas was put in glass vessels and analyzed in a Finnigan MAT Delta XP Plus mass spectrometer along with reference CO_2 gas at the New Mexico Tech Isotope Laboratory for determination of the $\delta^{18}O_{qtz}$ values. Oxygen yields greater than 90% were obtained after fluorination for all of the samples.

Calcite: Calcite samples were cleaned ultrasonically with distilled water to remove clays, dried and then powdered. Samples (0.25 mg) from Jarillas (n=12), Valdecañas (n=13), late stage veinlets (n=19), duplicates and mineral standards (IAEA CO-9, Solenhofen LS, and NBS 18) were placed in glass vessels and reacted with 100% H_3PO_4 at 25°C for 8 hours to extract CO_2 gas (McCrea, 1950). The evolved CO_2 gas was analyzed in the Finnigan MAT Delta XP Plus mass spectrometer at the New Mexico Tech for determination of $\delta^{18}O_{cal}$ and $\delta^{13}C$ values.

Sulfates: The alunite (n=4) and barite (CC-07-01) samples were powdered and then cleaned; alunite was cleaned with diluted HF for approximately one hour to remove any quartz and clays, rinsed with distilled water and dried, barite was only rinsed with distilled water and dried. The isotopic composition of sulfur in the SO_4 site of alunite and barite was determined from the SO_2 formed by combustion of the samples in an elemental analyzer. The bulk isotopic composition of oxygen in alunite and the SO_4 site in barite was determined from the CO produced by reacting alunite in a high temperature reducing furnace (TC/EA). For the analysis of the isotopic composition of oxygen in the SO_4 site, alunite was selectively dissolved in a heated solution of 0.5 N NaOH and the filtered solution was then titrated with HCl and re-precipitated as $BaSO_4$ following the methods of Wasserman et al. (1992). The re-precipitated barite was then reacted in the TC/EA. For hydrogen analysis, the alunite samples were reacted in the TC/EA to produce H_2 gas. Sample duplicates and standards were also combusted in the TC/EA. In all cases, the gas extracted was analyzed in a Finnigan MAT Delta Plus XP mass spectrometer by continuous flow at the New Mexico Tech Isotope Laboratory.

Inclusion fluids: δD values were determined for 8 quartz samples of Jarillas vein, 7 samples of Valdecañas vein and sample CH-09-01 from Fresnillo-SE. Samples with masses of approximately 15 mg were packed in silver cups and decrepitated at 1450°C in the TC/EA to form H_2 gas from the released water. The H_2 gas was then analyzed in continuous flow mode in the Finnigan MAT Delta XP Plus mass spectrometer at the New Mexico Tech. Standards (IAEA-CH7 and a benzoic acid) and two duplicates were run with the samples; the samples run in duplicate indicate a precision of ~3 per mil.

Results

All the isotope values are reported in ‰ (per mil) in this study. Oxygen and hydrogen isotope ratios are reported relative to the reference international standard VSMOW, carbon values are reported relative to PDB and sulfur relative to the Canyon del Diablo iron meteorite (CDT). Tables 5, 6 and 7 show the isotope data for quartz and calcite, and alunite and barite, respectively.

Oxygen: The $\delta^{18}O$ values of quartz associated with ore in Jarillas and Valdecañas veins and sample CH-09-01 from Fresnillo-SE range between 12.4 and 18.6 per mil. $\delta^{18}O$ values of calcite associated with ore and coexisting with quartz in Jarillas range from 10.7 to 15.3 per mil and are slightly lighter in Valdecañas ranging from 7.4 to 12.9 per mil. The $\delta^{18}O$ values of late stage calcite veins sampled at 100 m intervals are comparatively heavier than ore associated calcite and form a wide range from 12.01 to 18.56 per mil. Temperatures of isotopic equilibration for adjacent bands of quartz and calcite associated with ore were determined using the fractionation equation of Sharp and Kirschner (1994); for Jarillas, a temperature range between 59°C and 388°C was determined for all but one of the pairs; one pair produced a temperature of 1073°C, but

this is unrealistic and can be considered an outlier. Most of the temperatures calculated for Valdecañas vein are unreasonably low or high and indicate disequilibrium. The fluid $\delta^{18}O$ values were calculated using the temperatures of homogenization measured from fluid inclusions in quartz and calcite and the fractionation equations of Meheut et al. (2007) and Kim and O'Neil (1997), respectively. $\delta^{18}O_{water}$ value ranges are consistent in both veins; fluid values calculated for quartz range between 3.9 and 9.6 per mil and for the ore associated calcite between 5.9 and 10.9 per mil.

The $\delta^{18}O_{bulk}$ and $\delta^{18}O_{SO_4}$ values obtained for alunite and re-precipitated barite range between 15.2 and 32.7 per mil and between 24.0 and 31.2 per mil, respectively. The $\delta^{18}O_{OH}$ values were calculated using the $\delta^{18}O_{bulk}$ and $\delta^{18}O_{SO_4}$ values and the mass balance equation in Wasserman et al. (1992); $\delta^{18}O_{OH}$ range between 9.4 and 33.7 per mil. The temperatures of equilibration were calculated using the fractionation equations of Stoffregen et al. (1994); one temperature of 105°C and three unrealistic temperatures where obtained. $\delta^{18}O_{water}$ values were calculated assuming a temperature of 100°C which is probably accurate due to the occurrence of crystobalite and cinnabar associated with alunite in the steam-heated blanket. Additionally, Rye et al. (1992) suggested that alunite in the steam heated environment should form at temperatures between 90°C and 160°C. The calculated fluid values range between 4.7 and 11.9 ‰ and is similar to that for quartz and calcite. The $\delta^{18}O_{SO_4}$ determined for the barite sampled at surface in Fresnillo-SE is 12.3 per mil, and its fluid value for an average homogenization temperature of 150°C, is 2.8 per mil.

Table 5. Oxygen and hydrogen isotope data for quartz. $\delta^{18}O_{water}$ values were calculated using the fractionation equation of Meheut et al. (2007).

Sample	T°C	$\delta^{18}O_{mineral}$	$\delta^{18}O_{water}$	δD
Jarillas				
JV-FS95-2 (B)	230	13.3	4.0	-63.7
JV-FS95-2 (A)	230	16.4	7.1	-63.7
JV-FS95-3 (B)	230	16.3	7.0	
JV-FS95-3 (A)	230	17.2	7.9	
JV-FS95-4 (A)	230	16.2	6.9	
JV-FS95-4 (B)	230	17.4	8.1	
JV-FS95-4 (C)	230	18.3	9.0	
JV-G5-11 (B)	240	18.2	9.5	-70.3
JV-G5-2 (A)	240	16.8	8.2	
JV-G5-2 (C)	240	17.9	9.2	
JV-G5-2 (B)	240	18.0	9.3	
JV-G5-5 (2)	240	16.9	8.2	
JV-G5-5 (1)	240	18.3	9.6	
JV-I5-5 (1)	235	15.7	6.7	-65.4
JV-K7-4 (3)	226	16.6	7.1	-60.9
JV-K7-4 (9)	226	17.8	8.2	-60.9
JV-K7-11 (D)	226	15.8	6.2	
JV-K9-14 (3)	245	16.7	8.3	
JV-K9-14 (5)	245	17.4	9.0	
JV-K9-19 (2)	245	15.7	7.3	-68.9
JV-K9-19 (3)	245	16.6	8.3	-68.9
JV-K9-19 (4)	245	16.7	8.4	-68.9
JV-K9-19 (5)	245	17.4	9.1	-68.9
JV-K9-19 (1)	245	17.7	9.3	-68.9
JV-K9-20 (2)	245	14.9	6.6	
JV-K9-20 (7)	245	15.9	7.5	
JV-K9-20 (4)	245	15.9	7.6	
JV-K9-7 (2)	210	17.1	6.4	
JV-K9-7 (5-7)	210	17.9	7.2	
JV-K9-8 (2)	210	17.8	7.1	
JV-K9-8 (6)	210	18.6	7.9	
JV-S11-01	236	15.5	6.6	-70.0
JV-S5-01	227	15.9	6.4	-66.8
JV-S7-01	239	13.0	4.3	
JV-Q9-2	232	13.1	3.9	-52.9

Table 5. Continued.

Valdecañas				
VV-QF-09	261	12.4	4.9	
VV-EE-06	236	16.3	7.4	-61.1
VV-WC-02	249	15.3	7.2	-79.3
VV-KD-09	254	14.0	6.2	-54.3
VV-UD-01[1]	240	14.9	6.3	
VV-GD-02	240	16.8	8.1	-69.4
VV-OF-01	259	14.5	7.0	-56.6
VV-EE-10	236	15.4	6.4	
VV-EF-08A	251	12.5	4.5	
VV-ME-08				-62.4
Surface				
VR-09-01	100	29.9	9.0	
CH-09-01	180	14.1	0.9	-74.5

1. The temperature for this sample was assumed based on adjacent samples
Letters or numbers in parenthesis indicate different mineral bands within the sample

Hydrogen: δD values determined from inclusion fluid trapped in quartz associated with ore in Jarillas and Valdecañas veins (mineralizing stages 2 and 3) range from -70 to -53 per mil and -80 to -54 per mil respectively. Fluid inclusion studies revealed that primary and pseudo-secondary inclusions predominate in quartz from the two veins, consequently, the δD values should represent mostly the composition of the hydrothermal fluid that formed the quartz; however, most of the quartz from mineralizing stage three (associated with ore) is chalcedonic or recrystalized from chalcedony and it is possible that some of the inclusions that appear primary in origin, actually formed after recrystalization of the chalcedony, as documented by Sander and Black (1988). A δD value of -75 per mil was determined for the water in primary and pseudo-secondary inclusions of the barite sample CH-09-01.

Table 6. Oxygen and carbon isotope data for calcite. $\delta^{18}O_{water}$ values were calculated using the fractionation equation of O'Neil (1997).

Sample	T°C	$\delta^{13}C_{mineral}$	$\delta^{13}C_{CO2}$	$\delta^{18}O_{mineral}$	$\delta^{18}O_{water}$
Jarillas vein					
JV-K7-11 (2)-BE	226	-6.1	-5.3	15.3	10.4
JV-K9-8(2) B9	210	-7.9	-7.5	12.9	8.0
JV-K7-4 B10	226	-7.5	-6.6	13.9	9.0
JV-I5-5(5) B2	235	-7.5	-6.5	12.9	8.8
JV-K7-4 B10	226	-7.3	-6.5	12.8	7.9
JV-K7-11(2) BC	226	-7.0	-6.1	12.8	7.9
JV-K9-7(1) B1	210	-6.5	-6.1	15.1	10.2
JV-G5-11 BC	240	-8.2	-7.1	10.7	7.5
JV-K9-8 (2) B3	210	-6.8	-6.4	10.8	5.9
JV-G5-11 BA	240	-8.1	-7.0	11.2	7.9
JV-G5-11 BD	240	-6.9	-5.8	12.8	9.5
JV-K9-14(2) BG	245	-7.6	-6.4	10.9	8.5
Valdecañas vein					
EF-08A	251.0	-7.0	-5.7	12.2	10.2
EF-09	251.0	-4.0	-2.7	12.8	10.8
EF-10	251.0	-7.0	-5.6	8.9	6.9
KD-08	254.0	-8.1	-6.7	8.8	7.1
KD-05	254.0	-8.2	-6.8	10.6	8.8
GD-04	240.0	-9.1	-7.9	9.3	6.6
QF-9	261.0	-8.0	-6.5	7.4	6.1
QF-4	261.0	-7.0	-5.5	8.6	7.3
GB-04	227.0	-8.3	-7.5	10.4	6.8
UD-01	250.0	-8.1	-6.8	12.9	10.9
ME-02	248.0	-7.8	-6.6	9.0	6.8
OF-1	261.0	-7.0	-5.5	8.8	7.5
EE-10	240.0	-7.5	-6.4	9.7	7.0
Late calcite veins[1]					
G7-A04 (250)	130	-8.8	-11.2	18.3	6.0
G7-A05 (300)	135	-8.1	-10.3	15.1	3.4
G7-A06 (450)	140	-7.3	-9.2	18.6	7.3
G7-A07 (500)	145	-7.8	-9.5	15.5	4.8
G7-A08 (600)	150	-5.2	-6.7	13.2	3.0
G7-A09 (650)	155	-1.0	-2.3	15.5	5.8
G7-A10 (750)	160	-5.2	-6.3	14.1	4.9
K9-A01 (100)	110	-7.6	-11.1	18.0	3.4
K9-A02 (150)	115	-7.8	-11.0	15.1	1.0
K9-A03 (200)	120	-6.0	-8.9	14.8	1.3
K9-A04 (250)	125	-6.2	-8.8	17.6	4.8
K9-A05 (300)	130	-6.9	-9.3	16.0	3.7
K9-A06 (350)	135	-7.9	-10.1	14.7	2.9
K9-A08 (450)	140	-7.3	-9.3	15.7	4.5
K9-A10 (500)	145	-17.4	-19.1	16.5	5.8
K9-A11 (550)	150	-5.2	-6.7	16.2	6.0
K9-A12 (600)	155	-6.1	-7.4	16.0	6.3
K9-A13 (750)	160	-2.8	-3.9	15.4	6.2
K9-A14 (800)	165	-4.4	-5.3	12.0	3.3

1. The numbers in parenthesis in late calcite samples indicate the depth of sampling.
The temperatures for the Jarillas and Valdecañas samples were measured from fluid
inlcusions. The temperatures of the late calcites were assumed.

Table 7. Stable isotope data for sulfates. $\delta^{18}O_{water}$ values were calculated using the fractionation equation of Stoffregen et al. (1994).

Sample	Mineral	T°C	$\delta^{34}S$	$\delta^{18}O_{bulk}$	$\delta^{18}O_{SO4}$	$\delta^{18}O_{OH}$	$\delta^{18}O_{water}$	δD
VR-07-01	alunite	100.0	-1.6	21.4	27.7	17.1	8.4	-0.5
VR-07-05	alunite	100.0	-0.5	32.7	31.2	33.7	11.9	-5.5
VR-07-07	alunite	100.0	-0.6	25.3	29.3	22.7	10.0	-1.4
VV-IC-01	alunite	100.0	-1.2	15.2	24.0	9.4	4.7	-24.1
CC-07-01[1]	barite	150.0	2.5	n/a	12.3	n/a	2.8	

The temperatures for alunite samples were assumed, and the temperature for barite was determined from fluid inclusions

The δD values determined from alunite are heavy and form a range from -24.1 to -0.5 per mil. There is not a well-constrained fractionation equation for hydrogen in alunites at this low temperature, but Stoffregen et al. (1994), proposed that the fractionation values for alunite forming at temperatures between 150°C and 25°C should be between -6 and +4 per mil. Thus no fluid values were calculated for hydrogen in alunites, since it is possible that the deuterium fractionation for alunites in the steam-heated environment is close to zero; we therefore assume that the $\delta D_{mineral}$ values will be approximately equal to the δD_{water} values.

Sulfur: $\delta^{34}S$ values from alunite are remarkably consistent forming a range between -1.6 to -0.5 per mil. The $\delta^{34}S$ value for the analyzed barite from the veinlets outcropping in Fresnillo-SE is 2.5 per mil.

Carbon: $\delta^{13}C$ values determined from calcite samples associated with ore in Jarillas and Valdecañas form a narrow range from -8.2 to -6.1 per mil and a more spread range from -9.1 to -4.0 per mil respectively. The $\delta^{13}C$ values determined for late calcite veins sampled from the host rock every 100 m exhibit a wide range from -17.4 to -1.0 per mil. $\delta^{13}C_{CO2}$ fluid values using homogenization temperatures and the fractionation equation of

Ohmoto and Rye (1979) range between -7.9 and -2.7 per mil. $\delta^{13}C$ fluid values

calculated for late calcites, using a temperature range constrained by the temperature of

the steam-heated blanket (100°C) and the minimum temperature determined from fluid

inclusions in ore associated calcite (160°C), form a wide range between -11.2 and -2.3

per mil.

Discussion

Alunite

The near-zero $\delta^{34}S$ values of the alunite samples are consistent with a steam-

heated origin for the alteration blanket in Fresnillo-SW, however, the oxygen and

hydrogen isotopic compositions are consistent with compositions of alunites in high

sulfidation deposits (Rye et al., 1992; Rye, 2005). Evidence in support of steam-heated

origin besides the sulfur isotopes is the blanket like distribution of the alteration

(crystobalite, opaline-chalcedony, kaolinite, alunite). Isotopic equilibrium between

oxygen of the SO_4 and the OH sites in alunite is commonly attained in the low

temperatures of this environment (Rye et al., 1992; Rye, 2005), however we determined

unrealistic temperatures for three of the samples and one temperature of 105°C for

sample VR-07-07. We believe that the δD values in all of the alunite samples are heavier

than the possible range in δD for Tertiary meteoric water in the region. Rye (2005)

proposed that postdepositional retrograde hydrogen exchange in the OH site of alunite

occurs in magmatic hydrothermal alunites and that it also affects the reliability of the SO_4

and OH oxygen isotope fractionation for use as a geothermometer; however, he proposed

that this retrograde exchange is not significant in the low temperature steam-heated

environment. It is possible that the heavy δD values in the alunites of Fresnillo resulted

due to deuterium fractionation into the vapor phase at the time the fluids were boiling in the hydrothermal plume, and then post depositional retrograde hydrogen exchange contributed to make the alunites even heavier or alternatively, that the gases that formed the alunites have magmatic origin. Evidence in support of postdepositional exchange of hydrogen comes from the observation that the sample with the lightest hydrogen and oxygen composition is the one that was sampled ~50 m below surface (VV-IC-01), i.e. this sample has interacted less with surface meteoric water; the other three samples collected at the surface have heavier δD and $\delta^{18}O$ values. Another important consideration is that we do not know the real temperature of deposition of the alunites, since the temperature range for steam-heated alunites is wide, (90°C to 160°C) they could have been deposited at relatively high temperatures ~160°C and then been affected more strongly by retrograde exchange at low temperature. Something else that could be affecting the hydrogen isotope composition of alunite is substitution of potassium by NH_4^+ molecules, although we do not understand the effect that ammonia can impose in the δD values of alunite. Ammonia has been detected in some samples of alunite and interlayered illite-smectite in Fresnillo by Short Wave Infrared (SWIR) Spectroscopy (J. M. Velador, unpublished data, 2005).

Late calcite veinlets

Oxygen isotope ratios analyzed in late stage calcites sampled from 100 m below surface to 800 m depth in two drill-holes are consistently heavier than those of ore associated calcite. Heavier $\delta^{18}O$ values probably reflect the lower temperature of deposition of the late stage calcites. $\delta^{18}O$ values in late calcite get progressively lighter with depth as they approach the vein and get almost as light as the ore calcites when they

are proximal to the vein (Fig. 27). It is possible that a more systematic analysis of oxygen isotopes of calcite veins in exploration drill-holes in Fresnillo could be used in conjunction with detailed alteration core logging and chemical assays to assess exploration targets.
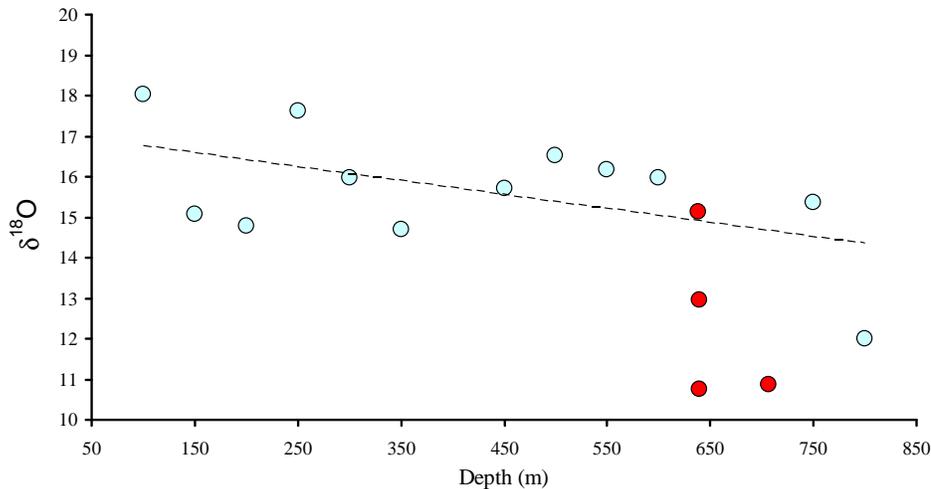
Fig. 27. Plot of $\delta^{18}O_{calcite}$ values vs. depth for drill hole K9. The blue circles represent samples of calcite at variable depths in the drill-hole and the red circles represent the values for ore associated calcite.

Source of fluids in epithermal deposits

The origin of the hydrothermal fluids that form epithermal deposits can be varied; from predominantly magmatic in HS epithermal deposits to predominantly meteoric in LS deposits (O'Neil and Silberman, 1974; Rye et al., 1992; Arribas et al., 1995; Hedenquist et al., 1998; Hedenquist et al., 2000; Cooke and Simmons, 2000). IS deposits in general have been suggested to have a closer affiliation with HS deposits and porphyries than LS deposits (Sillitoe and Hedenquist, 2003; Camprubí and Albinson, 2007), and thus the involvement of either meteoric or magmatic water at variable degrees can be determined in these deposits. In spite of Mexico being a very important IS province, only a few IS deposits have been studied in detail (Camprubí and Albinson,

2007) and thus detailed geochemical studies are needed in Mexico to understand these complex deposits. Isotope geochemistry and fluid inclusion studies of the Santo Niño vein and other Mexican IS deposits generally show the involvement of fluids with magmatic signatures (Simmons et al., 1988; Sillitoe and Hedenquist, 2003; Camprubí and Albinson, 2007).

Source of fluids in Fresnillo

The homogenization temperature range of 160°C to 320°C determined for the fluid inclusions in Jarillas and Valdecañas is typical of IS epithermal deposits (Hedenquist et al., 2000; Sillitoe and Hedenquist, 2003). Simmons et al. (1988), pointed out that fluid inclusions of the Santo Niño vein with salinities of up to10 wt % NaCl eq. likely indicate magmatic derivation of the hydrothermal fluids since no evaporites that could provide chlorine have been reported in the Fresnillo region, and if any connate water existed, it would have been squeezed out of the GT during accretion. The salinities determined for fluid inclusions in Jarillas and Valdecañas define a wide range from 0 to 11 wt % NaCl eq. and thus it is possible that these salinities up to 11 wt % NaCl eq. also represent pulses of brines of magmatic derivation. Simmons (1991), proposed that sphalerite and silver sulfosalts in Santo Niño were deposited by intermittently injected brines with salinities of 10 to 12 wt % NaCl eq. Further we'll discuss evidence that suggest that part of the broad variability in salinity (0 to 11 wt % NaCl eq.) of the Jarillas and Valdecañas inclusions could also be the result of extreme boiling of moderate salinity fluids, or mixing between high salinity fluids and diluted meteoric water.

The $\delta^{18}O_{water}$ and δD values determined for Santo Niño (Simmons et al. 1988; Benton, 1991), Jarillas, and Valdecañas veins plot within the Primary Magmatic Water

box, and thus are compatible with a magmatic origin for the fluids (Fig. 28). However, another possibility, as pointed out earlier by Simmons et al. (1988) and Benton (1991), is that these values resulted from deeply circulated meteoric water with δD composition between -30 and -60 per mil that exchanged oxygen with the sedimentary rocks of the GT. Other studies have shown that the isotopic composition of the fluids that formed the epithermal deposits of the Great Basin in the United States, is compatible with meteoric derivation, whereas the composition for fluids that formed alunite in some HS epithermal deposits is compatible with volcanic water (O'Neil and Silberman, 1974; Rye et al., 1992; Arribas et al., 1995) (Fig. 28). Some of the studied epithermal deposits from Mexico also plot in an area overlapping the primary magmatic water box, like Fresnillo, but generally they are more shifted towards the meteoric water line. Compared to the epithermal deposits of the Great Basin, some Mexican epithermal deposits and particularly Fresnillo do not have fluid compositions consistent with un-exchanged meteoric water. We interpret that the composition shown by the Fresnillo fluids is only consistent with either magmatic water, highly exchanged meteoric water (deeply circulated) or a mixture of both. In an attempt to determine the isotopic composition of Tertiary meteoric water we analyzed the δD composition of inclusion fluid in late quartz (CH-09-01) from an outcrop in Fresnillo-SE (shallow deposition) that presumably was formed by late meteoric fluids; the δD obtained was -74.5 per mil which plots within the range of ore related quartz and magmatic water; however, primary fluid inclusions with homogenization temperatures of ~200°C and pseudo-secondary inclusions with temperatures ~160°C were observed in this sample, and thus the δD value reflects the

71

average of two distinct fluids and does not help us constrain the composition of Tertiary meteoric water.
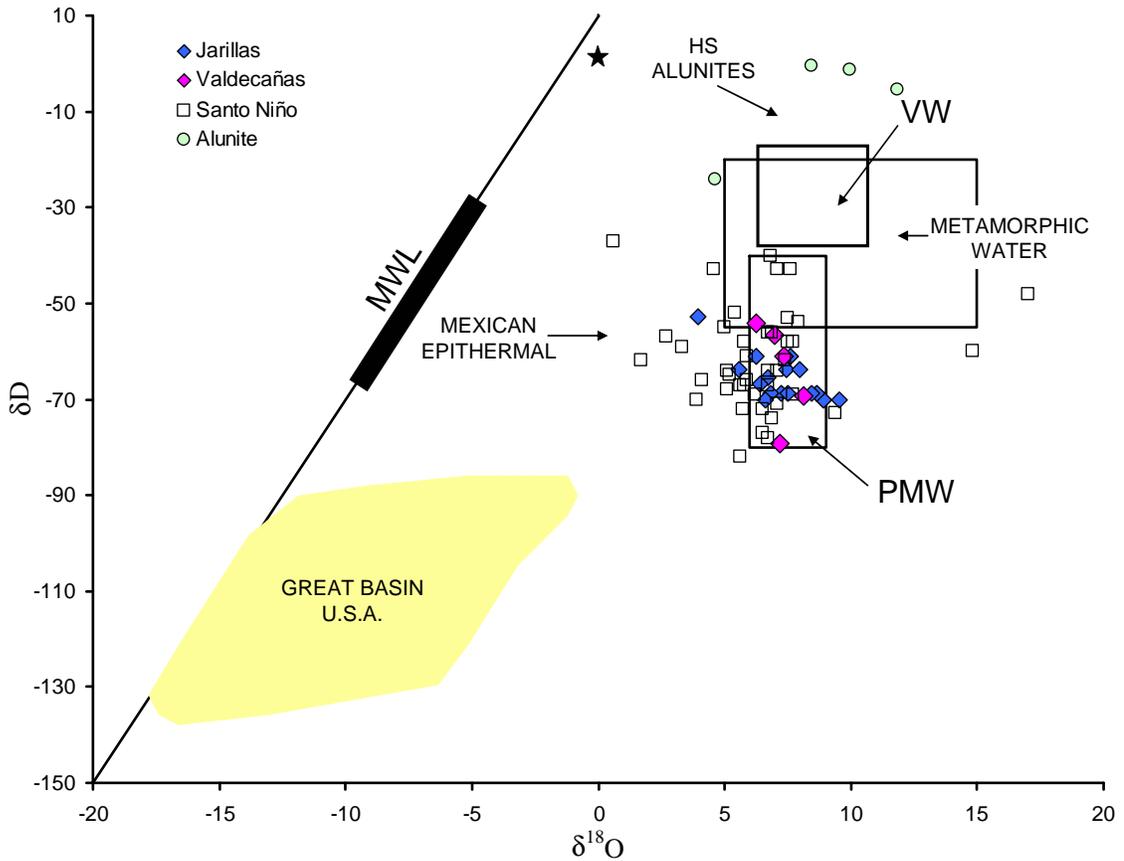
Fig. 28. $\delta^{18}O$ versus δD diagram (in per mil) showing data from Santo Niño, Jarillas, Valdecañas and alunite from Fresnillo. Explanation: PMW (Primary Magmatic Water box; Taylor, 1974), TMW (Tertiary Meteoric Water; Simmons, 1986), VW (volcanic water ; Taylor, 1974), HS Alunites (Alunites from high sulfidation deposits; Rye et al., 1992; Arribas et al., 1995), GREAT BASIN U.S.A. (several epithermal deposits from the Great Basin Nevada; O'Neil and Silberman, 1974), MEXICAN EPITHERMAL (Albinson et al., 2001).

Additionally we tried to constrain the isotopic composition of the Tertiary meteoric water by analyzing the $\delta^{18}O$ composition of opaline-chalcedony (VR-09-01) deposited in the steam-heated blanket (acid sulfate alteration affecting the Eocene tuffs

above Valdecañas vein presumably deposited above the paleowater table) and from late barite veinlets (CC-07-01) occurring at the surface in Fresnillo-SE; we calculated the $\delta^{18}O_{water}$ values of opaline-chalcedony for a temperature of 100°C (assuming a steam-heated environment) and 150°C (measured from pseudo-secondary fluid inclusions in barite). Unfortunately the two calculated $\delta^{18}O$ fluid values (9.0 and 2.8 per mil, respectively) are too heavy and do not indicate un-exchanged meteoric composition. The heavy fluid values of these two minerals are compatible with the composition of the fluids for ore associated quartz and calcite which could indicate that deep hydrothermal water and shallow meteoric water had similar isotopic composition.

Camprubí and Albinson (2007), suggested that the consistently heavy oxygen compositions of IS and LS epithermal deposits in Mexico, including Santo Niño vein are too heavy to be explained by boiling or water/rock interactions alone, and that they should reflect significant magmatic contributions. We believe that a distinction between magmatic water, deeply circulated exchanged water, or a mixture of magmatic and deeply circulated exchanged water is not possible by means of oxygen and hydrogen stable isotope analysis.

Plots of Ar/He vs. N_2/Ar and CO_2 vs. N_2/Ar ratios from Jarillas and Valdecañas indicate that the gases in fluid inclusions of these veins have a meteoric signature whereas gas analysis data of the Santo Niño vein indicates that the gases have magmatic composition (Benton, 1991; Albinson et al., 2001). Nevertheless, many of the samples from Jarillas and Valdecañas plot close to the edge of the calc-alkaline magmatic water box in the Ar/He vs. N2/Ar plot and that could be an indication that mixing between magmatic and meteoric fluids occurred (Figs 29 and 30). In conjunction, maximum

salinities of 11 wt % NaCl eq., heavy oxygen and hydrogen isotope ratios, and gas

chemistry ratios suggest that the hydrothermal fluids that formed the IS veins in Fresnillo

could have resulted from mixing between saline magmatic water and deeply circulated

meteoric water.

Source of sulfur and carbon

The consistent mineral δ^{34}S values determined for the veins in Fresnillo-SW

suggest that the veins were formed from a common source of sulfur and that all the veins

could be related to a single ore-forming event (Earthman et al., 2010; in preparation).

However, compared to the sulfur values around 0 ‰ from other epithermal systems

around the world, the sulfur values from Fresnillo and other Mexican epithermal deposits

hosted by the GT are lighter (-1.5 ‰ to -9.2 ‰) (Earthman et al., 2009). The

incorporation of sulfur from sedimentary rocks, which can contain light δ^{34}S values,

could explain the anomalous values seen in the veins (Earthman et al., 2010; in

preparation). Gonzalez et al. (1984), interpreted that the sulfur in sphalerite and galena of

the manto and vein deposits of the Fortuna-Proaño area, which are similar to those of

Fresnillo-SW, had a biogenic origin; they proposed that the sulfur was remobilized and

re-precipitated in galena and sphalerite by hydrothermal fluids in the Tertiary.

δ^{13}C values determined for calcites in Jarillas and Valdecañas are also light, and

are in agreement with those determined for Santo Niño vein by Simmons (1986), and

Benton (1991). Similarities in δ^{13}C values suggest that the source of carbon was also the

same for all veins, including the late calcite veins. The light values suggest that carbon

may have had its origin in the black shales of the GT as well. We believe that the light

and homogeneous δ^{34}S and δ^{13}C values in the district resulted because sulfur and carbon

were scavenged from the sediments at the time of hydrothermal water circulation or

alternatively, that assimilation and melting of xenoliths of the GT by a deep seated
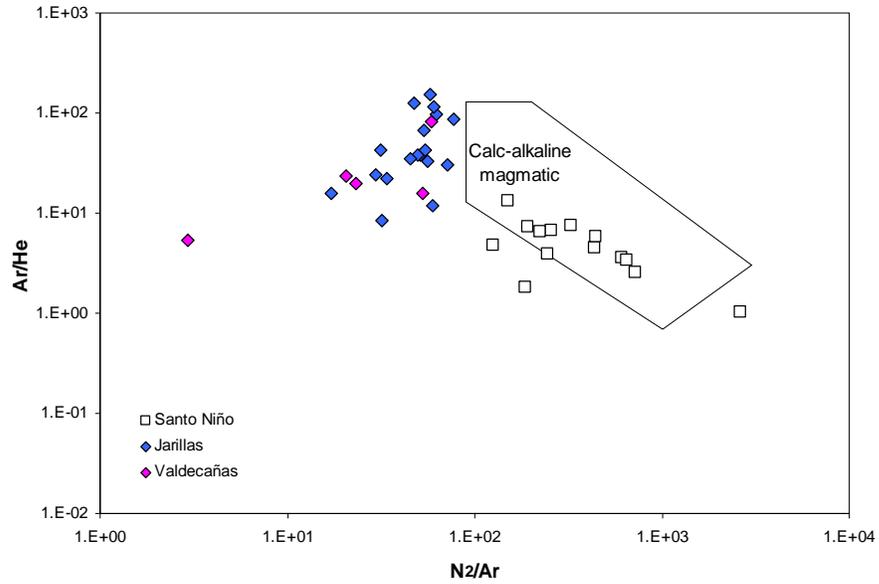
Fig. 29. N_2/Ar vs. Ar/He plot for fluid inclusion gas analyses data in from quartz and calcite of the Jarillas and Valdecañas veins; data for Santo Niño from Benton (1991). Calc-alkaline magmatic filed from Norman et al. (1997).
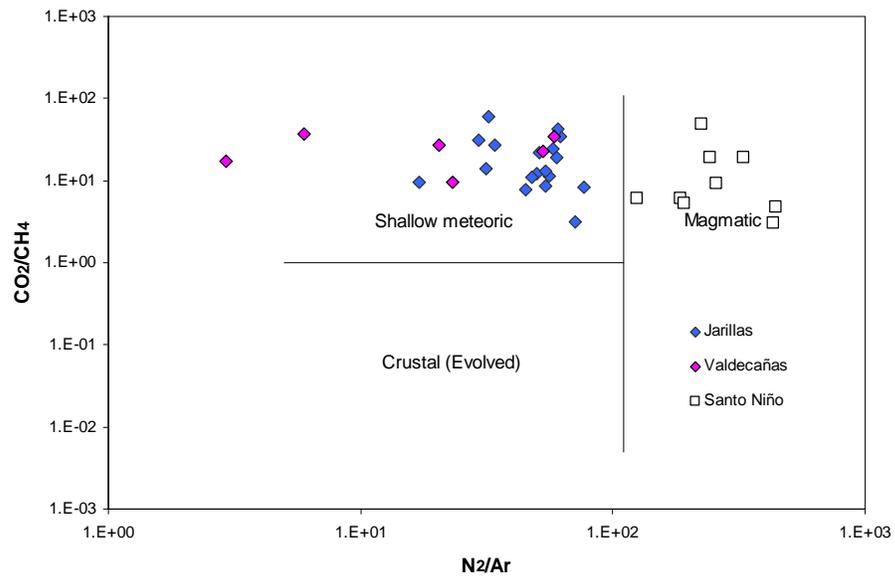
Fig. 30. N_2/Ar vs. CO_2/CH_4 plot for fluid inclusion gas analyses data from quartz and calcite of the Jarillas and Valdecañas veins; data for Santo Niño from Benton (1991). Shallow meteoric, magmatic and crustal waters fields from Blamey and Norman (2002).

magma chamber homogenized the sulfur and carbon isotopic composition of the magmatic fluids. Light sulfur values are reported for other Mexican epithermal deposits hosted by the GT (Guanajuato, La Guitarra, Taxco), which lead us to suggests that the GT could have acted as a local compositional anomaly that controlled the sulfur and carbon isotope values in those deposits.

Geochemistry of the Tertiary volcanic rocks in Fresnillo suggests that a change from trachitic-dacitic to rhyodacitic-rhyolitic compositions occurred after the hiatus in volcanism of the Upper Eocene (Orozco-Esquivel et al., 2002; Velador et al., 2010a; submitted). The hiatus marks also a change in the direction of extension that prevailed during the Oligocene in the Mesa Central (MC) (Nieto-Samaniego et al., 2007). A change in the chemistry of the volcanism after a hiatus in the Upper Eocene is also recorded in the SMOc province in the states of Durango and Chihuahua, and has been attributed to change in convergence rate and subduction angle (McDowell and Keizer, 1977; Damon et al., 1981; Clark et al., 1982). Differences in the geochemical composition between the Eocene and Oligocene volcanics in the MC have been attributed to a change of provenance from mantle derivation for the Eocene magmas to crustal derivation for the Oligocene magmas due to the onset of crustal extension which resulted as a consequence of the increase in subduction rate (Orozco-Esquivel et al., 2002; Nieto-Samaniego et al., 2007). Lead isotope studies done in galena samples from the Fortuna-Proaño area indicate that the lead was probably leached from the basement (De Cserna, et al., 1977). Mango (1992), interpreted that the lead from Fresnillo and Guanajuato is too radiogenic, which could indicate crustal derivation. Potra and MacFarlane (2009), reported lead isotope data for two porphyry copper deposits hosted by the GT and two manto-skarn

deposits hosted by the Sierra Madre Occidental terrane in souther Mexico and interpreted variable degrees of mixing between a mantle-derived Pb (for the porphyries) and a more radiogenic component, represented either by the basement or by the sedimentary rocks (for the manto-skarn deposits). A crustal source for Oligocene magmas responsible for mineralization and for the lead in the galenas of Fresnillo as suggested by some studies is compatible with the hypothesis that homogeneous sulfur and carbon values were the result of assimilation of crustal rocks (GT) in a deep seated magma chamber.

Sillitoe (2008) proposed that heterogeneously distributed metal preconcentrations, favourable redox conditions or other parameters in the mantle wedge or the upper crust could be the reason for the existence of metallogenic belts in the North and South American Cordillera. Campa and Coney 1982, investigated the distributions of the mineral resources in Mexico with respect to tectono stratigraphic terranes and showed that over 70% of the important gold and silver mines are located within three accreted terranes in western Mexico; one of them being the GT. Based on their findings, they proposed that the terranes controlled the distribution of the gold and silver resources in Mexico. We speculate that anomalous silver preconcentrations in the crust could also explain why there are notably silver-rich districts in Mexico; i.e. it is possible that silver was leached from the crust by hydrothermal fluid circulation at relatively shallow levels or that the magmas associated with the formation of the Mexican epithermal deposits assimilated crustal rocks with anomalously high silver concentrations at depth.

Physiochemical variations and fluid evolution

Early studies in the district described the differences in base metal and silver contents between the manto and chimney deposits (Stone and McArthy, 1942) and

between the base metal-rich manto and vein deposits in the Fortuna-Proaño area and the silver-rich veins of the Fresnillo-SE area; informally classified as "heavy sulfide" and "light sulfide" deposits, respectively (Chico, 1986). Ruvalcaba-Ruíz (1980), noted differences in Th and salinity between the manto and vein deposits and proposed the involvement of two types of fluids. Later, Simmons (1991) attributed the differences in base metal and silver contents between the manto and vein deposits of Fortuna-Proaño area and the silver-rich veins of Fresnillo-SE to a drop in the water table elevation before the formation of the silver-rich veins. Mineralogically, the Santo Niño and San Carlos veins are very similar to the Jarillas and Valdecañas veins, which suggest that they could have a common origin. Nonetheless, subtle differences have been observed, particularly in Au/Ag ratios (Velador et al., 2010b; in preparation); the Au/Ag ratios in Jarillas and Valdecañas can be 3 to 15 times greater than in Fresnillo-SE, suggesting district wide geochemical zoning. At the vein scale, galena and sphalerite are more abundant at deeper levels of the veins, gold occurs topographically higher but partially overlaps the base metals zone; silver occurs at higher elevations and overlaps the gold zone. This pattern of zoning at the vein scale is consistent with the zoning pattern proposed by Buchanan (1981) for epithermal veins.

Zoning of epithermal veins with greater base metal contents at depth and greater precious metal contents at shallow elevations has been observed in other Mexican IS epithermal deposits, and has been attributed to evolution in time and space of the hydrothermal fluids (Camprubí and Albinson, 2007). Fluid inclusion studies in Fresnillo reveal that the Jarillas and Valdecañas veins have greater mean and modal Th and salinity values than the Santo Niño vein. Figure 31 is a Th vs. salinity plot for fluid inclusion data

of the Santo Niño (Simmons, 1986), Jarillas and Valdecañas veins, and shows how the majority of data points from Santo Niño plot at lower Th and salinity values, whereas the data points of Jarillas and Valdecañas plot at greater Th and salinity. Similarly, it was determined that the ranges in $\log f S_2$ of Jarillas (-3.6 to -11.9) and Valdecañas (-5.2 to -11.7) are high with respect to the $\log f S_2$ values of Santo Niño (-10.5 to -17.9; Benton, 1991); and that these differences in sulfur fugacities suggest zoning at the district scale from more IS in the west to more LS to the east. Alternatively, these observations could indicate that the sources of fluids for Santo Niño and Jarillas-Valdecañas are different. If the veins were formed by the fluids with a common source, then the greater sulfur fugacities, temperatures, and salinities to the west could also indicate proximity to an intrusion. Unfortunately, we do not know the age of any of the veins in Fresnillo-SE, but because of similarities already mentioned between the veins of the two areas, it is possible that they are cogenetic.

Another line of evidence in support of fluid evolution in Fresnillo comes from mineralogy. The mineralogy of Jarillas and Valdecañas indicates that the system evolved from deposition of base metals as, sphalerite, galena and pyrite, to deposition base metals with silver sulfosalts associated with quartz, calcite, adularia and epidote, to deposition of carbonates, quartz and pyrargyrite, and finally to deposition of quartz, calcite and pyrite. Additionally, for the Jarillas and Valdecañas veins, petrography reveals that sphalerite from Stage 1 has dark-brown to black cores indicative of greater Fe contents, associated with chalcopyrite disease and inclusions of pyrrhotite, whereas rims are translucent, with no chalcopyrite and pyrrhotite. The iron content of sphalerite depends on sulfur activity; as the activity of sulfur increases, the activity of FeS decreases and causes the solubility
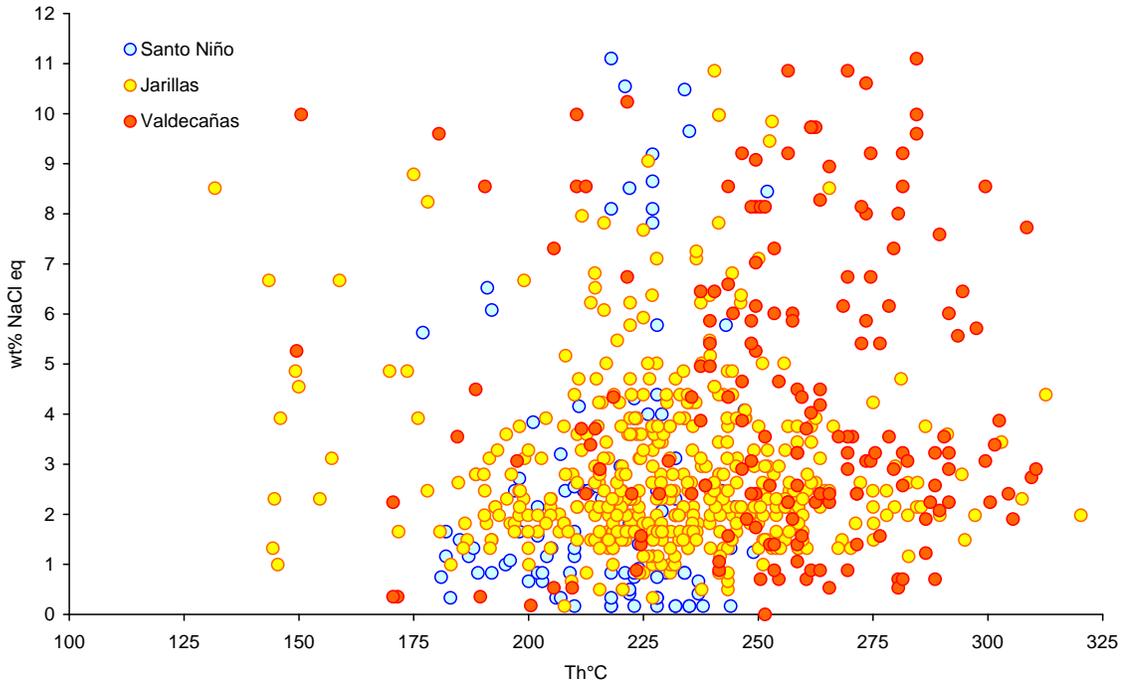
Fig. 31. Th vs. salinity plot for fluid inclusion data of Santo Niño (Simmons, 1986), Jarillas and Valdecañas veins showing trend of increasing temperature and salinity.

of iron in sphalerite to decrease (Vaughan and Craig, 1997). The presence of pyrrhotite in the cores but not in the rims of sphalerite is therefore interpreted to indicate a progressive increase in sulfur activity through time. If this ascertion is correct then it is possible that the fluids that deposited Stage 1 sulfides evolved from LS to HS compositions. Additionally, it is observed that low-Fe sphalerite in Stage 3 is occasionally accompanied of bands of quartz-hematite, which could also reflect that the increase in sulfur activity was accompanied by an increase in oxygen fugacity. Gemmell et al. (1988) similarly interpreted a progressive increase in both sulfur activity and oxygen fugacity from the early to the late mineralization stages based on mineralogy and mineral chemistry of the Santo Niño vein. Camprubí and Albinson (2007) found similar evidence consistent with

fluid evolution at La Guitarra, Mexico, where FeS molar contents in sphalerite also decrease through paragenesis.

Thus, it is possible that the variations observed at vein scale correspond to fluid evolution from LS to IS stage, reflecting boiling, mixing of hydrothermal fluids with meteoric water through time, or water-rock interaction. Initially, at low water rock ratios, the fluids would have been buffered more efficiently by host rocks; enduring later evolution of the system, at greater water-rock ratios, the buffering capacity of the host rock would lower. As a result, more reduced fluids would have deposited high-Fe sphalerite with pyrrhotite at Stage 1, and more oxidized fluids deposited low-Fe sphalerite and quartz-hematite bands at Stage 3. In comparison, a decrease in temperature and sulfur fugacity through paragenesis is attributed to fluid evolution caused by progressive influx of larger volumes of meteoric water in the Jeongju-Buan district, Korea (So and Yun, 1996).

Ore deposition

Boiling of fluids has been observed and suggested as the main mechanism for ore deposition in Fresnillo (Simmons, 1988; Dilley, 1993; Eckberg, 1999). In the Jarillas and Valdecañas veins, we see coexisting liquid-rich and vapour-rich inclusions which indicate boiling. Unfortunately, we were only able to homogenize two vapour-rich inclusions; both temperatures were consistent with the homogenization temperatures of the coexisting liquid-rich inclusions, as should be the case with simultaneous trapping of liquid and vapor phase during boiling. Discrimination plots of CO_2/N_2 gas ratios versus the log of total gas content for some samples show linear trends with negative slope which are indicative of boiling (Norman et al., 2002) (Fig. 32).
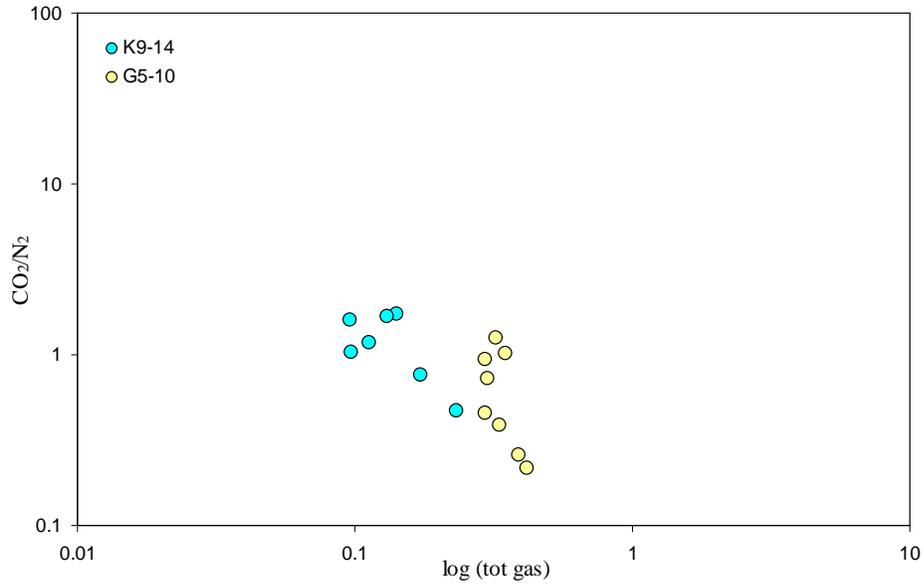
Fig. 32. CO_2/N_2 vs. log (tot gas) of two samples from Jarillas vein. The linear trend with negative slope suggest CO_2 loss due to boiling (Norman et al. 2002).

Other evidence that gives strong support to boiling conditions are the occurrence of adularia and epidote in Stage 3 of both veins, and bladed quartz after calcite in three holes in the Jarillas vein. Another evidence in favour of boiling conditions during ore deposition is the presence of chalcedonic quartz; which according to Fournier (1985) and Drummond and Ohmoto (1985), deposits due to quartz supersaturation of the fluids after boiling due to adiabatic steam loss and rapid cooling. In spite of all this evidence in favour of boiling, mixing with cooler meteoric water cannot be ruled out as a possible mechanism of deposition, at least at the late stages, due to the gas chemistry that suggest the involvement of meteoric water, including the occurrence of bands of quartz-hematite that could suggest incursion of oxidized meteoric water.

Conclusions

The fluid inclusion microthermometry and geochemistry data from Fresnillo still leave some unresolved questions about the source(s) of the mineralizing fluids.

Nonetheless, it has been determined that the veins in Fresnillo-SE and Fresnillo-SW are cogenetic, which permit us to interpret physiochemical zoning at the district scale and propose the possible location of the thermal center of the district.

At the vein scale, paragenetic observations indicate that fluids might have evolved from reduced LS to more oxidized IS solutions. In Fresnillo-SE, boiling has been documented and is suggested as the main process responsible for ore deposition. Evidences from gas analyses and mineralogy of the Jarillas and Valdecañas veins, in addition to coexisting liquid-rich and vapor-rich inclusions also suggest boiling conditions during ore deposition.

Maximum salinities of 11 wt % NaCl in Jarillas and Valdecañas suggest magmatic input to the hydrothermal fluids, whereas the heavy $\delta^{18}O$ and δD fluid values are compatible with either magmatic or exchanged meteoric water compositions. In addition, the heavy oxygen and hydrogen isotopic compositions of the alunites are also compatible with magmatic fluids. Gas ratios, on the other hand, suggest that both magmatic and meteoric water were involved during hydrothermal activity. In combination, fluid inclusion, oxygen and hydrogen stable isotope and gas data suggest that the hydrothermal fluids responsible for IS epithermal mineralization could have resulted from either magmatic fluids, deeply circulated and exchanged meteoric waters or a combination of the two.

Sulfur and carbon isotope data suggests that the GT could have been an important contributor of those elements to the hydrothermal fluids that formed the veins. Incorporation of sulfur and carbon to the hydrothermal fluids could have occurred by leaching of the elements during deep circulation of hydrothermal fluids or alternatively

due to assimilation and melting of GT xenoliths (or other rocks making up the basement) in a deep seated magma chamber.

Variations in average homogenization temperature and salinity, sulfur fugacity, and Au/Ag ratios describe a district wide zoning pattern from east to west. It is observed that temperature, salinity, sulfur fugacity and Au/Ag ratios increase from southeast to northwest, which could indicate that the source of heat and fluids lies to the northwest.

CHAPTER III

GEOCHEMICAL ZONING OF THE FRESNILLO INTERMEDIATE

SULFIDATION EPITHERMAL DISTRICT, ZACATECAS, MEXICO

Abstract

The Fresnillo district has produced silver almost continuously for over 450 years and at present contains total resources of approximately 1 BOz. The current production of the district is 7500 tonnes per day from veins averaging 300 to 700 grams per tonne of silver.

Silver ore occurs mainly as silver sulfosalts in intermediate sulfidation epithermal veins. The predominant minerals in the veins are quartz, calcite, pyrite, sphalerite, galena, pyrargyrite and arsenopyrite, in that order of abundance. The veins vary in length from 1.3 to 8.0 km and have average widths of 2.5 to 4.5 meters. Typically the veins strike east-west or northwest-southeast and dip either north or south at angles between 50 and 90 degrees. All the veins are blind to surface and hosted by the Guerrero Terrane volcanosedimentary sequence; the economic zones of the veins typically start 200 meters below surface and the ore bands have vertical extents between 200 and 400 meters.

Longitudinal sections of the veins illustrate that the base metals are concentrated at depth and precious metals at shallow levels which is consistent with metal zoning in boiling systems. Nevertheless, in Fresnillo the gold occurs associated with base metals and not above silver. In Fresnillo, the ore bands defined by Au

85

equivalent values greater than 5 ppm are located between the base metals zones and the high Ag/Pb bands. We observe that a late stage of mineralization carrying silver reached higher elevations in the vein and overlapped previous mineralizing stages, which modified the original metal ratios; particularly the Au/Ag ratios. Late mineralizing events could have deposited variable concentrations of silver across the district and thus, those later events could have modified the Au/Ag ratios differently in Fresnillo-SE and Fresnillo-SW.

Our results indicate that the gold concentrations and the Au/Ag ratios of the veins in Fresnillo-SW are consistently higher with respect to those of Fresnillo-SE, which is coincident with a trend of increasing average fluid inclusion homogenization temperatures, salinities and sulfur fugacity. High Au/Ag ratios and low base metal contents in the Saucito, San Antonio and San Mateo veins suggests that these veins occur distaly with respect to the possible center of the district. Therefore we suggest that the thermal center of the district was to the northwest of San Carlos and Valdecañas veins. We believe that overall, the hydrothermal fluids flowed laterally across the district from northwest to southeast imposing a district wide zoning pattern and that locally, in the open faults and fractures where the veins were formed, the fluids ascended vertically and boiled, causing vertical zoning.

Introduction

The Fresnillo mine has produced silver almost continuously for more than 450 years. It produced 400 MOz of silver during the 20th century. At present, Fresnillo is a world class district with Intermediate Sulfidation (IS) epithermal veins in two areas: Fresnillo-SE, which hosts the currently producing veins, e.g., Santo Niño and San Carlos;

and Fresnillo-SW, which contains a set of IS epithermal veins that were discovered in the last 6 years, e.g., Saucito, Jarillas and Valdecañas (Fig. 33). Hitherto, Fresnillo-SE contains resources (measured and indicated) of 52.7 Mt at an average grade of 374 grams per tonne of silver (~0.64 BOz). Extensive drilling exploration lead to the discovery of Saucito, Jarillas and Valdecañas veins in Fresnillo-SW which contains measured and indicated resources of approximately 0.17 BOz of silver. Total silver resources of the district (measured, indicated and inferred) are estimated to be approximately of 1BOz.

Dating of adularias in two veins of Fresnillo-SW revealed ages of 29.68 to 29.75 Ma for the IS epithermal veins and an age of 32.65 +/- 0.05 Ma for the Fortuna stock in the Fortuna-Proaño area, indicating that the Fortuna intrusion is too old to be the source of heat of hydrothermal activity related to vein deposition (Velador et al., 2010a; submitted). However, none of the veins in Fresnillo-SE have been dated so far, therefore it is not possible to determine whether the veins in the two areas are coeval. Similarities in mineralogy, paragenesis, and stable isotope geochemistry suggest that they could be cogenetic (Velador et al., 2010b; in preparation; Earthman et al., 2010; in preparation). In spite of the similarities shared by the veins, there are some physio-chemical variations that suggest zoning at the district and vein scale: variations are observed in fluid inclusion homogenization temperature (Th), salinity (wt% NaCl equivalent) and sulfur fugacity between Santo Niño vein (Fresnillo-SE) and Jarillas and Valdecañas veins (Fresnillo-SW) (Velador et al., 2010b; in preparation).

Major questions in the genesis of epithermal deposits are: what is the source of fluids and what was the fluid flow direction. The purpose of this study is to use chemical assay data from Santo Niño and San Carlos veins in Fresnillo-SE and from Saucito,

Jarillas and Valdecañas veins in Fresnillo-SW to investigate zoning in metal ratios and

metal concentrations across the district. The results from the study are interpreted in

conjunction with temperature, salinity and sulfur fugacity data to make inferences about

the possible locus of the thermal center of the district and fluid flow direction.
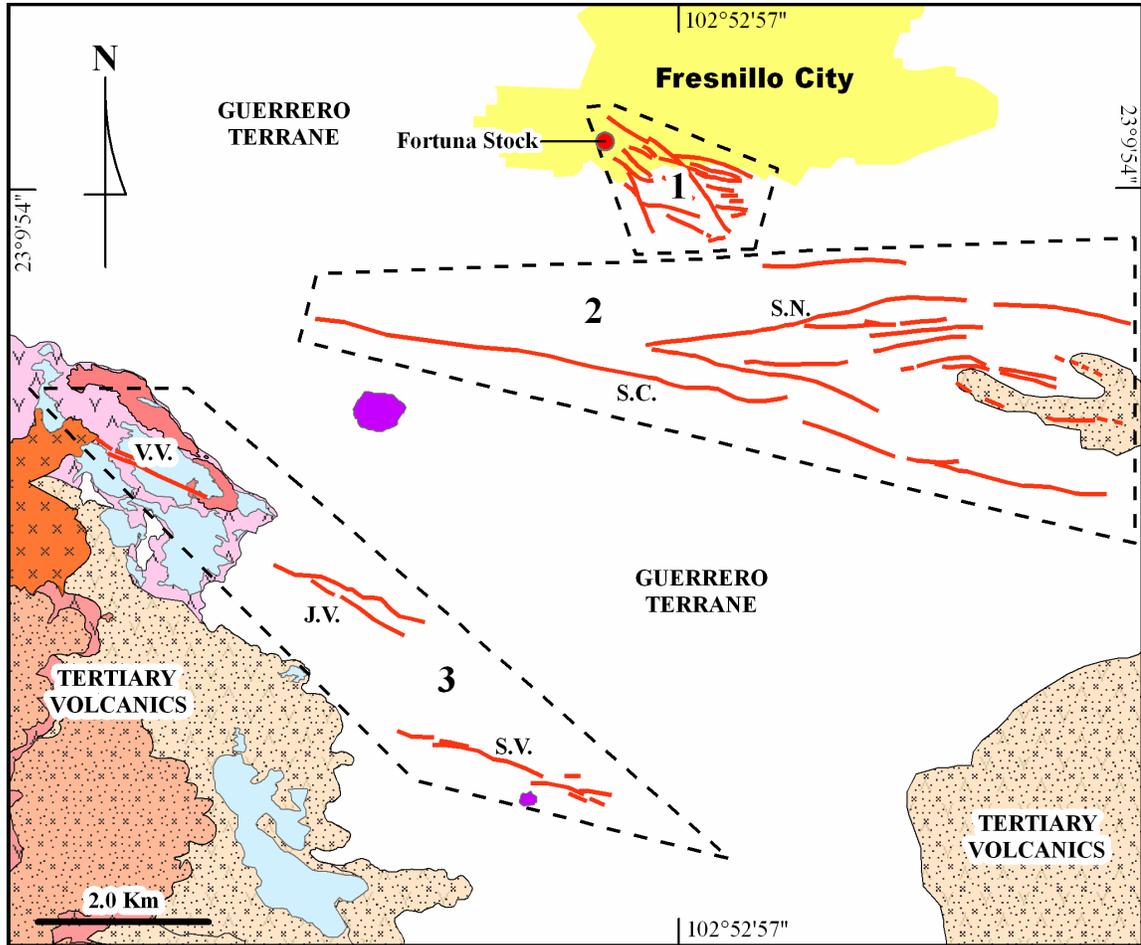
Fig.33. Geologic map of Fresnillo showing location of the Fortuna-Proaño area (1), Fresnillo-SE (2), Fresnillo-SW (3) and veins. Abbreviations; Santo Niño (S.N.), San Carlos (S.C.), Saucito (S.V.), Jarillas (J.V.) and Valdecañas (V.V.).

Geology

Fresnillo is located within the Mesa Central physiographic province (MC) which

is an elevated plateau comprised of marine sedimentary rocks of the Sierra Madre

Oriental (SMOr) terrane to the east and northeast and a sequence of volcanosedimentary rocks of the Guerrero Terrane (GT) to the southwest. These terranes are partially and unconformably overlain by volcanic rocks of the Sierra Madre Occidental (SMOc) in the western portions of the MC. The GT forms part of a collage of suspect terranes with arc affinity that were accreted to the west margin of Mexico during the Upper Cretaceous to Early Tertiary (Campa and Coney, 1982). The geochemistry, evolution and accretion of the GT are discussed by Campa and Coney (1982), Centeno-Garcia et al. (1993), and Mortensen et al. (2008).

In Fresnillo, the GT is separated into two domains; a predominantly sedimentary domain at the base and a predominantly volcanic domain on top. The sedimentary domain is separated into: "lower graywacke" consisting of a rhythmic sequence of graywackes interbedded with carbonaceous and calcareous shales and occasional tuffs and lava units; "middle unit" consisting of black carbonaceous and calcareous shales with occasional chert lenses and minor graywackes; and the "upper graywacke" consisting of alternating graywackes with minor black carbonaceous and calcareous shales, tuffs and lavas (De Cserna, 1976; Ruvalcaba-Ruiz and Thompson, 1988) (Fig. 34). The volcanic domain is locally described as the Chilitos formation, and consists of andesitic to basaltic lava flows with pillow lava structures, tuffs interbedded with black shales and graywackes, lenses of marls, limestones and laharic type volcanic epiclastic rocks (De Cserna, 1976; Ruvalcaba-Ruiz and Thompson, 1988). In Fresnillo, the GT outcrops are relatively small and limited to locations within the valley where there is no cover by Tertiary volcanics, conglomerate or alluvium.

The Tertiary section contains the Late Paleocene to Early Eocene Fresnillo conglomerate at the base (De Cserna, 1976; Ruvalcaba-Ruiz and Thompson, 1988), with overlying trachyte to dacite tuffs, and rhyolite to rhyodacite flows on top (J. M. Velador, unpublished data, 2005). Informal names of Valdecañas, Cierpe, Piedras and Altamira units have been assigned here to the Tertiary volcanics. The Valdecañas unit (44.73 Ma) rests on top of the conglomerate or directly on top of the GT and consists of hydrothermally altered dacite tuffs, whereas the Cierpe unit (40.83 to 40.92 Ma), that overlies the Valdecañas, consists of unaltered to oxidized crystal-lithic tuffs with compositions that straddle the trachyte and dacite fields in a Total Alkali Silica (TAS) diagram (J. M. Velador, unpublished data, 2005; Velador et al., 2010a, in preparation) (Fig. 34).
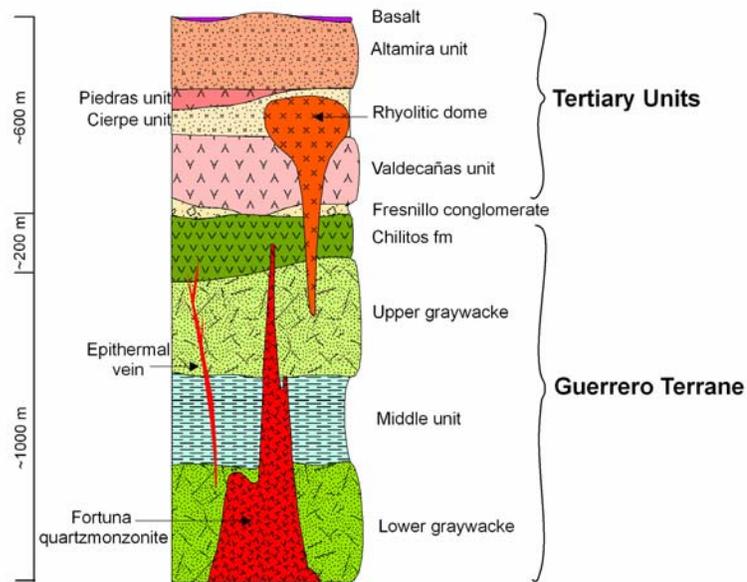
Fig. 34. Schematic stratigraphic column of the Fresnillo District.

The Piedras unit, an unaltered to oxidized crystal-lithic rhyolite tuff and the Altamira unit (31.04 Ma), a weakly to moderately altered porphyritic rhyodacite along with rhyolite domes (31.55 Ma) and flows are the major volcanic units resting

90

unconformably on the Eocene volcanics (J. M. Velador, unpublished data, 2005; Velador et al., 2010a, in preparation) (Fig. 34). Finally, common but sparse Miocene basalt flows represent the latest volcanism in the area (Nieto-Samaniego et al., 2007).

There are three types of intrusive rocks identified in Fresnillo; Middle Jurassic to Early Cretaceous mafic sills and dikes that form part of the GT; Oligocene quartz-monzonite and granodiorite in Fresnillo and Plateros, respectively; and Miocene basalt dikes. The Oligocene Fortuna stock (32.65 Ma) is spatially associated with mineralization in the Fortuna and Proaño areas (De Cserna, 1976; Ruvalcaba-Ruiz, 1980; Chico, 1986; Velador et al., 2010a, in preparation). This intrusion has been proposed as the ore generating stock for skarn, chimney and vein mineralization (De Cserna 1976; Garcia et al., 1991; Eckberg, 1999); however recent argon geochronology revealed that the intrusion is ~3 My older that IS epithermal mineralization which rules out its possible genetic connection with the veins (Velador et al., 2010a; in preparation).

Ore deposits

Mineralization in Fresnillo occurs in four areas: the Proaño area, the site for ore discovery in 1554, which contained silver mineralization in an oxidized stockwork; the Fortuna area, which contained silver, lead and zinc mineralization occurring in manto, chimney and vein deposits, spatially related to the Fortuna stock (De Cserna et al., 1977; Ruvalcaba-Ruiz, 1980; Chico, 1986); the Fresnillo-SE area which consists of high grade silver, lead and zinc, intermediate sulfidation epithermal veins such as Santo Niño and San Carlos (Trejo, 2001); and finally the recently discovered Fresnillo-SW area comprising the high-grade silver, gold, lead and zinc, intermediate sulfidation Saucito,

91

Jarillas and Valdecañas veins. In this study we refer to the Fortuna and Proaño deposits as the Fortuna-Proaño area.

Mineralization in Fresnillo-SE and Fresnillo-SW is blind to surface and for the most part hosted by the sedimentary units of the GT. The veins trend east-west to northwest-southeast, dip north or south at angles between 50° and 90°, have lengths varying between 1.3 to ~8 km and widths of 10's cm to 10's m. Typical vertical extents of ore bands vary from 200 to 400 meters.

Textural and mineralogical similarities, as well as stable isotope geochemistry, suggest a genetic connection between the veins of the Fresnillo-SE and Fresnillo-SW areas (Velador et al., 2010b, in preparation). The veins are characterized by occurrence of: argillic alteration, silicification and early brecciation of wall rock; deposition of massive sphalerite and galena at depth; deposition of alternating bands of sulfides (galena, sphalerite, pyrite, arsenopyrite, chalcopyrite and pyrrhotite), quartz, chalcedony, calcite, epidote and minor adularia; and deposition of late stage veins of barren quartz, calcite, and in some places fluorite. The silver sulfosalts (pyrargyrite, polybasite, stephanite and proustite), sulfides (acanthite, aguilarite) and electrum are the most important Ag-bearing minerals, and occur generally associated with galena and sphalerite or disseminated in quartz and calcite bands. Mineral deposition occurred in four stages in Santo Niño and San Mateo veins according to Gemmell (1986), and Dilley (1993). In Jarillas and Valdecañas, mineral deposition occurred in five stages; however three stages were the most important in terms of ore deposition, and they are present in the veins of both areas. Detailed descriptions of the mineralogy and paragenesis of the Santo Niño and Jarillas - Valdecañas veins are given in Gemmell et al. (1988) and Velador et al.

(2010b, in preparation), respectively. In general, all the veins show vertical zoning: base metals being more abundant at deeper levels and banded veins of quartz and calcite with lesser sulfides being more abundant at shallower levels.

Structure

Accretion of the GT to Mexico during the late Cretaceous to Early Tertiary led to a thin-skinned deformation defined by low-angle NW-trending thrusts-faults (Campa and Coney, 1982; Simmons, 1986; Trejo, 2001; Starling, 2006). Accretion occurred during the Laramide orogeny which operated in that part of Mexico between ~90 Ma and ~37 Ma (Nieto-Samaniego et al., 2007). Rhyolitic vulcanism and E-W to N-S extension started in the region in the Oligocene. The N-S extension was accompanied by sinistral trans-tensional reactivation of the low-angle NW thrust-faults, which produced the N-S extension produced E-W to NW-SE normal faults and tension fractures between the sets of reactivated NW thrust-faults, which facilitated hydrothermal fluid-flow and vein deposition at ~29.70 Ma (Starling, 2006; Nieto-Samaniego et al., 2007). Kinematic indicators, such as tension gashes, with orientation N70°W were observed in some of the scant outcrops of the GT. These indicators, along with the mineralized veins themselves, are evidence of the N-S extension of the Eocene - Oligocene. A second E-W extension event started in the Miocene which produced NNE and NW oriented normal faulting and tilting of the Eocene and Oligocene volcanics. The NNE and NW normal faults are interpreted to be post-mineralization and more representative of the Basin and Range type extension (Starling, 2006; Nieto-Samaniego et al., 2007).

Methods

Over 50,000 chemical assays from channel samples from all mine levels of the San Carlos and Santo Niño veins and assays of vein intercepts from over 250 drill-holes in Saucito, Jarillas and Valdecañas veins were used in this study. Assays covering 2576 meters of the central portion of Santo Niño and 4430 meters of the central portion of San Carlos veins were used. The assays for the Saucito, Jarillas and Valdecañas are from drill-holes that have average separations of 100 meters in the vertical direction and 200 meters in horizontal direction.

The chemical analyses for the Santo Niño and San Carlos veins were performed in the chemistry laboratory of the Fresnillo mine. Chemical analysis for Saucito Jarillas and Valdecañas were done commercially by ALS Chemex. In both cases, gold analyses are performed by fire assay atomic absorption spectrometry (AAS) and silver by inductively coupled plasma mass spectrometry (ICP-MS). High grade samples with gold concentrations >10 ppm and/or silver concentrations >200 ppm are analyzed by the fire assay gravimetric method. The Pb, Zn, Cu, As, Sb and Hg are analyzed by ICP-MS and those samples with Zn, Pb, and Cu concentrations >1% were also analyzed by AAS for more accuracy. Approximate detection limits for the elements are: Au=0.005 ppm, Ag=0.2 ppm, Pb, Zn and Cu=0.5 ppm.

Interpolation of data and creation of longitudinal sections for the five veins was done using the Kriging interpolation function built in the Surfer software, version 8.05. The basic statistics, minimum, maximum, mean and standard deviation were calculated for every vein. Correlation matrices were also calculated for every vein in order to identify the elements or metal ratios more suitable for plotting in longitudinal sections.

Results

94

The data used in this study is in units of parts per million (ppm) for Au, Ag, As and Sb and in per cent (%) for Pb, Zn, Cu, and Hg. Table 8, summarizes the basic statistics of the precious and base metal assay data and the calculated Au/Ag ratios. The average values for Au concentrations of the Fresnillo-SW veins range between 1.66 to 4.35 ppm, whereas the average Au concentrations of the two veins in Fresnillo-SE are 0.56 and 1.06 ppm. The average Pb+Zn values for all veins range between 1.52 and 4.60 per cent; the lowest value being for Saucito and the highest value being for Valdecañas vein. The Au/Ag ratios form a wide range from 1×10^{-3} (1:1000) in San Carlos vein to 5.6×10^{-2} (1:18) in Saucito vein. Cu values are generally low and erratic and occur at deeper levels. The average Cu values in the four veins that have copper assays in the data base, range from 0.02 to 0.09 per cent.

Correlation matrices were calculated for the assay data of every vein separately (Table 9). The calculations show that Ag and Sb have the highest correlation in Jarillas (0.9) and Valdecañas (0.7); there is no Sb data for the other veins. The high correlation between Ag and Sb supports the observation that pyrargyrite (Ag_3SbS_3) is the most abundant sulfosalt in both veins. On the other hand, the correlation coefficient of Ag with respect to Pb and Zn is never greater than 0.5 (0.1 to 0.5) which suggests that the spatial distribution of silver in the vein does not completely overlap that of lead and zinc. The correlation between Ag and Cu is low, and ranges between 0.0 and 0.3 and also suggests that silver and copper do not coexist. The correlation between Au and Ag (0.1 to 0.4) is low, as well as the correlation between Au and Pb, Zn and Cu (0.1 to 0.5), which suggests that the distribution of Au within the vein does not match exactly either the distribution of Ag, nor the distribution of base metals. In order to illustrate the

distribution of the elements in the veins, we prepared longitudinal sections for the five veins using the chemical assays and their corresponding "x" (easting) and "y" (elevation) coordinates.

Longitudinal sections of Ag/Pb, Au/Ag, Pb+Zn+Cu and Au equivalent (eq.) were plotted for the Jarillas, Valdecañas and Saucito veins of Fresnillo-SW; Pb+Zn was plotted only, instead of Pb+Zn+Cu, for Saucito vein due to the lack of Cu values in the data set (Figs. 35, 36, and 37). Longitudinal sections of Ag/Pb, Au/Ag and Pb+Zn+Cu were plotted for the central portions of the Santo Niño and San Carlos veins in Fresnillo-SE (Figs. 38 and 39). The sections for Au eq. of these veins were plotted, but they are not presented here because the distribution of the Au eq. representing the ore band, is almost identical to that of silver in the Ag/Pb section.

The longitudinal sections of the veins show that Pb, Zn and Cu are concentrated at depth and that the precious metals occur at shallow elevations, above the base metals zones. Additionally, the ore bands defined by Au eq. values greater than 5 ppm (gr/ton), have undulatory shapes and occur between the base metals zone and a band defined by high Ag/Pb ratios. The ratio used for calculating gold equivalent values was 1:63; 1 gram of gold equals 63 grams of silver and is based on the average prices of gold and silver for the present year.

Table 8. Summary table showing basic statistics for the veins, Santo Niño and San Carlos (Fresnillo-SE) and Saucito, Jarillas and Valdecañas (Fresnillo-SW).

	Minimun	Maximum	Mean	Std dev
Santo Niño (n=15960)				
Au ppm	0.00	69.90	1.06	2.22
Ag ppm	12.00	26347.00	991.21	1505.16
Pb %	0.00	29.57	0.88	1.37
Zn %	0.00	52.00	1.85	2.24
Cu %	0.00	1.02	0.07	0.21
Au/Ag	0.0E+00	2.1E-01	1.7e-3 (1:588)	4.5E-03
San Carlos (n=34103)				
Au ppm	0.00	161.00	0.56	1.77
Ag ppm	3.00	44376.00	1025.20	1625.68
Pb %	0.00	28.10	0.84	1.57
Zn %	0.00	43.36	1.41	2.02
Cu %	0.00	0.60	0.02	0.20
Au/Ag	0.0E+00	1.4E+00	1.0e-3 (1:1000)	9.5E-03
Saucito (n=90)				
Au ppm	0.01	23.10	4.35	5.17
Ag ppm	0.70	2510.00	306.84	443.86
Pb %	0.00	5.04	0.62	0.84
Zn %	0.00	9.87	0.90	1.63
Au/Ag	2.5E-04	5.9E-01	5.6e-2 (1:18)	9.8E-02
Jarillas (n=76)				
Au ppm	0.01	54.27	2.77	6.95
Ag ppm	0.30	4070.46	306.80	554.47
Pb %	0.00	4.71	0.66	0.82
Zn %	0.00	10.15	1.23	1.62
Cu %	0.00	0.45	0.06	0.08
As ppm[1]	0.00	>10000	1976.02	2062.89
Sb ppm	0.00	1866.01	183.81	245.19
Hg %	0.00	1.70	0.19	0.28
Au/Ag	5.3E-04	2.4E-01	1.8e-2 (1:55)	3.3E-02
Valdecañas (n=62)				
Au ppm	0.02	9.47	1.66	1.81
Ag ppm	4.75	2279.00	574.52	645.79
Pb %	0.00	10.11	1.69	2.01
Zn %	0.00	14.42	2.91	2.80
Cu %	0.00	0.81	0.09	0.12
As ppm[1]	89.00	>10000	2934.38	2747.95
Sb ppm	9.00	854.00	158.78	166.05
Hg %	0.00	0.98	0.19	0.21
Au/Ag	2.0E-04	4.0E-02	6.8e-3 (1:147)	8.7E-03

1. Only one value >10000 was found in each data set.

Values in parenthesis (ppm Au : ppm Ag)

Table 9. Correlation matrices for Santo Niño and San Carlos (Fresnillo-SE) and Saucito, Jarillas and Valdecañas (Fresnillo-SW).

Santo Niño

	Au	Ag	Pb	Zn	Cu
Au	1.0				
Ag	0.3	1.0			
Pb	0.4	0.4	1.0		
Zn	0.4	0.3	0.7	1.0	
Cu	0.1	0.1	0.2	0.2	1.0

San Carlos

	Au	Ag	Pb	Zn	Cu
Au	1.0				
Ag	0.2	1.0			
Pb	0.1	0.5	1.0		
Zn	0.1	0.5	0.7	1.0	
Cu	0.1	0.3	0.4	0.5	1.0

Saucito

	Au	Ag	Pb	Zn
Au	1.0			
Ag	0.4	1.0		
Pb	0.2	0.1	1.0	
Zn	0.2	0.2	0.9	1.0

Jarillas

	Au	Ag	Pb	Zn	Cu	Hg	As	Sb
Au	1.0							
Ag	0.1	1.0						
Pb	0.4	0.5	1.0					
Zn	0.2	0.3	0.8	1.0				
Cu	0.5	0.0	0.5	0.4	1.0			
Hg	0.1	0.2	0.2	0.2	0.1	1.0		
As	0.0	0.2	0.3	0.5	0.1	0.3	1.0	
Sb	0.1	0.9	0.6	0.4	0.0	0.2	0.5	1.0

Valdecañas

	Au	Ag	Pb	Zn	Cu	Hg	As	Sb
Au	1.0							
Ag	0.4	1.0						
Pb	0.2	0.4	1.0					
Zn	0.3	0.4	0.9	1.0				
Cu	0.1	0.1	0.8	0.7	1.0			
Hg	0.1	0.2	0.2	0.2	0.1	1.0		
As	0.4	0.2	0.1	0.4	0.0	0.2	1.0	
Sb	0.5	0.7	0.3	0.4	0.0	0.4	0.4	1.0
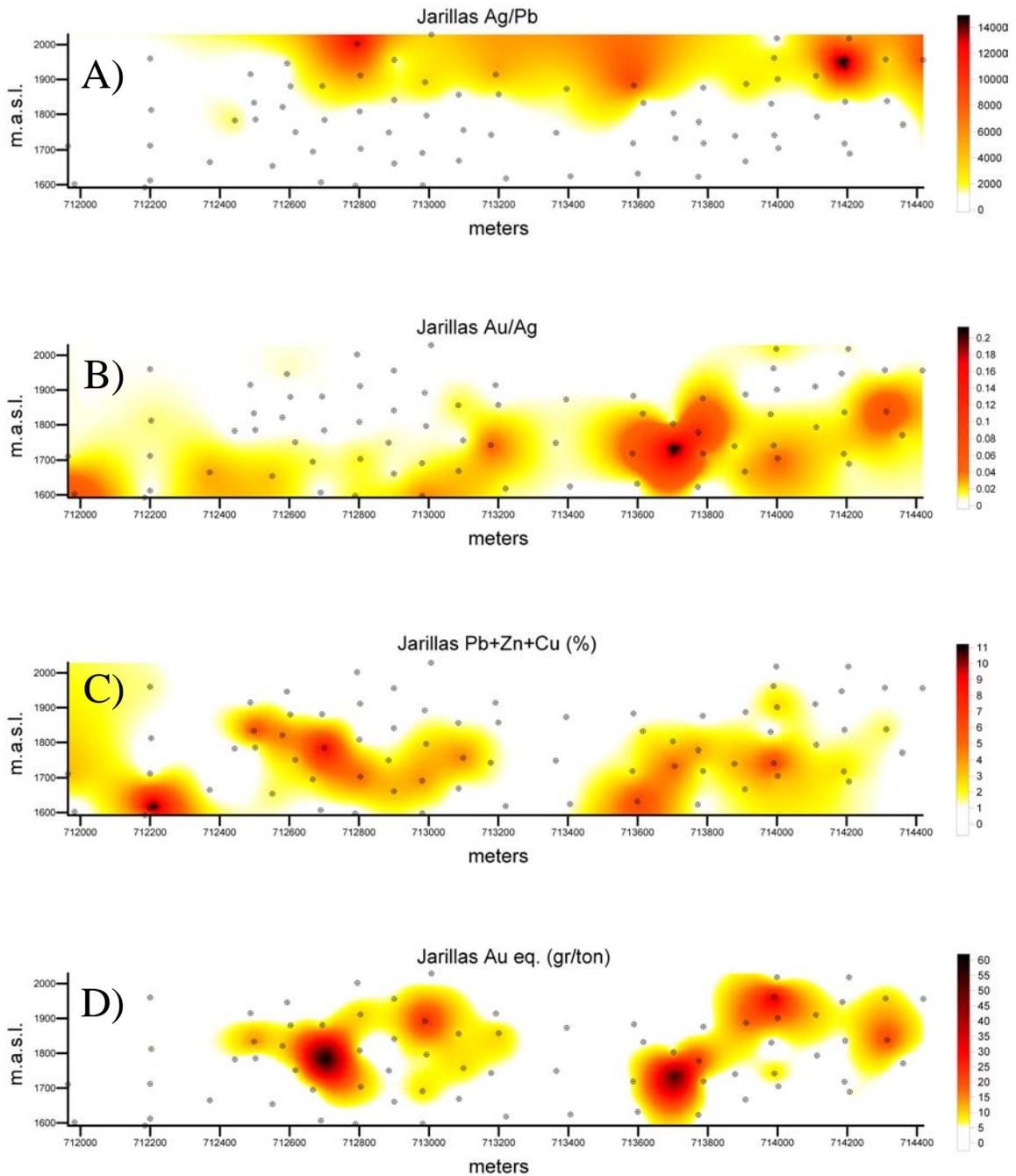
Fig. 35. Longitudinal sections of Jarillas vein. A) Ag/Pb ratios (>1000) showing the distribution of silver with respect to lead. B) Au/Ag ratios (>0.01) showing the distribution of gold with respect to silver. C) Pb+Zn+Cu (>1%). D) Distribution of gold equivalent values >5 gr/ton (ppm) showing the undulatory ore band. Elevation in meters above sea level (m.a.s.l.) and distance is in meters, the numbers represent the east coordinate in UTM.
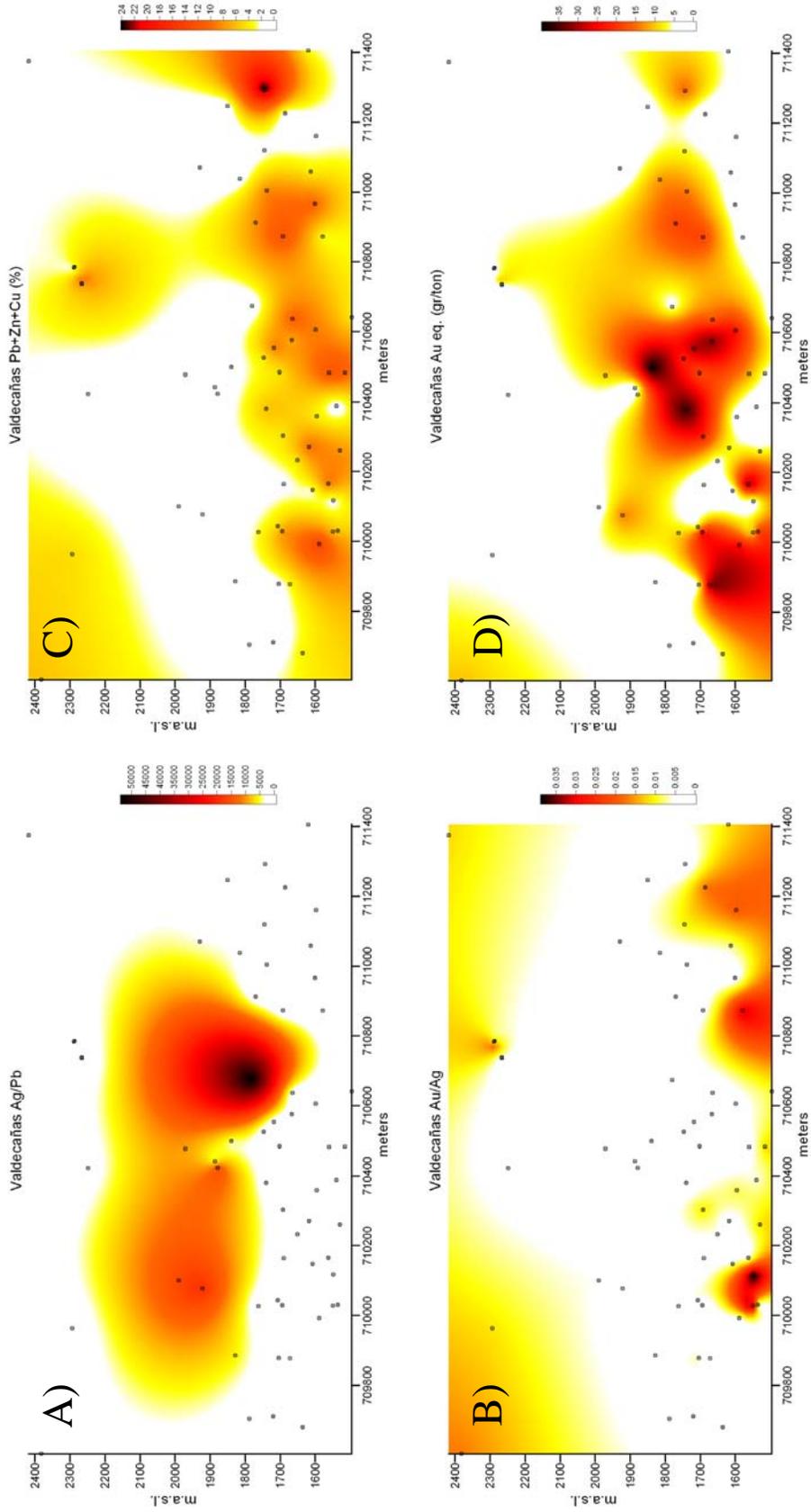
Fig. 36. Longitudinal sections for Valdecañas vein. A) Ag/Pb ratios (>2500) showing the distribution of silver with respect to lead. B) Au/Ag ratios (>0.005) showing the distribution of gold with respect to silver. C) Pb+Zn+Cu (>2%). D) Distribution of gold equivalent values >5 gr/ton (ppm) showing the undulatory ore band. Elevation and horizontal scale, same as in Figure 1. The small circles are the drill hole intercepts.
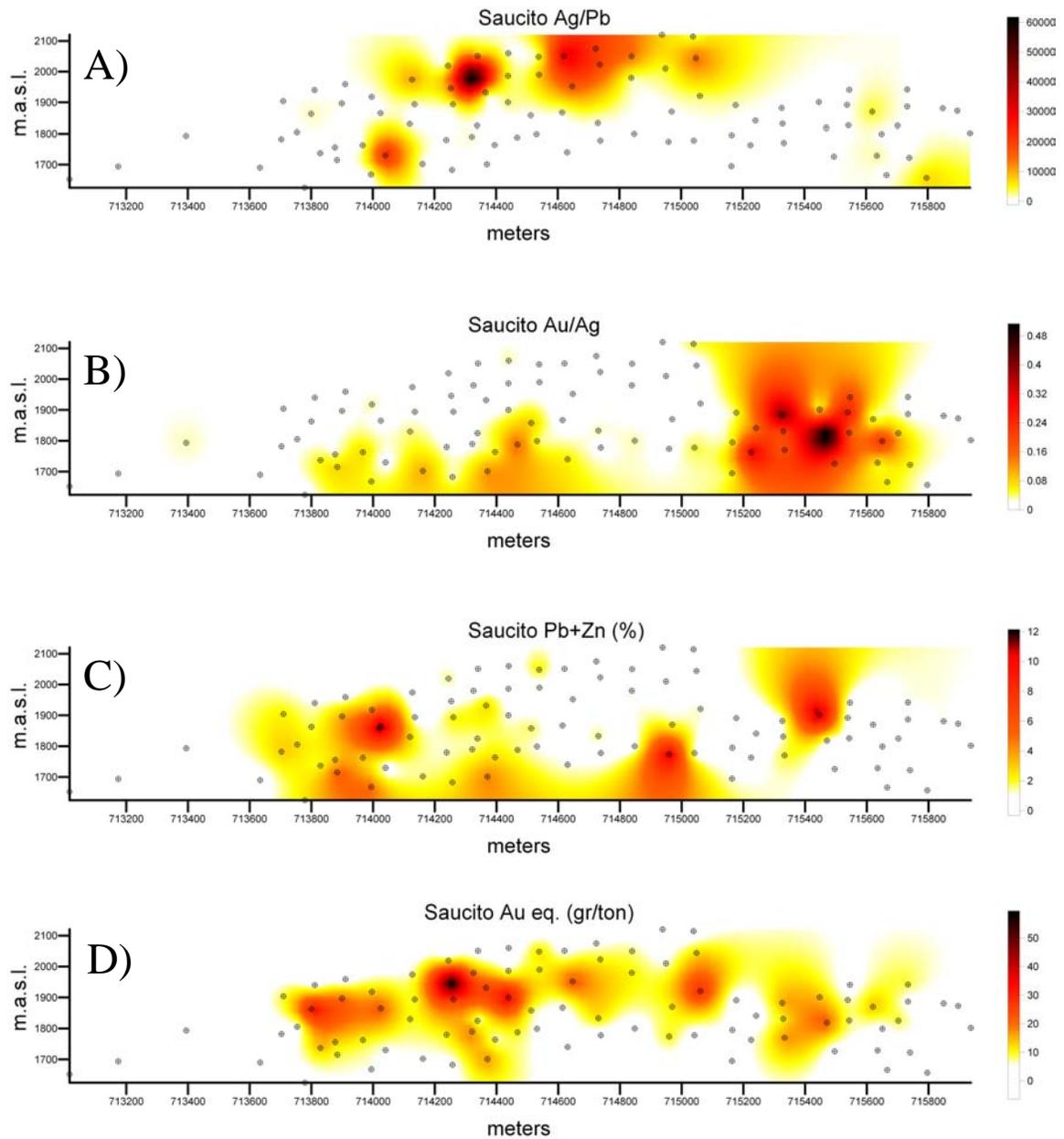
Fig. 37. Longitudinal sections of Saucito vein. A) Ag/Pb ratios (>2000) showing the distribution of silver with respect to lead. B) Au/Ag ratios (>0.03) showing the distribution of gold with respect to silver. C) Pb+Zn (>1%). D) Distribution of gold equivalent values >5 gr/ton (ppm) showing the undulatory ore band. Elevation in meters above sea level (m.a.s.l.) and distance is in meters, the numbers represent the east coordinate in UTM.
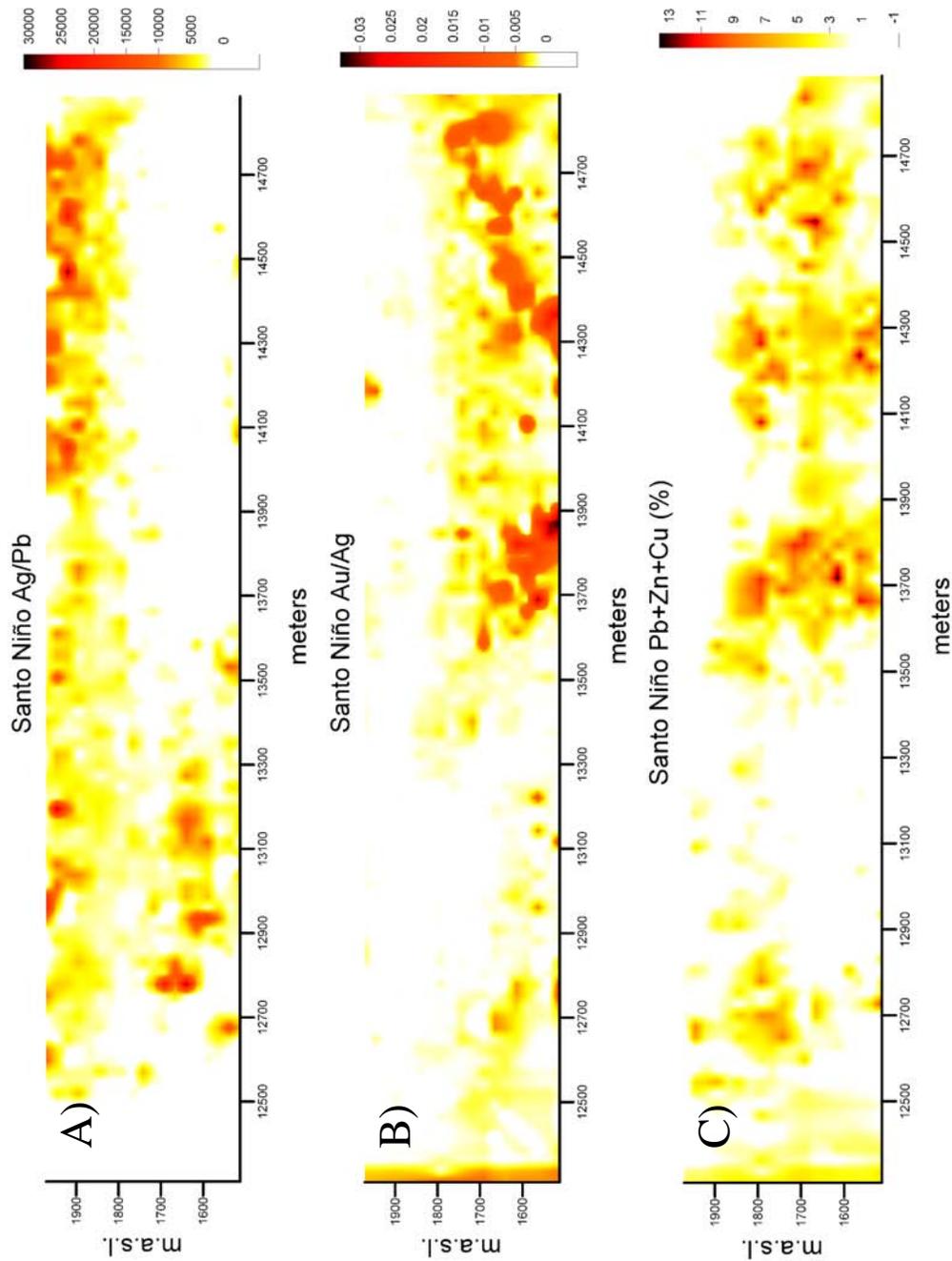
Fig. 38. Longitudinal sections for Santo Niño vein. A) Ag/Pb ratios (>2000) showing the distribution of silver with respect to lead. B) Au/Ag ratios (>0.001) showing the distribution of gold with respect to silver. C) Pb+Zn +Cu (>2%). Elevation and horizontal scale, same as in Figure 1.
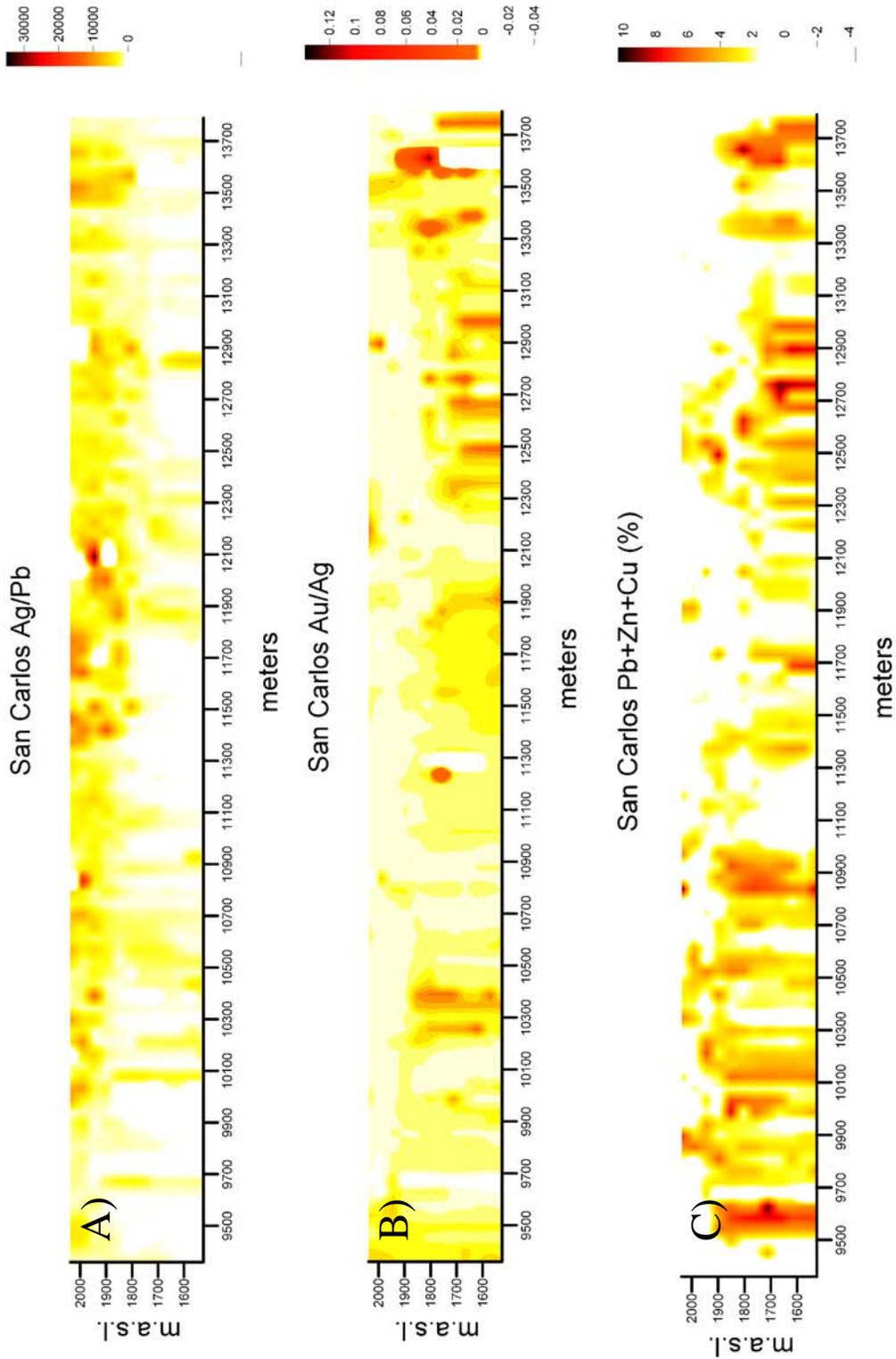
Fig. 39. Longitudinal sections for San Carlos vein. A) Ag/Pb ratios (>1000) showing the distribution of silver with respect to lead. B) Au/Ag ratios (>0.005) showing the distribution of gold with respect to silver. C) Pb+Zn+Cu (>2%). Elevation and horizontal scale, same as in Figure 1.

103

Discussion

Variations in metal concentrations and metal ratios are observed to occur between the Jarillas, Valdecañas and Saucito veins in Fresnillo-SW and the Santo Niño and San Carlos veins in Fresnillo-SE. Variations are also observed to occur at the scale of individual veins in vertical longitudinal sections. These variations at both scales are evidence of geochemical zoning. Homogenization temperatures, salinities and sulfur fugacity data also show variations at the district scale and may be related to fluid evolution (Velador et al., 2010b; in preparation).

Zoning at vein scale

The longitudinal sections show clearly that silver occurs at higher elevations with respect to base metals, which is supported by the observation that stage 3 (banded vein) and stage 4 (vein of quartz-carbonates with pyrargyrite) occur generally above the zone rich in base metals. The base metals occur at the deepest levels, whereas gold seems to occur in a zone overlapping and slightly above the base metals zone. SEM analyses done for metallurgical tests in the veins of Fresnillo-SW revealed that sphalerite contains inclusions of electrum (Fig. 40). Gold also overlaps partially the bottom of the silver zone. Hence, it appears that gold occurs in a band overlapping both the base metals and silver zones, which is confirmed by the distribution of Au eq. values greater than 5 ppm. This observation contradicts the typical zoning pattern caused by boiling in epithermal veins, where base metals occur at depth, silver at intermediate depth and gold at shallow depth (Buchanan, 1981; Drummond and Ohmoto, 1985). This anomalous position of the high Au grades associated with base metals and overlaid by a zone with high Ag/Pb ratios is also observed in the Cienega Mine, Durango, Mexico (De La Garza et al., 2001).

104

In the Purisima-Colon vein system, Pachuca, Mexico, the base metals are concentrated at depth, and there is an intermediate-depth zone with high silver grades overlapping the base metals zone (Dreier, 2005). In Jarillas and Valdecañas veins, a late mineralizing stage (stage 4) consisting of pyrargyrite associated with calcite, dolomite-ankerite and quartz, could be the responsible for the higher silver grades above and overlapping the gold zone (Fig. 41). The superposition of stage 4 upgraded the Ag grades of the veins and perhaps is responsible for the undulatory Au eq. bands sandwiched between the base metals and the high Ag/Pb bands in Jarillas, Valdecañas and Saucito veins.
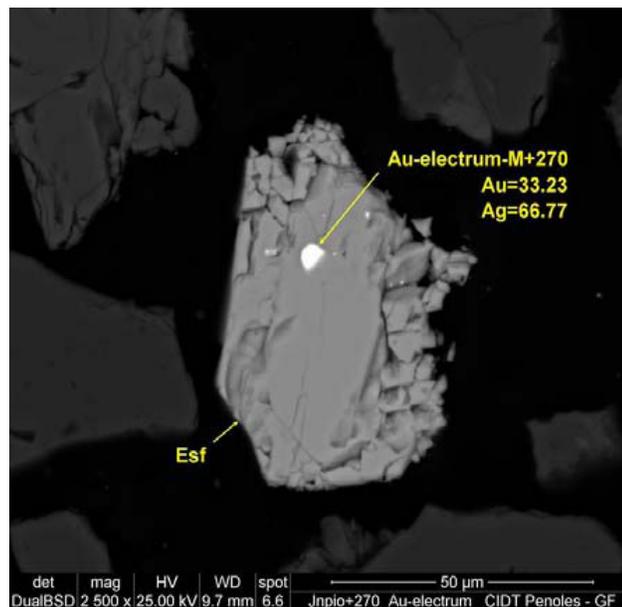
Fig. 40. SEM image showing an inclusion of electrum in sphalerite.

Zoning at the district scale

Direct observation of average Au concentration, allow us to see that the Santo Niño and San Carlos veins have lower gold values than the known ore band portions of the Jarillas, Valdecañas and Saucito veins. More interestingly is the fact that Saucito, being the southernmost vein in the district, has the highest average Au value.
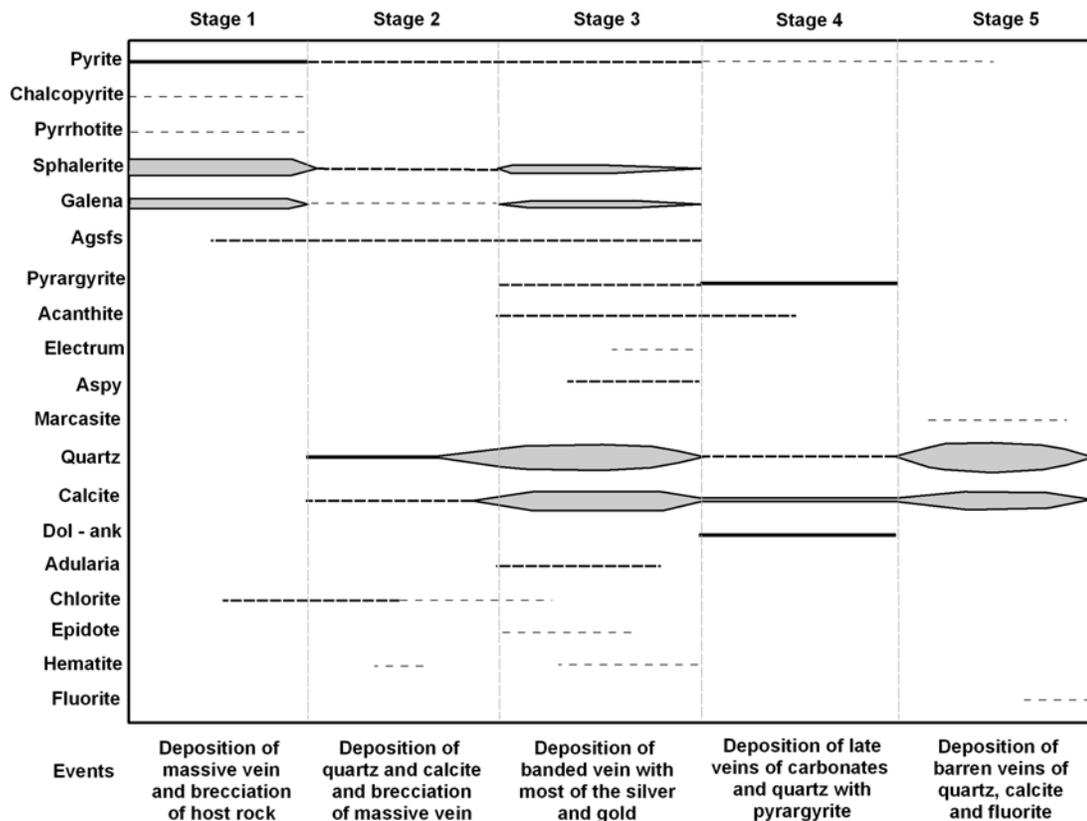
Fig. 41. Paragenetic sequence for Jarillas and Valdecañas veins.

Calculated Au/Ag ratios for Santo Niño and San Carlos range from 1:1000 to 1:588 whereas the mean range for Jarillas, Valdecañas and Saucito is 1:147 to 1:18. The Au/Ag ratios in Fresnillo-SW are 4 to 58 times bigger than those of Santo Niño and San Carlos veins. Average Pb and Zn values seem to be similar in Jarillas (Fresnillo-SW), Santo Niño and San Carlos (Fresnillo-SE). On the other hand, Valdecañas is the vein with the highest concentration of base metals whereas Saucito is the vein with the lowest concentration of base metals and higher gold concentration. Other veins with high gold to silver ratios and low base metals contents occur in the eastern-most part of the district; San Antonio (1:290) and San Mateo (1:480). The high Au/Ag ratios and low base metals

106

contents of Saucito, San Antonio and San Mateo with respect to the other veins could indicate that Saucito, San Antonio and San Mateo occur in the margins of the district based on the model of the porphyry to epithermal continuum proposed by Hedenquist et al. (1996). Based on the zoning patterns just described, the strike of the veins (east-west to northwest-southeast) which originally were just open fractures that controlled fluid flow, and the fluid inclusion and sulfur fugacity data, we infer that the fluid flow direction was from northwest to southeast and that the main source of heat and fluids was probably to the northwest. Other workers in Fresnillo have already suggested fluid flow direction from west to east at the vein scale. Simmons (1986), and Eckberg (1999), determined that homogenization temperatures and salinities decrease from west to east in Santo Niño and San Carlos veins respectively. Gemmell (1986) also determined flow direction from west to east on the basis of mineral zonation and $Sb/(Sb+As)$ and $Ag/(Ag+Cu)$ ratios in silver sulfosalts for the Santo Niño vein. Lateral fluid flow has been interpreted in other Mexican epithermal deposits like Topía (Loucks and Petersen, 1988), and Tayoltita (Clark, 1991). Figure 42 shows a map of Fresnillo with the veins, and isotherms that were interpolated visually based on fluid inclusion data and Au/Ag ratios. Notice that overall, the Au/Ag ratios are much higher in Fresnillo-SW than in Fresnillo-SE and therefore it is not possible to connect the contour lines for the Au/Ag ratios from the two areas. A possible explanation for that is that multiple mineralizing stages carrying silver or gold overlapped and modified the original Au/Ag ratios. Problems in metal ratio interpretations can arise due to overlap of different depositional periods (Goodell and Petersen, 1974; Bartos, 1990). We know of the presence of at least three mineralizing events carrying base metals, base metals-silver-gold, and silver in the

107

Fresnillo's veins, and they could account for the remarkable differences in Au/Ag between Fresnillo-SE and Fresnillo-SW. Nonetheless, in spite of the differences, the contours still define a trend of decreasing Au/Ag ratios to the northwest. Goodell and Petersen (1974), suggested that the rate of change of metal ratios along various paths can differ because of differences in depositional factors. Table 10 shows the average homogenization temperatures, salinities and sulfur fugacities of the veins. We hypothesize that the center of the district should have an intrusion that generated heat and that the fluids exsolved from that center evolved from hotter-saline and slightly oxidizing (IS) to cooler-diluted and reduced (LS) due to progressive neutralization of the fluids by interaction with host rocks, presumably some of them reduced black shales, from the center to the margin. Similar evidences of evolution from higher sulfidation state to lower sulfidation state have been proposed for Lepanto, Phillipines and La Guitarra, Mexico (Einaudi et al., 2003; Camprubi et al., 2007). We interpret that all together, metal concentrations, metal ratios, temperature, salinity and sulfur fugacity variations indicate that the thermal center of the district was to the northwest.

Table 10. Average homogenization temperatures, salinities and $\log f S_2$ and $\log f O_2$ ranges for Santo Niño (Simmons et al., 1988; Benton, 1991), Jarillas and Valdecañas.

Reference	Vein	Average Th°C	Average salinity in wt% NaCl eq.	Log fS2 (range)	Log fO2 (range)
Simmons, 1986; Benton, 1991	Santo Niño	217	2.5	-10 to -17	-38 to -47
This study	Jarillas	233	3.0	-4 to -12	-34 to -45
This study	Valdecañas	259	4.3	-5 to 12	-33 to -42
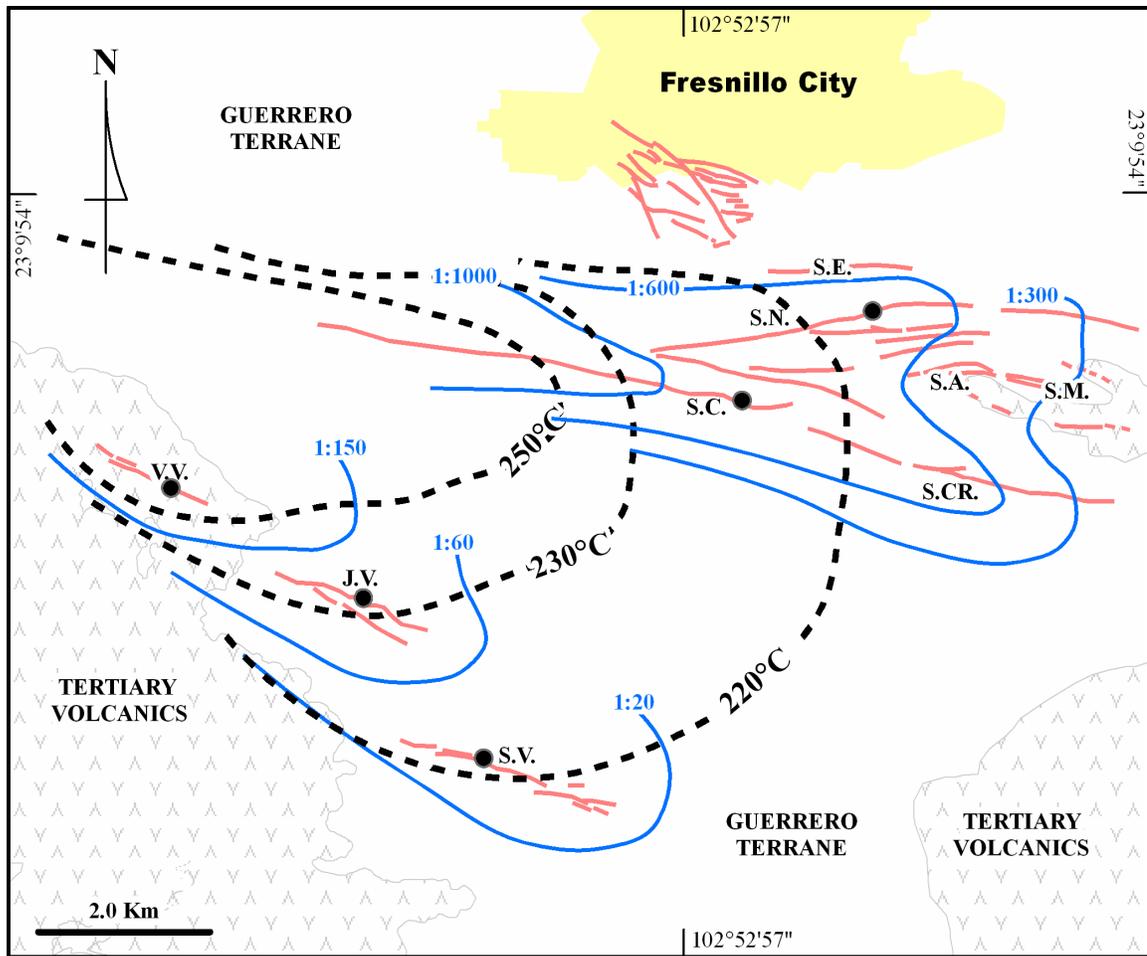
Fig. 42. Map of the Fresnillo District showing veins. The black dashed
contour lines are isotherms based on fluid inclusion data; interpolation was done visually.
The blue contour lines show the variations in Au/Ag ratios; 1 ppm Au : N ppm Ag.
Abbreviations; Santa Elena (S.E.), Santo Niño (S.N.), San Antonio (S.A.), San Mateo
(S.M.), San Carlos (S.C.), Santa Cruz (S.CR.), Saucito (S.V.) Jarillas (J.V.) and
Valdecañas (V.V.). Black dots are on veins with fluid inclusion data used for
interpretation of isotherms.

Conclusions

Longitudinal sections of the veins show that the base metals are concentrated at

depth and precious metals at shallow levels, which is in agreement with metal zoning in

boiling systems. Therefore, gold occurs low with respect to the high Ag/Pb band and

associated with sulfides, which causes that the ore band defined by Au eq. plots between

the base metals zone and the high Ag/Pb band. We determined that a late stage of mineralization carrying silver reached higher elevations in the vein and overlapped previous mineralizing stages, which modified the original metal ratios produced during boiling deposition; particularly Au/Ag. Later mineralizing events depositing silver at variable concentrations across the district could have modified the Au/Ag ratios differently in Fresnillo-SE and Fresnillo-SW.

Gold concentrations and Au/Ag ratios are consistently higher in Fresnillo-SW than in the Fresnillo-SE, which is coincident with a trend of increasing temperature, salinity and sulfur fugacity that indicate that the center of the district lies to the northwest. High Au/Ag ratios and low base metal contents in the Saucito, San Antonio and San Mateo veins suggests that these veins occur distaly with respect to the center of the district. In combination, metal contents, metal ratios, temperature, salinity, and sulfur fugacity suggest that the thermal center (presumably an intrusion), and maybe the source of some of the fluids that formed the IS veins is to the northwest. We believe that overall the fluids flowed laterally across the district from the northwest to the southeast, causing the district wide zoning; however locally in the open faults and fractures where the veins were formed, the fluids ascended vertically and boiled causing the zoning at the vein scale.

GENERAL CONCLUSIONS

One of the major questions posed at the outset of this work was whether all the Fresnillo IS veins are co-genetic, or was the Fresnillo district formed by super position of various ore forming processes over time. This chapter will utilize the results from the three papers to address those questions and their implications for future exploration in the district.

Mineralogy, paragenesis, fluid inclusion temperature and salinity ranges, and O, H, S, C isotopic compositions are similar for the IS epithermal veins throughout the district which indicates that the veins could be co-genetic (Chapter 2). Additionally our age data reported in chapter 1, shows that Jarillas and Valdecañas veins have the same age (29.68 +/- 0.10 Ma; 29.74 +/- 0.07 Ma; 29.75 +/- 0.12 Ma), therefore we know that at least these two veins are coeval. The similarities between the IS epithermal veins across the district described in chapter 2 lead us to believe that all the veins could be co-genetic and that they probably formed by one large hydrothermal event. Unfortunately we do not know the age of any of the veins in Fresnillo-SE, and besides we know that multiple pulses of intrusion and hydrothermal activity operated in Fresnillo; based on differences in age between the intrusion (32.65 +/-0.05 Ma), alunite deposition (30.56 +/- 0.04; 31.03 +/- 0.05) and mineralization (~29.70 Ma); and supported by the fact that there are other intrusions to the north of the district (Chapter 1). Therefore the question whether the

veins from Fresnillo-SE and Fresnillo-SW are coeval remains open and should be addressed by future geochronology work.

In conjunction, our fluid inclusion, stable isotope and gas chemistry data in chapter 2, indicate that the hydrothermal fluids could be either magmatic, deeply circulated (exchanged) meteoric water or a combination of the two types (Chapter 3). The zoning patterns across the district described in chapter 3, suggest that there was a source of heat and fluids to the northwest (i.e. an intrusion). The existence of an intrusion to the northwest as suggested in chapter 3, give us a constraint for the source of fluids, because an intrusion would have produced some magmatic fluids, and that would eliminate the possibility that the veins were formed exclusively by deeply circulated meteoric waters. We believe that both magmatic and deeply circulated meteoric fluids were important in the genesis of the Fresnillo veins. The zoning patterns shown in chapter 3 also have implications for fluid flow direction, because the fluids should flow outwards from the hot center of the district. Therefore the fluid flow direction should have been from northwest to southeast (Chapter 3), which is in agreement with previous studies done in individual veins in Fresnillo-SE (Simmons, 1986; Gemmell, 1986; Eckberg, 1999). Notice that a locus for the intrusion to the northwest implies that the Fortuna stock could not be the source for epithermal mineralization, which is also supported by the age of the intrusion reported in chapter 1. Figure 43 is a schematic genetic model for Fresnillo that illustrates our main interpretations from the three chapters; it shows an intrusion with age similar to the age of the veins (~29.70 Ma) releasing magmatic fluids that flow upwards and laterally, at intermediate depth the magmatic fluids mix with deeply circulated meteoric water that have exchanged oxygen and leached sulfur and carbon from the host

rock; after mixing the fluids ascend and find open structures were the fluids boil and deposit the ore. Notice that in the genetic model we speculate that at depth the fluids flow laterally and at shallow levels they ascend vertically which is compatible with our district-wide and vein-scale zonation patterns described in chapter 3. The model also accounts for the assimilation and melting of GT (black shales) in the magma chamber described in chapter 2.

The possibility of the existence of a blind intrusion to the northwest has, of course, important implications for future exploration in the district. There are several examples around the world that show that porphyry and epithermal systems form a continuum (Sillitoe, 1989; Vila and Sillitoe, 1991; and Hedenquist et al., 1997; Hedenquist et al., 1996; Muntean and Einaudi, 2001; Sillitoe and Hedenquist, 2003; Valencia et al., 2008; and Pudack et al., 2009), and for that reason it would be important to drill test this hypothesis in Fresnillo. Another important implication for the location of the center of the district is that mineralization could occur at both sides of such center; as long as the mechanical preparation of the host rock and the hydraulic gradient were favorable. We recommend that magnetic and gravity surveys should be performed in the northwest (in the valley immediately north of Sierra Valdecañas), to see if there is an indication of an intrusion body at depth; if that is the case, then drill the center of the anomaly to see if there are indications of alteration or mineralization.
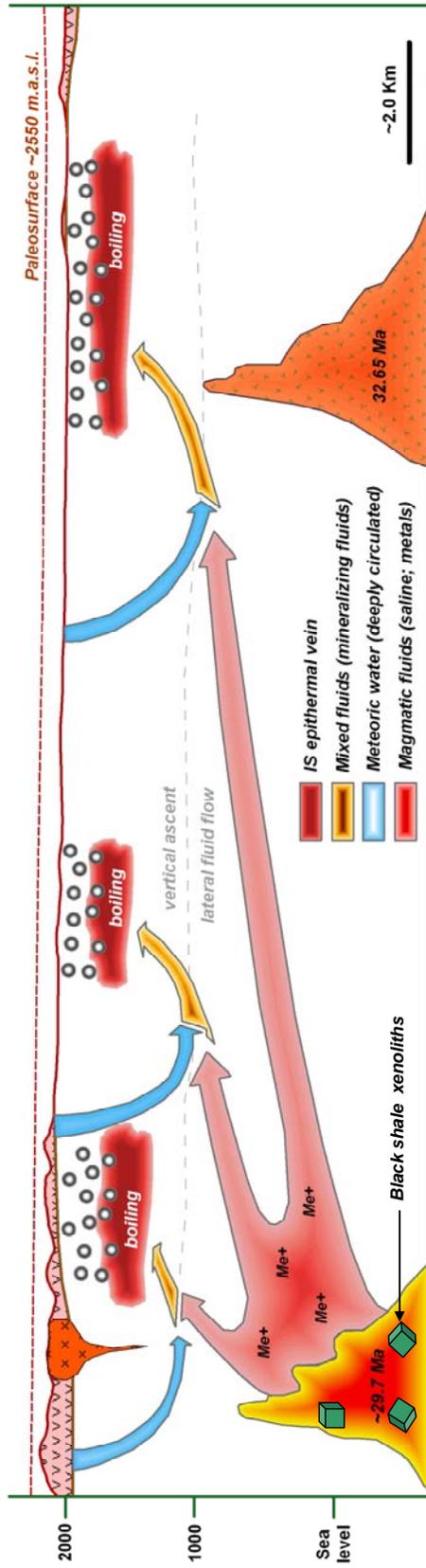
Fig. 43. Genetic model for the Fresnillo district. The model shows magmatic fluids derived from an intrusion that mix with deeply circulated meteoric water. At depth the fluids flow laterally and at shallow depths the fluids ascend vertically which is consistent with the district wide and vein zonation patterns.

114

REFERENCES

Albinson, T., 1988, Geologic Reconstruction of Paleosurfaces in the Sombrerete, Colorada, and Fresnillo Districts, Zacatecas State, Mexico: ECONOMIC GEOLOGY, vol. 83, p. 1647–1667.

Albinson, T., Norman, D.I., Cole, D., and Chomiak, B., 2001, Controls on Formation of Low-Sulfidation Epithermal Deposits in Mexico: Constraints from Fluid Inclusion and Stable Isotope Data: ECONOMIC GEOLOGY, Special Publication 8, p. 1 – 32.

Barton, P.B. Bethke, P.M., and Roedder, E., 1977, Environment of Ore Deposition in the Creede Mining District, San Juan Mountains, Colorado: Part III. Progress Toward Interpretation of the Chemistry of the Ore-Forming Fluid for the OH Vein: ECONOMIC GEOLOGY, vol. 72, pp. 1 – 24.

Bartos, P.J., 1990, Metal Ratios of the Quiruvilca Mining District, Northern Peru: ECONOMIC GEOLOGY, vol. 85, no. 7, p. 1629 – 1644.

Baumgartner, R., Fontboté, L., Spikings, R., Ovtcharova, M., Schaltegger, U., Schneider, J., Page, L., and Gutjahr, M., 2009, Bracketing the Age of Magmatic-Hydrothermal Activity at the Cerro de Pasco Epithermal Polymetallic Deposit, Central Peru: A U-Pb and $^{40}Ar/^{39}Ar$ Study: ECONOMIC GEOLOGY, vol. 104, p. 479–504.

Bayley, E.H., and Stevens, R.E., 1960, Selective Staining of K-Feldspar and Plagioclase on Rock Slabs and Thin Sections: The American Mineralogist, vol. 45, p. 1020–1025.

Campa, M.F., and Coney, P.J., 1983, Tectono- satratigraphic terranes and mineral resource distributions in Mexico: Canadian Journal of Earth Sciences, vol. 20, p. 1040–1051.

Blamey, N.J.F., and Norman, D.I., 2000, Fluid inclusion evidence for gold mineralization related to decalcification at the Pipeline Mine, Nevada, *in* Cluer, J.K., Price, J.G., Struhsacker, E.M., Hardyman, R.F., and Morris, C.L., eds., Geology and Ore Deposits 2000: The Great Basin and Beyond: Geological Society of Nevada Symposium Proceedings, May 15-18, 2000, p. 873 – 882.

Blamey, N.J.F., and Norman, D.I., 2002, "New Interpretations of Geothermal Fluid Inclusion Volatiles: Ar/He and N_2/Ar ratios - A Better Indicator of Magmatic Volatiles,

and Equilibrium Gas Geothermometry", 27th Workshop on geothermal reservoir engineering, CD.

Brown P.E., 1992, Fluid Inclusions Application, FLINCOR, version 1.4.

Buchanan, L.J., 1981, Precious Metal Deposits Associated with Volcanic Environments in the Southwest: In Relations of Tectonics to Ore Deposits in the Southern Cordillera, Eds. W.R. Dickson and W.D. Payne, Geological Society of Arizona, Digest 14, pp. 237 – 262.

Campa, M.F., and Coney, P.J., 1982, Tectono- satratigraphic terranes and mineral resource distributions in Mexico: Canadian Journal of Earth Sciences, vol. 20, p. 1040–1051.

Benton, L.D., 1991, Composition and source of the hydrothermal fluids of the San Mateo vein, Fresnillo, Mexico as determined from $^{87}Sr/$ ^{86}Sr, stable isotope and gas analyses: Unpublished Master's Thesis, New Mexico Institute of Mining and Technology, 55 p.

Camprubí, A., Cardellach, E., Canals, A., and Lucchini, R., 2001, The La Guitarra Ag-Au Low-Sulfidation Epithermal Deposit, Temascaltepec District, Mexico: Fluid Inclusion and Stable Isotope Data: ECONOMIC GEOLOGY, special pub. 8, p. 159–185.

Camprubí, A., Ferrari, L., Costa, M.A., Cardellach, E., and Canals, A., 2003, Ages of Epithermal Deposits in Mexico: Regional Significance and Links with Evolution of Tertiary Volcanism: ECONOMIC GEOLOGY, vol. 98, p. 1029–1037.

Camprubí, A., and Albinson, T., 2007, Epithermal deposits in Mexico: Update of current knowledge, and an empirical reclassification: Geological Society of America, Special Paper 422, p. 377–415.

Cathles, L.M., Erendi, A. H.J., and Barrie, T., 1997, How Long Can a Hydrothermal System Be Sustained by a Single Intrusive Event? ECONOMIC GEOLOGY, vol. 92, pp. 766 – 771.

Centeno-García, E., Ruiz, J., Coney, P.J., Patchett, P.J., and Ortega-Gutiérrez, F., 1993, Guerrero terrane of Mexico: Its role in the southern Cordillera from new geochemical data: Geology, v. 21, p. 419–422.

Chacko, T., Riciputi, L.R., Cole, D.R., and Horita, J., 1999, A new technique for determining equilibrium hydrogen isotope fractionation factors using the ion microprobe: Application to the epidote-water system. Geochimica et Cosmochimica Acta, vol. 63, pp. 1- 10.

Chico E., 1986, Mineralogy, paragenesis and fluid inclusion studies in three veins of the Fresnillo Mining District, Zacatecas, Mexico: Unpublished M.Sc. thesis, Dartmouth College, 115 p.

Clark, H.M., 1991, Geology of the Tayoltita Mine, San Dimas District, Durango: Geological Society of America, The Geology of North America, Ed. Guillermo P. Salas, vol. P-3, pp. 219 – 227.

Clark, K.F., Foster, C.T., and Damon, P.E., 1982, Cenozoic mineral deposits and subduction-related magmatic arcs in Mexico: Geological Society of America Bulletin, vol. 93, pp. 533 – 544.

Clayton, R.N., and Mayeda, T.K., 1963, The use of bromide pentafluoride in the extraction of oxygen from oxides and silicates for isotopic analysis, Geochemica et Cosmochemica Acta, vol. 27, pp. 43 – 52.

Conrad, J.E., McKee, E.H., Rytuba, J.J., Hash, J.T., and Utterback, W., 1993, Geochronology of the Sleeper Deposit, Humboldt County, Nevada: Epithermal Gold-Silver Mineralization Following Emplacement of a Silicic Flow-Dome Complex: ECONOMIC GEOLOGY, vol. 88, p. 317–327.

Cooke, D.R., and Simmons, S.F., 2000, Characteristics and Genesis of Epithermal Gold Deposits: Reviews in Economic Geology, vol. 13, p. 221–244.

Corbett, G.J., and Leach, T.M., 1988, Gold-Copper Systems: Structure, Alteration, and Mineralization: ECONOMIC GEOLOGY, Special Publication No. 6, pp. 201 – 214.

Damon, P.E., Shafiqullah, M., and Clark, K.F., 1983, Geochronology of the porphyry copper deposits and related mineralization in Mexico: Canadian Journal of Earth Sciences, vol. 20., pp. 1052 – 1071.

De Cserna, Z., 1976, Geology of the Fresnillo area, Zacatecas, Mexico: Geological Society of America, vol. 87, p.1191–1199.

De Cserna, Z., Delevaux, M.H., and Harris, D.C., 1977, Datos isotopicos, mineralogicos, y modelo genético propuesto para los yacimientos de plomo, zinc y plata de Fresnillo, Zacatecas: Revista del Instituto de Geología, UNAM, vol. 1, no. 1, p. 110–116.

Dilley L.M., 1993, Mineralogy and fluid inclusion study of the San Mateo vein, Fresnillo District Zacatecas Mexico, Unpublished Master's Thesis, New Mexico Institute of Mining and Technology, 137 p.

Dong, G., and Morrison, G.W., 1995, Adularia in epithermal veins, Queensland: morphology, structural state and origin: Mineralium Deposita, vol. 30. p. 11–19.

Dowling K., and Morrison G., 1989, Application of quartz textures to the classification of gold deposits using North Queensland examples, The Geology of Gold Deposits: The Perspective in1988, ECONOMIC GEOLOGY, monograph 6, pp. 342 – 355.

Dreier, J.E., 2005, The Environment of vein Formation and Ore Deposition in the Purisima-Colon Vein System, Pachuca Real del Monte District, Hidalgo, Mexico: ECONOMIC GEOLOGY, vol. 100, pp. 1325 – 1347.

Drummond, S.E., and Ohmoto, H., 1985, Chemical Evolution and Mineral Deposition in Boiling Hydrothermal Systems: ECONOMIC GEOLOGY, vol. 80, pp. 126 – 147.

Earthman, M.A., Velador, J.M., and Campbell, A.R., 2009, Stable Isotope Study of New Prospect Veins of the Fresnillo Silver District, Zacatecas, Mexico: Geological Society of America Abstracts with Programs, vol. 41, no.7, p. 681.

Earthman, M.A., 2010, Master's thesis in preparation.

Eckberg E., 1999, A fluid inclusion and cathodoluminescense study of the Santo Niño and San Carlos Vein Systems in the Fresnillo Silver District, Zacatecas, Mexico, Senior Honors Thesis, Earth Science Deptartment, Dartmouth College, 72 p.

Einaudi, M.T., Hedenquist, J.W., and Inan, E.E., 2003, Sulfidation state of fluids in active and extinct hydrothermal systems: transitions from porphyry to epithermal environments: ECONOMIC GEOLOGY, Special Publication, vol. 10, pp. 285 – 313.

Enríquez, E., 2004, Estudio de Inclusiones Fluidas de la Veta Saucito, Fresnillo, Zac: Internal report for Peñoles Industries, 30 p.

Escalona-Alcázar, F. de J., Delgado-Argote, L.A., Weber, B., Núñes-Peña, E.P., Valencia, V.A., and Ortiz-Acevedo, O., 2009, Kinematics and U-Pb dating of detrital zircons from the Sierra de Zacatecas, Mexico: Revista Mexicana de Ciencias Geológicas, vol. 26, no. 1, p. 48–64.

Etoh, J., Izawa, E., Watanabe, K., Taguchi, S., and Sekine, R., 2002, Bladded quartz and its relationship to gold mineralization in the Hishikari low-sulfidation epithermal gold deposit, Japan, Economic Geology, vol. 97, pp. 1841 – 1851.

Faure, K., Matsuhisa, Y., Metsugi, H., Mizota, C., and Hayashi, S., 2002, The Hishikari Au-Ag Epithermal Deposit, Japan: Oxygen and Hydrogen Isotope Evidence in Determining the Source of Paleohydrothermal Fluids: ECONOMIC GEOLOGY, vol. 97, p. 481–498.

Faure, K., 2003, δD Values of fluid inclusion water in quartz and calcite ejecta from active geothermal systems: do values reflect those of original hydrothermal water? ECONOMIC GEOLOGY, vol. 98, p. 657–660.

Foster, D.A., Harrison, T.M., Copeland, P., and Heizler, M.T., 1990, Effects of excess argon within large diffusion domains on K-feldspar age spectra: Geochimica et Cosmochimica Acta, vol. 54, p. 1699–1708.

Fournier, R.O., 1985, The behaviour of silica in hydrothermal solutions: in Berger, B.R., and Bethke, P.M., eds., Geology and Geochemistry of Epithermal Systems, 2. Reviews in Economic Geology, pp. 45 – 59.

Garcia, E., Querol., M.F., and Lowther, G.K., 1991, Geology of the Fresnillo Mining District, Zacatecas: Geological Society of America, The Geology of North America, Ed. Guillermo P. Salas, vol. P-3, pp. 383 – 394.

Gemmell, J.B., 1986, The Santo Niño Vein, Fresnillo District, Zacatecas, Mexico: Geology, Sulfide and Sulfosalt mineralogy, and Geochemistry: PhD Thesis, Dartmouth College, 244 p.

Gemmell, J.B., Simmons, S.F., and Zantop, H., 1988, The Santo Niño Silver-Lead-Zinc Vein, Fresnillo District, Zacatecas, Mexico: Part I. Structure, Vein Stratigraphy, and Mineralogy: ECONOMIC GEOLOGY, vol. 83, pp. 1597–1618.

González-Partida, E., 1984, Estudio microtermometrico del Distrito Minero de Fresnillo, Zacatecas: GEOMIMET, no. 130, pp. 17 – 21.

González-Partida, E., Arnold M. and Acosta E., 1984, Análisis Metalogenetico Preliminar del Distrito Minero de Fresnillo, Zacatecas Sobre la Base de 50 Medidas Isotópicas $\delta^{34}S$‰, GEOMIMET, no. 129, pp. 27 – 34.

Goodell, P.C., and Petersen, U., 1974, Julcani Mining District, Peru: A Study of Metal Ratios: ECONOMIC GEOLOGY, vol. 69, no. 3, p. 347 – 361.

Graham, C.M., Atkinson, J. and Harmon, R.S. (1984b). Hydrogen isotope fractionation in the system chlorite-water. NERC 6th Progress Report of Research 1981-1984, NERC Publication Series D, No. 25, pp. 1 39.

Hedenquist, J.W., 1987, Mineralization associated with volcanic-related hydrothermal systems in the circum-Pacific basin, Circum-Pacific Energy and Mineral Resources Conference, 4th, Singapore, August 17 – 22, 1986: Transactions, p. 513–524.

Hedenquist, J.W., Izawa, E., Arribas, A., and White, N.C., 1996, Epithermal Gold Deposits: Styles, Characteristics and Exploration: Resource Geology Special Publication, Society of Resource Geology, no. 1, 18 p.

Hedenquist, J.W., Arribas, A., Jr., and Reynolds, J.T., 1998, Evolution of an Intrusion-Centered Hydrothermal System: Far Southeast-Lepanto Porphyry and Epithermal Cu-Au Deposits, Philippines: ECONOMIC GEOLOGY, vol. 93, p. 373–404.

Hedenquist, J.W., Arribas, A. and Gonzalez-Urien, E., 2000, Exploration for Epithermal Gold Deposits, Reviews in Economic Geology, vol. 13, pp. 245 – 277.

Heizler, M.T., and Harrison, T.M., 1988, Multiple trapped argon isotope components revealed by $^{40}Ar/^{39}Ar$ isochron analysis: Geochimica et Cosmochimica Acta, vol. 52, p. 1295–1303.

Henley, R.W., Truesdell, A.H., Barton, P.B., Jr., and Whitney, J.A., 1984, Fluid-mineral equilibria in hydrothermal systems: Reviews in Economic Geology, v. 1, 267 p.

Henley, R.W., Hedenquist, J.W., and Roberts, P.J., 1986, Guide to active epithermal (Geothermal) systems and precious metal deposits of New Zealand, Monograph Series on Mineral Deposits, no. 26, pp. 1 – 22.

Henry, C.D., Elson, H.B., McIntosh, W.C., Heizler, M.T., and Castor, S.B., 1997, Brief Duration of Hydrothermal Activity at Round Mountain, Nevada, Determined from $^{40}Ar/^{39}Ar$ Geochronology: ECONOMIC GEOLOGY, vol. 92, p. 807–826.

Kapusta, Y., 2005, Reporte de fechamientos radiométricos por el método de K/Ar roca total, Unpublished Internal Report for Peñoles Industries, 2 p.

Kim, S.T. and O'Neil, J.R., 1997, Equilibrium and nonequilibrium oxygen isotope effects in synthetic carbonates: Geochimica et Cosmochimica Acta, vol. 61, pp. 3461 - 3475.

Kreczmer, M .J., 1977, The geology and geochemistry of the Fortuna mineralization, Fresnillo, Zacatecas, Mexico: Unpublished Master's Thesis, University of Toronto, 155 p.

Lang, B., Steintz, G., Sawkins, F.J., and Simmons, S.F., 1988, K/Ar Age Studies in the Fresnillo Silver District, Zacatecas, Mexico: ECONOMIC GEOLOGY, vol. 83, p. 1642–1646.

Leavitt, E.D., Spell, T.L., Goldstrand, P.M., and Arehart, P.M., 2004, Geochronology of the Midas Low-Sulfidation Epithermal Gold-Silver Deposit, Elko County, Nevada: ECONOMIC GEOLOGY, vol. 99, p. 1665–1686.

Loucks R.R., and Petersen U., 1988, Polymetallic Epithermal Fissure Vein Mineralization, Topia, Durango, Mexico: Part II. Silver Mineral Chemistry and High Resolution Patterns of Chemical Zoning in Veins: ECONOMIC GEOLOGY, vol. 83, 1529 – 1559.

Macdonald, A.J., 1978, The Geology and Genesis of the Cueva Santa Branch Silver, Lead, Zinc Manto Ore Body, Fresnillo Mine, Mexico: Masters Thesis, Department of Geological Sciences, University of Toronto, 129 p.

Macdonald, A.J., Kreczmar, M.J. and Kesler, S.E., 1986, Vein, manto and chimney mineralization at the Fresnillo silver – lead – zinc mine, Mexico: Canadian Journal of Earth Sciences, vol. 23, pp. 1603 – 1614.

Mango H.N., 1992, Origin of Epithermal Ag-Au-Cu-Pb-Zn Mineralization on the Veta Madre, Guanajuato, Mexico: Unpublished PhD Thesis, Dartmouth College, 201 p.

Marsh, T.M., Einaudi, M.T., and McWilliams, M., 1997, $^{40}Ar/^{39}Ar$ Geochronology of Cu-Au and Au-Ag Mineralization in the Potrerillos District, Chile: ECONOMIC GEOLOGY, vol. 92, p. 784–806.

McDougall, I., and Harrison, T.M., 1999, Geochronology and Thermochronology by the $^{40}Ar/^{39}Ar$ Method, Second Edition: New York, Oxford University Press 269 p.

McDowell, F.W., and Keizer, R.P., 1977, Timing of mid-Tertiary volcanism in the Sierra Madre Occidental between Durango City and Mazatlan, Mexico: Geological Society of America Bulletin, vol. 88, pp. 1479 – 1487.

McDowell, F.W., Housh, T.B., and Wark, D.A., 1999, Nature of the crust beneath west-central Chihuahua, Mexico, based upon Sr, Nd, and Pb isotopic compositions at the Tómochic volcanic center: Geological Society of America Bulletin, vol. 111, pp. 823 – 830.

Meheut, M, Lazzeri, M, Balan, E, Mauri, F., 2007, Equilibrium isotopic fractionation in the kaolinite, quartz, water system: Prediction from first-principles density-functional theory: Geochimica et Cosmochimica Acta, vol. 71, pp. 317 0- 3181.

Mortensen, J.K., Hall, B.V., Bissig, T., Friedman, R.M., Danielson, T., Oliver, J., Rhys D.A., Ross, K.V., and Gabites, J.E., 2008, Age and Paleotectonic Setting of Volcanogenic Massive Sulfide Deposits in the Guerrero Terrane of Central Mexico: Constraints from U-Pb Age and Pd Isotope Studies: ECONOMIC GEOLOGY, vol. 103, p. 117–140.

Muntean, J.L., and Einaudi, M.T., 2001, Porphyry-Epithermal Transition: Maricunga Belt, Northern Chile: ECONOMIC GEOLOGY, vol. 96, p. 743–772.

Nieto-Samaniego, A.F., Alaniz-Alvarez, S.A., and Camprubí, A., 2007, Mesa Central of México: Stratigraphy, structure, and Cenozoic tectonic evolution: Geological Society of America, Special paper 422, p. 41–70.

Norman, D.I., Moore, J.N. and Musgrave J., 1997, More on the use of fluid inclusion gaseous species as tracers in geothermal systems, Twenty-second workshop on geothermal reservoir engineering, Stanford University, Stanford, California, pp. 27 – 29.

Norman, D.I., Blamey, N., and Moore, J.N., 2002, Interpreting Geothermal Processes and Fluid Sources from Fluid Inclusion Organic Compounds and CO_2/N_2 Ratios: PROCEEDINGS, Twenty-Seventh Workshop on Geothermal Reservoir Engineering Stanford University, Stanford, California, 9 p.

Ohmoto, H. and Rye, R.O., 1979, Isotopes of sulfur and carbon, in Barnes, H. L. Ed., Geochemistry of Hydrothermal deposits, John Wiley & Sons, pp. 509 – 567.

O'Neil, J.R., and Taylor, H.P. Jr., 1967, The oxygen isotope and cation exchange chemistry of feldspars: American Mineralogist, vol. 52, pp. 1414 – 1437.

Orozco-Esquivel, M.T., Nieto-Samaniego, A.F., and Alaniz-Alvarez, S.A., 2002, Rhyolitic lava flows and domes: Journal of Volcanology and Geothermal Research, vol. 118, p. 37–56.

Potra, A. and MacFarlane, A.W., 2009, Ore Metal Sources in Tertiary Mineral Deposits of the Guerrero and Sierra Madre Terranes, Mexico, as inferred from lead isotope studies: Geological Society of America Abstracts with Programs, Vol. 41, No. 7, p. 438

Pudack, C., Halter, W.E., Heinrich, C.A., and Pettke, T., 2009, Evolution of Magmatic Vapor to Gold-Rich Epithermal Liquid: The Porphyry to Epithermal Transition at Nevados de Fatima, Northwest Argentina: ECONOMIC GEOLOGY, vol. 104, p. 449–477.

Rice, C.M., Steele, G.B., Barford, D.N., Boyce, A.J., and Pringle, M.S., 2005, Duration of Magmatic, Hydrothermal, and Supergene Activity at Cerro Rico de Potosi, Bolivia, ECONOMIC GEOLOGY, vol. 100, p.1647–1656.

Robinson, R.W., and Norman, D.I., 1984, Mineralogy and Fluid Inclusion Study of the Southern Amethyst Vein System, Creede Mining District, Colorado: ECONOMIC GEOLOGY, vol. 79, pp. 439 – 447.

Roedder E., 1984, Fluid Inclusions, Reviews in Mineralogy, Mineralogical Society of America, vol. 12, pp. 11 – 45.

Roedder, E. and Bodnar, R.J., 1980, Geologic pressure determinations from fluid inclusion studies, Ann. Rev. Earth Planet. Sci. vol. 8, pp. 263 – 301.

Ruvalcaba-Ruíz, D, 1980, Geology, alteration and fluid inclusions of the Santa Elena and Santo Niño fissure vein deposits in Fresnillo, Mexico: Unpublished M.Sc. thesis, Colorado State University, 86 p.

Ruvalcaba-Ruíz, D., and Thompson, T., 1988, Ore Deposits at the Fresnillo Mine, Zacatecas Mexico: ECONOMIC GEOLOGY, vol. 83, p. 1583–1596.

Rye R.O., Bethke P.M., and Wasserman M.D., 1992, The Stable Isotope Geochemistry of Acid Sulfate Alteration: ECONOMIC GEOLOGY, vol. 87, pp. 225 – 262.

Rye R.O., 2005, A review of the stable-isotope geochemistry of sulfate minerals in selected igneous environments and related hydrothermal systems: Chemical Geology, vol. 205, pp. 5 – 36.

Sander, M.V., and Black, J.E., 1988, Crystallization and recrystallization of growth-zoned vein quartz crystals from epithermal systems- implications for fluid inclusion studies: ECONOMIC GEOLOGY, vol. 83, pp. 1052 – 1060.

Sanematsu, K., Watanabe, K., Duncan, R.A., and Izawa, E., 2006, The History of Vein Formation Determined by $^{40}Ar/^{39}Ar$ Dating of Adularia in the Hosen-1 Vein at the Hishikari Epithermal Gold Deposit, Japan: ECONOMIC GEOLOGY, vol. 101, p. 685–698.

Sharp, Z.D., and Kirschner, D.L., 1994, Quartz-calcite oxygen isotope themometry: a calibration based on natural isotopic variations: Geochimica et Cosmochimica Acta, vol. 58, pp. 4491 - 4501.

Silberman, M.L., 1985, Geochronology of hydrothermal alteration and mineralization: Tertiary epithermal precious-metal deposits in the Great Basin: U. S. Geological Survey, bull. 1646, p. 55–70.

Sillitoe, R.H., 1985, Ore-related breccias in volcanoplutonic arcs: ECONOMIC GEOLOGY, vol. 80, pp. 1467 – 1514.

Sillitoe, R.H., 1989, Gold deposits in western Pacific island arcs: The magmatic Connection: ECONOMIC GEOLOGY Monograph, no. 6, p. 274–291.

Sillitoe, R.H. and Hedenquist J.W, 2003, Linkages between volcanotectonic settings, ore-fluid compositions, and epithermal precious-metal deposits: ECONOMIC GEOLOGY, Special Publication 10, pp. 315 – 343.

Sillitoe, R.H., 2008, Major Gold Deposits and Belts of the North and South American Cordillera: Distribution, Tectonomagmatic Settings, and Metallogenic Considerations: ECONOMIC GEOLOGY, vol. 103, pp. 663 – 687.

Simmons, S.F., 1986, Physio – Chemical Nature of the Mineralizing Solutions for the St. Niño Vein: Results form fluid inclusion, deuterium, oxygen and helium studies in the Fresnillo District, Zacatecas, Mexico: Unpublished Ph. D. thesis, Darmouth College, 191 p.

Simmons, S.F., Gemmell, J.B., and Sawkins, F.J., 1988, The Santo Niño Silver-Lead-Zinc Vein, Fresnillo District, Zacatecas, Mexico: Part II. Physical and Chemical Nature of Ore-Forming Solutions: ECONOMIC GEOLOGY, vol. 83, p. 1619–1641.

Simmons, S.F., 1991, Hydrologic Implications of Alteration and Fluid Inclusion Studies in the Fresnillo District, Mexico: Evidence for a Brine Reservoir and a Descending Water Table During the Formation of Hydrothermal Ag-Pb-Zn Orebodies: ECONOMIC GEOLOGY, vol. 91, pp. 204 – 212.

Singer, B., and Marchev, P., 2000, Temporal Evolution of Arc Magmatism and Hydrothermal Activity, Including Epithermal Gold Veins, Borovitsa Caldera, Southern Bulgaria: ECONOMIC GEOLOGY, vol. 95, p. 1155–1164.

Starling, T., 2006, Field Structural Analysis of the Juanicipio-Saucito Area, Zacatecas, Mexico: Unpublished internal report prepared for Servicios Industriales Peñoles, 7 p.

Stoffregen, R.E., Rye, R.O., & Wasserman, M.D. (1994) Experimental studies of alunite: Part I,18 O-16 O and D-H fractionation factors between alunite and water at 250-450 degrees C. Geochimica et Cosmochimica Acta 58, p. 903-916.

Stone, J.B., and McCarthy, J.C., 1948, Mineral and metal variations in the veins of Fresnillo, Zacatecas, Mexico: AIME Trans., vol. 148, pp. 91 – 106.

Taylor, H.P. Jr., 1974, The application of Oxygen and Hydrogen Isotope Studies to Problems of Hydrothermal Alteration and Ore Deposits: Economic Geology, vol. 69, p. 843–883.

Taylor, H.P. Jr., 1979. Oxygen and hydrogen isotope relationships in hydrothermal mineral deposits. In: Barnes, H.L. (Ed.), Geochemistry of Hydrothermal Ore Deposits, 2nd ed. Wiley, New York, pp. 236 – 318.

Trejo, P., 2001, Geology of the Fresnillo Southeast Mine, Fresnillo, Zacatecas, México: ECONOMIC GEOLOGY, Special Publication 8, p. 105–113.

Valencia, V.A., Eastoe, C., Ruiz, J., Ochoa-Landin, L., Gehrels, G., Gonzalez-Leon, C., Barra, F., and Espinoza, E., 2008, Hydrothermal Evolution of the Porphyry Copper Deposit at La Caridad, Sonora, Mexico, and the Relationship with a Neighbouring High-Sulfidation Epithermal Deposit: ECONOMIC GEOLOGY, vol. 103, p. 473–491.

Vaughan, D.J., and Craig, J.R., 1997, Sulfide Ore Mineral Stabilities, Morphologies, and Intergrowth Textures: Geochemistry of Hydrothermal Ore Deposits 3rd. ed., Edited by Hubert L. Barnes, pp. 367 – 434.

Velador, J.M., 2005, Inclusiones Fluidas, Mineralogia y Geoquímica de Veta Saucito y Geología y Geoquímica de Roca Total de Sierra de Valdecañas: Unpublished report for Servicios Industriales Peñoles 54 p.

Velador, J.M., Earthman M.A., and Campbell A.R., 2009, Spatial variation of physio–chemical conditions of the hydrothermal fluids in Fresnillo based on fluid inclusion studies: Geological Society of America Abstracts with Programs, Vol. 41, No. 7, p. 681

Velador, J.M., Heizler M.T., and Campbell A.R., 2010a, Timing of magmatic activity and mineralization and evidences of a long-lived hydrothermal system in the Fresnillo Silver District, Mexico: constrained by $^{40}Ar/^{39}Ar$ Geochronology: ECONOMIC GEOLOGY, submited.

Velador, J.M., Campbell, A.R., Earthman, M.A., and Blamey, N., 2010b, Physio-chemical Characteristics and Evolution of the Hydrothermal Fluids that Formed Intermediate Sulfidation Veins in Fresnillo, Mexico: in preparation

Velador, J.M., Campbell, A.R., Giles, D.A., Gomez, S.A., Vallejo, A., and Cruz, J., 2010c, Geochemical Zoning of the Fresnillo Intermediate Sulfidation Epithermal District, Zacatecas, Mexico, In preparation.

Vila, T., and Sillitoe, R.H., 1991, Gold-Rich Porphyry Systems in the Maricunga Belt, Northern Chile: ECONOMIC GEOLOGY, vol. 86, p. 1238–1260.

Warren, I., Archibald, D.A., and Simmons, S.F., 2008, Geochronology of Epithermal Au-Ag Mineralization, Magmatic-Hydrothermal Alteration, and Supergene Weathering in the El Peñon District, Northern Chile: ECONOMIC GEOLOGY, vol. 103, p. 851–864.

Wasserman, M. D., Rye, R. O., Bethke, P. M., and Arribas A. Jr., 1992, Methods for separation and total stable isotope analysis of alunite: U.S. Geological Survey, Open file report 92-9, 20 p.

White, N.C., and Hedenquist, J.W., 1990, Epithermal environments and styles of mineralization: variations and their causes, and guidelines for exploration: Journal of Geochemical Exploration, vol. 36, pp. 445 – 474.

APPENDICES

Appendix A1. Argon isotopic data for laser fusion analysis.

ID	$^{40}Ar/^{39}Ar$	$^{37}Ar/^{39}Ar$	$^{36}Ar/^{39}Ar$ (x 10^{-3})	$^{39}Ar_K$ (x 10^{-15} mol)	K/Ca	$^{40}Ar^*$ (%)	Age (Ma)	±1σ (Ma)
VR-07-12, Sanidine, J=0.0008215±0.06%, D=1.0006±0.001, NM-213G, Lab#=57526								
04	30.55	0.0107	0.4530	9.753	47.8	99.6	44.52	0.09
15	30.61	0.0110	0.5169	9.936	46.3	99.5	44.59	0.09
10	30.53	0.0089	0.2386	12.706	57.4	99.8	44.59	0.17
14	30.57	0.0091	0.2521	13.066	56.2	99.8	44.63	0.13
13	30.59	0.0095	0.3046	11.976	53.9	99.7	44.64	0.08
09	30.66	0.0110	0.5400	11.209	46.3	99.5	44.65	0.09
01	30.89	0.0099	1.226	17.904	51.3	98.8	44.69	0.07
07	30.72	0.0102	0.5480	5.557	49.9	99.5	44.73	0.09
06	31.88	0.0098	4.332	11.983	52.0	96.0	44.78	0.09
02	30.68	0.0094	0.2839	9.773	54.0	99.7	44.79	0.07
12	30.66	0.0119	0.2005	15.420	43.0	99.8	44.79	0.07
11	30.75	0.0118	0.5074	12.189	43.3	99.5	44.79	0.09
05	30.67	0.0101	0.0933	16.426	50.4	99.9	44.85	0.07
03	30.79	0.0099	0.3860	10.795	51.7	99.6	44.90	0.08
Mean age ± 1σ n=14 MSWD=1.70					50.3 ±8.9		44.73	0.04
LL-07-01, Sanidine, J=0.0008214±0.05%, D=1.0006±0.001, NM-213G, Lab#=57525								
01	31.00	0.0119	11.03	9.570	42.9	89.5	40.64	0.10
13	28.15	0.0105	1.132	10.181	48.7	98.8	40.75	0.08
02	27.91	0.0105	0.1047	10.959	48.8	99.9	40.84	0.08
12	28.02	0.0111	0.4833	7.655	45.8	99.5	40.85	0.07
03	28.06	0.0197	0.5845	12.789	25.9	99.4	40.86	0.07
09	28.27	0.0107	1.164	11.542	47.7	98.8	40.92	0.07
07	28.21	0.0184	0.9498	7.150	27.7	99.0	40.92	0.08
14	28.19	0.0235	0.7754	3.426	21.7	99.2	40.97	0.11
06	28.14	0.0106	0.5920	11.648	48.0	99.4	40.97	0.07
04	28.32	0.0109	1.109	7.390	47.0	98.8	41.02	0.07
11	28.07	0.0111	0.2616	8.213	46.0	99.7	41.02	0.07
15	28.02	0.0135	-0.0267	2.927	37.7	100.0	41.06	0.11
05	29.30	0.0250	3.847	12.842	20.4	96.1	41.26	0.11
Mean age ± 1σ n=13 MSWD=2.60					39.1 ±22.1		40.92	0.04
VR-07-17, Sanidine, J=0.0008206±0.05%, D=1.0006±0.001, NM-213G, Lab#=57524								
15	27.91	0.0106	0.5929	9.494	47.9	99.4	40.59	0.07
07	27.84	0.0100	0.3096	14.673	50.8	99.7	40.62	0.08
08	28.51	0.0114	2.290	8.335	44.6	97.6	40.74	0.08
12	28.07	0.0128	0.8106	5.242	39.9	99.2	40.74	0.08
10	27.99	0.0121	0.4724	13.636	42.1	99.5	40.77	0.11
06	28.01	0.0101	0.4351	6.966	50.4	99.5	40.81	0.07
04	28.05	0.0104	0.5664	10.925	49.2	99.4	40.82	0.08
03	27.98	0.0104	0.2269	7.841	49.1	99.8	40.86	0.07
02	28.16	0.0111	0.8289	10.143	45.8	99.1	40.86	0.09
05	28.04	0.0125	0.3988	7.106	40.8	99.6	40.86	0.07
13	28.10	0.0113	0.4740	5.675	45.1	99.5	40.92	0.07
09	28.31	0.0114	1.199	6.792	44.6	98.8	40.92	0.08
11	28.08	0.0096	0.4018	7.286	53.0	99.6	40.92	0.07
01	28.06	0.0090	0.2413	6.687	56.5	99.7	40.96	0.07
14	28.07	0.0141	0.1057	3.265	36.1	99.9	41.05	0.11
Mean age ± 1σ n=15 MSWD=2.32					45.9 ±11.3		40.83	0.04

Appendix A1. Continued

VR-07-38, Sanidine, J=0.0008193±0.05%, D=1.0006±0.001, NM-213G, Lab#=57523

07	23.54	0.0080	7.499	4.704	64.1	90.6	31.24	0.09
03	22.21	0.0087	2.611	17.383	58.5	96.5	31.41	0.07
06	22.51	0.0085	3.449	13.599	60.1	95.5	31.48	0.07
08	23.03	0.0092	5.172	11.820	55.2	93.4	31.50	0.07
15	21.81	0.0084	1.023	9.667	60.9	98.6	31.52	0.06
11	21.64	0.0081	0.4102	6.300	63.1	99.4	31.54	0.06
09	21.67	0.0084	0.4892	7.363	60.6	99.3	31.54	0.06
04	22.25	0.0102	2.389	14.170	49.9	96.8	31.57	0.06
12	22.28	0.0098	2.429	6.655	51.8	96.8	31.59	0.07
05	23.92	0.0081	7.962	13.086	62.8	90.2	31.60	0.07
02	21.79	0.0078	0.7219	9.314	65.2	99.0	31.61	0.06
01	21.77	0.0084	0.6205	16.412	61.1	99.2	31.62	0.05
13	21.83	0.0096	0.7682	5.928	52.9	99.0	31.66	0.07
14	22.23	0.0088	1.940	5.377	58.1	97.4	31.74	0.07
Mean age ± 1σ	n=14		MSWD=2.41			58.5 ±9.4	31.55	0.03

VR-08-02, Sanidine, J=0.0019421±0.14%, D=1.0014±0.001, NM-220B, Lab#=58018

07	14.01	0.0085	17.50	17.628	60.2	63.1	30.68	0.14
03	9.856	0.0087	3.353	26.570	58.5	89.9	30.76	0.15
12	9.525	0.0092	2.008	15.943	55.2	93.8	31.00	0.06
11	9.135	0.0086	0.6724	33.996	59.0	97.8	31.01	0.08
06	9.452	0.0072	1.730	19.595	70.5	94.6	31.02	0.06
05	16.13	0.0104	24.32	8.749	49.1	55.4	31.03	0.21
08	9.061	0.0098	0.3971	42.587	51.9	98.7	31.04	0.04
10	9.773	0.0086	2.803	15.870	59.1	91.5	31.04	0.07
13	10.55	0.0088	5.423	13.510	58.3	84.8	31.04	0.08
04	9.129	0.0087	0.5938	28.065	58.7	98.1	31.07	0.05
01	9.294	0.0084	1.139	34.974	60.8	96.4	31.08	0.06
14	9.425	0.0085	1.553	14.796	60.1	95.1	31.11	0.06
15	9.603	0.0075	2.118	9.014	67.9	93.5	31.15	0.08
# 09	9.165	0.0088	0.4666	36.256	58.3	98.5	31.32	0.06
# 02	10.10	0.0091	3.623	17.549	56.1	89.4	31.34	0.07
Mean age ± 1σ	n=13		MSWD=1.22			59.1 ±12.3	31.04	0.05

Notes:

Isotopic ratios corrected for blank, radioactive decay, and mass discrimination, not corrected for interfering reactions.

Errors quoted for individual analyses include analytical error only, without interfering reaction or J uncertainties.

Mean age is weighted mean age of Taylor (1982). Mean age error is weighted error

   of the mean (Taylor, 1982), multiplied by the root of the MSWD where MSWD>1, and also

   incorporates uncertainty in J factors and irradiation correction uncertainties.

Decay constants and isotopic abundances after Steiger and Jäger (1977).

symbol preceding sample ID denotes analyses excluded from mean age calculations.

Ages calculated relative to FC-2 Fish Canyon Tuff sanidine interlaboratory standard at 28.02 Ma

Decay Constant (LambdaK (total)) = 5.543e-10/a

Correction factors:

  $(^{39}Ar/^{37}Ar)_{Ca} = 0.0007 \pm 5e\text{-}05$

  $(^{36}Ar/^{37}Ar)_{Ca} = 0.00028 \pm 2e\text{-}05$

  $(^{38}Ar/^{39}Ar)_{K} = 0.013$

  $(^{40}Ar/^{39}Ar)_{K} = 0.01 \pm 0.002$

Appendix A2. Argon isotopic results for step-heated samples.

ID	Power/Temp (Watts/°C)	$^{40}Ar/^{39}Ar$	$^{37}Ar/^{39}Ar$	$^{36}Ar/^{39}Ar$ (x 10^{-3})	$^{39}Ar_K$ (x 10^{-15} mol)	K/Ca	$^{40}Ar^*$ (%)	^{39}Ar (%)	Age (Ma)	±1σ (Ma)
MP-08-01, K-Feldspar, 14.71 mg, J=0.0019364±0.12%, D=1.0014±0.001, NM-220B, LabX=58025-01										
Xi A	530	77.25	0.0259	140.9	2.37	19.7	46.1	0.3	120.29	1.40
Xi B	530	13.63	-0.0188	18.52	1.47	-	59.8	0.5	28.23	0.91
Xi C	580	16.33	-0.0010	14.60	1.96	-	73.6	0.7	41.46	0.64
Xi D	580	11.34	-0.0113	7.274	1.77	-	81.0	0.9	31.80	0.62
Xi E	630	14.77	0.0112	10.36	3.02	45.5	79.3	1.3	40.43	0.47
Xi F	630	10.02	0.0023	3.498	3.02	225.5	89.7	1.6	31.07	0.39
Xi G	680	11.95	0.0093	5.378	5.09	54.8	86.7	2.2	35.81	0.27
Xi H	680	9.436	-0.0077	1.300	5.17	-	95.9	2.8	31.31	0.22
Xi I	730	10.33	0.0080	3.448	6.85	63.8	90.1	3.6	32.19	0.19
Xi J	730	9.511	0.0096	1.767	7.55	53.3	94.5	4.5	31.10	0.16
Xi K	780	9.543	0.0030	1.057	7.91	170.1	96.7	5.4	31.93	0.14
Xi L	780	9.491	0.0028	1.049	8.8	180.2	96.7	6.5	31.76	0.14
Xi M	830	9.548	0.0073	0.8044	9.2	69.6	97.5	7.6	32.20	0.13
Xi N	830	9.492	0.0109	0.9845	11.6	46.8	96.9	8.9	31.83	0.11
Xi O	880	9.543	0.0076	0.6711	11.8	66.9	97.9	10.3	32.32	0.10
Xi P	880	9.518	0.0107	0.5618	13.8	47.5	98.3	11.9	32.35	0.10
Xi Q	930	9.470	0.0110	0.5787	12.4	46.2	98.2	13.4	32.16	0.10
R	930	9.581	0.0065	0.5142	15.6	78.6	98.4	15.3	32.61	0.09
S	980	9.632	0.0070	0.6958	13.8	73.2	97.9	16.9	32.60	0.09
T	980	9.719	0.0074	0.8875	17.5	68.7	97.3	18.9	32.70	0.08
U	1030	9.871	0.0035	1.440	14.8	144.1	95.7	20.7	32.67	0.10
V	1030	9.829	0.0044	1.154	19.6	117.1	96.5	23.0	32.81	0.08
W	1080	10.08	0.0060	2.055	18.1	85.6	94.0	25.1	32.78	0.09
X	1080	9.849	0.0067	1.404	22.3	76.6	95.8	27.8	32.63	0.10
Y	1130	10.01	0.0075	2.142	26.9	68.4	93.7	30.9	32.44	0.09
Z	1180	9.867	0.0094	1.481	37.7	54.1	95.6	35.4	32.61	0.07
Xi AA	1180	9.910	0.0095	1.153	72.7	53.8	96.6	43.9	33.09	0.06
Xi AB	1180	9.962	0.0072	1.027	78.9	70.5	97.0	53.2	33.40	0.06
Xi AC	1180	10.37	0.0125	1.588	75.5	40.8	95.5	62.2	34.24	0.06
Xi AD	1180	10.82	0.0054	3.123	64.0	93.7	91.5	69.7	34.22	0.07
Xi AE	1280	9.736	0.0067	0.3234	78.7	75.9	99.0	79.0	33.34	0.06
Xi AF	1330	9.833	0.0073	0.3998	59.3	70.2	98.8	86.0	33.59	0.05
Xi AG	1380	10.03	0.0099	0.6077	32.1	51.5	98.2	89.8	34.07	0.06
Xi AH	1580	10.62	0.0146	0.6396	86.7	35.0	98.2	100.0	36.05	0.05
Integrated age ± 1σ			n=34		847.9	60.3	K2O=11.43%		33.78	0.06
Plateau ± 1σ	steps R-Z	n=9	MSWD=1.57	186.108				21.9	32.65	0.05
Isochron±1σ	steps R-Z	n=9	MSWD=1.77			$^{40}Ar/^{36}Ar=$	291.3±16.3		32.67	0.09

JV-G5-9, Adularia, 4.59 mg, J=0.0008213±0.06%, D=1.0006±0.001, NM-213H, LabX=57531-01

X	A	650	192.5	0.0336	568.4	0.92	15.2	12.7	3.0	35.97	1.52
	B	750	29.39	0.0101	29.89	2.24	50.5	69.9	10.3	30.20	0.38
	C	850	22.54	0.0205	7.880	2.94	24.9	89.7	19.9	29.70	0.26
	D	920	22.05	0.0096	7.315	2.09	53.2	90.2	26.8	29.23	0.34
	E	1000	26.40	0.0038	19.77	3.19	133.6	77.9	37.2	30.21	0.28
	F	1075	22.82	0.0058	9.267	4.75	87.6	88.0	52.8	29.52	0.18
	G	1110	23.81	0.0053	11.45	3.50	95.9	85.8	64.2	30.02	0.23
	H	1180	25.51	0.0024	16.64	2.94	217.0	80.7	73.9	30.26	0.27
	I	1210	26.33	0.0037	19.68	1.66	138.8	77.9	79.3	30.14	0.43
	J	1250	27.40	0.0022	23.16	1.47	231.0	75.0	84.1	30.20	0.49
	K	1300	28.49	0.0100	25.62	1.70	51.1	73.4	89.7	30.74	0.46
X	L	1400	28.02	0.0291	24.68	3.15	17.6	74.0	100.0	30.45	0.27
	Integrated age ± 1σ			n=12		30.5	49.2	K2O=3.11%		30.19	0.13
	Plateau ± 1σ		steps B-K	n=10	MSWD=1.91	26.5			86.7	29.89	0.13
	Isochron±1σ		steps A-L	n=12	MSWD=1.36		$^{40}Ar/^{36}Ar=$	304.4±1.9		29.75	0.12

JV-K9-17, Adularia, 8.15 mg, J=0.0008204±0.06%, D=1.0006±0.001, NM-213H, LabX=57530-01

Xi	A	650	1483.1	0.0922	4894.9	2.25	5.5	2.5	1.0	53.47	8.86
Xi	B	750	86.87	0.2185	224.5	9.1	2.3	23.7	5.0	30.18	0.52
Xi	C	850	30.13	0.2131	33.39	11.2	2.4	67.3	9.9	29.77	0.14
X	D	920	23.73	0.0151	11.11	10.2	33.8	86.2	14.4	30.01	0.10
Xi	E	1000	29.75	0.0100	32.17	21.0	51.0	68.1	23.6	29.72	0.15
X	F	1075	22.77	0.0073	7.867	24.4	70.0	89.8	34.4	30.02	0.07
X	G	1110	25.16	0.0044	15.22	17.8	115.8	82.1	42.2	30.32	0.09
X	H	1180	25.62	0.0042	17.12	19.7	120.5	80.3	50.9	30.18	0.10
X	I	1210	25.80	0.0042	17.33	10.0	121.5	80.2	55.3	30.35	0.13
	J	1250	27.62	0.0065	22.86	10.0	78.2	75.5	59.7	30.63	0.15
	K	1300	29.36	0.0074	28.76	16.2	68.9	71.1	66.8	30.62	0.12
	L	1680	28.80	0.0084	26.47	75.6	61.0	72.8	100.0	30.79	0.09
	Integrated age ± 1σ			n=12		227.6	18.9	K2O=13.08%		30.59	0.17
	Plateau ± 1σ		steps J-L	n=3	MSWD=0.81	101.842			44.7	30.71	0.07
	Isochron±1σ		steps D-L	n=8	MSWD=1.06		$^{40}Ar/^{36}Ar=$	321.6±3.6		29.68	0.10

VV-GD-13, Adularia, 18 mg, J=0.0019393±0.12%, D=1.0014±0.001, NM-220B, LabX=58020-01

X	A	650	114.2	0.0008	350.3	18.7	607.8	9.3	2.2	36.77	1.60
X	B	750	13.16	0.0040	21.03	59.5	127.8	52.7	9.0	24.10	0.16
X	C	850	9.147	0.0024	4.799	51.7	212.4	84.5	15.0	26.81	0.07
X	D	920	8.397	0.0005	1.103	34.3	1010	96.1	19.0	27.99	0.06
X	E	1000	8.449	0.0015	0.7368	64.4	350.5	97.4	26.4	28.54	0.05
X	F	1075	8.555	0.0012	1.022	64.4	426.4	96.5	33.8	28.61	0.05
X	G	1110	8.965	0.0007	2.332	38.6	760.6	92.3	38.3	28.69	0.07
X	H	1140	9.232	0.0010	3.158	27.5	510.3	89.9	41.5	28.77	0.10
X	I	1170	9.521	0.0011	4.473	20.2	478.1	86.1	43.8	28.43	0.11
X	J	1210	9.870	0.0008	5.199	19.3	645.6	84.4	46.0	28.89	0.12
X	K	1250	10.48	0.0023	7.311	27.4	221.5	79.4	49.2	28.84	0.10
X	L	1275	10.84	-0.0001	8.405	35.7	-	77.1	53.3	28.97	0.11
X	M	1300	11.00	0.0010	8.692	51.1	535.3	76.6	59.2	29.24	0.10
	N	1400	10.72	0.0005	7.236	318.8	1007	80.0	100.0	29.74	0.07
	Integrated age ± 1σ			n=15		866.0	439.8	K2O=9.53%		28.94	0.10
	Step N ± 1σ			n=1		318.823			40.8	29.74	0.07

VV-IC-01, Alunite, 10 mg, J=0.0008211±0.06%, D=1.0032±0.0012, NM-213H, LabX=57534-01

Xi A	2	436.5	0.1204	1366.9	0.062	4.2	7.5	0.0	47.7	9.2
Xi B	3	63.41	-0.0055	140.0	1.97	-	34.8	1.5	32.37	0.49
Xi C	4	26.69	-0.0035	16.92	5.74	-	81.3	5.6	31.84	0.14
Xi D	5	22.38	-0.0009	4.095	11.2	-	94.6	13.7	31.082	0.080
E	6	21.33	-0.0008	1.642	34.0	-	97.7	38.3	30.622	0.049
F	8	21.32	0.0002	1.715	48.0	2698	97.6	73.0	30.562	0.047
G	10	21.60	-0.0001	2.836	32.2	-	96.1	96.2	30.496	0.052
Xi H	11	54.36	0.0804	120.6	5.22	6.3	34.5	100.0	27.55	0.38
Integrated age ± 1σ			n=8		138.3	193.0	K2O=6.47%		30.579	0.063
Plateau ± 1σ	steps E-G	n=3	MSWD=1.54	114.1				82.5	30.563	0.040
Isochron±1σ	steps E-G	n=3	MSWD=0.64		$^{40}Ar/^{36}Ar=$	240±40			30.73	0.11

VR-07-05, Alunite, 9.7 mg, J=0.0008219±0.07%, D=1.0032±0.0012, NM-213H, LabX=57533-01

Xi B	2	543.6	0.9487	1712.7	0.028	0.54	6.9	0.0	55	11
Xi C	3	46.33	0.0345	95.29	0.93	14.8	39.2	0.8	26.75	0.47
D	4	26.55	0.0199	18.86	3.32	25.7	79.0	3.4	30.85	0.14
E	5	25.15	0.0136	13.51	6.17	37.6	84.1	8.3	31.11	0.12
F	6	23.75	0.0130	9.117	20.5	39.3	88.7	24.7	30.951	0.071
G	8	23.12	0.0114	6.491	50.5	44.8	91.7	65.0	31.173	0.057
H	10	23.17	0.0111	7.164	25.5	46.0	90.9	85.4	30.948	0.068
I	12	29.44	0.0154	28.59	15.0	33.1	71.3	97.3	30.87	0.13
J	14	94.74	0.0530	248.7	2.57	9.6	22.4	99.4	31.24	0.73
Xi K	16	198.0	0.1156	608.9	0.76	4.4	9.2	100.0	26.7	1.9
Integrated age ± 1σ			n=10		125.3	35.8	K2O=6.03%		30.988	0.084
Plateau ± 1σ	steps D-J	n=7	MSWD=2.13	123.5				98.6	31.026	0.053
Isochron±1σ	steps D-J	n=7	MSWD=2.47		$^{40}Ar/^{36}Ar=$	294.3±2.9			31.050	0.070

Notes:

Isotopic ratios corrected for blank, radioactive decay, and mass discrimination, not corrected for interfering reactions.

Errors quoted for individual analyses include analytical error only, without interfering reaction or J uncertainties.

Integrated age calculated by summing isotopic measurements of all steps.

Integrated age error calculated by quadratically combining errors of isotopic measurements of all steps.

Plateau age is inverse-variance-weighted mean of selected steps.

Plateau age error is inverse-variance-weighted mean error (Taylor, 1982) times root MSWD where MSWD>1.

Plateau error is weighted error of Taylor (1982).

Decay constants and isotopic abundances after Steiger and Jäger (1977).

X symbol preceding sample ID denotes analyses excluded from plateau age calculations.

i symbol preceding sample ID denotes analyses excluded from isochron age calculations.

- symbol indicates no detectable 37Ar

Weight percent K_2O calculated from ^{39}Ar signal, sample weight, and instrument sensitivity.

Ages calculated relative to FC-2 Fish Canyon Tuff sanidine interlaboratory standard at 28.02 Ma

Decay Constant (LambdaK (total)) = 5.543e-10/a

Correction factors:

NM-213	NM-220
$(^{39}Ar/^{37}Ar)_{Ca} = 0.00068 \pm 5e\text{-}05$	$(^{39}Ar/^{37}Ar)_{Ca} = 0.0007 \pm 5e\text{-}05$
$(^{36}Ar/^{37}Ar)_{Ca} = 0.00028 \pm 2e\text{-}05$	$(^{36}Ar/^{37}Ar)_{Ca} = 0.00028 \pm 2e\text{-}05$
$(^{38}Ar/^{39}Ar)_K = 0.0125$	$(^{38}Ar/^{39}Ar)_K = 0.013$
$(^{40}Ar/^{39}Ar)_K = 0 \pm 0.0004$	$(^{40}Ar/^{39}Ar)_K = 0.01 \pm 0.002$

Appendix B. Description of samples collected at surface.

Sample	East	North	Description/Alteration	Veinlets
VR-07-01	711,682	2,559,543	Tuff, quartz alunite	Alunite
VR-07-05	711,497	2,559,813	Tuff, quartz alunite	Alunite
VR-07-07	711,383	2,559,926	Tuff, quartz alunite	Alunite
VR-07-12	711,769	2,559,202	Tuff	
VR-07-17	711,343	2,557,913	Tuff	
CC-07-01	720,133	2,560,948	GT-graywacke, chloritized	Barite
LL-07-01	721,681	2,561,115	Tuff	
VR-07-38	708,590	2,559,720	Rhylitic dome	
VR-08-02	710,426	2,555,886	Altamira rhyodacite	
VR-09-01	711,636	2,556,260	Chalcedony blanket	
CH-09-01	717,407	2,560,334	GT-andesite, chloritized	Quartz

East and north coordinates in UTM, datum Nad-27, Zone 13N
GT (Guerrero Terrane, volcanic sedimentary sequence)

Appendix C. Longitudinal section with drill holes.
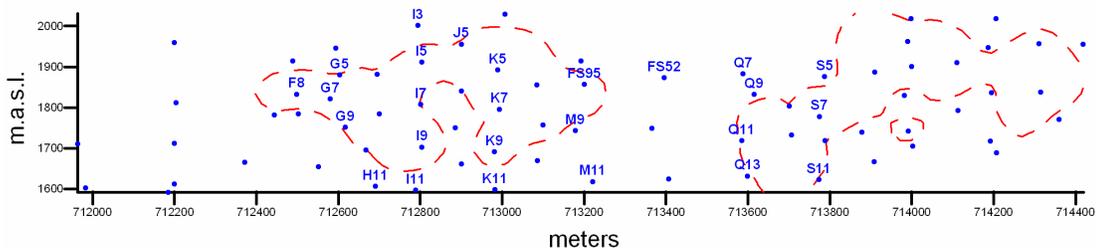
Location of drill holes studied from Jarillas vein. Blue circles represent drill-hole intercepts; only the drill-holes studied are labelled. Red dashed line approximately represents the ore zone. Elevation in meters above sea level (m.a.s.l.), and horizontal scale (easting coordinate; UTM) in meters.

Appendix D. Petrographic descriptions for samples of Jarillas vein.

JV-G5-01: Banded vein of quartz, calcite and sulfides, that is cross cut by late quartz micro veins. This sample shows sphalerite with chalcopyrite disease, pyrite occurs disseminated in quartz and calcite and replacing sphalerite and galena. Polybasite, myargirite and pyrargyrite occur disseminated in calcite and quartz. Late micro veins of quartz cross cut early calcite, quartz and coarse grains of sphalerite.

JV-G5-02: Banded vein of quartz, calcite and sulfides that is cross cut by late quartz micro veins. This sample shows clearly that pyrite replaces sphalerite and silver sulfosalts

131

(polybasite, pyrargyrite). There is microcrystalline quartz with disseminated grains of pyrite and sphalerite. In this sample pyrite and sphalerite are abundant but the amount of silver sulfosalts diminishes with respect to sample JV-G5-01.

JV-G5-04: Banded vein of quartz, calcite and sulfides. In this sample most of the pyrite occurs in euhedral cubes and less commonly replaces sphalerite. Sphalerite was observed to be associated with polybasite. There are also cubes of pyrite that seem to be replaced by late pyrargyrite.

JV-G5-05: Banded vein of quartz, calcite, sulfides and hematite. In this sample sphalerite replaces galena, and pyrite and arsenian-pyrite replace sphalerite. Pyrite also occurs included in sphalerite and galena. There are polybasite, acanthite and pyrargyrite inclusions in sphalerite. This sample contains more galena than sphalerite.

JV-G5-07: Brecciated vein with sulfides bordered by quartz, calcite and chlorite. In this sample sphalerite replaces galena and pyrite replaces sphalerite and galena. Sphalerite contains abundant chalcopyrite disease and inclusions of pyrargyrite and acanthite. Early pyrite occurs included in galena and sphalerite. Pyrargyrite is associated and replaced by pyrite.

JV-G5-15: Banded vein; there are thin bands of sulfosalts. Sphalerite contains abundant inclusions of chalcopyrite, pyrargyrite, pyrrhotite and galena. Sphalerite is the most abundant sulfide, followed by arsenian-pyrite, pyrite and arsenopyrite. Early pyrite is included in sphalerite and galena, and late pyrite replaces sphalerite and galena. A very late pyrargyrite borders the late pyrite. Late pyrargyrite is associated with calcite.

JV-G5-08: Banded veins of quartz, calcite and sphalerite with disseminated sulfosalts. Sphalerite in this sample has dark cores due to high Fe contents. Sphalerite replaces galena, pyrite replaces sphalerite and arsenian-pyrite – arsenopyrite replaces pyrite.

JV-G5-09: Banded vein; thick bands of quartz and sphalerite; adularia crystals were observed in this sample. The sphalerite in this sample also has cores rich in Fe and chalcopyrite disease, chalcopyrite also occurs as independent grains and as large inclusions (100μm) in sphalerite. Sphalerite also contains inclusions of pyrite, galena, sulfosalts, and pyrrhotite. Late pyrite and arsenian-pyrite border sphalerite.

JV-G5-11: Banded vein of quartz, calcite and sulfides; there are late quartz and dolomite-ankerite in vugs between bands. The sample contains galena, sphalerite pyrite and arsenopyrite in that order of deposition. Sphalerite has generally low iron contents but it shows abundant inclusions of silver sulfosalts, galena and sometimes very tiny inclusions of chalcopyrite.

JV-G5-11: Banded vein of quartz, chalcedonic quartz, calcite and sulfides (predominantly pyrite and sphalerite). The sample consists of galena, sphalerite, pyrite, pyrargyrite, acanthite, aguilarite, arsenopyrite. In this sample sphalerite has inclusions of galena, pyrite, silver sulfosalts (pyrargyrite and polybasite?), and less chalcopyrite. Inclusions of sphalerite were observed in acanthite.

FS-95-01: Banded vein consisting of quartz, calcite, white phylosilicates (illite-smectite), and sulfides (sphalerite, pyrite, galena). This sample contains sphalerite, galena, pyrargyrite, pyrite, arsenian-pyrite and arsenopyrite. Sphalerite contains inclusions of galena, pyrite and pyrargyrite but galena was also observed with inclusions of sphalerite

and pyrargyrite, therefore galena and sphalerite were co-deposited. Arsenian-pyrite and arsenopyrite are the latest minerals in the paragenesis.

FS-95-02: Banded vein; colloform bands of white and black chalcedony and calcite. This sample contains pyrite and pyrargyrite. Pyrargyrite is associated with calcite and they are late with respect to the chalcedony bands. Adularia was observed being replaced by a white phylosilicate (sericite).

FS-95-03: Banded and brecciated vein. This sample is barren, it contains coarse grains of arsenian-pyrite and rhombs of arsenopyrite. There are brecciated or broken bands of chalcedony and sometimes quartz-hematite; the bands are broken by late barren quartz. Small adularia grains altered to sericite were also observed.

FS-95-04: Banded vein; coarse banding. The vein contains thick bands of quartz with disseminated arsenian-pyrite and arsenopyrite and less calcite; calcite mainly interstitial.

JV-G7-11: Banded vein, multiple bands of quartz, chalcedony and calcite. The chalcedony in these bands shows typical colloform banding and feathery textures. The sample contains pyrite, sphalerite, chalcopyrite, acanthite, and electrum? The grains of electrum (<50 μm) were observed in quartz alone and associated with acanthite.

JV-G7-13: Massive vein of sphalerite, pyrite, galena with less interstitial quartz. The sphalerite grains are zoned, they contain cores with abundant chalcopyrite disease; the abundant chalcopyrite makes the cores look yellow. The rims of the crystals have progressively much less chalcopyrite. Other minerals occurring as inclusions in sphalerite are galena, undifferentiated silver sulfosalts (too small) and pyrrhotite. The quartz that occurs in this sample makes up ~10% volume, it occurs interstitial, cementing brecciated grains of sulfides and in micro-veins cross cutting big sulfide grains. Minor amounts of

calcite also occur interstitial. Sphalerite and galena are early and pyrite is late. Galena also contains inclusions of sulfosalts.

JV-G7-02: Banded vein showing bands of sphalerite, pyrite, galena, calcite and quartz. There are late stage calcite veins cross cutting the banding. Sphalerite contains inclusions of silver sulfosalts (aguilarite?), galena, pyrite and chalcopyrite. There are late pyrite micro-veins that cross cut sphalerite bands. There is a vein of epidote that cross cuts sphalerite.

JV-G7-06: Vein of sulfides that are being cross cut by a crustiform banded vein. The crustified vein has vugs at the center filled with calcite and big euhedral crystals of pyrargyrite. The quartz in the banded vein is chalcedonic with colloform textures. Sphalerite forms bands and contains inclusions of pyrargyrite, acanthite, galena and chalcopyrite. Pyrite is late and also early.

JV-G7-09: Crustiform banded vein with colloform chalcedonic quartz and calcite. The sample contains sphalerite, galena, pyrite and acanthite in that paragenesis. Sphalerite contains inclusions of galena and chalcopyrite. Epidote was observed.

JV-G9-06: Banded vein of quartz and calcite with disseminated sphalerite and silver sulfosalts. This sample contains adularia and epidote. The sample contains sphalerite, pyrite, galena, pyrargyrite and acanthite in that paragenesis. Sphalerite contains inclusions of galena.

JV-I11-03: Banded vein of multi-stages of quartz and calcite with disseminated sphalerite. Epidote was observed associated with calcite. The sample contains chalcopyrite, galena, sphalerite, pyrite and arsenian-pyrite. Chalcopyrite occurs as

135

discrete grains and as inclusions in sphalerite. Arsenian-pyrite is the latest sulfide mineral.

JV-I5-02: Banded vein of quartz and calcite with sulfides and coarse pyrargyrite. There are bands of colloform chalcedony, some of these bands are broken by late quartz and calcite. There altered (sericitized) adularia grains. The sample contains galena, sphalerite, pyrite, acanthite and arsenian-pyrite in that paragenetic order. Sphalerite contains inclusions of pyrargyrite and chalcopyrite; looks like sulfosalt and chalcopyrite disease.

JV-I5-05: Banded vein of quartz, calcite, pyrite and sphalerite. The sample contains galena, sphalerite, pyrite, pyrargyrite, acanthite and arsenian pyrite in that paragenetic order. Sphalerite contains abundant inclusions of pyrargyrite.

JV-I5-06: Banded vein with colloform textures of chalcedony with disseminated pyrite. The sample contains sphalerite with inclusions of pyrargyrite and early pyrite. There are also late pyrite, pyrargyrite (discrete grains), acanthite and arsenian-pyrite.

JV-I7-03: Banded vein of quartz and calcite bearing disseminated pyrite and sphalerite. The sample contains galena, sphalerite, pyrite, acanthite and arsenian-pyrite in that paragenetic order.

JV-I7-04: Banded vein, quartz, calcite and bands of quartz hematite. The sample contains chalcopyrite, pyrite, electrum? and arsenopyrite. Some arsenopyrite grains are up to ~900 µm.

JV-I9-01: Banded vein of quartz, calcite, sphalerite and galena; colloform textures. There are both, quartz and chalcedony, the chalcedony bands show radial extinction (feathery). The sample contains galena, sphalerite, pyrite, acanthite, and arsenian-pyrite. Sphalerite

contains inclusions of pyrargyrite, tetrahedrite, aguilarite? and chalcopyrite. Thin bands of hematite were also observed.

JV-I9-06: Banded vain of quartz and sulfides. The banded vein seems to be cross cutting and brecciating a vein of massive sulfides because some sphalerite grains are sub-rounded and cross cut by quartz micro-veins. There are big sphalerite grains, zoned with variable amounts of chalcopyrite disease from band to band of sphalerite. There also inclusions of tetrahedrite-tennantite in sphalerite; thin micro-veins of pyrargyrite cross cut sphalerite grains. The quartz micro-veins contain small grains of sphalerite probably broken from the vein of massive sulfides. A thin banded vein of chalcedonic quartz cross cuts the previous quartz and the massive sulfides. The sample contains pyrite, galena, sphalerite, pyrite in that paragenetic order.

JV-I9-07: Banded vein of quartz, calcite and sphalerite. The bands of sphalerite also contain galena, pyrite and pyrargyrite and late arsenian-pyrite. The sphalerite grains contain inclusions of sulfosalts (tertrahedrite – tennantite, miargyrite?).

JV-I9-08: Crustified banded vein of quartz and sulfides. There are zoned bands of sphalerite; the sphalerite of the band at the center is iron rich, whereas the sphalerite at in the bands at the edges is iron poor. There is also a band of galena inter-grown with sphalerite. Some sphalerite grains contain chalcopyrite disease and inclusions of sphalerite. The minerals are early pyrite, galena, sphalerite, pyrite and arsenian-pyrite in that paragenetic order. Late quartz breaks the bands of sphalerite and galena.

JV-K11-02: Banded vein of quartz, chalcedony, calcite and epidote. Very few disseminated sulfides. There are galena, sphalerite, pyrite pyrargyrite and late arsenian-pyrite. Sphalerite contains inclusions of chalcopyrite.

JV-K11-05: Banded vein of quartz, chalcedony, calcite and epidote. Epidote bears interstitial calcite. There is also adularia being altered to sericite. The disseminated sulfides are not abundant. There are sphalerite, pryrite, pyrargyrite and late acanthite.

JV-K11-07: Banded vein of quartz, chalcedony, calcite, epidote and sulfides. The sample contains galena, sphalerite, pyrite, pyrargyrite and arsenian pyrite. Sphalerite contains chalcopyrite and pyrargyrite inclusions. There is early and late pyrite. Late calcite breaks bands of chalcedony. There are hematite bands and hematite filling fractures. Adularia was observed associated with epidote.

JV-K5-01: Banded vein of quartz and calcite with disseminated pyrite and silver sulfosalts. The vein shows dissolution cavities between bands probably due to acid leaching by late hydrothermal fluids. There are adularia grains but they are deeply sericitized. There are small grains of acanthite rimmed by arsenian-pyrite. No other sulfides were observed.

JV-K5-02: Banded vein of quartz, calcite and sulfides, cross cut by late veins of calcite bearing pyrargyrite. The sample contains galena, sphalerite, pyrite, arsenian-pyrite and pyrargyrite in that paragenetic order. Sphalerite and galena contain inclusions of silver sulfosalts (pyrargyrite, aguilarite, tetrahedrite – tennantite). There is band of chalcedonic quartz with arsenian-pyrite with dendritic habit; this habit in arsenian-pyrite was probably caused because arsenian-pyrite was in suspension in the colloidal silica, not in solution in a fluid. Late calcite veins with pyrargyrite cross cut the bands of chalcedonic quartz.

JV-K5-04: Banded vein of calcite and quartz with disseminated sulfides. The vein presents dissolution cavities probably due to the passage of latter acidic fluids. The

sample contains galena, sphalerite, pyrite, pyrargyrite and arsenian-pyrite in that paragenetic order.

JV-K5-05: Banded vein of quartz, chalcedony, calcite and epidote with disseminated sulfides and bearing dissolution cavities. The sample contains early pyrite, galena, sphalerite, pyrite and arsenopyrite in that paragenetic order. Sphalerite contains inclusions of undifferentiated (very small) silver sulfosalts and chalcopyrite.

JV-I7-04: Banded vein of quartz, calcite, quartz-hematite and epidote. The bands are broken by a late stage of quartz. Only pyrite and arsenian-pyrite were observed in this sample.

JV-K7-04: Banded vein of quartz, calcite and sulfides. Some bands are actually chalcedony with radial extinction (feathery). The sample contains early pyrite, galena, sphalerite and late pyrite in that paragenetic order. Sphalerite contains inclusions of pyrargyrite and chalcopyrite.

JV-K7-11: Banded vein of quartz chalcedony, calcite and sulfides. The sample contains early pyrite, galena, sphalerite and late pyrite. The sphalerite of this sample contains abundant inclusions of pyrrhotite and lesser chalcopyrite.

JV-K7-06: Banded vein of quartz and calcite. There are bands of sphalerite and galena broken by late calcite. The sample contains early pyrite, galena, sphalerite and late pyrite. Sphalerite contains inclusions of silver sulfosalts.

JV-K7-09: Banded vein of quartz, chalcedony, calcite and sulfides. The sample contains bands of sphalerite and galena that were broken by late calcite carrying pyrargyrite and quartz. The sample contains early pyrite, galena, sphalerite, pyrite, arsenopyrite (rhombs)

and pyrargyrite in that paragenetic order. Sphalerite contains big inclusions of chalcopyrite (up to 400 μm).

JV-K9-01: Banded vein of quartz, chalcedony, calcite and sulfides being cross cut by late veinlets of quartz with pyrargyrite. There are bands of chalcedony and sulfides that are broken by late stage microcrystalline quartz and calcite. The sample contains early pyrite, galena, sphalerite, and late pyrite. Pyrargyrite and chalcopyrite were only observed as inclusions in sphalerite.

JV-K9-12: Brecciated vein of massive sulfides. The sample contains coarse grains of sphalerite rimmed by thin layers of pyrite. Sphalerite was deposited on top of the layers of pyrite and seems to occur as cement to the galena-pyrite grains. Late quartz and calcite also brecciate and cement the sulfides, including sphalerite. Silver sulfosalts were not observed.

JV-K9-13: Banded vein of quartz, calcite, sulfides and epidote. The banded vein is cross cut by a late colloform banded vein of chalcedony. The sample has vugs that have been filled by late quartz and dolomite-ankerite carrying pyrargyrite. The sample contains early pyrite, galena, sphalerite, late pyrite and pyrargyrite. Sphalerite contains inclusions of silver sulfosalts (tetrahedrite-tennantite) and chalcopyrite.

JV-K9-14: Banded vein of quartz, chalcedony, calcite and sulfides. Some of the chalcedony bands show radial feathery and spherulitic structures. Epidote was also observed in this sample. All the bands are cross cut by thin calcite veinlets. The sample contains chalcopyrite, early and late pyrite, very fine grain undifferentiated sulfosalts (polybasite, aguilarite, tetrahedrite-tennatite) and electrum. Unfortunately the paragenetic

relations between the silver sulfosalts and electrum are not clear but it appears that electrum is late with respect to silver in this sample.

JV-K9-17: Banded vein of quartz, chalcedony and calcite with disseminated pyrite. This sample shows multiple bands of quartz and chalcedony broken by late calcite. Epidote and adularia were also observed associated with the bands of chalcedony. Only disseminated pyrite was observed in this sample.

JV-K9-18: Banded vein of quartz, chalcedony and calcite. There are bands of coarse anhedral quartz and chalcedony. Calcite is late with respect to quartz and chalcedony. Only disseminated pyrite was observed.

JV-K9-19: Banded vein of quartz, chalcedony and calcite. There are multiple bands of quartz and chalcedony with feathery and spherulitic structures. Calcite occurs interstitial in quartz bands and filling vugs between bands of chalcedony. Only disseminated pyrite was observed.

JV-K9-20: Banded vein of quartz, chalcedony and calcite with disseminated galena, sphalerite and pyrite. The sample contains early pyrite, galena, sphalerite and late pyrite disseminated in quartz-chalcedony bands. Some of these bands with sulfides appear to be brecciated by a late stage of calcite. Sphalerite contains inclusions of chalcopyrite.

JV-K9-22: Banded vein of quartz, chalcedony, calcite and sulfides. There are late veins of calcite cross cutting the banding and also calcite getting between bands and breaking them. The sample contains early pyrite, galena, polybasite, tetrahedrite, sphalerite, late pyrite and pyrargyrite in that paragenetic order. Sphalerite contains inclusions of silver sulfosalts (polybasite, tetrahedrite-tennantite).

JV-K9-05: Banded vein of quartz, chalcedony, epidote and calcite. The chalcedony bands show the typical feathery textures. Epidote has interstitial calcite. The sample contains abundant disseminated early pyrite, galena, sphalerite late pyrite and pyrargyrite in that paragenetic order. Sphalerite contains inclusions of undifferentiated silver sulfosalts and chalcopyrite. In this sample a band of epidote has disseminated sphalerite and pyrite.

JV-K9-07: Banded vein of quartz, chalcedony and calcite with disseminated sulfides. Some of the early bands of quartz and chalcedony are broken by late quartz and calcite and cross cut by late calcite veins. The sample contains early pyrite, galena, sphalerite, late pyrite in the paragenetic order. The sphalerite in this sample is zoned; it has cores rich in iron with abundant chalcopyrite disease and rims poor in iron, and inclusions of galena and silver sulfosalts instead of chalcopyrite.

JV-K9-08: Banded vein of quartz, chalcedony and calcite with disseminated sulfides. The banded vein is cross cut by late calcite veins. The sample contains early pyrite, galena, sphalerite, late pyrite, pyrargyrite and acanthite in that paragenetic order. Sphalerite contains inclusions of gray silver sulfosalts (aguilarite?) and chalcopyrite. Additionally, a band of sphalerite is cross cut by abundant micro-veins of pyrargyrite and quartz.

JV-M11-01: Brecciated banded vein. The sample is a breccia with clasts of banded vein cemented by calcite. The bands are made up of quartz, chalcedony and sphalerite-galena. There are also epidote grains cross cut by calcite veins. The sample contains only pyrite, galena and sphalerite.

JV-M11-02: Late stage, barren vein. It appears that it is a vein of calcite and epidote with large vugs filled by late coarse grain anhedral quartz. No sulfides were observed.

JV-Q11-01: Banded vein of quartz, chalcedony and calcite with disseminated sulfides. The sample contains early pyrite, galena, sphalerite, late pyrite and arsenian-pyrite in that paragenetic order. Sphalerite has inclusions of gray silver sulfosalts and moderate to weak chalcopyrite disease. One grain of silver sulfosalts in sphalerite has one inclusion of chalcopyrite.

JV-Q11-02: Banded vein of quartz, chalcedony, calcite and sulfides (sphalerite, galena and pyrite). There are broken bands of sulfides; broken by calcite. The sample contains early pyrite, galena, sphalerite, late pyrite and arsenian-pyrite in that paragenetic order. Sphalerite contains inclusions of chalcopyrite.

JV-Q11-04: Banded vein of quartz, chalcedony and calcite. The sample is complex, it is a brecciated banded vein; broken bands of quartz and chalcedony. It shows dissolution vugs probably left by the passage of late acidic fluids. There are only disseminated pyrite and sphalerite in this sample.

JV-Q9-02: Breccia vein. The sample has large quartz grains cemented by calcite. Also there is a late stage calcite filling vugs. The sample contains only disseminated pyrite and sphalerite.

JV-Q9-04: Brecciated banded vein. There are broken bands of sphalerite, galena and pyrite. Calcite is the mineral that brecciated the banded vein. There are bands of hematite in this sample. The sample contains early pyrite, galena, sphalerite, and late pyrite in that paragenetic order. Sphalerite is almost free of chalcopyrite disease, although it contains some very small silver sulfosalts inclusions.

Appendix E. Fluid inclusions data for Jarillas vein.

Sample	Band	Mineral	Th°C	T_{mice}	NaCl wt% eq.	Density	P (bars)	Depth (m)	Stage
Chi-P76-09	xtl-2-3	euh-qtz	193.4	-2.4	3.9	0.90	11	122	surface/late
Chi-P76-09	xtl-2-3	euh-qtz	196.0	-2.4	3.9	0.90	12	133	surface/late
Chi-P76-09	xtl-2-1	euh-qtz	165.9	-2.6	4.2	0.94	6	64	surface/late
Chi-P76-09	xtl-2-3	euh-qtz	292.3	-2.6	4.2	0.77	72	938	surface/late
Chi-P76-09	xtl-2-3	euh-qtz	190.2	-2.7	4.4	0.91	10	110	surface/late
Chi-P76-09	xtl-2-3	euh-qtz		-2.7	4.4				surface/late
Chi-P76-09	xtl-2-1	euh-qtz	175.8	-2.8	4.5	0.93	7	76	surface/late
Chi-P76-09	xtl-2-1	euh-qtz	165.9	-2.9	4.7	0.94	6	64	surface/late
Chi-P76-09	xtl-2-1	euh-qtz		-2.9	4.7				surface/late
Chi-P76-09	xtl-2-3	euh-qtz	257.3	-3.1	5.0	0.84	41	491	surface/late
Chi-P76-09	xtl-2-3	euh-qtz	296.2	-3.1	5.0	0.78	72	924	surface/late
Chi-P76-09	xtl-1	euh-qtz	177.3	-3.9	6.2	0.94	8	85	surface/late
Chi-P76-09	xtl-1	euh-qtz	231.0	-3.9	6.2	0.88	25	283	surface/late
Chi-P76-09	xtl-1	euh-qtz	201.8	-4.3	6.8	0.92	13	141	surface/late
Chi-P76-09	xtl-2-1	euh-qtz	152.3				5		surface/late
Chi-P76-09	xtl-1	euh-qtz	177.3				8		surface/late
Chi-P76-09	xtl-1	euh-qtz	350.6				160		surface/late
Chi-P76-09	xtl-1	euh-qtz	360.3				177		surface/late
JV-F8-01	4	coarse qtz	222.1	-1.2	2.0	0.85	20	234	3
JV-F8-01	4	coarse qtz	217.3	-1.3	2.1	0.86	18	209	3
JV-F8-01	4	coarse qtz	233.7	-1.3	2.1	0.84	26	310	3
JV-F8-01	1	coarse-euh-qtz	230.8	-1.4	2.3	0.84	25	296	3
JV-F8-01	1	coarse-euh-qtz	257.7	-1.4	2.3	0.80	41	511	3
JV-F8-01	1	coarse-euh-qtz	231.7	-1.5	2.5	0.85	25	296	3
JV-F8-01	4	coarse qtz	215.4	-1.6	2.6	0.87	18	207	3
JV-F8-01	4	coarse qtz	226.9	-1.6	2.6	0.85	23	270	3
JV-F8-01	1	coarse-euh-qtz	228.9	-1.7	2.8	0.85	24	282	3
JV-F8-01	7	clowdy qtz	226.9	-2.3	3.8	0.86	23	266	3
JV-F8-01	7	clowdy qtz	222.1	-2.9	4.7	0.88	20	228	3
JV-F8-01	5	clowdy qtz	149.3	-3.0	4.9	0.96	5	52	3
JV-F8-01	3	coarse-euh-qtz	222.1	-3.6	5.8	0.89	20	225	3
JV-F8-01	1	coarse-euh-qtz	225.0	-3.7	5.9	0.89	22	248	3
JV-F8-01	1	coarse-euh-qtz		-3.7	5.9				3
JV-F8-01	1	coarse-euh-qtz	222.1	-3.9	6.2	0.89	20	224	3
JV-F8-01	3	coarse-euh-qtz	237.5	-3.9	6.2	0.88	28	320	3
JV-F8-01	3	coarse-euh-qtz	246.2	-3.9	6.2	0.86	33	382	3
JV-F8-01	3	coarse-euh-qtz	226.9	-4.0	6.4	0.89	23	259	3
JV-F8-01	3	coarse-euh-qtz	239.4	-4.0	6.4	0.87	29	332	3
JV-F8-01	3	coarse-euh-qtz	225.0	-4.9	7.7	0.90	22	244	3
JV-F8-01	5	clowdy qtz	106.6			0.85	5	59	3
JV-F8-01	5	clowdy qtz	160.8			0.85	6	71	3
JV-F8-01	3	coarse-euh-qtz	222.1			0.85	20	237	3
JV-FS52-1	2	coarse qtz	217.4	-1.0	1.7	0.86	18	210	3
JV-FS52-1	2	coarse qtz	218.4	-1.0	1.7	0.86	19	222	3
JV-FS52-1	3	clean cal		-1.1	1.8				3
JV-FS52-1	2	coarse qtz	222.3	-1.1	1.8	0.85	20	235	3
JV-FS52-1	2	coarse qtz	236.8	-1.1	1.8	0.83	28	337	3
JV-FS52-1	3	clean cal	207	-1.0	2	0.87	15	172	3
JV-FS52-1	2	coarse qtz	210.6	-1.3	2.1	0.87	16	184	3

Appendix E. Continued

Sample	Band	Mineral	Th°C	T_{mice}	NaCl wt% eq.	Density	P (bars)	Depth (m)	Stage
JV-FS52-1		2 coarse qtz	198.9	-1.4	2.3	0.89	12	136	3
JV-FS52-1		3 clean cal	216.4	-1.5	2.5	0.87	18	208	3
JV-FS52-1		4 ep	251.4	-1.5	2.5	0.82	36	441	3
JV-FS52-1		2 coarse qtz	198.0	-1.5	2.5	0.89	12	135	3
JV-FS52-1		6 clean cal	210	-1.7	3	0.88	16	182	3
JV-FS52-1		4 ep		-1.7	2.8				3
JV-FS52-1		6 clean cal	202.8	-1.9	3.1	0.89	13	146	3
JV-FS52-1		4 ep	217	-1.9	3	0.87	18	207	3
JV-FS52-1		6 clean cal	211.6	-2.0	3.3	0.88	16	182	3
JV-FS52-1		6 clean cal	229.1	-2.1	3.4	0.86	24	280	3
JV-FS52-1		6 clean cal	210.6	-2.2	3.6	0.88	16.0	181.2	3
JV-FS52-1		6 clean cal	207.7	-2.3	3.8	0.89	15	169	3
JV-FS52-1		6 clean cal	204	-2.4	4	0.89	14	157	3
JV-FS-95-1	F	cal	209.4	-0.4	0.7	0.86	15	175	3
JV-FS-95-1	B	cal	216.9	-2.1	3.4	0.87	18	206	3
JV-FS-95-1	B	cal	228.3	-2.1	3.4	0.86	23	268	3
JV-FS-95-1	F	cal	212.7	-2.2	3.6	0.88	17	193	3
JV-FS-95-1	D	cal	221.6	-2.2	3.6	0.87	20	230	3
JV-FS-95-1	A	cal	223.5	-2.2	3.6	0.87	21	242	3
JV-FS-95-1	F	cal	224.5	-2.2	3.6	0.87	22	248	3
JV-FS-95-1	B	cal	227.3	-2.2	3.6	0.86	23	267	3
JV-FS-95-1	F	cal	198.0	-2.3	3.8	0.90	12	134	3
JV-FS-95-1	F	cal	215.0	-2.3	3.8	0.88	18	205	3
JV-FS-95-1	A	cal	223.5	-2.4	3.9	0.87	21	241	3
JV-FS-95-1	A	cal	223.5	-2.4	3.9	0.87	21	241	3
JV-FS-95-1	A	cal	223.5	-2.4	3.9	0.87	21	241	3
JV-FS-95-1	C	Clowdy qtz	233.9	-2.4	3.9	0.86	26	304	3
JV-FS-95-1	C	Clowdy qtz	233.9	-2.4	3.9	0.86	26	304	3
JV-FS-95-1	C	Clowdy qtz	233.9	-2.4	3.9	0.86	26	304	3
JV-FS-95-1	E	cal	216.0	-2.6	4.2	0.88	18	204	3
JV-FS-95-1	E	cal	230.1	-2.6	4.2	0.87	24	277	3
JV-FS-95-1	F	coarse qtz	219.8	-2.6	4.2	0.88	20	228	3
JV-FS-95-1	F	cal	233.0	-2.7	4.4	0.86	26	302	3
JV-FS-95-1	F	comb qtz	150.0	-2.8	4.5	0.95	5	53	3
JV-FS-95-1	E	cal	226.4	-2.9	4.7	0.87	22	252	3
JV-FS-95-1	E	cal	281.1	-2.9	4.7	0.79	61	768	3
JV-FS-95-1	E	qtz	232.0	-2.9	4.7	0.87	25	288	3
JV-FS-95-1	B	cal	243.4	-3.0	4.9	0.85	31	363	3
JV-FS-95-1	F	comb qtz	169.7	-3.0	4.9	0.94	7	75	3
JV-FS-95-1	E	cal	216.9	-3.1	5.0	0.89	18	203	3
JV-FS-95-1	E	cal	255.6	-3.1	5.0	0.84	40	478	3
JV-FS-95-1	E	coarse qtz	237.7	-3.1	5.0	0.86	28	325	3
JV-FS-95-1	E	coarse qtz	250.9	-3.1	5.0	0.84	36	427	3
JV-FS-95-1	E	qtz		-3.1	5.0				3
JV-FS-95-1	E	coarse qtz		-3.1	5.0				3
JV-FS-95-1	E	coarse qtz	239.6	-3.2	5.2	0.86	29	337	3
JV-FS-95-1	E	qtz		-3.2	5.2				3
JV-FS-95-1	F	chal qtz	163.1			0.85	6	71	3
JV-FS-95-1	F	chal qtz	163.1			0.85	6	71	3

Appendix E. Continued

Sample	Band	Mineral	Th°C	T_{mice}	NaCl wt% eq.	Density	P (bars)	Depth (m)	Stage
JV-FS-95-1	F	chal qtz	163.1			0.85	6	71	3
JV-FS-95-1	F	chal qtz	215.0			0.85	18	213	3
JV-FS-95-1	F	qtz	139.5			0.85	5	59	
JV-FS-95-1	D	coarse qtz	145.2			0.85	5	59	
JV-G5-1(1)	1 and 3	cal	239.6	-0.8	1.3	0.82	35	426	2
JV-G5-1(1)	1 and 3	cal	242.5	-0.8	1.3	0.82	31	379	2
JV-G5-1(1)	1 and 3	cal	258.7	-0.8	1.3	0.79	46	583	2
JV-G5-1(1)	1 and 3	cal	258.7	-0.8	1.3	0.79	46	583	2
JV-G5-1(1)	1 and 3	cal	258.7	-0.8	1.3	0.79	46	583	2
JV-G5-1(1)	1 and 3	cal	260.6	-0.8	1.3	0.79	48	608	2
JV-G5-1(1)	1 and 3	cal	268.3	-0.9	1.5	0.77	58	749	2
JV-G5-1(1)	1 and 3	cal	295.0	-0.9	1.5	0.72	76	1053	2
JV-G5-1(1)	6	qtz	253.9	-1.2	2.0	0.81	40	497	3
JV-G5-1(1)	1 and 3	cal	253.9	-1.3	2.1	0.81	40	496	2
JV-G5-1(1)	1 and 3	cal	284.5	-1.3	2.1	0.75	64	849	2
JV-G5-1(1)	1 and 3	cal	285.5	-1.3	2.1	0.75	65	864	2
JV-G5-1(1)	4 and 5	cal	249.2	-1.3	2.1	0.82	46	564	3
JV-G5-1(1)	4 and 5	cal	255.8	-1.3	2.1	0.80	42	522	3
JV-G5-1(1)	4 and 5	cal	256.8	-1.3	2.1	0.80	43	535	3
JV-G5-1(1)	4 and 5	cal	256.8	-1.3	2.1	0.80	43	535	3
JV-G5-1(1)	4 and 5	cal	256.8	-1.3	2.1	0.80	43	535	3
JV-G5-1(1)	4 and 5	cal	258.7	-1.3	2.1	0.80	46	576	3
JV-G5-1(1)	4 and 5	cal	258.7	-1.3	2.1	0.80	46	576	3
JV-G5-1(1)	4 and 5	cal	258.7	-1.3	2.1	0.80	46	576	3
JV-G5-1(1)	4 and 5	cal	279.7	-1.3	2.1	0.76	63	827	3
JV-G5-1(1)	4 and 5	qtz	257.8	-1.3	2.1	0.80	44	549	3
JV-G5-1(1)	A	chal	231.0	-1.5	2.5	0.85	25	296	3
JV-G5-1(1)	A	chal	231.0	-1.5	2.5	0.85	25	296	3
JV-G5-1(1)	A	chal	234.8	-1.5	2.5	0.84	29	345	3
JV-G5-1(1)	A	chal	241.5	-1.5	2.5	0.83	37	445	3
JV-G5-1(1)	1 and 3	cal	262.5	-1.6	2.6	0.80	44	550	2
JV-G5-1(1)	1 and 3	cal	241.5	-1.7	2.8	0.83	37	444	2
JV-G5-1(1)	1 and 3	cal	241.5	-1.7	2.8	0.83	37	444	2
JV-G5-1(1)	4 and 5	cal	237.7	-1.8	3.0	0.84	32	380	3
JV-G5-1(1)	1 and 3	cal	242.5	-2.7	4.4	0.85	38	448	2
JV-G5-1(1)	1 and 3	cal	244.4	-2.7	4.4	0.85	40	472	2
JV-G5-1(1)	1 and 3	cal	237.7			0.85	28	331	2
JV-G5-1(1)	1 and 3	cal	252.0			0.85	37	438	2
JV-G5-1(1)	1 and 3	cal	262.5			0.85	44	520	2
JV-G5-1(1)	A	chal	236.7			0.85	28	331	3
JV-G5-3	1	euh-qtz grain	192.0	-0.9	1.5	0.89	11	124	4
JV-G5-3	1	euh-qtz grain	210.6	-0.9	1.5	0.86	16	185	4
JV-G5-3	1	euh-qtz grain	221.2	-0.9	1.5	0.85	20	235	4
JV-G5-3	1	euh-qtz grain	206.7	-1.0	1.7	0.87	15	172	4
JV-G5-3	1	euh-qtz grain	221.2	-1.0	1.7	0.85	20	235	4
JV-G5-3	1	euh-qtz grain	222.1	-1.0	1.7	0.85	20	235	4
JV-G5-3	1	euh-qtz grain	190.8	-1.1	1.8	0.89	10	112	4
JV-G5-3	1	euh-qtz grain	239.4	-1.1	1.8	0.83	29	351	4
JV-G5-3	1	euh-qtz grain	219.2	-1.2	2.0	0.86	19	221	4

Appendix E. Continued

Sample	Band	Mineral	Th°C	T_{mice}	NaCl wt% eq.	Density	P (bars)	Depth (m)	Stage
JV-G5-3	1	euh-qtz grain	224.0	-1.2	2.0	0.85	21	247	4
JV-G5-3	1	euh-qtz grain	210.6	-1.3	2.1	0.87	16	184	4
JV-G5-3	1	euh-qtz grain	220.2	-1.3	2.1	0.86	20	233	4
JV-G5-3	1	euh-qtz grain	224.0	-1.3	2.1	0.85	21	246	4
JV-G5-3	1	euh-qtz grain	223.1	-1.4	2.3	0.86	21	245	4
JV-G5-3	1	euh-qtz grain	214.4	-1.6	2.6	0.87	17	195	4
JV-G5-3	1	euh-qtz grain	228.9	-1.6	2.6	0.85	24	282	4
JV-G5-3	1	euh-qtz grain	188.5	-1.7	2.8	0.90	10	111	4
JV-G5-3	1	euh-qtz grain	188.5	-1.7	2.8	0.90	10	111	4
JV-G5-3	1	euh-qtz grain	190.3	-1.7	2.8	0.90	10	111	4
JV-G5-3	1	euh-qtz grain	226.0			0.85	22	260	4
JV-G7-11	10	cal	243.4	-0.3	0.5	0.81	31	385	3
JV-G7-11	2	qtz	220.5	-0.3	0.5	0.84	27	321	3
JV-G7-11	2	qtz	220.5	-0.3	0.5	0.84	27	321	3
JV-G7-11	2	qtz	237.7	-0.3	0.5	0.82	32	393	3
JV-G7-11	10	cal	243.4	-0.4	0.7	0.81	31	384	3
JV-G7-11	10	cal	225.1	-0.5	0.8	0.84	22	263	3
JV-G7-11	10	cal	243.4	-0.5	0.8	0.81	31	383	3
JV-G7-11	11	cal	183.1	-0.6	1.0	0.89	9	101	3
JV-G7-11	11	cal	227.0	-0.6	1.0	0.84	23	275	3
JV-G7-11	3	chal qtz	270.2	-0.8	1.3	0.75	51	684	3
JV-G7-11	4	dirty cal	216.7	-0.9	1.5	0.86	18	210	3
JV-G7-11	3	prism qtz	251.1	-0.9	1.5	0.80	36	448	3
JV-G7-11	4	clean cal	232.0	-1.2	2.0	0.84	25	298	3
JV-G7-11	4	cal	239.6	-1.2	2.0	0.83	29	350	3
JV-G7-11	9	cal	244.4	-1.2	2.0	0.82	32	390	3
JV-G7-11	4	clean cal	246.3	-1.2	2.0	0.82	33	403	3
JV-G7-11	4	cal	192.8	-1.3	2.1	0.89	11	123	3
JV-G7-11	4	cal	192.8	-1.3	2.1	0.89	11	123	3
JV-G7-11	4	clean cal	243.4	-1.3	2.1	0.83	31	376	3
JV-G7-11	4	clean cal	246.3	-1.3	2.1	0.82	33	402	3
JV-G7-11	4	clean cal	263.5	-1.3	2.1	0.79	45	570	3
JV-G7-11	10	cal	220.5	-1.4	2.3	0.86	20	233	3
JV-G7-11	9	cal	239.6	-1.5	2.5	0.83	29	348	3
JV-G7-11	4	clean cal	240.6	-1.5	2.5	0.83	30	361	3
JV-G7-11	6	brown cal	256.8	-1.5	2.5	0.81	41	509	4
JV-G7-11	6	brown cal	257.8	-1.5	2.5	0.80	41	510	4
JV-G7-11	9	cal	260.6	-1.5	2.5	0.80	44	551	4
JV-G7-11	6	clean cal	275.0	-1.5	2.5	0.78	55	710	4
JV-G7-11	9	cal	282.6	-1.6	2.6	0.76	63	827	3
JV-G7-11	6	brown cal	256.8	-1.6	2.6	0.81	41	507	4
JV-G7-11	4	dirty cal	208.1	-1.7	2.8	0.88	15	170	3
JV-G7-11	6	clean cal		-1.7	2.8				4
JV-G7-11	2	qtz	242.5	-1.7	2.8	0.83	38	456	3
JV-G7-11	11	cal	227.0	-1.8	3.0	0.86	23	268	3
JV-G7-11	4	cal	249.2	-1.8	3.0	0.83	35	424	3
JV-G7-11	4	cal		-1.8	3.0				3
JV-G7-11	2	qtz	238.7	-1.8	3.0	0.84	33	393	3
JV-G7-11	4	clean cal	157.1	-1.9	3.1	0.94	5	53	3

Appendix E. Continued

Sample	Band	Mineral	Th°C	T_{mice}	NaCl wt% eq.	Density	P (bars)	Depth (m)	Stage
JV-G7-11	6	clean cal	291.2	-2.2	3.6	0.76	71	933	4
JV-G7-11	6	clean cal	266.4	-2.3	3.8	0.81	48	595	4
JV-G7-11	6	clean cal	286.4	-2.3	3.8	0.77	66	855	4
JV-G7-11	6	clean cal	232.9	-2.4	3.9	0.86	26	303	3
JV-G7-11	4	cal	247.2	-2.4	3.9	0.84	34	406	3
JV-G7-11	12	cal	146.0	-2.4	3.9	0.95	5	53	
JV-G7-11	3	qtz	173.6	-3.0	4.9	0.92	7	76	3
JV-G7-11	12	cal	88.1			0.85	6	71	3
JV-G7-11	3	cal	105.8			0.85	5	59	3
JV-G7-11	4	cal	110.5			0.85	5	59	3
JV-G7-11	4	cal	217.6			0.85	19	225	3
JV-G7-11	4	cal	219.5			0.85	19	225	3
JV-G7-11	4	cal	249.2			0.85	35	414	3
JV-G7-11	6	clean cal	244.4			0.85	32	379	4
JV-G7-11	12	cal	97.8			0.85	5	59	
JV-G7-11	11	ep - qtz	246.3			0.85	33	390	3
JV-G7-11	11	ep - qtz	250.1			0.85	36	426	3
JV-G7-11	2	qtz	101.1			0.85	5	59	3
JV-H11-01	1	coarse euh qtz	259.2	-1.2	1.7	0.80	41	515	4
JV-H11-01	1	coarse euh qtz	250.0	-1.1	1.8	0.81	36	444	4
JV-H11-01	1	coarse qtz	219.2	-1.4	2.3	0.86	19	221	4
JV-H11-01	1	coarse qtz	242.3	-1.4	2.3	0.83	31	374	4
JV-H11-01	1	coarse qtz	251.0	-1.6	2.6	0.82	36	440	4
JV-H11-01	1	coarse euh qtz	191.8			0.85	11	130	4
JV-H11-01	1	coarse euh qtz	213.5			0.85	17	201	4
JV-H11-01	1	coarse euh qtz	218.3			0.85	19	225	4
JV-H11-01	1	coarse euh qtz	222.1			0.85	20	237	4
JV-H11-01	1	coarse euh qtz	238.5			0.85	28	331	4
JV-H11-03	6	adul	228.9	-1.0	1.7	0.84	24	285	3
JV-H11-03	5	coarse qtz	225.0	-1.1	1.8	0.85	22	259	3
JV-H11-03	6	coarse euh qtz	227.9	-1.2	2.0	0.85	23	272	3
JV-H11-03	3	coarse qtz	248.1	-1.2	2.0	0.82	34	417	3
JV-H11-03	1	coarse qtz	258.8	-1.3	2.1	0.80	42	526	3
JV-H11-03	5	med qtz	275.1	-1.3	2.1	0.77	55	713	3
JV-H11-03	1	coarse qtz	277.9	-1.5	2.5	0.77	58	754	3
JV-H11-03	5	med qtz	261.6	-1.6	2.6	0.80	44	550	3
JV-H11-03	5	coarse qtz	284.7	-1.6	2.6	0.76	65	856	3
JV-H11-03	5	coarse qtz	253.4	-1.7	2.8	0.82	38	466	3
JV-H11-03	1	coarse qtz	260.7	-1.7	2.8	0.80	47	585	3
JV-H11-03	5	med qtz	230.8	-1.9	3.1	0.85	25	293	3
JV-H11-03	6	qtz + adul	263.5	-1.9	3.1	0.80	45	560	3
JV-H11-03	7	chal qtz		-2.0	3.3				3
JV-H11-03	3	micro-qtz	241.4	-2.1	3.4	0.84	30	356	3
JV-H11-03	3	micro-qtz	261.6	-2.3	3.8	0.81	44	541	3
JV-H11-03	7	chal qtz	222.1	-2.4	3.9	0.87	20	229	3
JV-H11-03	7	chal qtz	262.5	-2.4	3.9	0.82	44	540	3
JV-H11-03	1	coarse qtz	312.6	-2.7	4.4	0.73	98	1342	3
JV-H11-03	5	coarse qtz	227.9	-3.1	5.0	0.88	23	263	3
JV-H11-03	1	coarse qtz	246.3	-4.0	6.4	0.87	33	382	3

Appendix E. Continued

Sample	Band	Mineral	Th°C	T_{mice}	NaCl wt% eq.	Density	P (bars)	Depth (m)	Stage
JV-H11-03	3	micro-qtz	143.5	-4.2	6.7	0.97	5	51	3
JV-H11-03	1	coarse qtz	158.8	-4.2	6.7	0.96	5	52	3
JV-H11-03	1	coarse qtz	199.0	-4.2	6.7	0.92	12	131	3
JV-H11-03	1	coarse qtz	244.3	-4.3	6.8	0.87	32	367	3
JV-H11-03	6	qtz + adul	227.9	-4.5	7.1	0.89	23	257	3
JV-H11-03	3	micro-qtz	236.6	-4.5	7.1	0.88	28	317	3
JV-H11-03	1	coarse qtz	250.1	-4.5	7.1	0.87	36	415	3
JV-H11-03	3	micro-qtz	236.6	-4.6	7.3	0.88	28	317	3
JV-H11-03	3	micro-qtz	241.4	-5.0	7.8	0.89	31	345	3
JV-H11-03	1	coarse qtz	175.0	-5.7	8.8	0.96	7	73	3
JV-H11-03	1	coarse qtz	240.5	-7.3	10.9	0.91	30	323	3
JV-H11-03	3	micro-qtz	153.9			0.85	5	59	3
JV-H11-03	6	qtz + adul	168.6			0.85	6	71	3
JV-H11-03	6	qtz + adul	169.5			0.85	6	71	3
JV-H11-03	6	qtz + adul	178.2			0.85	8	95	3
JV-H11-03	1	coarse qtz	195.2			0.85	11	130	3
JV-H11-03	1	coarse qtz	212.6			0.85	17	201	3
JV-H11-03	1	coarse qtz	237.6			0.85	28	331	3
JV-H11-03	1	coarse qtz	240.5			0.85	30	349	3
JV-H11-03	5	coarse qtz	241.4			0.85	30	355	3
JV-H11-03	1	coarse qtz	248.1			0.85	34	402	3
JV-H11-03	1	coarse qtz	248.2			0.85	34	402	3
JV-H11-03	1	coarse qtz	259.7			0.85	43	509	3
JV-H11-03	7	chal qtz	260.6			0.85	44	520	3
JV-H11-03	3	micro-qtz	262.5			0.85	44	520	3
JV-H11-03	1	coarse qtz	290.4			0.85	70	828	3
JV-H11-03	1	coarse qtz	360.7			0.85	179	2117	3
JV-I5-2	2	chal qtz	207.8	-0.1	0.2	0.86	15	175	3
JV-I5-2	1	cal	230.9	-0.5	0.8	0.83	25	302	3
JV-I5-2	1	cal	230.9	-0.6	1.0	0.83	25	301	3
JV-I5-2	2	coarse qtz	251.1	-0.6	1.0	0.80	36	451	3
JV-I5-2	1	cal	252.0	-0.9	1.5	0.80	37	461	3
JV-I5-2	1	cal	254.9	-0.9	1.5	0.80	39	489	3
JV-I5-2	2	chal qtz	186.6	-0.9	1.5	0.89	9	101	3
JV-I5-2	2	chal qtz	191.9	-0.9	1.5	0.89	11	124	3
JV-I5-2	2	coarse qtz	223.2	-1.0	1.7	0.85	21	247	3
JV-I5-2	4	qtz	226.1	-1.1	1.8	0.85	22	260	3
JV-I5-2	1	qtz	275.1	-1.1	1.8	0.77	55	718	3
JV-I5-2	4	qtz		-1.1	1.8				3
JV-I5-2	2	coarse qtz	251.1	-1.2	2.0	0.81	36	444	3
JV-I5-2	5	cal	213.6	-1.3	2.1	0.87	17	196	3
JV-I5-2	1	qtz	255.9	-1.3	2.1	0.80	40	498	3
JV-I5-2	4	coarse qtz	252.0	-1.4	2.3	0.81	37	456	3
JV-I5-2	1	qtz	255.9	-1.4	2.3	0.81	40	496	3
JV-I5-2	1	cal	198.2	-1.5	2.5	0.89	12	135	3
JV-I5-2	5	cal	264.5	-1.5	2.5	0.79	46	579	3
JV-I5-2	4	cal	294.3	-1.7	2.8	0.74	75	1009	3
JV-I5-2	4	qtz	252.0	-1.8	3.0	0.82	37	451	3
JV-I5-2	5	cal	224.1	-1.9	3.1	0.86	21	244	3

Appendix E. Continued

Sample	Band	Mineral	Th°C	T_{mice}	NaCl wt% eq.	Density	P (bars)	Depth (m)	Stage
JV-I5-2	6	cal	227.0	-2.0	3.3	0.86	23	267	3
JV-I5-2	5	cal	252.0	-2.0	3.3	0.82	37	450	3
JV-I5-2	5	cal	255.9	-2.0	3.3	0.82	40	490	3
JV-I5-2	2	qtz	177.9			0.85	8	95	3
JV-I5-2	2	qtz	223.2			0.85	21	248	3
JV-I5-2	2	coarse qtz	233.8			0.85	26	308	3
JV-I5-2	1	qtz	248.2			0.85	34	402	3
JV-I9-7	4	qtz	241.5	-0.5	0.8	0.81	30	369	3
JV-I9-7	1	cal	231.8	-0.6	1.0	0.83	25	302	3
JV-I9-7	1	cal	227.0	-0.7	1.2	0.84	23	274	3
JV-I9-7	1	cal	231.8	-0.7	1.2	0.83	25	301	3
JV-I9-7	6	cal	236.6	-1.0	1.7	0.83	28	338	3
JV-I9-7	6	cal	245.3	-1.0	1.7	0.82	32	392	3
JV-I9-7	8	chal qtz	248.2	-1.1	1.8	0.81	34	418	3
JV-I9-7	5 -6	cal	245.3	-1.3	2.1	0.82	32	389	3
JV-I9-7	8	chal qtz	249.1	-1.3	2.1	0.82	35	429	3
JV-I9-7	8	cal	195.3	-1.4	2.3	0.89	11	124	3
JV-I9-7	9	cal	254.0	-1.4	2.3	0.81	38	470	3
JV-I9-7	9	cal	259.7	-1.4	2.3	0.80	43	538	3
JV-I9-7	5 -6	cal	243.4	-1.5	2.5	0.83	31	374	3
JV-I9-7	9	qtz	233.8	-1.7	2.8	0.85	26	308	3
JV-I9-7	5 -6	cal	235.7	-2.0	3.3	0.85	27	319	3
JV-I9-7	4	clean cal	243.4	-2.3	3.8	0.84	31	368	3
JV-I9-7	4	clean cal	241.5	-2.7	4.4	0.85	30	352	3
JV-I9-7	10	cal	240.5	-2.8	4.5	0.85	29	340	3
JV-I9-7	10	cal	240.5	-2.8	4.5	0.85	29	340	3
JV-I9-7	3	coarse qtz	244.3	-3.0	4.9	0.85	32	376	3
JV-I9-7	1	cal	231.8			0.85	25	296	3
JV-I9-7	1	cal	231.8			0.85	25	296	3
JV-I9-7	10	cal	233.8			0.85	26	308	3
JV-I9-7	5 -6	cal	237.6			0.85	28	331	3
JV-I9-7	10	cal	238.6			0.85	28	331	3
JV-I9-7	8	cal	243.4			0.85	31	367	3
JV-I9-7	2	chal qtz	222.2			0.85	20	237	3
JV-I9-7	2	chal qtz	224.1			0.85	21	248	3
JV-I9-7	8	chal qtz	249.1			0.85	35	414	3
JV-I9-7	2	chal qtz	328.0			0.85	120	1419	3
JV-J5-02	5	clean cal	215.5	-0.3	0.5	0.85	18	212	4
JV-J5-02	2, 4	micro-qtz	212.6	-0.5	0.8	0.86	17	199	3
JV-J5-02	5	clean cal	200.1	-0.6	1.0	0.87	13	149	4
JV-J5-02	5	clean cal	218.4	-0.6	1.0	0.85	19	224	4
JV-J5-02	5	clean cal	229.0	-0.6	1.0	0.83	24	288	4
JV-J5-02	5	clean cal	217.4	-0.8	1.3	0.86	18	211	4
JV-J5-02	2, 4	micro-qtz	230.9	-0.8	1.3	0.83	25	300	3
JV-J5-02	2, 4	micro-qtz	243.4	-0.8	1.3	0.82	31	380	3
JV-J5-02	2, 4	micro-qtz	253.0	-0.8	1.3	0.80	38	476	3
JV-J5-02	2, 4	micro-qtz	254.0	-0.8	1.3	0.80	38	476	3
JV-J5-02	2, 4	micro-qtz	267.4	-0.8	1.3	0.77	48	620	3
JV-J5-02	2, 4	micro-qtz	255.9	-0.9	1.5	0.80	40	503	3

Appendix E. Continued

Sample	Band	Mineral	Th°C	T_{mice}	NaCl wt% eq.	Density	P (bars)	Depth (m)	Stage
JV-J5-02	2, 4	micro-qtz	275.1	-0.9	1.5	0.76	55	722	3
JV-J5-02	2, 4	micro-qtz	202.0	-1.0	1.7	0.88	13	148	3
JV-J5-02	2, 4	micro-qtz	227.0	-1.0	1.7	0.84	23	273	3
JV-J5-02	2, 4	micro-qtz	254.0	-1.0	1.7	0.80	38	474	3
JV-J5-02	2, 4	micro-qtz	186.2	-1.1	1.8	0.90	9	100	3
JV-J5-02	2, 4	micro-qtz	207.8	-1.1	1.8	0.87	15	172	3
JV-J5-02	5	clean cal	190.4	-1.2	2.0	0.89	10	112	4
JV-J5-02	5	clean cal	214.5	-1.2	2.0	0.86	18	203	4
JV-J5-02	1	coarse radial	232.8	-1.2	2.0	0.84	26	310	3
JV-J5-02	2, 4	coarse euh	278.0	-1.2	2.0	0.76	58	760	3
JV-J5-02	2, 4	micro-qtz	272.2	-1.6	2.6	0.78	53	678	3
JV-J5-02	3	coarse euh	215.5	-1.7	2.8	0.87	18	207	4
JV-J5-02	1	coarse radial	233.8	-3.0	4.9	0.87	26	300	3
JV-J5-02	5	clean cal	221.3			0.85	20	237	4
JV-J5-02	2, 4	chal qtz	247.2			0.85	34	402	3
JV-K11-3	1	coarse-euh-qtz	191.6	-0.8	1.3	0.89	11	124	3
JV-K11-3	1	coarse-euh-qtz	171.7	-1.0	1.7	0.91	7	77	3
JV-K11-3	1	coarse-euh-qtz	180.8	-1.0	1.7	0.90	8	89	3
JV-K11-3	1	coarse-euh-qtz	199.9	-1.0	1.7	0.88	13	148	3
JV-K11-3	1	coarse-euh-qtz		-1.0	1.7				3
JV-K11-3	1	coarse-euh-qtz	196.0	-1.1	1.8	0.89	12	136	3
JV-K11-3	1	coarse-euh-qtz	197.0	-1.1	1.8	0.88	12	136	3
JV-K11-3	1	coarse-euh-qtz	198.0	-1.2	2.0	0.88	12	136	3
JV-K11-3	1	coarse-euh-qtz	199.9	-1.2	2.0	0.88	13	147	3
JV-K11-3	1	coarse-euh-qtz	241.7	-1.2	2.0	0.83	31	376	3
JV-K11-3	1	coarse-euh-qtz	204.8	-1.3	2.1	0.88	14	159	3
JV-K11-3	1	coarse-euh-qtz	215.5	-1.3	2.1	0.87	18	208	3
JV-K11-3	1	coarse-euh-qtz	235.9	-1.3	2.1	0.84	27	323	3
JV-K11-3	1	coarse-euh-qtz	240.7	-1.3	2.1	0.83	30	362	3
JV-K11-3	1	coarse-euh-qtz	250.5	-1.3	2.1	0.81	36	442	3
JV-K11-3	1	coarse-euh-qtz	194.2			0.85	11	130	3
JV-K11-3	1	coarse-euh-qtz	199.9			0.85	13	154	3
JV-K11-3	1	coarse-euh-qtz	247.5			0.85	34	402	3
JV-K11-3	1	coarse-euh-qtz	261.2			0.85	44	520	3
JV-K11-3	1	coarse-euh-qtz	267.0			0.85	48	568	3
JV-K5-2	vein B	cal	218.4	-0.8	1.3	0.85	19	223	4
JV-K5-2	4 to 6	qtz	185.8	-0.8	1.3	0.89	9	101	3
JV-K5-2	2	qtz	250.1	-0.8	1.3	0.80	36	448	3
JV-K5-2	3	cal	232.8	-0.9	1.5	0.83	26	312	3
JV-K5-2	vein B	cal	227.0	-0.9	1.5	0.84	23	273	4
JV-K5-2	4 to 6	qtz	213.6	-0.9	1.5	0.86	17	198	3
JV-K5-2	3	cal	229.9	-1.0	1.7	0.84	24	286	3
JV-K5-2	4 to 6	qtz	259.7	-1.0	1.7	0.79	43	544	3
JV-K5-2	vein B	cal	229.0	-1.1	1.8	0.84	24	285	4
JV-K5-2	1	cal	202.0	-1.2	2.0	0.88	13	148	3
JV-K5-2	1	cal	219.3	-1.2	2.0	0.86	19	221	3
JV-K5-2	2	qtz	217.4	-1.2	2.0	0.86	18	209	3
JV-K5-2	2	qtz	221.3	-1.2	2.0	0.86	20	234	3
JV-K5-2	1	qtz	259.7	-1.2	2.0	0.80	43	541	3

151

Appendix E. Continued

Sample	Band	Mineral	Th°C	T_{mice}	NaCl wt% eq.	Density	P (bars)	Depth (m)	Stage
JV-K5-2	vein B	cal	220.3	-1.3	2.1	0.86	20	233	4
JV-K5-2	vein B	cal	246.3	-1.3	2.1	0.82	33	402	4
JV-K5-2	4 to 6	cal	204.9	-1.4	2.3	0.88	14	159	3
JV-K5-2	4 to 6	cal	222.2	-1.4	2.3	0.86	20	233	3
JV-K5-2	3	cal	239.5	-1.4	2.3	0.83	29	348	3
JV-K5-2	4 to 6	cal		-1.5	2.5				3
JV-K5-2	3	cal	214.5	-1.8	3.0	0.87	17	195	3
JV-K5-2	4 to 6	qtz	223.2	-2.4	3.9	0.87	21	241	3
JV-K5-2	2	qtz	219.3	-3.4	5.5	0.89	19	213	3
JV-K5-2	3	cal	200.1			0.85	13	154	3
JV-K5-2	vein B	pyr	112.9			0.85	5	59	4
JV-K9-10	1	coarse-euh-qtz	204.8	-0.8	1.3	0.87	14	161	3
JV-K9-10	1	coarse-euh-qtz		-0.8	1.3				3
JV-K9-10	1	coarse-euh-qtz	214.5	-0.9	1.5	0.86	18	203	3
JV-K9-10	1	coarse-euh-qtz	215.5	-1.0	1.7	0.86	18	209	3
JV-K9-10	1	coarse-euh-qtz	220.3	-1.0	1.7	0.85	20	234	3
JV-K9-10	1	coarse-euh-qtz	228.1	-1.0	1.7	0.84	23	273	3
JV-K9-10	1	coarse-euh-qtz	231.0	-1.0	1.7	0.84	25	298	3
JV-K9-10	1	coarse-euh-qtz	207.7	-1.1	1.8	0.87	15	172	3
JV-K9-10	1	coarse-euh-qtz	218.4	-1.1	1.8	0.86	19	221	3
JV-K9-10	1	coarse-euh-qtz		-1.1	1.8				3
JV-K9-10	1	coarse-euh-qtz	204.8	-1.2	2.0	0.88	14	160	3
JV-K9-10	1	coarse-euh-qtz	232.0	-1.2	2.0	0.84	25	298	3
JV-K9-10	1	coarse-euh-qtz	235.9	-1.2	2.0	0.83	27	324	3
JV-K9-10	1	coarse-euh-qtz	204.8	-1.4	2.3	0.88	14	159	3
JV-K9-10	1	coarse-euh-qtz	210.6	-1.6	2.6	0.88	16	183	3
JV-K9-13		qtz	282.6	-1.2	2.0	0.75	63	836	3
JV-K9-13		qtz	220.4	-1.5	2.5	0.86	20	232	3
JV-K9-13		qtz	235.4	-1.6	2.6	0.84	27	321	3
JV-K9-13		qtz	231.4	-1.7	2.8	0.85	25	294	3
JV-K9-13		qtz	220.4	-1.8	3.0	0.87	20	231	3
JV-K9-13		qtz	251.5	-1.8	3.0	0.82	36	438	3
JV-K9-13		qtz	254.5	-1.8	3.0	0.82	38	466	3
JV-K9-13		qtz	224.4	-1.9	3.1	0.86	21	244	3
JV-K9-13		qtz	245.5	-1.9	3.1	0.83	32	385	3
JV-K9-13		qtz	228.4	-2.1	3.4	0.86	23	268	3
JV-K9-13		qtz	258.5	-2.1	3.4	0.82	41	503	3
JV-K9-13		qtz	222.4	-2.2	3.6	0.87	20	230	3
JV-K9-13		qtz	227.4	-2.2	3.6	0.86	23	267	3
JV-K9-13		qtz	229.4	-2.2	3.6	0.86	24	279	3
JV-K9-13		qtz	256.5	-2.3	3.8	0.82	40	487	3
JV-K9-13		qtz	258.5	-2.3	3.8	0.82	41	501	3
JV-K9-13		qtz	215.4	-2.6	4.2	0.88	18	204	3
JV-K9-13		qtz	235.4	-2.6	4.2	0.86	27	315	3
JV-K9-13		qtz	236.4	-2.6	4.2	0.86	27	315	3
JV-K9-13		qtz	252.5	-6.2	9.5	0.89	37	418	3
JV-Q13-01	1	coarse-euh-qtz	145.4	-0.6	1.0	0.93	5	54	4
JV-Q13-01	1	coarse-euh-qtz	162.5			0.85	6	71	4
JV-Q13-01	1	coarse-euh-qtz	184.7			0.85	9	106	4

Appendix E. Continued

Sample	Band	Mineral	Th°C	T_{mice}	NaCl wt% eq.	Density	P (bars)	Depth (m)	Stage
JV-Q13-01	1 euh-qtz		189.1			0.85	10	118	4
JV-Q7-01	4 clean cal		234.7	-0.8	1.3	0.83	27	326	4
JV-Q7-01	4 clean cal		217.4	-0.9	1.5	0.86	18	210	4
JV-Q7-01	4 clean cal			-0.9	1.5				4
JV-Q7-01	4 clean cal		234.7	-1.0	1.7	0.83	27	325	4
JV-Q7-01	4 clean cal		235.7	-1.1	1.8	0.83	27	325	4
JV-Q7-01	3 ep		221.3	-1.4	2.3	0.86	20	233	3
JV-Q7-01	3 ep		178.0	-1.5	2.5	0.91	8	88	3
JV-Q7-01	3 ep		265.5	-1.5	2.5	0.79	48	600	3
JV-Q7-01	3 ep		184.7	-1.6	2.6	0.90	9	100	3
JV-Q7-01	1 coarse qtz		246.3	-2.4	3.9	0.84	33	393	3
JV-Q7-01	3 dirty cal		216.5	-3.8	6.1	0.90	18	200	3
JV-Q7-01	3 coarse qtz		213.6	-3.9	6.2	0.90	17	188	3
JV-Q7-01	3 coarse qtz		214.5	-4.1	6.5	0.90	18	194	3
JV-Q7-01	3 dirty cal		216.5	-5.0	7.8	0.91	18	197	3
JV-Q7-01	3 dirty cal		211.6	-5.1	8.0	0.92	16	174	3
JV-Q7-01	3 dirty cal		178.1	-5.3	8.2	0.95	8	84	3
JV-Q7-01	3 ep		265.5	-5.5	8.5	0.86	48	552	3
JV-Q7-01	1 chal qtz		131.7	-5.5	8.5	0.99	4	40	3
JV-Q7-01	1 coarse qtz		226.1	-5.9	9.1	0.91	22	241	3
JV-Q7-01	1 coarse qtz		253.0	-6.5	9.8	0.89	38	427	3
JV-Q7-01	1 coarse qtz		241.5	-6.6	10.0	0.90	31	338	3
JV-Q7-01	1 coarse qtz		241.5	-6.6	10.0	0.90	31	338	3
JV-Q7-01	3 dirty cal		238.6			0.85	29	343	3
JV-Q7-01	4 clean cal		209.7			0.85	16	189	4
JV-Q7-01	3 ep		268.4			0.85	49	580	3
JV-Q7-01	3 coarse qtz		233.8			0.85	26	308	3
JV-Q7-01	1 coarse qtz		242.4			0.85	31	367	3
JV-Q7-01	3 coarse qtz		278.0			0.85	68	804	3
JV-Q7-01	1 coarse qtz		301.1			0.85	83	982	3
JV-Q9-2	1 coarse-euh-qtz		228.1	-0.7	1.2	0.84	23	275	3
JV-Q9-2	1 coarse-euh-qtz		241.7	-0.7	1.2	0.82	31	380	3
JV-Q9-2	2 cal		220.3	-0.9	1.5	0.85	20	235	3
JV-Q9-2	2 cal		229.1	-0.9	1.5	0.84	24	286	3
JV-Q9-2	1 coarse-euh-qtz		227.1	-0.9	1.5	0.84	23	273	3
JV-Q9-2	1 coarse-euh-qtz		251.4	-0.9	1.5	0.81	36	447	3
JV-Q9-2	2 cal		197.0	-1.0	1.7	0.88	12	136	3
JV-Q9-2	2 cal		208.7	-1.0	1.7	0.87	15	173	3
JV-Q9-2	2 cal			-1.0	1.7				3
JV-Q9-2	1 coarse-euh-qtz		219.3	-1.0	1.7	0.86	19	222	3
JV-Q9-2	1 coarse-euh-qtz		221.3	-1.0	1.7	0.85	20	235	3
JV-Q9-2	1 coarse-euh-qtz		228.1	-1.0	1.7	0.84	23	273	3
JV-Q9-2	1 coarse-euh-qtz		229.1	-1.0	1.7	0.84	24	285	3
JV-Q9-2	1 coarse-euh-qtz		229.1	-1.0	1.7	0.84	24	285	3
JV-Q9-2	1 coarse-euh-qtz		233.0	-1.0	1.7	0.84	26	311	3
JV-Q9-2	1 coarse-euh-qtz		234.9	-1.0	1.7	0.83	27	325	3
JV-Q9-2	1 coarse-euh-qtz		234.9	-1.0	1.7	0.83	27	325	3
JV-Q9-2	1 coarse-euh-qtz		235.9	-1.0	1.7	0.83	27	325	3
JV-Q9-2	1 coarse-euh-qtz		241.7	-1.0	1.7	0.82	31	378	3

Appendix E. Continued

Sample	Band	Mineral	Th°C	T_{mice}	NaCl wt% eq.	Density	P (bars)	Depth (m)	Stage
JV-Q9-2	1	coarse-euh-qtz		-1.0	1.7				3
JV-Q9-2	2	cal	193.6	-1.2	2.0	0.89	11	124	3
JV-Q9-2	1	coarse-euh-qtz	233.0			0.85	26	308	3
JV-S11-01	4	chal qtz	227.0	-0.2	0.3	0.83	23	277	3
JV-S11-01	5	coarse qtz	224.1	-0.5	0.8	0.81	32	396	3
JV-S11-01	1	cal	226.1	-0.7	1.2	0.84	22	262	3
JV-S11-01	3	cal	215.5	-0.8	1.3	0.86	18	210	3
JV-S11-01	3	cal	218.4	-0.8	1.3	0.85	19	223	3
JV-S11-01	2	qtz	234.7	-0.8	1.3	0.83	27	326	3
JV-S11-01	2	qtz	144.3	-0.8	1.3	0.94	5	53	
JV-S11-01	3	cal	217.4	-0.9	1.5	0.86	18	210	3
JV-S11-01	2	qtz	245.3	-1.1	1.8	0.82	32	391	3
JV-S11-01	5	qtz	258.8	-1.1	1.8	0.80	42	528	3
JV-S11-01	2	qtz	289.5	-1.2	2.0	0.74	70	939	3
JV-S11-01	4	chal qtz	297.2	-1.2	2.0	0.73	78	1076	3
JV-S11-01	3	cal	233.8	-1.3	2.1	0.84	26	310	3
JV-S11-01	3	cal	229.0	-1.4	2.3	0.85	24	283	3
JV-S11-01	1	ep	190.5	-1.5	2.5	0.90	10	111	3
JV-S11-01	1	ep	196.3	-1.7	2.8	0.89	12	135	3
JV-S11-01	1	ep	191.4	-1.9	3.1	0.90	10	111	3
JV-S11-01	1	ep	199.1	-1.9	3.1	0.89	12	135	3
JV-S11-01	5	qtz	212.6			0.85	17	201	3
JV-S11-01	5	qtz	224.1			0.85	21	248	3
JV-S5-01B	2	coarse qtz	220.2	-1.3	2.1	0.86	20	233	3
JV-S5-01B	2	coarse qtz	144.6	-1.4	2.3	0.97	5	52	3
JV-S5-01B	2	coarse qtz	234.6	-1.6	2.6	0.84	27	321	3
JV-S5-01B	2	coarse qtz	193.2	-2.0	3.3	0.90	11	122	3
JV-S5-01B	2	coarse qtz	200.0	-2.0	3.3	0.89	13	146	3
JV-S5-01B	1	coarse qtz	175.9	-2.4	3.9	0.92	7	76	3
JV-S5-01B	1	coarse qtz		-2.4	3.9				3
JV-S5-01B	1	coarse qtz	234.6	-2.6	4.2	0.86	27	315	3
JV-S5-01B	1	coarse qtz	275.1	-2.6	4.2	0.80	55	689	3
JV-S5-01B	1	coarse qtz	239.4	-3.4	5.5	0.87	29	335	3
JV-S5-01B	2	coarse qtz	214.4	-4.3	6.8	0.91	17	188	3
JV-S5-01B	1	coarse qtz	177.8			0.85	8	95	3
JV-S5-01B	2	coarse qtz	189.4			0.85	10	118	3
JV-S5-01B	2	chal qtz	200.9			0.85	13	154	3
JV-S5-01B	2	coarse qtz	201.9			0.85	13	154	3
JV-S5-01B	2	coarse qtz	211.5			0.85	16	189	3
JV-S5-01B	1	coarse qtz	225.0			0.85	22	260	3
JV-S5-01B	1	coarse qtz	236.6			0.85	28	331	3
JV-S7-01	2	coarse qtz	225.0	-0.7	1.2	0.84	22	261	4
JV-S7-01	2	coarse qtz	282.8	-0.7	1.2	0.74	63	849	4
JV-S7-01	2	coarse qtz	200.0	-0.8	1.3	0.88	13	148	4
JV-S7-01	1	coarse qtz	254.8	-0.8	1.3	0.80	39	490	4
JV-S7-01	2	coarse qtz	233.7	-0.9	1.5	0.83	26	313	4
JV-S7-01	2	coarse qtz	236.6	-0.9	1.5	0.83	28	339	4
JV-S7-01	1	coarse qtz	244.3	-0.9	1.5	0.82	32	392	4
JV-S7-01	2	coarse qtz	259.7	-0.9	1.5	0.79	43	545	4

154

Appendix E. Continued

Sample	Band	Mineral	Th°C	T_{mice}	NaCl wt% eq.	Density	P (bars)	Depth (m)	Stage
JV-S7-01	2 coarse qtz			-0.9	1.5				4
JV-S7-01	2 coarse qtz		223.1	-1.0	1.7	0.85	21	247	4
JV-S7-01	2 coarse qtz		256.8	-1.0	1.7	0.80	41	515	4
JV-S7-01	1 coarse qtz		203.8	-1.1	1.8	0.88	14	160	4
JV-S7-01	2 coarse qtz		219.2	-1.2	2.0	0.86	19	221	4
JV-S7-01	4 coarse qtz		219.2	-1.4	2.3	0.86	19	221	4
JV-S7-01	1 coarse qtz		220.2	-1.5	2.5	0.86	20	232	4
JV-S7-01	1 coarse qtz		279.9	-1.8	3.0	0.77	60	777	4
JV-S7-01	1 coarse qtz		216.3	-1.9	3.1	0.87	18	206	4
JV-S7-01	1 coarse qtz		237.5	-1.9	3.1	0.84	28	332	4
JV-S7-01	1 coarse qtz		249.1	-2.0	3.3	0.83	35	423	4
JV-S7-01	1 coarse qtz		261.6	-2.1	3.4	0.81	44	544	4
JV-S7-01	1 coarse qtz		303.0	-2.1	3.4	0.74	85	1156	4
JV-S7-01	2 coarse qtz		220.2	-2.3	3.8	0.87	20	229	4
JV-S7-01	4 coarse qtz		225.0	-2.7	4.4	0.87	22	252	4
JV-S7-01	4 coarse qtz		234.6	-2.7	4.4	0.86	27	314	4
JV-S7-01	1 coarse qtz		226.0	-3.1	5.0	0.88	22	251	4
JV-S7-01	1 coarse qtz		229.8			0.85	24	284	4
JV-S7-01	1 coarse qtz		247.1			0.85	34	402	4
JV-S7-07	2 coarse qtz		271.2	-1.1	1.8	0.77	52	672	3
JV-S7-07	2 coarse qtz		232.7	-1.2	2.0	0.84	26	310	3
JV-S7-07	3 coarse euh qtz		320.3	-1.2	2.0	0.68	108	1600	3
JV-S7-07	4 coarse qtz		198.1	-1.3	2.1	0.89	12	136	3
JV-S7-07	2 coarse qtz		215.4	-1.3	2.1	0.87	18	208	3
JV-S7-07	2 coarse qtz		217.3	-1.3	2.1	0.86	18	209	3
JV-S7-07	3 coarse euh qtz		218.3	-1.4	2.3	0.86	19	220	3
JV-S7-07	3 coarse euh qtz		227.9	-1.4	2.3	0.85	23	271	3
JV-S7-07	3 coarse euh qtz		224.0	-1.5	2.5	0.86	21	245	3
JV-S7-07	3 coarse euh qtz		240.4	-1.5	2.5	0.83	29	348	3
JV-S7-07	3 coarse euh qtz			-1.5	2.5				3
JV-S7-07	4 coarse qtz		219.2	-1.6	2.6	0.86	19	220	3
JV-S7-07	4 coarse qtz		240.4	-1.6	2.6	0.84	29	347	3
JV-S7-07	2 clean cal		220.2	-1.7	2.8	0.86	20	231	3
JV-S7-07	1 coarse crist qtz		221.2	-1.7	2.8	0.86	20	232	3
JV-S7-07	3 coarse euh qtz		245.2	-1.8	3.0	0.83	32	385	3
JV-S7-07	3 coarse euh qtz		243.3	-1.9	3.1	0.84	31	371	3
JV-S7-07	2 coarse qtz			-1.9	3.1				3
JV-S7-07	4 coarse qtz		225.0	-2.0	3.3	0.86	22	255	3
JV-S7-07	3 coarse euh qtz		243.3	-2.1	3.4	0.84	31	369	3
JV-S7-07	4 coarse qtz		195.2	-2.2	3.6	0.90	11	122	3
JV-S7-07	1 coarse crist qtz		222.1	-2.2	3.6	0.87	20	230	3
JV-S7-07	4 coarse qtz		226.9	-2.3	3.8	0.86	23	266	3
JV-S7-07	1 coarse crist qtz		230.8	-2.3	3.8	0.86	25	291	3
JV-S7-07	1 coarse crist qtz		230.8	-2.3	3.8	0.86	25	291	3
JV-S7-07	3 coarse euh qtz		243.3	-2.4	3.9	0.84	31	367	3
JV-S7-07	1 coarse crist qtz		247.1	-2.4	3.9	0.84	34	406	3
JV-S7-07	4 coarse qtz		247.1	-2.5	4.1	0.84	34	405	3
JV-S7-07	2 clean cal		222.1			0.85	20	237	3
JV-S7-07	1 coarse crist qtz		235.6			0.85	27	319	3

Appendix E. Continued

Sample	Band	Mineral	Th°C	T_{mice}	NaCl wt% eq.	Density	P (bars)	Depth (m)	Stage
M-11-2		qtz	154.6	-1.4	2.3	0.93	12	129	5
M-11-2		qtz	307.4	-1.4	2.3	0.71	90	1269	5
M-11-2		qtz	245.3	-1.6	2.6	0.83	42	508	5
M-11-2		qtz	228.1	-2.3	3.8	0.86	23	267	5
M-11-2		qtz	235.8	-2.3	3.8	0.85	30	352	5
M-11-2		qtz	250.1	-2.3	3.8	0.83	36	433	5
M-11-2		qtz	245.3	-2.4	3.9	0.84	42	500	5
M-11-2		qtz	210.0	-2.7	4.4	0.89	16	180	5
M-11-2		qtz	218.6	-2.7	4.4	0.88	25	284	5
M-11-2		qtz	222.4	-2.7	4.4	0.88	30	342	5
M-11-2		qtz	230.1	-2.7	4.4	0.87	24	277	5
M-11-2		qtz	210.9	-2.9	4.7	0.89	18	202	5
M-11-2		qtz	214.8	-2.9	4.7	0.89	21	236	5
M-11-2		qtz	208.1	-3.2	5.2	0.90	30	334	5

Band refers to arbitrary number assigned to individual bands within the studied sample.

Abbreviations: qtz (quartz), cal (calcite), ep (epidote), adul (adularia), pyr (pyrargyrite), chal (chalcedony) euh (euhedral grain).

Appendix F. Incremental crushing gas chemistry data for Jarillas and Valdecañas veins; gas species concentrations in mol %.

Sample	Mineral	Crush	H_2	He	CH_4	H_2O	N_2	H_2S	Ar	CO_2
K9-13-GA	Quartz	8297a	3.29E-05	6.27E-05	7.33E-03	99.78	9.33E-02	2.67E-03	2.53E-03	9.59E-02
K9-13-GA	Quartz	8297b	0.00E+00	6.49E-05	6.00E-03	99.80	8.31E-02	2.85E-03	2.47E-03	7.99E-02
K9-13-GA	Quartz	8297c	0.00E+00	6.88E-06	6.74E-03	99.87	3.81E-02	8.31E-04	1.74E-03	7.03E-02
K9-13-GA	Quartz	8297d	0.00E+00	6.23E-06	5.05E-03	99.91	2.68E-02	4.28E-04	6.00E-04	4.63E-02
K9-13-GA	Quartz	8297e	0.00E+00	9.43E-05	9.79E-03	99.85	3.06E-02	9.34E-04	1.48E-03	9.24E-02
K9-13-GA	Quartz	8297g	0.00E+00	4.81E-07	1.22E-02	99.80	3.79E-02	5.60E-04	1.45E-03	1.25E-01
K9-13-GA	Quartz	8297h	0.00E+00	0.00E+00	1.52E-02	99.79	7.26E-02	0.00E+00	1.79E-03	1.01E-01
K9-13-GA	Quartz	8297j	0.00E+00	4.42E-05	1.25E-02	99.71	4.49E-02	2.34E-03	2.79E-03	2.10E-01
K9-20-GA	Quartz	8298a	0.00E+00	1.45E-04	1.48E-02	99.78	3.75E-02	4.20E-04	6.30E-04	1.47E-01
K9-20-GA	Quartz	8298b	0.00E+00	2.81E-04	9.00E-03	99.77	3.09E-02	5.61E-03	2.18E-03	1.46E-01
K9-20-GA	Quartz	8298c	0.00E+00	3.26E-05	1.44E-02	99.82	5.25E-02	1.91E-03	2.03E-03	8.87E-02
K9-20-GA	Quartz	8298d	0.00E+00	4.38E-05	1.27E-02	99.82	3.53E-02	2.79E-03	1.99E-03	1.02E-01
K9-20-GA	Quartz	8298e	0.00E+00	2.32E-05	1.19E-02	99.84	4.61E-02	1.25E-03	1.69E-03	8.46E-02
K9-20-GA	Quartz	8298f	0.00E+00	0.00E+00	1.27E-02	99.85	2.49E-02	4.68E-04	1.36E-03	9.18E-02
K9-20-GA	Quartz	8298g	0.00E+00	1.99E-05	1.33E-02	99.86	2.85E-02	1.21E-03	1.51E-03	7.90E-02
K9-20-GA	Quartz	8298h	0.00E+00	4.60E-05	1.41E-02	99.84	2.54E-02	2.02E-03	1.82E-03	9.50E-02
K9-20-GA	Quartz	8298j	0.00E+00	1.91E-05	1.08E-02	99.89	2.82E-02	1.03E-03	1.46E-03	5.69E-02
K9-8-GA	Quartz	8300a	0.00E+00	4.87E-04	1.51E-02	99.64	1.28E-01	0.00E+00	1.66E-03	2.08E-01
K9-8-GA	Quartz	8300b	0.00E+00	3.00E-04	2.04E-02	99.65	1.74E-01	9.26E-05	2.67E-03	1.36E-01
K9-8-GA	Quartz	8300c	0.00E+00	0.00E+00	2.51E-02	99.37	3.66E-01	8.76E-04	4.91E-03	2.23E-01
K9-8-GA	Quartz	8300d	0.00E+00	8.51E-05	3.15E-02	99.38	3.54E-01	1.29E-03	5.00E-03	2.13E-01
K9-8-GA	Quartz	8300e	0.00E+00	3.03E-05	1.46E-02	99.70	1.81E-01	4.25E-04	2.75E-03	9.37E-02
K9-8-GA	Quartz	8300f	0.00E+00	7.61E-05	2.77E-02	99.54	1.36E-01	1.33E-03	3.07E-03	2.81E-01
K9-8-GA	Quartz	8300g	0.00E+00	3.54E-05	3.71E-02	99.41	2.14E-01	8.27E-04	4.54E-03	3.20E-01
K9-19-GA	Quartz	8301a	0.00E+00	0.00E+00	4.97E-02	99.58	1.50E-01	8.53E-04	2.00E-03	2.10E-01
K9-19-GA	Quartz	8301b	0.00E+00	5.74E-05	2.33E-02	99.76	1.03E-01	9.58E-04	1.46E-03	1.02E-01
K9-19-GA	Quartz	8301c	0.00E+00	0.00E+00	2.61E-02	99.67	6.98E-02	7.53E-04	1.29E-03	2.21E-01

Appendix F. Continued.

Sample	Mineral	Crush	SO$_2$	C$_2$H$_4$	C$_2$H$_6$	C$_3$H$_6$	C$_3$H$_8$	C$_4$H$_8$	C$_4$H$_{10}$	Benzene
K9-13-GA	Quartz	8297a	3.42E-04	3.11E-03	2.21E-03	0.00E+00	1.12E-02	1.81E-04	1.67E-03	1.17E-04
K9-13-GA	Quartz	8297b	3.20E-04	3.27E-03	1.49E-03	0.00E+00	1.39E-02	2.21E-04	2.05E-03	7.75E-05
K9-13-GA	Quartz	8297c	1.46E-04	2.15E-03	9.36E-04	0.00E+00	9.73E-03	9.18E-05	1.24E-03	0.00E+00
K9-13-GA	Quartz	8297d	5.21E-05	1.16E-03	6.96E-04	0.00E+00	6.53E-03	0.00E+00	9.02E-04	4.94E-04
K9-13-GA	Quartz	8297e	3.47E-04	1.95E-03	1.25E-03	0.00E+00	8.68E-03	1.99E-04	1.01E-03	1.62E-05
K9-13-GA	Quartz	8297g	0.00E+00	3.04E-03	1.99E-03	0.00E+00	1.38E-02	9.15E-05	2.13E-03	2.44E-04
K9-13-GA	Quartz	8297h	8.95E-04	2.20E-03	1.45E-03	6.19E-04	1.16E-02	1.85E-04	4.56E-04	4.15E-04
K9-13-GA	Quartz	8297j	3.01E-04	3.17E-03	1.44E-03	0.00E+00	1.44E-02	2.27E-04	1.89E-03	1.42E-04
K9-20-GA	Quartz	8298a	8.81E-04	1.37E-03	3.28E-03	0.00E+00	8.70E-03	7.64E-04	1.70E-03	0.00E+00
K9-20-GA	Quartz	8298b	5.31E-04	4.72E-03	1.97E-03	0.00E+00	2.04E-02	3.13E-04	3.24E-03	2.13E-04
K9-20-GA	Quartz	8298c	3.14E-04	2.81E-03	1.27E-03	0.00E+00	1.15E-02	1.61E-04	1.72E-03	1.58E-04
K9-20-GA	Quartz	8298d	2.82E-04	3.03E-03	1.44E-03	0.00E+00	1.43E-02	2.05E-04	1.67E-03	6.07E-05
K9-20-GA	Quartz	8298e	1.79E-04	2.34E-03	1.12E-03	0.00E+00	9.81E-03	2.27E-04	1.85E-03	1.48E-04
K9-20-GA	Quartz	8298f	4.85E-04	3.37E-03	1.07E-03	0.00E+00	1.50E-02	2.86E-04	2.39E-03	0.00E+00
K9-20-GA	Quartz	8298g	2.67E-04	1.83E-03	8.21E-04	0.00E+00	9.59E-03	7.27E-05	7.51E-04	1.05E-04
K9-20-GA	Quartz	8298h	2.45E-04	3.05E-03	1.14E-03	0.00E+00	1.30E-02	1.25E-04	1.59E-03	9.58E-05
K9-20-GA	Quartz	8298j	2.37E-04	2.28E-03	9.00E-04	0.00E+00	9.65E-03	5.48E-05	1.28E-03	6.47E-06
K9-8-GA	Quartz	8300a	0.00E+00	0.00E+00	7.09E-03	1.45E-03	1.02E-03	7.66E-04	0.00E+00	7.41E-05
K9-8-GA	Quartz	8300b	0.00E+00	4.50E-03	1.85E-05	0.00E+00	2.03E-03	0.00E+00	3.91E-03	1.00E-03
K9-8-GA	Quartz	8300c	5.15E-04	1.84E-03	2.15E-03	0.00E+00	1.98E-03	0.00E+00	1.09E-03	0.00E+00
K9-8-GA	Quartz	8300d	9.13E-04	1.62E-03	4.20E-03	0.00E+00	3.29E-03	4.19E-04	1.10E-03	7.75E-04
K9-8-GA	Quartz	8300e	1.84E-04	3.55E-04	1.75E-03	0.00E+00	8.94E-04	1.87E-04	3.71E-04	0.00E+00
K9-8-GA	Quartz	8300f	5.14E-04	1.32E-03	3.16E-03	6.72E-04	2.37E-03	8.06E-05	0.00E+00	1.77E-04
K9-8-GA	Quartz	8300g	3.01E-04	9.64E-04	5.04E-03	0.00E+00	3.29E-03	4.69E-04	4.46E-04	6.87E-05
K9-19-GA	Quartz	8301a	0.00E+00	1.41E-03	3.74E-03	2.24E-03	4.53E-03	8.82E-04	0.00E+00	0.00E+00
K9-19-GA	Quartz	8301b	2.58E-04	5.40E-04	2.94E-03	0.00E+00	2.49E-03	2.35E-04	2.91E-04	1.92E-04
K9-19-GA	Quartz	8301c	4.00E-04	2.34E-03	3.60E-03	0.00E+00	4.68E-03	2.42E-04	1.42E-03	3.51E-04

Appendix F. Continued.

Sample	Mineral	Crush	H_2	He	CH_4	H_2O	N_2	H_2S	Ar	CO_2
K9-19-GA	Quartz	8301d	0.00E+00	0.00E+00	1.01E-01	99.56	8.76E-02	7.77E-04	1.39E-03	2.14E-01
K9-19-GA	Quartz	8301e	0.00E+00	1.87E-04	5.01E-02	99.63	1.87E-01	5.79E-04	2.44E-03	1.14E-01
K9-19-GA	Quartz	8301f	0.00E+00	1.27E-04	1.09E-01	99.36	2.01E-01	1.28E-03	2.39E-03	3.09E-01
K9-19-GA	Quartz	8301g	0.00E+00	0.00E+00	2.62E-01	99.37	1.21E-01	9.55E-04	1.65E-03	1.92E-01
K9-5-GA	Quartz	8302a	4.56E-04	1.05E-04	1.12E-02	99.54	8.99E-02	3.80E-03	2.16E-03	3.40E-01
K9-5-GA	Quartz	8302b	0.00E+00	4.11E-05	2.41E-02	99.60	9.68E-02	9.15E-04	1.19E-03	2.67E-01
K9-5-GA	Quartz	8302c	2.10E-03	4.06E-05	1.88E-02	99.58	4.05E-02	2.41E-03	1.09E-03	3.47E-01
K9-5-GA	Quartz	8302d	0.00E+00	2.02E-05	1.78E-02	99.62	5.50E-02	2.42E-04	5.72E-04	3.03E-01
K9-5-GA	Quartz	8302e	0.00E+00	0.00E+00	2.00E-02	99.50	8.24E-02	5.59E-04	1.03E-03	3.94E-01
K9-5-GA	Quartz	8302f	0.00E+00	1.95E-05	1.47E-02	99.49	1.99E-02	2.22E-03	1.04E-03	4.67E-01
K9-5-GA	Quartz	8302g	0.00E+00	5.33E-05	9.95E-03	99.61	2.69E-02	3.25E-03	1.08E-03	3.38E-01
K9-5-GA	Quartz	8302h	0.00E+00	4.06E-05	1.72E-02	99.60	2.72E-02	1.67E-03	8.85E-04	3.45E-01
K9-5-GA	Quartz	8302j	8.32E-04	3.26E-05	1.90E-02	99.43	9.40E-03	2.15E-03	8.17E-04	5.27E-01
K9-19-GA	Quartz	8303a	0.00E+00	1.48E-05	8.18E-03	99.81	7.11E-02	1.26E-03	1.38E-03	1.05E-01
K9-19-GA	Quartz	8303b	0.00E+00	0.00E+00	1.55E-02	99.81	4.86E-02	2.00E-04	8.01E-04	1.16E-01
K9-19-GA	Quartz	8303c	0.00E+00	1.11E-05	2.12E-02	99.66	5.52E-02	9.11E-04	7.40E-04	2.50E-01
K9-19-GA	Quartz	8303d	0.00E+00	7.41E-05	1.33E-02	99.76	2.89E-02	4.00E-04	5.11E-04	1.91E-01
K9-19-GA	Quartz	8303e	0.00E+00	2.66E-05	1.96E-02	99.70	4.41E-02	1.41E-03	1.10E-03	2.30E-01
K9-19-GA	Quartz	8303f	0.00E+00	0.00E+00	2.95E-02	99.55	7.14E-02	5.64E-05	8.28E-04	3.38E-01
K9-19-GA	Quartz	8303g	0.00E+00	0.00E+00	2.74E-02	99.61	6.20E-02	0.00E+00	8.70E-04	2.93E-01
K9-19-GA	Quartz	8303h	0.00E+00	3.84E-05	2.81E-02	99.59	4.55E-02	1.56E-03	1.12E-03	3.24E-01
K9-19-GA	Quartz	8303j	0.00E+00	8.94E-05	2.41E-02	99.56	6.08E-02	1.62E-03	1.29E-03	3.45E-01
K9-20-GA	Quartz	8304a	0.00E+00	2.71E-05	2.23E-02	99.72	5.19E-02	1.42E-03	8.35E-04	2.01E-01
K9-20-GA	Quartz	8304b	0.00E+00	6.69E-05	2.06E-02	99.58	1.07E-01	1.59E-03	2.22E-03	2.84E-01
K9-20-GA	Quartz	8304c	0.00E+00	3.94E-05	1.80E-02	99.56	3.98E-02	3.19E-03	1.28E-03	3.70E-01
K9-20-GA	Quartz	8304d	4.80E-04	9.53E-05	1.16E-02	99.53	1.55E-02	3.68E-03	1.38E-03	4.31E-01
K9-20-GA	Quartz	8304e	0.00E+00	3.41E-05	1.64E-02	99.70	3.55E-02	7.00E-04	5.75E-04	2.41E-01

Appendix F. Continued.

Sample	Mineral	Crush	SO$_2$	C$_2$H$_4$	C$_2$H$_6$	C$_3$H$_6$	C$_3$H$_8$	C$_4$H$_8$	C$_4$H$_{10}$	Benzene
K9-19-GA	Quartz	8301d	0.00E+00	2.96E-03	1.12E-02	0.00E+00	1.43E-02	7.02E-04	8.74E-04	5.39E-04
K9-19-GA	Quartz	8301e	0.00E+00	4.25E-03	1.83E-03	6.92E-04	5.64E-03	4.04E-04	2.45E-04	6.64E-04
K9-19-GA	Quartz	8301f	9.87E-04	2.60E-03	8.35E-03	9.83E-04	7.81E-03	7.59E-04	0.00E+00	3.47E-05
K9-19-GA	Quartz	8301g	2.17E-03	2.73E-03	1.93E-02	0.00E+00	2.01E-02	2.18E-03	1.77E-03	9.23E-05
K9-5-GA	Quartz	8302a	4.54E-04	1.78E-03	2.77E-03	0.00E+00	2.92E-03	2.39E-04	4.64E-04	1.39E-04
K9-5-GA	Quartz	8302b	2.28E-04	5.18E-04	2.06E-03	0.00E+00	1.27E-03	2.99E-04	2.26E-04	3.45E-04
K9-5-GA	Quartz	8302c	2.79E-04	9.34E-04	1.77E-03	1.49E-04	1.89E-03	1.23E-04	1.24E-04	1.36E-04
K9-5-GA	Quartz	8302d	6.39E-05	1.20E-04	2.49E-03	2.80E-04	2.82E-03	0.00E+00	0.00E+00	0.00E+00
K9-5-GA	Quartz	8302e	7.40E-04	7.53E-04	1.91E-03	4.84E-04	1.45E-03	3.64E-04	1.00E-05	0.00E+00
K9-5-GA	Quartz	8302f	2.57E-04	8.90E-04	1.91E-03	0.00E+00	1.67E-03	9.82E-05	4.45E-04	3.31E-05
K9-5-GA	Quartz	8302g	3.67E-04	1.45E-03	2.48E-03	0.00E+00	2.46E-03	1.85E-04	4.24E-04	1.02E-04
K9-5-GA	Quartz	8302h	2.64E-04	9.15E-04	2.10E-03	0.00E+00	2.55E-03	1.43E-04	5.75E-04	1.64E-04
K9-5-GA	Quartz	8302j	1.52E-04	9.17E-04	2.27E-03	0.00E+00	2.44E-03	1.64E-04	4.00E-04	1.03E-04
K9-19-GA	Quartz	8303a	2.00E-04	5.85E-04	1.32E-03	1.73E-04	1.32E-03	1.17E-04	9.99E-05	5.76E-05
K9-19-GA	Quartz	8303b	7.50E-04	1.38E-04	3.59E-03	0.00E+00	2.41E-03	4.37E-04	4.26E-04	0.00E+00
K9-19-GA	Quartz	8303c	0.00E+00	8.81E-04	2.67E-03	0.00E+00	2.85E-03	0.00E+00	5.40E-04	6.22E-04
K9-19-GA	Quartz	8303d	1.69E-04	1.23E-03	2.08E-03	0.00E+00	2.55E-03	0.00E+00	1.21E-03	4.70E-04
K9-19-GA	Quartz	8303e	1.62E-04	1.05E-03	1.85E-03	0.00E+00	2.26E-03	6.41E-05	8.26E-04	3.09E-04
K9-19-GA	Quartz	8303f	2.70E-04	4.77E-04	3.32E-03	0.00E+00	2.15E-03	7.34E-04	7.32E-04	1.17E-04
K9-19-GA	Quartz	8303g	5.02E-04	6.81E-04	3.40E-03	0.00E+00	1.97E-03	6.96E-04	1.27E-03	0.00E+00
K9-19-GA	Quartz	8303h	7.05E-04	1.22E-03	1.71E-03	0.00E+00	2.20E-03	7.71E-05	8.37E-04	0.00E+00
K9-19-GA	Quartz	8303j	1.56E-04	4.22E-04	2.27E-03	1.80E-04	1.68E-03	1.37E-04	1.47E-04	1.46E-04
K9-20-GA	Quartz	8304a	1.55E-04	7.99E-04	2.06E-03	0.00E+00	1.63E-03	4.01E-04	1.93E-04	0.00E+00
K9-20-GA	Quartz	8304b	5.10E-05	9.77E-04	2.38E-03	0.00E+00	1.72E-03	0.00E+00	3.38E-04	0.00E+00
K9-20-GA	Quartz	8304c	3.17E-04	1.64E-03	3.13E-03	0.00E+00	2.56E-03	1.84E-04	3.06E-04	1.17E-04
K9-20-GA	Quartz	8304d	4.25E-04	1.77E-03	3.55E-03	0.00E+00	3.73E-03	2.39E-04	5.91E-04	1.29E-04
K9-20-GA	Quartz	8304e	4.25E-04	2.70E-04	3.06E-03	5.26E-04	2.06E-03	2.46E-04	0.00E+00	0.00E+00

160

Appendix F. Continued.

Sample	Mineral	Crush	H_2	He	CH_4	H_2O	N_2	H_2S	Ar	CO_2
K9-20-GA	Quartz	8304f	0.00E+00	2.50E-06	1.97E-02	99.56	6.97E-02	7.88E-04	9.31E-04	3.43E-01
K9-20-GA	Quartz	8304g	0.00E+00	5.26E-05	1.36E-02	99.42	1.47E-02	2.23E-03	9.64E-04	5.37E-01
K9-20-GA	Quartz	8304h	0.00E+00	3.84E-05	1.72E-02	99.68	3.69E-02	1.30E-03	6.37E-04	2.62E-01
K9-1-GA	Quartz	8305a	0.00E+00	7.15E-05	2.30E-01	85.02	3.77E+00	1.69E-03	4.31E-03	8.74E+00
K9-1-GA	Quartz	8305b	0.00E+00	0.00E+00	2.02E-02	99.36	3.08E-01	4.42E-04	4.30E-03	2.91E-01
K9-1-GA	Quartz	8305c	0.00E+00	4.43E-05	2.31E-02	99.31	3.03E-01	1.28E-03	4.25E-03	3.45E-01
K9-1-GA	Quartz	8305d	0.00E+00	3.40E-06	1.56E-02	98.64	7.32E-01	2.06E-03	1.44E-02	5.83E-01
K9-1-GA	Quartz	8305e	0.00E+00	6.94E-05	1.50E-02	99.10	6.22E-01	2.46E-03	8.32E-03	2.49E-01
K9-1-GA	Quartz	8305f	0.00E+00	4.47E-05	1.75E-02	99.32	2.12E-01	1.67E-03	3.95E-03	4.36E-01
K9-1-GA	Quartz	8305g	0.00E+00	3.14E-05	1.22E-02	99.20	4.39E-01	2.40E-03	9.63E-03	3.31E-01
K9-1-GA	Quartz	8305h	0.00E+00	2.80E-05	1.59E-02	99.46	2.20E-01	2.67E-03	4.40E-03	2.88E-01
K9-1-GA	Quartz	8305j	0.00E+00	4.89E-05	1.16E-02	99.41	2.86E-01	3.44E-03	6.21E-03	2.75E-01
K9-14-GA	Quartz	8306a	0.00E+00	4.89E-05	8.92E-03	99.90	3.98E-02	1.16E-03	5.58E-04	4.12E-02
K9-14-GA	Quartz	8306b	0.00E+00	3.06E-05	1.20E-02	99.77	1.44E-01	1.59E-03	2.02E-03	6.73E-02
K9-14-GA	Quartz	8306c	0.00E+00	3.59E-05	6.98E-03	99.83	8.85E-02	2.26E-03	1.96E-03	6.69E-02
K9-14-GA	Quartz	8306d	0.00E+00	5.21E-05	9.68E-03	99.89	4.42E-02	1.49E-03	8.43E-04	5.21E-02
K9-14-GA	Quartz	8306e	0.00E+00	3.47E-05	9.67E-03	99.86	4.46E-02	2.57E-03	1.11E-03	7.68E-02
K9-14-GA	Quartz	8306f	0.00E+00	0.00E+00	1.37E-02	99.90	2.85E-02	8.17E-04	3.15E-04	4.52E-02
K9-14-GA	Quartz	8306g	0.00E+00	3.22E-05	9.03E-03	99.87	4.12E-02	2.70E-03	9.35E-04	6.92E-02
K9-3-GA	Calcite	8307a	0.00E+00	6.78E-05	3.05E-02	99.37	1.47E-01	5.05E-04	1.02E-03	4.48E-01
K9-3-GA	Calcite	8307b	0.00E+00	1.18E-04	1.89E-02	99.63	4.80E-02	1.14E-03	6.26E-04	2.99E-01
K9-3-GA	Calcite	8307c	0.00E+00	0.00E+00	2.45E-02	99.44	7.87E-02	8.99E-04	6.98E-04	4.42E-01
K9-3-GA	Calcite	8307d	0.00E+00	6.15E-05	1.59E-02	99.49	3.18E-02	1.32E-03	8.40E-04	4.51E-01
K9-3-GA	Calcite	8307e	0.00E+00	4.59E-05	2.41E-02	99.47	5.17E-02	1.40E-03	9.32E-04	4.50E-01
K9-3-GA	Calcite	8307f	0.00E+00	3.27E-05	2.73E-02	99.32	4.34E-02	2.71E-05	3.98E-04	6.02E-01
K9-3-GA	Calcite	8307g	0.00E+00	3.39E-05	1.50E-02	99.68	1.27E-02	7.75E-04	3.69E-04	2.91E-01
K9-3-GA	Calcite	8307h	0.00E+00	6.21E-05	6.79E-02	99.26	9.42E-02	5.34E-04	6.62E-04	5.72E-01

Appendix F. Continued.

Sample	Mineral	Crush	SO$_2$	C$_2$H$_4$	C$_2$H$_6$	C$_3$H$_6$	C$_3$H$_8$	C$_4$H$_8$	C$_4$H$_{10}$	Benzene
K9-20-GA	Quartz	8304f	2.65E-04	1.69E-03	2.42E-03	0.00E+00	2.60E-03	4.10E-04	7.53E-04	5.87E-05
K9-20-GA	Quartz	8304g	3.18E-04	9.10E-04	2.56E-03	0.00E+00	2.11E-03	1.96E-04	3.86E-04	1.05E-04
K9-20-GA	Quartz	8304h	1.08E-04	7.71E-04	2.51E-03	1.33E-04	1.80E-03	2.17E-04	1.83E-04	1.15E-04
K9-1-GA	Quartz	8305a	1.08E+00	2.08E-02	2.09E-05	6.52E-01	1.72E-02	1.29E-03	1.56E-02	4.49E-01
K9-1-GA	Quartz	8305b	1.27E-03	2.24E-03	5.59E-03	0.00E+00	1.07E-03	5.91E-04	1.70E-03	0.00E+00
K9-1-GA	Quartz	8305c	0.00E+00	3.68E-03	6.31E-03	0.00E+00	3.78E-03	0.00E+00	3.96E-03	8.94E-04
K9-1-GA	Quartz	8305d	4.91E-04	3.38E-03	4.65E-03	0.00E+00	2.66E-03	0.00E+00	8.02E-04	4.57E-04
K9-1-GA	Quartz	8305e	2.22E-04	1.18E-03	3.81E-03	0.00E+00	1.76E-03	1.94E-04	5.15E-04	1.45E-04
K9-1-GA	Quartz	8305f	9.08E-04	1.46E-03	4.56E-03	9.41E-04	4.25E-03	1.36E-04	0.00E+00	6.83E-05
K9-1-GA	Quartz	8305g	2.33E-04	8.12E-04	2.50E-03	0.00E+00	1.92E-03	7.35E-05	1.98E-04	6.45E-05
K9-1-GA	Quartz	8305h	2.68E-04	6.60E-04	3.00E-03	0.00E+00	1.85E-03	1.50E-04	2.04E-04	1.03E-04
K9-1-GA	Quartz	8305j	3.77E-04	9.39E-04	2.69E-03	0.00E+00	1.70E-03	1.16E-04	4.09E-04	1.34E-04
K9-14-GA	Quartz	8306a	3.86E-04	4.61E-04	1.97E-03	0.00E+00	1.35E-03	2.80E-04	3.76E-04	1.60E-04
K9-14-GA	Quartz	8306b	4.10E-04	7.45E-04	2.27E-03	0.00E+00	1.35E-03	1.57E-04	3.01E-04	2.24E-04
K9-14-GA	Quartz	8306c	2.88E-04	8.10E-04	2.68E-03	0.00E+00	1.71E-03	1.37E-04	3.70E-04	9.72E-05
K9-14-GA	Quartz	8306d	1.13E-04	6.55E-04	1.70E-03	0.00E+00	1.61E-03	2.36E-04	2.93E-04	9.98E-05
K9-14-GA	Quartz	8306e	2.83E-04	1.16E-03	2.58E-03	0.00E+00	2.35E-03	1.82E-04	5.42E-04	1.17E-04
K9-14-GA	Quartz	8306f	1.03E-03	1.53E-03	1.41E-03	0.00E+00	2.54E-03	0.00E+00	8.85E-04	0.00E+00
K9-14-GA	Quartz	8306g	2.86E-04	9.84E-04	2.62E-03	0.00E+00	2.70E-03	2.10E-04	4.71E-04	1.16E-04
K9-3-GA	Calcite	8307a	5.37E-04	0.00E+00	3.20E-03	0.00E+00	3.75E-04	5.54E-04	1.63E-03	0.00E+00
K9-3-GA	Calcite	8307b	4.51E-04	1.47E-04	2.34E-03	2.42E-04	1.59E-03	8.33E-05	0.00E+00	6.59E-06
K9-3-GA	Calcite	8307c	2.65E-04	6.51E-04	2.06E-03	0.00E+00	3.42E-03	7.22E-04	1.06E-03	2.49E-04
K9-3-GA	Calcite	8307d	7.33E-04	4.94E-04	2.62E-03	0.00E+00	2.16E-03	8.88E-05	4.57E-04	1.28E-04
K9-3-GA	Calcite	8307e	2.77E-04	4.05E-04	2.48E-03	2.30E-04	1.98E-03	1.91E-04	1.91E-05	2.81E-05
K9-3-GA	Calcite	8307f	3.66E-04	4.12E-04	2.44E-03	0.00E+00	2.70E-03	4.18E-04	5.87E-04	5.43E-04
K9-3-GA	Calcite	8307g	6.35E-05	6.59E-05	1.12E-03	0.00E+00	7.82E-04	6.99E-05	1.02E-04	8.51E-05
K9-3-GA	Calcite	8307h	0.00E+00	8.02E-04	2.81E-03	0.00E+00	1.25E-03	0.00E+00	6.83E-04	3.63E-04

162

Appendix F. Continued.

Sample	Mineral	Crush	H_2	He	CH_4	H_2O	N_2	H_2S	Ar	CO_2
K9-8-GA	Calcite	8308a	0.00E+00	6.11E-05	3.65E-02	99.15	4.14E-01	5.69E-03	8.55E-03	2.87E-01
K9-8-GA	Calcite	8308b	0.00E+00	5.14E-05	2.84E-02	99.23	4.59E-01	2.47E-03	7.58E-03	2.20E-01
K9-8-GA	Calcite	8308c	0.00E+00	4.87E-05	1.85E-02	99.33	3.16E-01	5.10E-03	6.68E-03	2.54E-01
K9-8-GA	Calcite	8308d	0.00E+00	6.17E-05	1.98E-02	99.29	3.11E-01	6.00E-03	6.82E-03	2.83E-01
K9-22-GA	Quartz	8309b	0.00E+00	0.00E+00	1.41E-02	99.58	1.19E-01	1.58E-04	1.46E-03	2.78E-01
K9-22-GA	Quartz	8309c	0.00E+00	0.00E+00	1.43E-02	99.66	1.00E-01	4.01E-04	1.47E-03	2.17E-01
K9-22-GA	Quartz	8309d	0.00E+00	2.49E-04	2.27E-02	99.59	1.95E-01	8.83E-04	2.56E-03	1.81E-01
K9-22-GA	Quartz	8309e	0.00E+00	0.00E+00	1.84E-02	99.60	2.26E-01	0.00E+00	2.88E-03	1.44E-01
K9-22-GA	Quartz	8309f	0.00E+00	1.70E-04	2.45E-02	99.57	2.15E-01	1.19E-03	2.81E-03	1.75E-01
K9-22-GA	Quartz	8309g	0.00E+00	0.00E+00	1.91E-02	99.63	1.94E-01	1.86E-04	2.53E-03	1.49E-01
K9-22-GA	Quartz	8309h	0.00E+00	5.33E-05	2.33E-02	99.61	1.79E-01	3.68E-04	2.35E-03	1.76E-01
K9-21-GA	Calcite	8310a	0.00E+00	0.00E+00	1.96E-02	99.76	8.85E-02	0.00E+00	6.78E-04	1.26E-01
K9-21-GA	Calcite	8310b	0.00E+00	0.00E+00	1.64E-02	99.84	6.30E-02	5.82E-04	6.72E-04	7.65E-02
K9-21-GA	Calcite	8310c	0.00E+00	7.30E-05	1.50E-02	99.72	9.54E-02	3.20E-03	1.79E-03	1.61E-01
K9-21-GA	Calcite	8310d	0.00E+00	8.22E-05	2.76E-02	99.66	1.07E-01	1.18E-03	8.97E-04	1.95E-01
K9-21-GA	Calcite	8310e	0.00E+00	5.09E-05	1.88E-02	99.66	1.00E-01	2.47E-03	1.83E-03	2.13E-01
K9-21-GA	Calcite	8310f	0.00E+00	4.50E-05	1.13E-02	99.71	1.29E-01	2.94E-03	2.21E-03	1.39E-01
K9-21-GA	Calcite	8310g	0.00E+00	0.00E+00	2.63E-02	99.64	8.30E-02	9.30E-04	1.10E-03	2.49E-01
K9-21-GA	Calcite	8310h	0.00E+00	9.96E-05	1.91E-02	99.69	1.05E-01	1.51E-03	1.63E-03	1.79E-01
K9-19-GA	Calcite	8311a	0.00E+00	5.94E-05	8.84E-03	99.59	2.65E-01	1.70E-03	3.12E-03	1.23E-01
K9-19-GA	Calcite	8311b	0.00E+00	1.13E-04	4.60E-03	99.75	7.54E-02	4.42E-03	2.13E-03	1.55E-01
K9-19-GA	Calcite	8311c	8.81E-05	6.47E-05	7.46E-03	99.66	5.29E-02	8.00E-03	1.82E-03	2.60E-01
K9-19-GA	Calcite	8311d	0.00E+00	3.58E-05	9.82E-03	99.77	5.82E-02	3.23E-03	9.85E-04	1.49E-01
K9-19-GA	Calcite	8311e	0.00E+00	1.61E-05	8.26E-03	99.69	4.79E-02	5.68E-03	1.22E-03	2.40E-01
K9-19-GA	Calcite	8311f	7.07E-04	4.60E-05	9.22E-03	99.66	2.56E-02	8.78E-03	1.40E-03	2.83E-01
K9-19-GA	Calcite	8311g	0.00E+00	5.51E-05	8.38E-03	99.67	2.62E-02	9.40E-03	1.39E-03	2.72E-01
G5-1-GA	Quartz	8313a	0.00E+00	0.00E+00	1.88E-02	98.71	9.35E-01	1.68E-03	1.40E-02	3.10E-01

163

Appendix F. Continued.

Sample	Mineral	Crush	SO_2	C_2H_4	C_2H_6	C_3H_6	C_3H_8	C_4H_8	C_4H_{10}	Benzene
K9-8-GA	Calcite	8308a	8.11E-04	0.00E+00	9.14E-02	1.28E-03	2.70E-03	3.88E-04	4.30E-04	1.89E-04
K9-8-GA	Calcite	8308b	7.31E-04	0.00E+00	4.25E-02	0.00E+00	2.36E-03	0.00E+00	5.91E-04	3.99E-04
K9-8-GA	Calcite	8308c	7.18E-04	0.00E+00	7.01E-02	0.00E+00	2.44E-03	3.74E-04	5.26E-04	1.85E-04
K9-8-GA	Calcite	8308d	8.21E-04	0.00E+00	8.22E-02	0.00E+00	2.75E-03	4.16E-04	5.05E-04	2.11E-04
K9-22-GA	Quartz	8309b	0.00E+00	1.60E-03	1.37E-03	0.00E+00	3.67E-03	0.00E+00	1.33E-03	6.53E-04
K9-22-GA	Quartz	8309c	0.00E+00	2.59E-03	2.13E-05	0.00E+00	3.69E-04	2.02E-04	5.54E-03	1.10E-03
K9-22-GA	Quartz	8309d	0.00E+00	8.64E-04	4.24E-04	0.00E+00	7.65E-04	4.05E-04	1.12E-03	0.00E+00
K9-22-GA	Quartz	8309e	4.68E-04	3.49E-04	2.99E-03	0.00E+00	3.65E-03	4.09E-04	1.11E-03	5.75E-04
K9-22-GA	Quartz	8309f	5.63E-04	0.00E+00	3.76E-03	2.30E-04	1.29E-03	8.63E-04	8.26E-05	0.00E+00
K9-22-GA	Quartz	8309g	3.69E-05	1.43E-04	3.21E-03	0.00E+00	3.08E-03	0.00E+00	8.70E-04	8.90E-05
K9-22-GA	Quartz	8309h	7.58E-04	3.97E-03	4.33E-05	0.00E+00	0.00E+00	0.00E+00	5.76E-03	0.00E+00
K9-21-GA	Calcite	8310a	0.00E+00	5.77E-04	1.80E-04	3.47E-05	0.00E+00	4.96E-04	0.00E+00	0.00E+00
K9-21-GA	Calcite	8310b	4.96E-04	0.00E+00	1.21E-03	0.00E+00	3.80E-04	1.58E-04	5.63E-05	0.00E+00
K9-21-GA	Calcite	8310c	2.49E-04	1.02E-03	2.33E-03	0.00E+00	1.51E-03	1.06E-04	2.31E-04	7.31E-05
K9-21-GA	Calcite	8310d	3.43E-04	1.32E-03	1.11E-03	0.00E+00	3.17E-03	7.99E-04	0.00E+00	4.33E-04
K9-21-GA	Calcite	8310e	2.23E-04	7.04E-04	1.89E-03	0.00E+00	1.36E-03	2.08E-04	2.87E-04	7.05E-05
K9-21-GA	Calcite	8310f	2.63E-04	9.37E-04	2.02E-03	0.00E+00	1.83E-03	1.37E-04	3.59E-04	1.07E-04
K9-21-GA	Calcite	8310g	2.43E-04	9.07E-04	1.27E-03	0.00E+00	8.46E-04	4.31E-04	4.25E-04	1.94E-04
K9-21-GA	Calcite	8310h	3.81E-05	3.46E-04	1.30E-03	3.27E-04	1.22E-03	9.79E-05	0.00E+00	0.00E+00
K9-19-GA	Calcite	8311a	2.39E-04	0.00E+00	3.33E-03	0.00E+00	1.78E-03	6.89E-04	3.96E-04	0.00E+00
K9-19-GA	Calcite	8311b	4.24E-04	1.46E-03	3.03E-03	0.00E+00	3.34E-03	2.07E-04	4.60E-04	1.04E-04
K9-19-GA	Calcite	8311c	4.68E-04	1.45E-03	2.78E-03	0.00E+00	3.17E-03	2.19E-04	5.88E-04	1.00E-04
K9-19-GA	Calcite	8311d	1.63E-04	5.97E-04	1.34E-03	0.00E+00	1.47E-03	1.64E-04	3.77E-04	3.54E-05
K9-19-GA	Calcite	8311e	2.66E-04	6.82E-04	1.58E-03	0.00E+00	1.79E-03	2.03E-04	2.81E-04	1.05E-04
K9-19-GA	Calcite	8311f	3.16E-04	1.18E-03	2.56E-03	0.00E+00	2.50E-03	1.95E-04	4.44E-04	9.14E-05
K9-19-GA	Calcite	8311g	4.25E-04	1.33E-03	2.71E-03	0.00E+00	2.70E-03	1.78E-04	6.40E-04	1.71E-04
G5-1-GA	Quartz	8313a	0.00E+00	7.98E-04	2.12E-03	0.00E+00	0.00E+00	1.70E-03	4.37E-04	0.00E+00

164

Appendix F. Continued.

Sample	Mineral	Crush	H_2	He	CH_4	H_2O	N_2	H_2S	Ar	CO_2
G5-1-GA	Quartz	8313b	0.00E+00	1.14E-04	3.31E-03	99.79	1.27E-01	3.31E-03	3.03E-03	6.72E-02
G5-1-GA	Quartz	8313c	0.00E+00	8.03E-06	2.42E-02	99.41	4.20E-01	2.04E-05	5.67E-03	1.33E-01
G5-1-GA	Quartz	8313d	0.00E+00	3.78E-05	1.08E-02	99.73	1.22E-01	1.96E-03	1.92E-03	1.29E-01
G5-1-GA	Quartz	8313e	0.00E+00	1.85E-05	5.88E-03	99.84	7.08E-02	1.28E-03	1.17E-03	7.38E-02
G5-1-GA	Quartz	8313f	0.00E+00	2.82E-06	1.07E-02	99.69	1.51E-01	7.09E-04	2.34E-03	1.45E-01
G5-1-GA	Quartz	8313g	1.47E-05	3.70E-05	1.49E-02	99.61	1.87E-01	2.15E-03	3.01E-03	1.75E-01
G5-1-GA	Quartz	8313h	0.00E+00	4.01E-05	1.16E-02	99.65	1.74E-01	2.24E-03	2.84E-03	1.54E-01
G5-1-GA	Quartz	8313j	0.00E+00	4.43E-05	1.78E-02	99.74	7.81E-02	1.38E-03	1.39E-03	1.58E-01
G5-3-GA	Quartz	8314a	0.00E+00	4.04E-05	1.64E-02	99.27	5.08E-02	4.74E-03	3.12E-03	6.51E-01
G5-3-GA	Quartz	8314b	0.00E+00	0.00E+00	3.16E-02	99.10	1.40E-01	5.65E-04	1.51E-03	7.15E-01
G5-3-GA	Quartz	8314c	1.88E-03	3.99E-05	1.66E-02	99.27	5.92E-03	2.97E-03	9.70E-04	6.95E-01
G5-3-GA	Quartz	8314d	0.00E+00	5.36E-05	2.87E-02	99.34	1.18E-01	1.90E-03	1.83E-03	5.09E-01
G5-3-GA	Quartz	8314e	0.00E+00	4.17E-05	8.63E-03	99.56	3.53E-03	2.13E-03	5.61E-04	4.25E-01
G5-3-GA	Quartz	8314f	5.68E-04	8.00E-05	1.16E-02	99.67	2.53E-02	3.10E-03	9.60E-04	2.81E-01
G5-3-GA	Quartz	8314g	0.00E+00	4.61E-06	2.52E-02	99.51	6.27E-02	5.50E-04	7.08E-04	3.92E-01
G5-3-GA	Quartz	8314h	0.00E+00	3.90E-05	1.65E-02	99.67	4.16E-02	1.21E-03	8.36E-04	2.68E-01
G5-3-GA	Quartz	8314j	0.00E+00	1.93E-04	2.11E-02	99.72	4.20E-02	5.77E-04	1.48E-04	2.14E-01
G5-5-GA	Quartz	8315a	0.00E+00	0.00E+00	2.06E-02	98.26	1.45E+00	2.98E-03	1.88E-02	2.36E-01
G5-5-GA	Quartz	8315b	0.00E+00	5.77E-05	1.32E-02	99.14	6.56E-01	1.41E-03	8.90E-03	1.72E-01
G5-5-GA	Quartz	8315c	0.00E+00	3.97E-05	1.78E-02	99.56	2.35E-01	1.55E-03	3.54E-03	1.79E-01
G5-5-GA	Quartz	8315d	0.00E+00	3.12E-05	1.14E-02	99.71	1.27E-01	1.22E-03	1.89E-03	1.42E-01
G5-5-GA	Quartz	8315e	0.00E+00	4.05E-04	3.64E-03	99.81	1.26E-01	3.72E-03	2.69E-03	5.07E-02
G5-5-GA	Quartz	8315f	0.00E+00	0.00E+00	2.23E-02	99.50	2.32E-01	6.78E-04	2.63E-03	2.31E-01
G5-5-GA	Quartz	8315g	0.00E+00	7.89E-05	9.89E-03	99.53	2.47E-01	2.69E-03	4.59E-03	1.96E-01
G5-5-GA	Quartz	8315h	0.00E+00	4.86E-05	8.10E-03	99.66	1.11E-01	2.54E-03	2.43E-03	2.11E-01
G5-10-GA	Quartz	8316a	0.00E+00	0.00E+00	1.36E-02	99.65	1.59E-01	6.70E-04	1.99E-03	1.62E-01
G5-10-GA	Quartz	8316b	0.00E+00	0.00E+00	6.06E-03	99.68	1.35E-01	3.07E-04	1.88E-03	1.69E-01

165

Appendix F. Continued.

Sample	Mineral	Crush	SO_2	C_2H_4	C_2H_6	C_3H_6	C_3H_8	C_4H_8	C_4H_{10}	Benzene
G5-1-GA	Quartz	8313b	3.01E-04	1.38E-03	2.18E-03	0.00E+00	1.86E-03	1.72E-04	2.69E-04	9.62E-05
G5-1-GA	Quartz	8313c	6.61E-04	4.52E-04	2.00E-03	4.98E-04	8.82E-04	6.22E-04	0.00E+00	0.00E+00
G5-1-GA	Quartz	8313d	2.46E-04	7.84E-04	1.28E-03	0.00E+00	1.15E-03	2.15E-04	2.68E-04	9.76E-05
G5-1-GA	Quartz	8313e	9.64E-05	4.69E-04	8.71E-04	0.00E+00	8.18E-04	8.26E-05	1.10E-04	2.24E-05
G5-1-GA	Quartz	8313f	1.20E-04	7.87E-04	1.03E-03	0.00E+00	8.19E-04	9.86E-05	4.78E-04	0.00E+00
G5-1-GA	Quartz	8313g	1.97E-04	6.48E-04	1.55E-03	2.70E-05	1.55E-03	1.19E-04	1.19E-04	5.65E-05
G5-1-GA	Quartz	8313h	1.33E-04	9.44E-04	1.66E-03	0.00E+00	1.56E-03	1.91E-04	3.32E-04	8.16E-05
G5-1-GA	Quartz	8313j	2.01E-04	6.51E-04	1.22E-03	0.00E+00	1.08E-03	1.02E-04	2.78E-04	0.00E+00
G5-3-GA	Quartz	8314a	2.99E-04	1.12E-03	2.58E-03	0.00E+00	2.14E-03	1.80E-04	4.73E-04	1.31E-04
G5-3-GA	Quartz	8314b	0.00E+00	1.39E-03	2.24E-03	0.00E+00	3.26E-03	7.02E-04	2.67E-03	1.20E-03
G5-3-GA	Quartz	8314c	2.56E-04	7.12E-04	2.34E-03	0.00E+00	1.98E-03	1.63E-04	2.39E-04	1.04E-04
G5-3-GA	Quartz	8314d	2.06E-04	2.96E-04	2.07E-03	0.00E+00	1.27E-03	2.45E-04	5.52E-04	0.00E+00
G5-3-GA	Quartz	8314e	2.05E-04	6.32E-04	1.61E-03	0.00E+00	1.81E-03	1.09E-04	2.35E-04	5.85E-05
G5-3-GA	Quartz	8314f	2.93E-04	1.37E-03	2.82E-03	0.00E+00	2.55E-03	1.77E-04	4.94E-04	8.89E-05
G5-3-GA	Quartz	8314g	0.00E+00	7.15E-04	3.52E-03	0.00E+00	2.05E-03	0.00E+00	2.26E-03	0.00E+00
G5-3-GA	Quartz	8314h	2.33E-04	7.48E-04	1.68E-03	0.00E+00	1.43E-03	1.38E-04	6.35E-04	5.60E-05
G5-3-GA	Quartz	8314j	4.52E-04	3.78E-04	2.05E-03	0.00E+00	2.56E-03	0.00E+00	2.79E-04	5.45E-04
G5-5-GA	Quartz	8315a	0.00E+00	5.59E-03	7.16E-04	0.00E+00	3.08E-03	0.00E+00	1.61E-03	0.00E+00
G5-5-GA	Quartz	8315b	2.79E-04	6.02E-04	1.72E-03	1.48E-04	1.16E-03	1.20E-04	7.78E-05	4.61E-05
G5-5-GA	Quartz	8315c	7.23E-05	5.59E-04	1.37E-03	0.00E+00	1.15E-03	7.44E-05	1.59E-04	7.47E-05
G5-5-GA	Quartz	8315d	2.03E-04	5.97E-04	1.64E-03	0.00E+00	1.23E-03	2.03E-04	3.21E-04	0.00E+00
G5-5-GA	Quartz	8315e	3.24E-04	8.09E-04	1.88E-03	0.00E+00	2.21E-03	2.20E-04	4.95E-04	1.56E-04
G5-5-GA	Quartz	8315f	8.14E-04	1.38E-03	2.77E-03	0.00E+00	1.90E-03	5.83E-04	4.03E-03	0.00E+00
G5-5-GA	Quartz	8315g	2.71E-04	9.28E-04	2.26E-03	0.00E+00	2.17E-03	1.51E-04	3.12E-04	1.03E-04
G5-5-GA	Quartz	8315h	2.74E-04	9.78E-04	1.96E-03	0.00E+00	1.77E-03	1.99E-04	2.71E-04	2.07E-05
G5-10-GA	Quartz	8316a	0.00E+00	2.20E-03	5.18E-03	6.28E-05	2.26E-03	1.03E-03	0.00E+00	0.00E+00
G5-10-GA	Quartz	8316b	0.00E+00	2.71E-03	3.26E-03	0.00E+00	9.23E-04	4.66E-04	1.56E-03	5.29E-04

166

Appendix F. Continued.

Sample	Mineral	Crush	H_2	He	CH_4	H_2O	N_2	H_2S	Ar	CO_2
G5-10-GA	Quartz	8316c	1.90E-02	4.77E-05	2.13E-01	86.98	3.24E+00	2.36E-03	5.04E-03	9.49E+00
G5-10-GA	Quartz	8316d	0.00E+00	4.51E-05	3.64E-03	99.61	2.97E-01	2.75E-03	4.80E-03	7.69E-02
G5-10-GA	Quartz	8316e	0.00E+00	8.54E-06	9.62E-03	99.58	3.28E-01	1.42E-03	4.52E-03	7.06E-02
G5-10-GA	Quartz	8316f	0.00E+00	3.87E-05	1.06E-02	99.67	2.25E-01	1.56E-03	3.55E-03	8.73E-02
G5-10-GA	Quartz	8316g	0.00E+00	2.70E-05	5.04E-03	99.70	1.94E-01	1.01E-03	3.03E-03	8.81E-02
G5-10-GA	Quartz	8316h	0.00E+00	4.75E-05	6.14E-03	99.70	1.65E-01	2.74E-03	3.04E-03	1.19E-01
G5-10-GA	Quartz	8316j	0.00E+00	4.85E-05	5.71E-03	99.70	1.44E-01	2.91E-03	3.29E-03	1.34E-01
GD-4-GA	Quartz	8317a	0.00E+00	6.33E-05	5.38E-03	99.47	2.20E-01	2.25E-03	3.98E-03	2.95E-01
GD-4-GA	Quartz	8317b	0.00E+00	4.97E-04	4.88E-03	99.64	7.81E-02	5.32E-03	2.79E-03	2.57E-01
GD-4-GA	Quartz	8317c	0.00E+00	1.84E-04	4.22E-03	99.73	1.64E-02	3.69E-03	8.78E-04	2.40E-01
GD-4-GA	Quartz	8317d	0.00E+00	3.95E-05	6.78E-03	99.53	2.11E-02	2.30E-03	1.25E-03	4.34E-01
GD-4-GA	Quartz	8317e	0.00E+00	1.78E-04	4.25E-03	99.72	5.33E-02	3.34E-03	1.57E-03	2.07E-01
GD-4-GA	Quartz	8317f	0.00E+00	2.15E-04	3.70E-03	99.63	5.77E-02	4.01E-03	1.77E-03	2.95E-01
GD-4-GA	Quartz	8317g	0.00E+00	4.84E-05	5.58E-03	99.55	8.87E-03	3.40E-03	9.58E-04	4.19E-01
GD-4-GA	Quartz	8317h	0.00E+00	5.17E-05	4.22E-03	99.67	1.33E-02	3.12E-03	8.78E-04	2.99E-01
GD-4-GA	Quartz	8317j	0.00E+00	1.75E-05	4.78E-03	99.70	5.80E-02	1.14E-03	1.06E-03	2.28E-01
GD-4-GA	Quartz	8318a	0.00E+00	6.69E-05	4.24E-03	98.87	9.19E-01	3.00E-03	1.43E-02	1.81E-01
GD-4-GA	Quartz	8318b	0.00E+00	9.59E-05	4.55E-03	98.87	8.36E-01	1.85E-03	1.07E-02	2.67E-01
GD-4-GA	Quartz	8318c	0.00E+00	4.22E-05	6.90E-03	99.58	1.52E-01	2.30E-03	2.80E-03	2.47E-01
GD-4-GA	Quartz	8318d	0.00E+00	0.00E+00	6.91E-03	99.57	1.67E-01	4.29E-04	2.14E-03	2.46E-01
GD-4-GA	Quartz	8318e	0.00E+00	0.00E+00	1.16E-02	99.29	2.98E-01	1.12E-03	4.01E-03	3.85E-01
GD-4-GA	Quartz	8318f	0.00E+00	5.38E-05	6.84E-03	99.54	3.63E-02	2.32E-03	1.50E-03	4.13E-01
GD-4-GA	Quartz	8318g	0.00E+00	7.38E-05	8.52E-03	98.97	7.17E-01	1.33E-03	1.11E-02	2.70E-01
GD-4-GA	Quartz	8318h	0.00E+00	4.51E-05	9.18E-03	99.57	9.07E-02	1.83E-03	1.80E-03	3.25E-01
GD-8-GA	Quartz	8319a	0.00E+00	3.82E-05	6.00E-03	99.75	1.11E-01	2.10E-03	1.81E-03	1.28E-01
GD-8-GA	Quartz	8319b	0.00E+00	3.12E-05	5.30E-03	99.81	5.11E-02	2.48E-03	1.47E-03	1.24E-01
GD-8-GA	Quartz	8319c	0.00E+00	4.50E-07	6.29E-03	99.83	3.08E-02	1.79E-04	5.72E-04	1.20E-01

Appendix F. Continued.

Sample	Mineral	Crush	SO_2	C_2H_4	C_2H_6	C_3H_6	C_3H_8	C_4H_8	C_4H_{10}	Benzene
G5-10-GA	Quartz	8316c	8.28E-04	8.49E-03	1.93E-02	0.00E+00	1.01E-02	2.38E-04	1.14E-03	8.83E-04
G5-10-GA	Quartz	8316d	2.11E-04	9.93E-04	2.14E-03	0.00E+00	1.73E-03	1.28E-04	3.06E-04	7.71E-05
G5-10-GA	Quartz	8316e	1.64E-04	5.37E-04	1.41E-03	0.00E+00	1.20E-03	4.97E-05	1.72E-04	5.71E-05
G5-10-GA	Quartz	8316f	1.84E-04	7.52E-04	1.75E-03	0.00E+00	1.36E-03	1.00E-04	3.68E-04	4.08E-05
G5-10-GA	Quartz	8316g	3.04E-04	3.44E-04	1.47E-03	0.00E+00	1.41E-03	1.09E-04	5.90E-05	0.00E+00
G5-10-GA	Quartz	8316h	2.39E-04	8.50E-04	2.18E-03	0.00E+00	1.93E-03	1.39E-04	2.46E-04	6.52E-05
G5-10-GA	Quartz	8316j	2.65E-04	1.02E-03	2.28E-03	0.00E+00	1.93E-03	1.49E-04	2.27E-04	5.99E-05
GD-4-GA	Quartz	8317a	1.90E-04	1.05E-03	2.33E-03	0.00E+00	2.04E-03	1.24E-04	2.84E-04	8.36E-05
GD-4-GA	Quartz	8317b	5.12E-04	9.45E-04	2.71E-03	0.00E+00	5.57E-03	2.23E-04	4.59E-04	1.60E-04
GD-4-GA	Quartz	8317c	3.16E-04	9.88E-04	2.27E-03	0.00E+00	2.65E-03	1.76E-04	3.36E-04	9.97E-05
GD-4-GA	Quartz	8317d	2.92E-04	6.37E-04	2.11E-03	8.65E-05	1.76E-03	1.64E-04	1.27E-04	3.38E-05
GD-4-GA	Quartz	8317e	2.13E-04	8.52E-04	2.17E-03	0.00E+00	2.98E-03	1.38E-04	2.64E-04	7.54E-05
GD-4-GA	Quartz	8317f	2.02E-04	1.06E-03	3.03E-03	0.00E+00	3.47E-03	1.05E-04	2.58E-04	7.44E-05
GD-4-GA	Quartz	8317g	1.46E-04	1.17E-03	2.97E-03	2.56E-04	2.44E-03	1.58E-04	1.76E-04	2.30E-05
GD-4-GA	Quartz	8317h	1.83E-04	1.04E-03	2.41E-03	0.00E+00	2.41E-03	1.02E-04	2.43E-04	6.98E-05
GD-4-GA	Quartz	8317j	0.00E+00	3.14E-05	2.08E-03	0.00E+00	1.12E-03	1.52E-04	2.46E-04	1.36E-04
GD-4-GA	Quartz	8318a	2.86E-04	5.66E-04	2.75E-03	0.00E+00	1.85E-03	8.31E-05	2.33E-04	5.82E-05
GD-4-GA	Quartz	8318b	0.00E+00	3.57E-04	3.21E-03	0.00E+00	1.38E-03	2.57E-04	3.88E-04	0.00E+00
GD-4-GA	Quartz	8318c	2.17E-04	7.50E-04	1.88E-03	0.00E+00	1.38E-03	9.81E-05	2.32E-04	5.04E-05
GD-4-GA	Quartz	8318d	7.27E-04	1.78E-04	3.02E-03	6.26E-04	9.95E-04	0.00E+00	0.00E+00	1.40E-04
GD-4-GA	Quartz	8318e	2.19E-04	2.44E-05	2.32E-03	0.00E+00	1.90E-03	1.98E-04	1.03E-03	6.53E-04
GD-4-GA	Quartz	8318f	1.79E-04	7.29E-04	2.55E-03	0.00E+00	1.38E-03	1.07E-04	2.21E-04	4.32E-05
GD-4-GA	Quartz	8318g	5.98E-04	0.00E+00	9.30E-03	7.99E-05	7.64E-03	2.17E-04	0.00E+00	2.54E-04
GD-4-GA	Quartz	8318h	1.37E-04	4.81E-04	2.30E-03	9.03E-05	1.15E-03	1.05E-04	1.10E-04	5.11E-05
GD-8-GA	Quartz	8319a	9.21E-05	6.66E-04	2.07E-03	8.01E-05	1.06E-03	7.70E-05	1.22E-04	5.66E-05
GD-8-GA	Quartz	8319b	2.06E-04	8.00E-04	2.33E-03	0.00E+00	1.23E-03	9.58E-05	1.83E-04	1.49E-04
GD-8-GA	Quartz	8319c	8.08E-04	8.11E-05	3.39E-03	0.00E+00	1.47E-03	3.42E-04	1.73E-03	0.00E+00

168

Appendix F. Continued.

Sample	Mineral	Crush	H_2	He	CH_4	H_2O	N_2	H_2S	Ar	CO_2
GD-8-GA	Quartz	8319d	0.00E+00	8.48E-05	6.70E-03	99.90	3.62E-02	8.16E-04	5.33E-04	5.24E-02
GD-8-GA	Quartz	8319e	0.00E+00	9.40E-05	1.17E-02	99.59	4.56E-02	2.02E-03	1.13E-03	3.42E-01
GD-8-GA	Quartz	8319f	0.00E+00	1.90E-05	6.53E-03	99.88	2.90E-02	0.00E+00	2.94E-04	8.31E-02
GD-8-GA	Quartz	8319g	0.00E+00	0.00E+00	5.72E-03	99.85	2.88E-02	6.18E-05	4.70E-04	1.08E-01
GD-8-GA	Quartz	8319h	0.00E+00	0.00E+00	4.73E-03	99.89	2.69E-02	0.00E+00	2.94E-04	7.47E-02
GD-10-GA	Quartz	8320a	0.00E+00	1.92E-06	9.36E-03	99.04	6.85E-01	3.33E-04	8.25E-03	2.57E-01
GD-10-GA	Quartz	8320b	0.00E+00	3.32E-05	5.82E-03	99.43	3.59E-01	2.35E-03	5.61E-03	1.91E-01
GD-10-GA	Quartz	8320c	1.72E-03	3.75E-05	4.32E-03	99.65	1.30E-01	2.55E-03	2.44E-03	2.06E-01
GD-10-GA	Quartz	8320d	0.00E+00	4.39E-05	3.77E-03	99.76	4.56E-02	1.03E-03	1.07E-03	1.87E-01
GD-10-GA	Quartz	8320e	0.00E+00	4.82E-05	4.41E-03	99.74	1.16E-01	1.05E-03	1.64E-03	1.34E-01
GD-10-GA	Quartz	8320f	0.00E+00	3.03E-05	6.12E-03	99.52	2.72E-01	1.64E-03	4.16E-03	1.89E-01
GD-10-GA	Quartz	8320g	0.00E+00	5.69E-05	4.00E-03	99.45	4.03E-01	2.82E-03	6.31E-03	1.30E-01
GD-10-GA	Quartz	8320h	1.30E-04	4.65E-05	6.91E-03	99.72	7.87E-02	2.00E-03	1.58E-03	1.87E-01
OF-09-GA	Quartz	8321a	0.00E+00	7.31E-05	1.93E-02	99.38	2.67E-02	2.91E-03	4.57E-04	5.63E-01
OF-09-GA	Quartz	8321b	0.00E+00	4.69E-05	7.01E-03	99.66	0.00E+00	1.79E-03	3.02E-04	3.31E-01
OF-09-GA	Quartz	8321c	0.00E+00	5.07E-05	6.46E-03	99.81	0.00E+00	1.84E-03	2.95E-04	1.81E-01
OF-09-GA	Quartz	8321d	0.00E+00	7.14E-05	1.70E-02	99.50	9.53E-03	2.64E-03	3.47E-04	4.64E-01
OF-09-GA	Quartz	8321e	0.00E+00	7.97E-05	3.46E-02	99.41	3.54E-02	1.92E-03	3.76E-04	5.15E-01
OF-09-GA	Quartz	8321f	0.00E+00	5.59E-05	1.47E-02	99.51	1.24E-02	2.31E-03	5.75E-04	4.55E-01
OF-09-GA	Quartz	8321g	0.00E+00	5.59E-05	2.40E-02	99.48	0.00E+00	2.65E-03	4.58E-04	4.85E-01
OF-09-GA	Quartz	8321h	0.00E+00	1.37E-04	9.53E-03	99.43	0.00E+00	5.64E-03	5.73E-04	5.44E-01

Appendix F. Continued.

Sample	Mineral	Crush	SO_2	C_2H_4	C_2H_6	C_3H_6	C_3H_8	C_4H_8	C_4H_{10}	Benzene
GD-8-GA	Quartz	8319d	0.00E+00	5.08E-04	1.28E-03	0.00E+00	3.58E-04	3.67E-05	4.71E-04	7.65E-05
GD-8-GA	Quartz	8319e	8.90E-05	1.74E-04	3.85E-03	4.43E-04	2.13E-03	2.86E-04	3.75E-05	2.36E-04
GD-8-GA	Quartz	8319f	0.00E+00	2.38E-04	1.99E-03	0.00E+00	1.27E-03	0.00E+00	3.02E-04	1.67E-04
GD-8-GA	Quartz	8319g	0.00E+00	2.99E-04	2.61E-03	0.00E+00	1.09E-03	0.00E+00	8.73E-04	1.95E-04
GD-8-GA	Quartz	8319h	7.62E-04	6.98E-04	2.92E-03	0.00E+00	1.16E-03	1.61E-04	1.32E-03	0.00E+00
GD-10-GA	Quartz	8320a	1.84E-04	2.82E-04	3.17E-03	7.06E-04	1.33E-03	1.83E-04	0.00E+00	0.00E+00
GD-10-GA	Quartz	8320b	5.95E-05	4.74E-04	1.96E-03	2.07E-04	1.06E-03	5.14E-05	6.79E-05	4.02E-05
GD-10-GA	Quartz	8320c	2.08E-04	7.95E-04	1.97E-03	0.00E+00	1.30E-03	1.58E-04	3.05E-04	7.80E-05
GD-10-GA	Quartz	8320d	1.93E-04	2.98E-04	1.55E-03	3.41E-04	1.26E-03	1.44E-04	0.00E+00	7.70E-05
GD-10-GA	Quartz	8320e	2.76E-04	3.18E-04	1.59E-03	0.00E+00	9.68E-04	0.00E+00	2.02E-04	1.19E-04
GD-10-GA	Quartz	8320f	2.12E-04	3.28E-04	1.46E-03	2.64E-04	7.46E-04	6.55E-05	1.12E-05	1.05E-05
GD-10-GA	Quartz	8320g	9.45E-05	7.40E-04	2.55E-03	6.67E-05	1.78E-03	8.68E-05	1.57E-04	3.94E-05
GD-10-GA	Quartz	8320h	1.72E-04	6.67E-04	1.85E-03	0.00E+00	1.09E-03	1.21E-04	2.94E-04	6.24E-05
OF-09-GA	Quartz	8321a	5.66E-04	0.00E+00	3.79E-03	2.53E-04	9.43E-04	4.85E-04	2.26E-05	0.00E+00
OF-09-GA	Quartz	8321b	1.30E-04	5.61E-04	1.65E-03	6.43E-05	1.43E-03	9.33E-05	8.13E-05	3.51E-05
OF-09-GA	Quartz	8321c	1.75E-04	5.26E-04	1.74E-03	0.00E+00	1.39E-03	9.31E-05	1.41E-04	6.15E-05
OF-09-GA	Quartz	8321d	2.97E-04	4.03E-04	2.31E-03	0.00E+00	1.29E-03	3.05E-04	3.75E-04	5.11E-05
OF-09-GA	Quartz	8321e	2.58E-04	4.70E-06	3.75E-03	0.00E+00	1.83E-03	1.94E-04	7.90E-04	3.97E-05
OF-09-GA	Quartz	8321f	1.92E-04	6.65E-04	1.95E-03	0.00E+00	1.25E-03	1.12E-04	3.72E-04	1.04E-04
OF-09-GA	Quartz	8321g	2.67E-04	5.66E-04	2.58E-03	0.00E+00	1.73E-03	2.15E-04	3.51E-04	6.76E-05
OF-09-GA	Quartz	8321h	3.97E-04	1.46E-03	3.25E-03	0.00E+00	2.75E-03	2.66E-04	4.13E-04	1.77E-04